

A Thesis Submitted for the Degree of PhD at the University of Warwick

Permanent WRAP URL:

<http://wrap.warwick.ac.uk/90316>

Copyright and reuse:

This thesis is made available online and is protected by original copyright.

Please scroll down to view the document itself.

Please refer to the repository record for this item for information to help you to cite it.

Our policy information is available from the repository home page.

For more information, please contact the WRAP Team at: wrap@warwick.ac.uk

Towards the Stabilisation of Enzymes *via* the Synthesis of Protein-Polymer Conjugates

Alice Charlotte Hill



Department of Chemistry

Submitted for the degree of Doctor of Philosophy

January 2017

Table of Contents

Table of Contents.....	I
List of Figures, Schemes and Tables.....	XII
Figures.....	XII
Schemes.....	XXVII
Tables.....	XXVIII
Acknowledgements.....	XXXII
Declaration of Authorship.....	XXXIII
Summary of Thesis.....	XXXIV
Abbreviations.....	XXXV
1 Introduction.....	1
1.1 Introduction.....	2
1.2 Protein Structure.....	2
1.2.1 Primary Structure.....	2
1.2.2 Secondary Structure.....	3
1.2.2.1 α -Helices.....	4
1.2.2.2 β -Sheets.....	5
1.2.2.3 β -Turns.....	6
1.2.3 Tertiary Structure.....	7
1.2.4 Quaternary Structure.....	9
1.3 Activity of Enzymes.....	10
1.4 Inhibition of Enzymes.....	12

1.4.1	Irreversible Inhibition.....	12
1.4.2	Reversible Inhibition	12
1.5	Denaturation and Inactivation of Proteins	14
1.6	Enzyme Stabilisation	16
1.6.1	Extremophile Enzymes.....	17
1.6.2	Protein Engineering.....	17
1.6.3	Additives.....	18
1.6.4	Polymeric Additives.....	19
1.6.5	Encapsulation.....	21
1.6.6	Post-translational Protein Modification	23
1.6.6.1	Chemical Modification	23
1.6.6.2	Immobilisation	26
1.7	Protein-polymer Conjugates	29
1.7.1	Polymerisation Techniques.....	30
1.7.1.1	Atom-Transfer Radical Polymerisation	31
1.7.1.2	Reversible-Addition Fragmentation Chain-Transfer Polymerisation	34
1.7.2	Synthetic Approaches	37
1.7.2.1	“Grafting to”	38
1.7.2.2	In Situ Formation of Protein-Polymer Conjugates	39
1.7.3	Site-Selectivity.....	43
1.8	Concluding Remarks.....	44
1.9	References	45

2	Synthesis and Characterisation of Site-Selective Protein Macro-Initiators	56
2.1	Abstract	57
2.2	Introduction	57
2.2.1	Chemical Modification of Proteins.....	57
2.2.2	Post-Translational Modification of Proteins	58
2.2.3	Synthesis of Polymer-Functionalised Proteins.....	59
2.2.4	Structure and Activation of α -Chymotrypsin	61
2.3	Results and Discussion	64
2.3.1	Conjugation of Initiator to Chymotrypsin	64
2.3.2	pH and Concentration Profile of CT-MI 2.1 Conjugation.....	68
2.3.3	Continuous Formation of Intermediates	73
2.3.4	Locating Modified Sites in CT-MI 2.1 Species	75
2.3.5	Activity of α -CT Macro-Initiator Species	86
2.3.6	Stability of α -CT Macro-Initiator Species	88
2.3.6.1	Thermal Stability	88
2.3.6.2	Autolytic Stability	93
2.3.6.3	Secondary Enzyme Stability	94
2.3.7	Other Methods of Conjugation to α -CT	96
2.4	Conclusions	100
2.5	Experimental	102
2.5.1	Materials	102
2.5.2	Instrumentation	102

2.5.2.1	¹ H Nuclear Magnetic Resonance (NMR) and ¹³ C NMR Spectroscopy	102
2.5.2.2	Matrix-Assisted Laser Desorption/Ionization Time-of-Flight (MALDI-ToF) Mass Spectrometry	102
2.5.2.3	Fourier Transform Infrared (FTIR) Spectroscopy	103
2.5.2.4	Liquid Chromatography–Mass Spectrometry (LC-MS)	103
2.5.2.5	Ultraviolet-Visible (UV-Vis) Spectroscopy	103
2.5.2.6	Zeta Potential	103
2.5.2.7	Thermal Shift Assay	103
2.5.2.8	Differential Scanning Calorimetry (DSC)	104
2.5.3	Software	104
2.5.4	Enzyme Kinetic Studies	104
2.5.4.1	pNA Protease Assay	104
2.5.4.2	α-CT Stability Assays	104
2.5.4.3	Michaelis-Menten Kinetics and Parameters	105
2.5.4.4	Glucose Oxidase Stability Assays	105
2.5.5	Synthesis of I-NHS 2.1	105
2.5.5.1	Synthesis of 3-(2-Bromo-2-methylpropionylamino)propionic acid	105
2.5.5.2	Synthesis of 2,5-Dioxo-1-pyrrolidinyl 3-(2-bromo-2-methylpropionylamino) propionate (I-NHS 2.1)	106
2.5.6	Typical Synthesis of a α-CT Macro-Initiator (CT-MI)	107
2.5.7	Synthesis of I-NHS 2.2	107
2.5.7.1	Synthesis of 3-(2-Bromo-propionylamino)propionic acid	107

2.5.7.2	Synthesis of 2,5-Dioxo-1-pyrrolidinyl 3-(2-bromo-propionylamino)propionate (I-NHS 2.2).....	108
2.5.8	Azidation of CT-MI-NHS 2.2.13 (CT-MI 2.3)	108
2.5.9	Typical Tryptic Digestion of Proteins	108
2.5.10	Synthesis of I-BA 2.1	109
2.5.10.1	Synthesis of 4-(2-Hydroxyethoxy)-benzaldehyde	109
2.5.10.2	Synthesis of 2-(4-Formyl-phenoxy)ethyl 2-bromo-2-methylpropanoate	109
2.5.11	Typical Synthesis of CT-MI-BA	110
2.6	References	111
3	Effects of Polymeric Grafting Density on the Stabilisation of α -Chymotrypsin.....	116
3.1	Abstract.....	117
3.2	Introduction	117
3.3	Results and Discussion	120
3.3.1	Synthesis and Characterisation of CT-PGMA PPCs	120
3.3.1.1	Size Exclusion Chromatography (SEC) Characterisation	122
3.3.1.2	Ultraviolet-Visible (UV-Vis) Characterisation.....	126
3.3.1.3	Poly(acrylamide) Gel Electrophoresis (PAGE) Characterisation	127
3.3.1.4	Summary of Characterisation of CT-PGMA PPCs.....	131
3.3.2	Activity of CT-PGMA PPCs.....	133
3.3.2.1	Batch-to-Batch α -CT Variation	133
3.3.2.2	Michaelis-Menten of CT-PGMA PPCs	138
3.3.3	Stability of CT-PGMA PPCs.....	141

3.3.3.1	Thermal Stability of α -CT and PGMA	141
3.3.3.2	Thermal Stability of CT-PGMA PPCs	145
3.3.3.3	Secondary Enzyme Stability of CT-MI and CT-PGMA PPCs.....	151
3.4	Conclusions	153
3.5	Experimental.....	155
3.5.1	Materials	155
3.5.2	Instrumentation	155
3.5.2.1	^1H Nuclear Magnetic Resonance (NMR) and ^{13}C NMR Spectroscopy	155
3.5.2.2	Size Exclusion Chromatography (SEC).....	155
3.5.2.3	Ultraviolet-Visible (UV-Vis) Spectroscopy.....	155
3.5.2.4	Sodium Dodecyl Sulfate Poly(acrylamide) Gel Electrophoresis (SDS-PAGE)	156
3.5.2.5	Matrix-Assisted Laser Desorption/Ionization Time-of-Flight (MALDI-ToF) Mass Spectrometry	156
3.5.2.6	Dynamic Light Scattering (DLS)	156
3.5.2.7	Circular Dichroism (CD).....	157
3.5.2.8	Conductivity	157
3.5.2.9	Thermal Shift Assay	157
3.5.2.10	Small Angle X-Ray Scattering (SAXS)	157
3.5.3	Enzyme Kinetic Studies	158
3.5.3.1	pNA Protease Assay	158
3.5.3.2	α -CT Stability Assays	158
3.5.3.3	Michaelis-Menten Kinetics and Parameters.....	159

3.5.3.4	Glucose Oxidase Stability Assays	159
3.5.4	Synthesis of Glycerol Methacrylate (GMA).....	159
3.5.5	Typical Polymerisation of GMA to Synthesise α -CT-PPCs.....	160
3.5.6	Typical Polymerisation of GMA to Synthesise PGMA	160
3.5.7	Typical Hydrolysis of CT-PGMA/PGMA	161
3.6	References	162
4	The Effect of Grafted Polymer Functionality upon the Stability of α -Chymotrypsin.....	166
4.1	Abstract.....	167
4.2	Introduction	167
4.3	Results and Discussion	173
4.3.1	Comparison of Hydrophilic Polymers.....	173
4.3.1.1	Synthesis and Characterisation of CT-PHPMA PPCs.....	173
4.3.1.2	Activity of CT-PHPMA PPCs.....	176
4.3.1.3	Stability of CT-PHPMA PPCs.....	177
4.3.2	Comparison of Linear and Comb-Like Polymers	187
4.3.2.1	Synthesis and Characterisation of CT-POEGMA PPCs	188
4.3.2.2	Activity of CT-POEGMA PPCs	189
4.3.2.3	Stability of CT-POEGMA PPCs	190
4.3.3	Comparison of Molecular Weight of Comb-Like Hydrophilic Polymers	192
4.3.4	Comparison of Comb-Length of Hydrophilic Monomers.....	198
4.4	Conclusions	204
4.5	Experimental.....	207

4.5.1	Materials	207
4.5.2	Instrumentation	207
4.5.2.1	¹ H Nuclear Magnetic Resonance (NMR) and ¹³ C NMR Spectroscopy	207
4.5.2.2	Ultraviolet-Visible (UV-Vis) Spectroscopy	207
4.5.2.3	Sodium Dodecyl Sulfate Poly(acrylamide) Gel Electrophoresis (SDS-PAGE)	208
4.5.2.4	Dynamic Light scattering (DLS)	208
4.5.2.5	Thermal Shift Assay	208
4.5.3	Enzyme Kinetic Studies	208
4.5.3.1	pNA Protease Assay	208
4.5.3.2	CT Stability Assays	209
4.5.3.3	Michaelis-Menten Kinetics and Parameters	209
4.5.3.4	Glucose Oxidase Stability Assays	209
4.5.4	Synthesis of <i>N</i> -(2-Hydroxypropyl)methacrylamide (HPMA)	210
4.5.5	Typical Polymerisation of HPMA/OEGMA to Synthesise α -CT-PPCs.....	210
4.5.6	Synthesis of Triethylene Glycol Methyl Ether Methacrylate (TEGMA).....	211
4.6	References	212
5	Synthesis of Protein-Polymer Conjugates from Laundry-Specific Enzymes	215
5.1	Abstract	216
5.2	Introduction	216
5.2.1	Laundry Formulations	216
5.2.2	Laundry-Specific Protease Enzymes.....	218
5.2.3	Laundry-Specific Lipase Enzymes.....	219

5.3	Results and Discussion	223
5.3.1	Effectiveness of α -Chymotrypsin and α -Chymotrypsin PPCs in Laundry Applications.....	223
5.3.2	Laundry-Specific Protease Enzymes.....	227
5.3.2.1	Structure and Properties of Laundry-Specific Protease Enzymes.....	227
5.3.2.2	Synthesis of Macro-Initiators from Laundry Specific Protease Enzymes.....	229
5.3.2.3	Activity of Macro-Initiators from Laundry Specific Protease Enzymes.....	235
5.3.2.4	Stability of Macro-Initiators from Laundry Specific Protease Enzymes.....	240
5.3.2.5	Synthesis and characterisation of Protein-Polymer Conjugates from Laundry-Specific Protease Enzymes.....	242
5.3.3	Laundry-Specific Lipase Enzymes.....	246
5.3.3.1	Structure of Laundry Specific Lipase Enzymes.....	246
5.3.3.2	Synthesis of Macro-Initiators from Laundry Specific Lipase Enzymes.....	249
5.3.3.3	Synthesis and Characterisation of Protein-Polymer Conjugates from Laundry-Specific Lipase Enzymes.....	261
5.3.4	Towards One-Pot Storage of Protease and Lipase Enzymes.....	267
5.4	Conclusions	268
5.5	Experimental	270
5.5.1	Materials	270
5.5.2	Instrumentation	270
5.5.2.1	^1H Nuclear Magnetic Resonance (NMR) and ^{13}C NMR Spectroscopy.....	270
5.5.2.2	Industrial Stain testing	270

5.5.2.3	Matrix-Assisted Laser Desorption/Ionization Time-of-Flight (MALDI-ToF) Mass Spectrometry	271
5.5.2.4	Ultraviolet-Visible (UV-Vis) Spectroscopy.....	271
5.5.2.5	Sodium Dodecyl Sulfate Poly(acrylamide) Gel Electrophoresis (SDS-PAGE)	271
5.5.2.6	Thermal Shift Assay.....	272
5.5.3	Software.....	272
5.5.4	Enzyme Kinetic Studies	272
5.5.4.1	pNA Protease Assay	272
5.5.4.2	pNP Lipase Assay.....	272
5.5.4.3	Stability Assays.....	273
5.5.4.4	Michaelis-Menten Kinetics and Parameters.....	273
5.5.5	Synthesis of ATRP Initiators	273
5.5.5.1	Synthesis of Carboxylic Acid Initiator 3-(2-Bromo-2-methylpropionylamino) propionic acid (I-COOH 5.1).....	273
5.5.5.2	Synthesis of N-Hydroxysuccinimide Initiator 2,5-Dioxo-1-pyrrolidinyl 3-(2-bromo-2-methylpropionylamino) propionate (I-NHS 2.1).....	274
5.5.6	Typical Synthesis of Protein Macro-Initiators.....	275
5.5.6.1	Utilising I-NHS 2.1	275
5.5.6.2	Utilising I-COOH 5.1	275
5.5.7	Synthesis of Glycerol Methacrylate (GMA).....	275
5.5.8	Typical Polymerisation of GMA to Synthesise Protein-Polymer Conjugates (UL1-PGMA and Lx-PGMA).....	276
5.6	References	277

6	Conclusions and Future Work.....	280
6.1	Conclusions	281
6.2	Future Work.....	283

List of Figures, Schemes and Tables

Figures

Figure 1.1 Schematic representations of primary, secondary, tertiary, and quaternary structures of proteins.....	2
Figure 1.2 Chemical structure of an L-amino acid.	3
Figure 1.3 Schematic representation of the hydrogen bonding present within an α -helix with the location of R-groups represented by dots. Taken from Bugg. ³	4
Figure 1.4 Schematic representation of the hydrogen bonding present within parallel and anti-parallel β -Sheets.....	5
Figure 1.5 Schematic representation of the crystal structure of human thioredoxin (IERU) highlighting the twist in the β -sheet shown in red. ²⁰ Blue represents α -helix, pink represents random coil and red represents β -sheets. PDB crystal structure references are identified in bold.	6
Figure 1.6 General structure of β -turns.....	6
Figure 1.7 Schematic representations of interactions that contribute to the tertiary structure of proteins. Reproduced from Janecek <i>et al.</i> ²⁴	7
Figure 1.8 Energy landscapes of protein folding. a) Simplified small protein folding showing a single energy minimum. Taken from Dobson. ³⁵ b) Simplified energy funnel indicating presence of a local energy minima. Taken from Dill and Chan. ³⁶	9
Figure 1.9 Lineweaver-Burk Plot.....	11
Figure 1.10 Schematic representations of the three different types of reversible enzyme inhibition.....	13
Figure 1.11 Graphical representations of the Lineweaver-Burk plots of the three different types of reversible enzyme inhibition a) competitive c) uncompetitive c) noncompetitive. ^{49, 50}	14
Figure 1.12 Schematic representation of the denaturing process of proteins.....	15

Figure 1.13 Hofmeister lyotropic series. ⁸⁹	19
Figure 1.14 Chemical structure of poly(di(carboxylatophenoxy))phosphazene (PCPP).....	20
Figure 1.15 Schematic representation of enzyme encapsulation and the effects of selectively permeable membranes.....	22
Figure 1.16 Residual activity of HRP with bis(<i>N</i> -hydrosuccinimide ester) cross-linkers. Adapted from Ryan <i>et al.</i> ¹¹⁰	24
Figure 1.17 Schematic representation of reductive alkylation of L-lysine residues.....	26
Figure 1.18 Schematic representation of the adsorption of lipase onto glutaraldehyde-modified silica nanoparticles. Reproduced from Jesionowski <i>et al.</i> ¹²⁰	27
Figure 1.19 Schematic representation of the effect of single point and multipoint immobilisation on enzyme rigidity. Taken from Fernandez-Lafuente <i>et al.</i> ¹¹⁶	28
Figure 1.20 Timeline highlighting for advances in protein-polymer conjugates. Reproduced from Pelegri-O'Day <i>et al.</i> ¹⁴⁰	30
Figure 1.21 Mechanism for ATRP. ^{159, 161}	31
Figure 1.22 ATRP equilibrium constants, K_{ATRP} , for various nitrogen-based ligands with the initiator ethyl α -bromoisobutyrate in the presence of Cu(I)Br in MeCN at 22 °C. Colour key:(red) N2; (black) N3 and N6; (blue) N4. Symbol key: (solid) amine/imine; (open) pyridine; (left-half-solid) mixed; (■) linear; (▲) branched; (●) cyclic. Taken from Tang <i>et al.</i> ¹⁶⁴	32
Figure 1.23 Examples of ATRP initiator structures employed to form linear, branched, or polymeric star morphologies.	33
Figure 1.24 Proposed general mechanism of RAFT/MADIX polymerisation. I = initiator, M = monomer, P = polymer, R and Z = RAFT group functionalities. Reproduced from Moad <i>et al.</i> ¹⁷⁶	35
Figure 1.25 The generic structure of a RAFT CTA. Taken from Willcock and O'Reilly. ¹⁷⁹	36
Figure 1.26 Guidelines for appropriate RAFT CTA selection for controlled polymerisations. S = styrenes, MA = methacrylates, AA = acrylic acid, AM = acrylamide, AN = acrylonitriles,	

MMA = methyl methacrylate, and VAc = vinyl acetate. Dotted lines indicate that there is only partial control over the polymerisation. Taken from Moad <i>et al.</i> ¹⁸²	37
Figure 1.27 Schematic representation of the three main strategies for formation of PPCs: a) “grafting to” b) “grafting from” and c) “grafting through”	38
Figure 1.28 MALDI-TOF mass spectrum of α -CT-PEG PPCs synthesised <i>via</i> a “grafting to” method. Reproduced from Lele <i>et al.</i> ¹⁹⁷	39
Figure 1.29 Synthesis of a protein macro-initiator for the production of PPCs <i>via</i> a “grafting from” approach. Taken from Bontempo <i>et al.</i> ²⁰¹	40
Figure 1.30 Cleavable ATRP initiator employed by Averick <i>et al.</i> ²⁰⁰	41
Figure 1.31 Synthesis of single enzyme nanogels <i>via</i> the “grafting through” approach. Taken from Yan <i>et al.</i> ¹⁹⁸	43
Figure 2.1 Schematic representation of examples of non-natural amino acids utilised by Deiters <i>et al.</i> that can be reacted using biorthogonal chemistries to natural residues. ¹⁰	58
Figure 2.2 Schematic representation of examples of protein macro-initiators utilised in RDRP to form PPCs in literature reports. ²⁴⁻²⁶	60
Figure 2.3 Schematic representation of the formation of active α -CT from the inactive zymogen, chymotrypsinogen.	61
Figure 2.4 Schematic representation of a) the catalytic triad (Ser195, His57 and Asp102) present in α -CT’s active site and b) charge relay system occurring within α -CT’s catalytic triad.....	63
Figure 2.5 a) Primary structure and b) crystal structure (4CHA) ⁴⁹ of α -CT. L-Lysine residues have been highlighted in pink and the three <i>N</i> -termini highlighted in yellow. PDB crystal structure references are identified in bold.	64
Figure 2.6 ¹ H NMR spectra of a) native α -CT and b) α -CT macro-initiator species (CT-MI 2.1) synthesised using 3.3 eq. of initiator per amine at pH 8.0, in D ₂ O at 400 MHz. The yellow region highlights the disappearance of an impurity at 3.0 ppm and the blue region highlights the appearance of I-NHS 2.1 peaks at 1.5 ppm.	66

Figure 2.7. MALDI-ToF mass spectra for α -CT and CT-MI 2.1 recorded using a positive linear mode.....	67
Figure 2.8. a) MALDI-ToF mass spectra and b) Average number of functionalised sites as determined by MALDI-ToF of α -CT at various time intervals after the addition of I-NHS 2.1 . Error bars are displayed as the standard deviation of the distribution based on the assumption of a Gaussian fit of the MALDI-ToF mass spectra.	68
Figure 2.9 a) MALDI-ToF mass spectra of CT-MI 2.1 species synthesised using 3.3 equivalents of I-NHS 2.1 per amine at varying pH values b) Average number of functionalised sites as determined by MALDI-ToF of α -CT at various pH values after the addition of I-NHS 2.1 . Error bars are displayed as the standard deviation of the distribution based on the assumption of a Gaussian fit of the MALDI-ToF mass spectra.	69
Figure 2.10 MALDI-TOF mass spectra of CT-MI 2.1 species formed at varying concentrations of I-NHS 2.1 when the conjugation reaction was carried out at a) pH 4.0, b) pH 6.0, and c) pH 8.0.	71
Figure 2.11 MALDI-TOF mass spectra of CT-MI 2.1 species formed at in a continuous manner using a) 1 equivalent and b) 3.3 equivalents of initiator of I-NHS 2.1 per amine.	74
Figure 2.12 Crystal structure of α -CT(4CHA) ⁴⁹ highlighting the positions of L-lysine residues with respect to hydrophobic and hydrophilic residues. L-Lysine residues have been highlighted in pink, <i>N</i> -termini in yellow, hydrophobic residues (Ala, Gly, Val, Leu, Ile, Met, and Phe) are shown in red and hydrophilic residues (Arg, His, Glu, Asp, Asn, Gln, Thr, Ser and Cys) in blue.....	76
Figure 2.13 Crystal structure of α -CT (4CHA) ⁴⁹ highlighting position of L-lysine residues with respect to acidic and basic residues. L-Lysine residues have been highlighted in pink, <i>N</i> -termini in yellow, acidic residues (Asp and Glu) are shown in green and basic residues (Arg and His) in cyan.....	76
Figure 2.14 Predicted pK _a values of amine groups in L-lysine residues within α -CT compared with the average pK _a of L-lysine at 10.5. All values have been calculated by the DEPTH server. ⁶¹	78

Figure 2.15 Chemical Structure of FAM-NHS used in the experiments conducted aiming to locate modification sites within α -CT.	78
Figure 2.16 MALDI-ToF mass spectra of CT-FAM species synthesised at pH 8.0 at varying concentrations of FAM-NHS . Errors are reported as the standard deviation of the distribution based on the assumption of a Gaussian fit of the MALDI-ToF mass spectra.	79
Figure 2.17 Chemical structure of CTA-NHS 2.1 used in the attempt to locate the conjugation sites within α -CT.....	80
Figure 2.18 MALDI-ToF mass spectra of CT-CTA species synthesised at pH 8.0 at varying concentrations of CTA-NHS 2.1 . Errors are reported as the standard deviation of the distribution based on the assumption of a Gaussian fit of the MALDI-ToF mass spectra.	80
Figure 2.19 MALDI-ToF mass spectra of α - CT-MI 2.2 species synthesised at varying pH values using 3.3 equivalents of I-NHS 2.2 per amine.....	82
Figure 2.20 FTIR spectra of CT-MI before (2.2.13) and after azidation (2.3). Inset shows an enlargement of the region from 2300 to 2000 cm^{-1}	83
Figure 2.21 MALDI-ToF mass spectra of CT-MI 2.2 species before and after azidation.....	84
Figure 2.22 LC-MS chromatograms obtained from the tryptic digestion of α -CT and the CT-MI species CT-MI 2.1.1 and CT-MI 2.1.10 , recorded at $\lambda = 280 \text{ nm}$	85
Figure 2.23 Initial velocity of α -CT-catalysed hydrolysis upon exposure to varying conditions. A - purified by dialysis, B - exposed to reaction conditions, C - exposed to NHS and dialysis, D - purified by ultrafiltration. Each data point is based on the average of four repeats of pNA assay with standard deviation displayed as error.	87
Figure 2.24 Thermal stability profiles of α -CT and CT-MI 2.1 species at pH 8.0, 40 °C. Each data point is based on the average of four repeats of pNA assay with standard deviation displayed as error. Initial catalytic velocity at $t = x$ is divided by their relative initial catalytic velocity at $t = 0$ to calculate residual activity.	89

Figure 2.25 Activity half-life at 40 °C for α -CT and CT-MI 2.1 species extracted from the linear regression of $\ln(\text{residual activity})$ against time.....	90
Figure 2.26 Zeta potential values of α -CT and CT-MI 2.1 species in water.	90
Figure 2.27 Schematic representation of dye-protein binding during thermal shift assays.	91
Figure 2.28 T_m of native α -CT by a) DSC, 50 mg/mL in water, 1 °C/min ramp rate and b) thermal shift assay, 5 mg/mL in water with SYPRO orange, excitation $\lambda = 492$ nm, emission $\lambda = 610$ nm.	92
Figure 2.29 a) Thermal shift assay profile of native α -CT and initiator-functionalized α -CT, 5 mg/mL in water with SYPRO orange, excitation $\lambda = 492$ nm, emission $\lambda = 610$ nm and b) graph displaying T_m of α -CT and CT-MI 2.1 species. Values are obtained from triplicate repeats and error is displayed as standard deviation.....	93
Figure 2.30 a) MALDI-ToF mass spectra of CT-MI 2.1.10 stored in solution at RT at various time points b) Average molar masses as determined by MALDI-ToF spectroscopy of CT-MI 2.1.10 at various time intervals in various storage conditions. Errors bars are displayed as the standard deviation of the distribution based on the assumption of a Gaussian fit of the MALDI-ToF mass spectra.	94
Figure 2.31 Schematic representation of the <i>o</i> -dianisidine assay for glucose oxidase.	95
Figure 2.32 Stability profiles of GO_x incubated with α -CT and CT-MI species at various time intervals at pH 5.0, 30 °C. Each data point is based on the average of four repeats of <i>o</i> -dianisidine assay with standard deviation displayed as error.	95
Figure 2.33. ^1H NMR spectra of a) I-BA 2.1 and b) Imine formation reaction between benzylamine and I-BA 2.1 in dichloromethane. ^1H NMR solvent: CDCl_3 , 400 MHz. Green highlights aldehyde peak disappearance and red highlights the appearance of imine peak.....	97
Figure 2.34. ^1H NMR spectra of a) I-BA 2.1 and b) secondary amine formation reaction between Boc-Lys and I-BA 2.1 with single addition of sodium cyanoborohydride (10 eq.) MeOD, 400 MHz. Blue highlights formation of product species at 7.65 and 6.75 ppm.....	98

Figure 2.35. Initial hydrolysis rate of α -CT after with incubation at 3 °C, (CT) in water, (CT-NaCNBH ₃) with sodium cyanoborohydride (10 eq.), (CT-NHS) with NHS (6.6 eq.). Each data point is based on the average of four repeats of pNA assay with standard deviation displayed as error.	99
Figure 2.36. MALDI-ToF mass spectra of CT-MI-BA species synthesised at pH 8.0, 10 eq. of I-BA 2.1 and varying concentrations of NaCNBH ₃ . Errors are reported as the standard deviation of the distribution based on the assumption of a Gaussian fit of the MALDI-ToF mass spectra.	100
Figure 3.1 Thermal stability of native and modified Glucose oxidase (GO _x) with PPEGA incubated at 70 °C. Reproduced from Luo <i>et al.</i> ¹²	118
Figure 3.2 Schematic representation of targeted CT-PGMA structures.....	121
Figure 3.3 Molecular weight distributions of CT-PGMA 3.10.5 with and without the presence of 2 equivalents of I-NHS 2.1 obtained by SEC in DMF.....	123
Figure 3.4 Molecular weight distributions of PGMA 3.1 before and after (PGMA 3.1H) obtained by SEC in DMF.	125
Figure 3.5 SDS-PAGE gel of Native α -CT visualised by Coomassie Brilliant Blue. Lane 1: Protein ladder, lane 2: Native α -CT.	128
Figure 3.6 SDS-PAGE gel of CT-PGMAs visualised by Coomassie Brilliant Blue. Lane 1: Protein ladder, lane 2: PGMA 3.1 , lane 3: Native α -CT, lane 4: CT-PGMA 3.1.5 , lane 5: CT-PGMA 3.1.25 , lane 6: CT-PGMA 3.1.50 , lane 7: CT-PGMA 3.5.5 , lane 8: CT-PGMA 3.10.5 . Samples were run on various PAGE gels.....	129
Figure 3.7 Activity half-lives of native α -CT batches at 40 °C based on pNA assay extracted from the linear regression of ln(residual activity) against time.	134
Figure 3.8 MALDI-ToF mass spectra for α -CT batch one and two recorded using a positive linear mode.....	135

Figure 3.9 Size distributions averaged by intensity for α -CT batch one and two in water at 25 °C.	136
Figure 3.10 Far-UV CD spectra of native α -CT batch 1 and 2 run at 20 °C.....	137
Figure 3.11 Relationship between K_m and the molecular weight of PPC as determined by UV-Vis spectroscopy.....	140
Figure 3.12 Crystal structure of α -CT (4CHA) ³⁷ highlighting the location of the active site and the relative position of the <i>N</i> -terminus. Residues within the active site have been highlighted in red, <i>N</i> -terminus in yellow.....	141
Figure 3.13 Molecular weight distributions of PGMA 3.1-3.5 obtained by SEC in DMF.	142
Figure 3.14 Thermal stability profiles of α -CT incubated with PGMA 3.2-3.5 at pH 8.0, 40 °C. a) α -CT and PGMA 3.2-3.5 at 85 equivalents per α -CT b) α -CT and PGMA 3.3 at varying concentrations. Each data point is based on the average of four repeats of <i>p</i> NA assay with standard deviation displayed as error.	144
Figure 3.15 Factor of half-life increase for CT-MI 2.1.X and CT-PGMA PPC species at 40 °C and pH 8.0 extracted from the linear regression of ln(residual activity) against time and normalised to the corresponding batch of α -CT.....	146
Figure 3.16 Schematic representation of the ability of polymers to prevent solvent-protein interactions based on the effect of increasing grafting density.	147
Figure 3.17 a) Thermal shift assay profile of native α -CT, CT-MI 2.1.10 , and CT-PGMA 3.10.5 , 5 mg/mL in water with SYPRO orange, excitation $\lambda = 492$ nm, emission $\lambda = 610$ nm and b) graph displaying half-lives of α -CT CT-MI 2.1.10 , and CT-PGMA 3.10.5 species. Values are obtained from triplicate repeats and error is displayed as standard deviation.....	148
Figure 3.18 Scattering profiles of a) α -CT and b) CT-PGMA 3.10.5 of $I(q)$ plotted against q at varying temperatures.....	149
Figure 3.19 of a) Kratky plots of α -CT of $q^2I(q)$ plotted against q and b) dimensionless Kratky plots of CT-PGMA 3.10.5 of $(R_gq)^2I(q)/I(0)$ plotted against R_gq at varying temperatures.	150

Figure 3.20 Stability profiles of GO _x incubated with α -CT, CT-MI 2.1.10 , and CT-PGMA 3.10.5 at various time intervals at pH 5.0, 30 °C. Each data point is based on the average of four repeats of <i>o</i> -dianisidine assay with standard deviation displayed as error.....	152
Figure 4.1 Chemical structures of trehalose and a trehalose-modified styrenic monomer utilised by Mancini <i>et al.</i> ⁹	168
Figure 4.2 Schematic representation of the effect of charged grafted polymers on the substrate affinity and selectivity observed by Murata <i>et al.</i> ¹⁰	169
Figure 4.3 Schematic representation of the phase diagrams associated with the LCST and UCST transitions observed within thermoresponsive polymer solutions. Reproduced from Phillips <i>et al.</i> ¹⁵	170
Figure 4.4 Schematic representation of responsive polymer species preventing access to the active site by undergoing a transition from Stayton <i>et al.</i> ²⁸	171
Figure 4.5 Schematic representation of the effect of combining UCST and LCST monomers to generate diblock polymers grafted to a protein from Cummings <i>et al.</i> ³⁵	171
Figure 4.6 Chemical structures of GMA and HPMA.....	173
Figure 4.7 a) Weight percentage protein and molecular weights of CT-PHPMA PPCs extracted from absorbance at $\lambda = 280$ nm b) SDS-PAGE gel of CT-PHPMA PPCs visualised by Coomassie Brilliant Blue. Lane 1: Ladder, lane 2: PHPMA , lane 3: Native α -CT, lane 4: CT-PHPMA 4.1.5 , lane 5: CT-PHPMA 4.1.25 , lane 6: CT-HPMA 4.10.5	175
Figure 4.8 Factor of activity half-life increase compared to α -CT for CT-PGMA PPCs and CT-PHPMA PPCs at 40 °C and pH 8.0 extracted from the linear regression of ln(residual activity) against time.....	178
Figure 4.9 Initial velocity of α -CT, CT-PGMA 3.10.5 , and CT-PHPMA 4.10.5 species at t = 0, before and after storage at -20 °C, at pH 8.0. Each data point is based on the average of four repeats of <i>p</i> NA assay with standard deviation displayed as error.....	180

Figure 4.10 Stability profiles of α -CT, CT-PGMA 3.10.5 and CT-PHPMA 4.10.5 species at pH 8.0 incubated at a) 4 °C and b) 20 °C. Each data point is based on the average of four repeats of pNA assay with standard deviation displayed as error.	182
Figure 4.11 Factor of activity half-life increase for CT-PGMA 3.10.5 and CT-PHPMA 4.10.5 species at 4 °C and 20 °C, pH 8.0 extracted from the linear regression of ln(residual activity) against time.....	183
Figure 4.12 a) Thermal shift assay profile of native α -CT, CT-PGMA 3.10.5 , and CT-PHPMA 4.10.5 , at 5 mg/mL in water with SYPRO orange, excitation $\lambda = 492$ nm, emission $\lambda = 610$ nm and b) graph displaying the half-lives of α -CT, CT-PGMA 3.10.5 , and CT-PHPMA 4.10.5 species. Values are obtained from triplicate repeats and error is displayed as standard deviation.	185
Figure 4.13 Stability profiles of GOx incubated with α -CT, CT-PGMA 3.10.5 , and CT-PHPMA 4.10.5 at various time intervals at pH 5.0, 30 °C. Each data point is based on the average of four repeats of <i>o</i> -dianisidine assay with standard deviation displayed as error....	186
Figure 4.14 Chemical structure comparison of GMA to OEGMA.....	187
Figure 4.15 Factor of activity half-life increase for CT-PGMA and CT-POEGMA PPC species compared with native α -CT at 40 °C and pH 8.0 extracted from the linear regression of ln(residual activity) against time.....	190
Figure 4.16 Schematic representation of possible morphologies of CT-PGMA 3.10.5 and CT-POEGMA 4.10.5	191
Figure 4.17 Factor of activity half-life increase for CT-POEGMA 4.10.2-4.10.20 species compared to native α -CT at 40 °C and pH 8.0 extracted from the linear regression of ln(residual activity) against time.....	194
Figure 4.18 Initial velocity of α -CT, CT-POEGMA 4.10.5 , and CT-POEGMA 4.10.20 species at t=0 before and after storage at -20 °C, pH 8.0. Each data point is based on the average of four repeats of pNA assay with standard deviation displayed as error.	195

Figure 4.19 Residual activity stability profiles of a) CT-POEGMA 4.10.5 and b) CT-POEGMA 4.10.20 . All samples were incubated at pH 8.0 at both 4 and 20 °C. Each data point is based on the average of four repeats of <i>p</i> NA assay with standard deviation displayed as error.	196
Figure 4.20 Number average size distributions of CT-POEGMA 4.10.20 at 5 and 25 °C.	197
Figure 4.21 Chemical structures of TEGMA, OEGMA ₄₅₀ , and OEGMA ₉₀₀	199
Figure 4.22 Dependence of hydrodynamic diameter of CT-PTEGMA 4.10.5 , CT-POEGMA₄₅₀ 4.10.5 , and CT-POEGMA₉₀₀ 4.10.5 on temperature measured in pH 8.0 buffer. a) full range of observed D_h and b) displays an enlargement of the region from 0 to 50 nm.	201
Figure 4.23 Catalytic half-lives for CT-PTEGMA 4.10.5 , CT-POEGMA₄₅₀ 4.10.5 , and CT-POEGMA₉₀₀ 4.10.5 at pH 8.0 at a) 30 °C and b) 40 °C extracted from the linear regression of $\ln(\text{residual activity})$ against time. Accurate half-life values cannot be extracted for α -CT at 30 °C due to methodology described in Section 4.3.1.3.1.	203
Figure 4.24 Schematic representation of the proposed effective structures of CT-PTEGMA 4.10.5 , CT-POEGMA₄₅₀ 4.10.5 , and CT-POEGMA₉₀₀ 4.10.5	204
Figure 5.1 Schematic representation of the interaction of surfactants with hydrophobic stains	217
Figure 5.2 Schematic representation of the hydrolysis of triglycerides to form glycerol and fatty acid chains.	220
Figure 5.3 Crystal structure of TLL in the a) closed (1DU4), and b) open (1EIN) positions with the active site shown in blue. ²¹ The structure is represented as i) the secondary structure ii) the surface structure. PDB crystal structure references are identified in bold. With thanks to Dr. Katherine Farrance.	221
Figure 5.4 The effect of Ecoboost™ formulation upon activity of α -CT. Each data point is based on the average of four repeats of <i>p</i> NA assay with standard deviation displayed as error.	223
Figure 5.5 Experimental procedure for industrial stain testing.	225

Figure 5.6 a) Layout of samples in stain plates and resulting stain test plates after exposure to α -CT, CT-PGMA 3.10.5 , CT-PHPMA 4.10.5 , CT-POEGMA 4.10.5 and CT-POEGMA 4.10.20 with b) blood and c) blood, milk and ink.	226
Figure 5.7 Crystal structure of savinase (1SVN). ¹⁴ L-Lysine residues have been highlighted in pink and the <i>N</i> -terminus highlighted in yellow.	228
Figure 5.8 Predicted pK_a values of amine groups in L-lysine residues within savinase compared with the average pK_a of L-lysine at 10.5. All values have been calculated by the DEPTH server. ²⁸	228
Figure 5.9 MALDI-ToF mass spectra of UL1-MI 2.1 species formed at varying concentrations of I-NHS 2.1 when the conjugation reaction was carried out at a) pH 8.0, b) pH 10.0, and c) pH 12.0.	230
Figure 5.10 Average number of initiator functionalised sites of UL1 as determined by MALDI-ToF with I-COOH 5.1 and various conjugation reagents. Error bars are displayed as the standard deviation of the distribution of sites functionalised based on the assumption of a Gaussian fit of the MALDI-ToF mass spectra.	233
Figure 5.11 MALDI-ToF mass spectra of UL1-MI 5.1 species formed at pH 8.0 using 10 equivalents of I-COOH 5.1 and varying concentrations of EDC.HCl.....	234
Figure 5.12 Residual activity of UL1-MI 5.1 species after purification by dialysis for 48 hours against deionised water. Each data point is based on the average of four repeats of the <i>p</i> NA assay with standard deviation displayed as error bars.....	235
Figure 5.13 Initial velocity of native UL1 upon exposure to varying concentrations of NHS, EDC.HCl, and EDC urea. Equivalents of the additive were calculated as equivalents per amine. Each data point is based on the average of four repeats of the <i>p</i> NA assay with standard deviation displayed as error bars.....	237
Figure 5.14 Residual activity of UL1-MI 5.1.5 upon exposure to varying purification conditions relative to native UL1. A - purified by 96 hours of dialysis against deionised water, B – purified	

by precipitation into methanol, C – purified by spin filtering with a MWCO of 10 kDa, D – purified with a desalting column, E – purified by ultrafiltration with a MWCO of 5 kDa. Each data point is based on the average of four repeats of the <i>pNA</i> assay with standard deviation displayed as error bars.	238
Figure 5.15 a) Thermal stability profiles of UL1 and UL1-MI 5.1 species in Ecoboost™ formulation at 40 °C. Each data point is based on the average of four repeats of <i>pNA</i> assay with standard deviation displayed as error bars. b) Activity half-life at 40 °C for UL1 and UL1-MI 5.1 species extracted from the linear regression of ln(residual activity) against time.	240
Figure 5.16 Graph displaying T_m of UL1 and UL1-MI 5.1 species. T_m values were extracted from thermal shift assays at 5 mg/mL in water with SYPRO orange, excitation $\lambda = 492$ nm, emission $\lambda = 610$ nm. Values are obtained from triplicate repeats and error is displayed as standard deviation.	241
Figure 5.17 a) Thermal stability profiles of UL1 and UL1-PGMA PPC species in Ecoboost™ formulation at 40 °C. Each data point is based on the average of four repeats of <i>pNA</i> assay with standard deviation displayed as error bars. b) Activity half-life at 40 °C for UL1 and UL1-PGMA PPC species extracted from the linear regression of ln(residual activity) against time.	245
Figure 5.18 Graph displaying T_m of UL1 and UL1-PGMA PPC species. T_m values were extracted from thermal shift assays at 5 mg/mL in water with SYPRO orange, excitation $\lambda = 492$ nm, emission $\lambda = 610$ nm. Values are obtained from triplicate repeats and error is displayed as standard deviation.	246
Figure 5.19 Kyte-Doolittle plot of (A) TLL, (B) Lipolase, and (C) Lipex. The highlighted boxes emphasise locations in which a change in the hydrophobicity is observed, with thanks to Dr Katherine Farrance and Dr Dietmar Lang.	248
Figure 5.20 Crystal structure of a) PFL (1VA4), ⁴² and b) TLL (1DU4). ²¹ L-Lysine residues have been highlighted in pink and the <i>N</i> -termini highlighted in yellow. PDB crystal structure references are identified in bold.	250

Figure 5.21 MALDI-ToF mass spectra of a) native PFL and b) PFL species formed using 3.3 equivalents of I-NHS 2.1 per amine when the conjugation reaction was carried out at a range of pH values.	251
Figure 5.22 MALDI-ToF mass spectra of a) native TLL and b) TLL species formed using 3.3 equivalents of I-NHS 2.1 per amine when the conjugation reaction was carried out at a range of pH values.	253
Figure 5.23 MALDI-ToF mass spectra of Lipex species formed a) native Lipex b) using 10 equivalents of I-NHS 2.1 per amine at varying pH and c) at pH 8.0 using varying concentrations of I-NHS 2.1	254
Figure 5.24 MALDI-ToF mass spectra of Lx-MI 5.1 species formed at pH 8.0 using a) 20 equivalents of EDC.HCl and varying concentrations of I-COOH 5.1 and b) 10 equivalents of I-COOH 5.1 and varying concentrations of EDC.HCl.	256
Figure 5.25 Initial velocity of native Lipex upon exposure to varying concentrations of NHS, EDC.HCl, and EDC urea. Equivalents of the additive (NHS, EDC.HCl or EDC Urea) were calculated as equivalents per amine. Each data point is based on the average of four repeats of <i>p</i> NP assay with standard deviation displayed as error bars.	258
Figure 5.26 Activity half-life at 40 °C in Ecoboost™ formulation for Lipex and Lx-MI 5.1 species extracted from the linear regression of ln(residual activity) against time from aliquots analysed with the <i>p</i> NP assay. Each data point is based on the average of four repeats of <i>p</i> NP assay with standard deviation displayed as error bars.	260
Figure 5.27 Graph displaying T_m of Lipex and Lx-MI 5.1 species. T_m values were extracted from thermal shift assays at 5 mg/mL in water with SYPRO orange, excitation $\lambda = 492$ nm, emission $\lambda = 610$ nm. Values are obtained from triplicate repeats and error is displayed as standard deviation.	261

Figure 5.28 Initial velocity of a) Lx-PGMA 5.1.50 and b) Lx-PGMA 5.5.10 upon exposure to varying concentrations of DMSO. Each data point is based on the average of four repeats of <i>p</i> NP assay with standard deviation displayed as error bars.....	264
Figure 5.29 Thermal stability profiles of Lipex and Lx-PGMA 5.1.10 species in Ecoboost™ formulation at 40 °C. Each data point is based on the average of four repeats of <i>p</i> NP assay with standard deviation displayed as error bars.	265
Figure 5.30 Graph displaying T_m of Lipex and Lx-PGMA PPC species. T_m values were extracted from thermal shift assays at 5 mg/mL in water with SYPRO orange, excitation $\lambda = 492$ nm, emission $\lambda = 610$ nm. Values are obtained from triplicate repeats and error is displayed as standard deviation.	266
Figure 5.31 Stability profiles of Lipex incubated with UL1 and UL1-PGMA PPC species at various time intervals in Ecoboost™ formulation at 40 °C. Each data point is based on the average of four repeats of <i>p</i> NP assay with standard deviation displayed as error bars.....	267

Schemes

Scheme 2.1 Schematic representation of primary amines on the α -CT reacting with an NHS active ester, I-NHS 2.1 , to form CT-MI 2.1	65
Scheme 2.2 Schematic representation of the attachment of I-NHS 2.2 to α -CT and intended subsequent modification to azide and “click” of fluorescent ABM tag. TCEP = (tris(2-carboxyethyl)phosphine), TBTA = tris[(1-benzyl-1H-1,2,3-triazol-4-yl)methyl]amine.	81
Scheme 2.3 Schematic representation of the post-conjugation modification reaction of the secondary bromide to azide.	83
Scheme 2.4 Schematic representation of the <i>p</i> NA assay for proteases.....	86
Scheme 2.5 Schematic for the formation of secondary amine, from I-BA 2.1 , sodium cyanoborohydride and L-lysine residues.	98
Scheme 3.1 Schematic representation of ATRP of GMA from the surface of CT-MI 2.1 to form CT-PGMA	122
Scheme 3.2 Schematic representation of acidic hydrolysis of a PPC.....	124
Scheme 5.1 Reaction of primary amines on UL1 with I-NHS 2.1 to form UL1-MI 2.1	229
Scheme 5.2 Reaction of primary amines on UL1 with I-COOH 5.1 to form UL1-MI 5.1	232
Scheme 5.3 Reaction of primary amines on UL1 with I-COOH 5.1 to form UL1-MI 5.1 with the production of EDC urea from EDC.	236
Scheme 5.4 Reaction of primary amines on Lipex with I-COOH 5.1 to form Lx-MI 5.1	255
Scheme 5.5 Hydrolysis of 4-nitrophenyl dodecanoate employed in the <i>p</i> NP assay for the detection of lipase activity.....	257

Tables

Table 2.1 Average degree of attachment of I-NHS 2.1 initiator for CT-MI 2.1 species synthesised at varying pH values of initiator as determined by MALDI-ToF analysis. Errors are reported as the standard deviation of the distribution based on the assumption of a Gaussian fit of the MALDI-ToF mass spectra.....	70
Table 2.2. Average degree of attachment of I-NHS 2.1 initiator for CT-MI 2.1 species synthesised at varying pH values and concentrations of initiator as determined by MALDI-ToF analysis. Errors are reported as the standard deviation of the distribution based on the assumption of a Gaussian fit of the MALDI-ToF mass spectra.....	73
Table 2.3 Average degree of attachment of the initiator species onto α -CT forming CT-MI 2.1 in a single continuous manner with varying concentrations of initiator and solution pH, as determined by MALDI-ToF MS analysis. Errors are reported as the standard deviation of the distribution based on the assumption of a Gaussian fit of the MALDI-ToF mass spectra.....	74
Table 2.4. Comparison of average degree of attachment of 3.3 equivalents of I-NHS 2.1/2.2 initiator at varying pH values as determined by MALDI-ToF analysis. Errors are reported as the standard deviation of the distribution based on the assumption of a Gaussian fit of the MALDI-ToF mass spectra.....	82
Table 2.5 Michaelis-Menten Parameters of α -CT, CT-MI 2.1.1 , and CT-MI 2.1.10 based on the <i>p</i> NA assay.....	88
Table 3.1. Targeted molecular weights and grafting densities of CT-PGMA PPCs.	120
Table 3.2 Molecular weights and dispersities for PGMA 3.1 before and after hydrolysis (determined by SEC in DMF against poly(methyl methacrylate) standards).....	125
Table 3.3 Percentage protein and molecular weights of CT-PGMA PPCs extracted from the intensity of absorbance at $\lambda = 280$ nm.....	127
Table 3.4. Extracted molecular weights and dispersities of native α -CT and CT-PGMAs from densitometric analysis of SDS-PAGE gel using ImageJ.....	129

Table 3.5. Summary CT-PGMA s with UV-Vis spectroscopy and SDS-PAGE characterisation...	132
Table 3.6 Michaelis-Menten Parameters of batches of α -CT based on the <i>p</i> NA assay.....	133
Table 3.7 Conductivity of batches of α -CT dissolved in water at 1 mg/mL and 20 °C.....	138
Table 3.8 Michaelis-Menten Parameters of CT-PGMA PPCs based on the <i>p</i> NA assay.....	139
Table 3.9 Molecular weights and dispersities for PGMA 3.2-3.5 (determined by SEC in DMF against poly(methyl methacrylate) standards).....	142
Table 4.1. Targeted molecular weights and grafting densities of CT-PHPMA PPCs.....	174
Table 4.2. Summary CT-PGMA PPC and CT-PHPMA PPC characterisation with UV-Vis spectroscopy and SDS-PAGE analysis.....	176
Table 4.3 Michaelis-Menten Parameters of α -CT and CT-PHPMA PPCs based on the <i>p</i> NA assay.	177
Table 4.4 Summary of catalytic half-lives for α -CT, CT-PGMA 3.10.5 , and CT-PHPMA 4.10.5 at 4 °C, 20 °C, and 40 °C. Half-lives at 40 °C have been normalised to a native α -CT half-life of 13.2 minutes.	183
Table 4.5. Summary of CT-PGMA PPCs and CT-POEGMA PPCs with characterisation data from UV-Vis spectroscopy and SDS-PAGE analysis.....	188
Table 4.6 Michaelis-Menten Parameters of α -CT and CT-POEGMA PPCs based on the <i>p</i> NA assay.	189
Table 4.7. Summary CT-POEGMA 4.10.2-4.10.20 characterisation with UV-Vis spectroscopy and SDS-PAGE analysis.....	192
Table 4.8 Michaelis-Menten Parameters of α -CT and CT-POEGMA 4.10.2-4.10.20 based on the <i>p</i> NA assay.....	193
Table 4.9 Summary of catalytic half-lives for α -CT, CT-PGMA 3.10.5 , CT-POEGMA 4.10.5 , and 4.10.20 at 4 °C, 20 °C, and 40 °C. Half-lives at 40 °C have been normalised to a native α -CT half-life of 13.2 minutes.	198

Table 4.10. Summary of CT-PTEGMA 4.10.5 , CT-POEGMA₄₅₀ 4.10.5 , and CT-POEGMA₉₀₀ 4.10.5 characterisation with UV-Vis spectroscopy and SDS-PAGE analysis.....	199
Table 4.11 Michaelis-Menten parameters of α -CT and CT-PTEGMA 4.10.5 , CT-POEGMA₄₅₀ 4.10.5 , and CT-POEGMA₉₀₀ 4.10.5 based on the pNA assay.....	202
Table 5.1. Average degree of attachment of I-NHS 2.1 initiator for UL1-MI 2.1 species synthesised at varying pH values and concentrations of initiator as determined by MALDI-ToF analysis. Errors are reported as the standard deviation of the distribution based on the assumption of a Gaussian fit of the MALDI-ToF mass spectra.	231
Table 5.2. Average degree of attachment of I-COOH 5.1 initiator for UL1-MI 5.1 species synthesised at varying pH values and concentrations of EDC.HCl as determined by MALDI-ToF analysis. Errors are reported as the standard deviation of the distribution based on the assumption of a Gaussian fit of the MALDI-ToF mass spectra.	234
Table 5.3 Michaelis-Menten Parameters of UL1 and UL1-MI 5.1 species based on the pNA assay.	239
Table 5.4. Summary UL1-PGMA PPC characterisation from UV-Vis spectroscopy and SDS-PAGE analysis.....	243
Table 5.5 Michaelis-Menten Parameters of UL1 and UL1-PGMA PPCs based on the pNA assay.	243
Table 5.6. Average degree of attachment of I-NHS 2.1 initiator for PFL-MI 5.1 species synthesised at varying pH values as determined by MALDI-ToF analysis. Errors are reported as the standard deviation of the distribution based on the assumption of a Gaussian fit of the MALDI-ToF mass spectra.	251
Table 5.7. Average degree of attachment of I-NHS 2.1 initiator for Lx-MI 2.1 species synthesised at pH 8.0 and varying concentrations of initiator as determined by MALDI-ToF analysis. Errors are reported as the standard deviation of the distribution based on the assumption of a Gaussian fit of the MALDI-ToF mass spectra.....	254

Table 5.8. Average degree of attachment of I-COOH 5.1 initiator for Lx-MI 5.1 species synthesised at pH 8.0 and varying concentrations of initiator and EDC.HCl as determined by MALDI-ToF analysis. Errors are reported as the standard deviation of the distribution based on the assumption of a Gaussian fit of the MALDI-ToF mass spectra.	256
Table 5.9 Michaelis-Menten Parameters of Lipex and Lx-MI 5.1 species based on the <i>p</i> NP assay.	259
Table 5.10. Summary of Lx-PGMA PPC characterisation from UV-Vis spectroscopy and SDS-PAGE analysis.....	262
Table 5.11 Michaelis-Menten Parameters of Lipex and Lx-PGMA PPCs based on the <i>p</i> NP assay.	263

Acknowledgements

I would like to thank Rachel O'Reilly, for giving me the opportunity to work within her group. I am grateful for all of the encouragement and support you have provided (even when some things weren't going to plan) but also for the occasional push I needed to get me to where I am now.

I would also like to thank Unilever for funding and my industrial contacts: Ezat Khosdel, Dietmar Lang, and Andrew Cook for providing useful scientific discussions and for allowing me to perform application testing within their facilities at Port Sunlight.

A huge thank you to Dafni, Anaïs, Guillaume, Kay, Becky, Jon and Lewis for proof-reading, as without them I am unsure if this thesis would have made any sense. Thank you also to Annette for allowing me to follow her across the country and for always being there to give me perspective when it was needed. To everyone in the O'Doveilly groups, both past and present group members, thank you for allowing me to escape to the world outside the lab. This includes the special group of people that were able to put up with me through all of my different moods and who taught me the best meal of the day is brunch, to appreciate the art of spoken word singing, and that I can definitely run a half-marathon if I need to. At times you all had more faith in me than I did in myself, and without you I wouldn't have finished this thesis!

Finally I would like to thank my family, because even if they didn't understand what I did or why I did it, they were always there to encourage and support me. More specifically to my parents, I would like to thank you for understanding my crazy moments, for teaching me the determination I needed to get through this and for the support when after 17 years of education I signed up for 3 more. You have always been there for me when I needed anything from home-cooked meals in stressful times, car maintenance advice, or just someone to talk to - thank you for everything.

Declaration of Authorship

This thesis is submitted to the University of Warwick in support of my application for the degree of Doctor of Philosophy. It has been composed by the author and has not been submitted in any previous application for any degree. All of the work presented in this thesis (including data generated and data analysis) was conducted by the author unless otherwise stated. Any experiments or data analysis conducted by other persons is clearly stated within each chapter

- The SAXS characterisation in Chapter 3 was acquired and analysed by Dr Anaïs Pitto-Barry from Professor Rachel O'Reilly's group of the University of Warwick.
- The stain test data and images in Chapter 5 were acquired by Andrew Cook from the Home Care division of Unilever Research and Development.

Summary of Thesis

This thesis explores the use of protein-polymer conjugates to enhance the stability of various enzymatic species.

Chapter 1 gives an overview of the current literature covering mechanisms of enzyme denaturation and various approaches to enhance stability of enzymatic species

Chapter 2 evaluates the synthesis of protein macro-initiators from α -chymotrypsin and the ability to tune the initiator grafting density by employing control of pH and concentration.

Chapter 3 examines the production of protein-polymer conjugates from α -chymotrypsin utilising atom transfer radical polymerisations with a hydrophilic monomer, glycerol methacrylate, and investigates the effects of altering the polymeric grafting densities on enzyme stability.

Chapter 4 investigates the functionality and architecture of the grafted polymer on the surface of α -Chymotrypsin and the subsequent effects on both activity and stability of the protein-polymer conjugate.

Chapter 5 discusses the challenges of employing the chemistries used to synthesise both protein macro-initiators and protein-polymer conjugates on enzymes specific to laundry applications.

Abbreviations

$^3J_{H-H}$	Vicinal proton coupling constant
a_0	Contact area of hydrophilic segment
ABM	Aminobromomaleimide
AIBN	Azobisisobutyronitrile
ARGET	Activators regenerated by electron transfer
ATRP	Atom transfer radical polymerisation
BSA	Bovine serum albumin
c	Concentration
CalB	<i>Candida antarctica</i> lipase B
CD	Circular Dichroism
CTA	Chain transfer agent
d	Doublet
Da	Dalton
D_h	Hydrodynamic diameter
DLS	Dynamic light scattering
D_M	Molecular weight distribution
DMA	<i>N,N</i> -Dimethylacrylamide
DMAP	4-Dimethylaminopyridine
DMF	<i>N,N</i> -Dimethylformamide
DMSO	Dimethyl sulfoxide
DSC	Differential scanning calorimetry
E	Enzyme
eATRP	Electrochemically mediated ATRP
EDC urea	1-(Dimethylamino)-3-(3-ethylureido)propane
EDC.HCl	<i>N</i> -(3-Dimethylaminopropyl)- <i>N'</i> -ethylcarbodiimide hydrochloride

EG-NHS	Ethylene glycol bis(<i>N</i> -hydroxysuccinimide ester)
ES	Enzyme-substrate
ESI-MS	Electrospray ionisation mass spectroscopy
FDA	Food and drug administration
FTIR	Fourier transform infrared spectroscopy
GC	Gas chromatography
GMA	Glycerol methacrylate
GO _x	Glucose oxidase
HATU	1-[Bis(dimethylamino)methylene] 1H-1,2,3-triazolo[4,5]pyridinium 3-oxid hexafluorophosphate
HBTU	2-(1H-benzotriazol-1-yl) 1,1,3,3-tetramethyluronium hexafluorophosphate
HMTETA	1,1,4,7,10,10-hexamethyltriethylenetetramine
HPMA	<i>N</i> -(2-Hydroxypropyl)methacrylamide
HRP	Horseradish peroxidase
I	Inhibitor
<i>I</i>	Scattering Intensity
IFN- α	α -Interferon
k_{act}	Rate of activation
K_{ATRP}	ATRP equilibrium constant
k_{cat}	Catalytic constant
k_{deact}	Rate of deactivation
K_m	Michaelis constant
<i>L</i>	Path Length
LAM	Less activated monomer
l_c	Length of hydrophobic chain
LC-MS	Liquid chromatography–mass spectrometry

LCST	Lower critical solution temperature
m	multiplet
MADIX	Macromolecular design <i>via</i> interchange of xanthates
MALDI-ToF	Matrix-assisted laser desorption/ionisation time-of-flight
MAM	More activated monomer
MI	Macro-initiator
M_n	Number-average molecular weight
M_w	Weight-average molecular weight
MWCO	Molecular weight cut-off
NHS	<i>N</i> -Hydroxysuccinimide
NMP	Nitroxide-mediated radical polymerisation
NMR	Nuclear magnetic resonance
OEGMA	oligo(ethylene glycol) methacrylate
OEGMA ₃₆₀	OEGMA with a M_n of 360 g mol ⁻¹
OEGMA ₄₅₀	OEGMA with a M_n of 450 g mol ⁻¹
OEGMA ₉₀₀	OEGMA with a M_n of 900 g mol ⁻¹
OmpF	Outer membrane protein F
p	Packing parameter
PCPP	Poly(di(carboxylatophenoxy)phosphazene)
PDEAAm	Poly(<i>N,N</i> -diethylacrylamide)
PDMAEMA	Poly(dimethylaminoethyl methacrylate)
PDMS	Poly(dimethylsiloxane)
PEG	Poly(ethylene glycol)
PFL	Lipase from <i>Pseudomonas fluorescens</i>
PGMA	Poly(glycerol methacrylate)
PHPMA	Poly(<i>N</i> -(2-hydroxypropyl)methacrylamide)

pI	Point of ionisation
PMOXA	Poly(2-methyl-2-oxazoline)
pNA	p -Nitroaniline
PNIPAm	Poly(N -isopropylacrylamide)
pNP	p -Nitrophenol
PNVP	Poly(N -vinylpiperidone)
PPC	Protein-polymer conjugate
PPEGA	Poly(polyethylene glycol acrylate)
PVA	Poly(vinyl alcohol)
PyBOP	Benzotriazol-1-yl-oxytripyrrolidinophosphonium
q	Wave vector
RAFT	Reversible addition-fragmentation chain transfer
RDRP	Reversible-deactivation radical polymerisation
R_g	Radius of gyration
ROMP	Ring-opening metathesis polymerisation
ROP	Ring-opening polymerisation
s	Singlet
SA-NHS	Suberic acid bis(N -hydroxysuccinimide ester)
SARA	Supplemental activator and reducing agent
SAXS	Small-angle X-ray scattering
SBAm	Sulfobetaine methacrylamide
SDS-PAGE	Sodium dodecyl sulfate poly(acrylamide) gel electrophoresis
SEC	Size exclusion chromatography
SET-LRP	Single electron transfer living radical polymerisation
SRI	Stain removal index
t	Triplet

TBTU	2-(1H Benzotriazole-1-yl)-1,1,3,3-tetramethyluronium tetrafluoroborate
TEA	Triethylamine
TEGMA	Triethylene glycol methacrylate
TLL	Lipase from <i>Thermomyces Lanuginosa</i>
T_m	Melting temperature
UCST	Upper critical solution temperature
UL1	Unilever Protease 1
UV-Vis	Ultraviolet-visible
v	Volume of hydrophobic chain
α -CT	α -Chymotrypsin
δ	Chemical shift
ΔE	Change in colour
ϵ	Molar absorption coefficient
θ	Scattering angle
λ	Wavelength
ρ	Conductivity

1 Introduction

1.1 Introduction

Nature is able to catalyse many biological reactions through the use of enzymes.^{1,2} As catalysts they are highly specific only catalysing the reaction of defined substrates in a narrow window of optimum conditions. Enzymes are a subclass of proteins whose activity is dependent upon the unique structure and folding of the polypeptide.³ The folding creates internal pockets to allow catalysis to occur, referred to as active sites and it is the morphology of these pockets that determines the enzymes substrate specificity.^{4,5} Significant research has been conducted into trying to replicate enzymes and create enzyme mimics though many do not achieve the same catalytic rate or substrate specificity.^{6,7}

1.2 Protein Structure

As mentioned, the ability of enzymes to catalyse reactions is dependent upon their structure. As a protein, enzyme structure can be divided into four separate levels of organisation: primary, secondary, tertiary and quaternary structures (Figure 1.1).^{3,8}

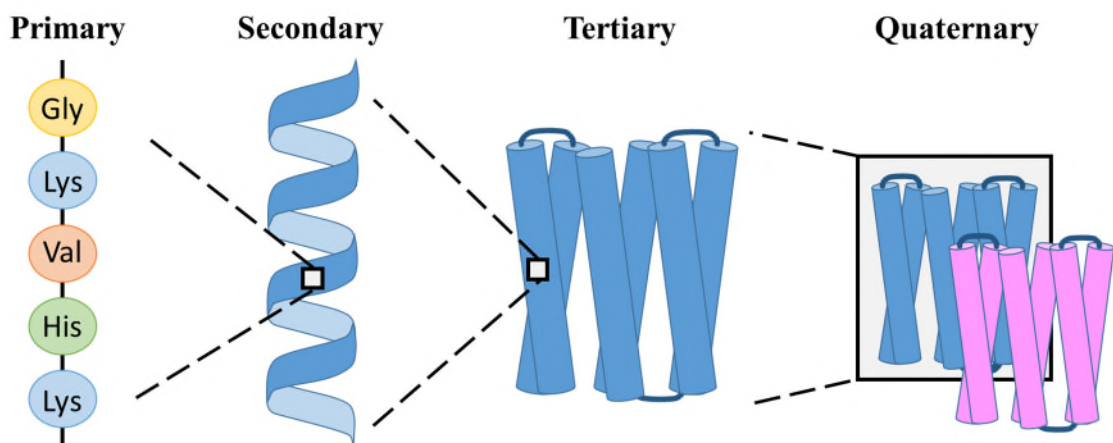


Figure 1.1 Schematic representations of primary, secondary, tertiary, and quaternary structures of proteins.

1.2.1 Primary Structure

The primary structure of a protein is the sequence in which the amino acids are coded within DNA to produce the protein.⁸ These are typically reported from the *N*-terminus to the *C*-terminus in a

linear fashion. Amino acids possess a chiral centre and can exist in both an L- or D- isomer, however most naturally occurring proteins consist of almost entirely of L-amino acids, and therefore all proteins are chiral species.⁹ In nature, there exists 22 natural L- α -amino acids, however only 20 have found to be coded for within the genetic material. These amino acids can be combined in an almost infinite number of ways to produce proteins with a vast range of structures and functions.¹⁰ The functionality of an amino acid is controlled by the nature of the side chain, R (Figure 1.2), which can introduce hydrophobic, hydrophilic, acidic, basic, or polar properties within the molecule.

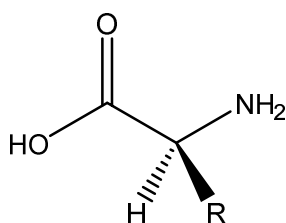


Figure 1.2 Chemical structure of an L-amino acid.

In addition to the natural amino-acids that exist, unnatural amino-acids possessing a wide range of functionalities have been synthesised.^{11, 12} Many of these structures contain moieties that react bioorthogonally to the natural amino acids and create functional handles that provide new synthetic routes to modify enzymes. For example, Deiters *et al.* successfully expressed non-natural amino acids containing alkyne and azide functionalities into human superoxide dismutase.¹³ This enabled the binding of dyes containing alkyne and azide moieties to the newly introduced residues without impacting any other residues due to the reactions between azide and alkyne functionalities being bioorthogonal to reactions that can take place between the natural amino acid residues.¹⁴

1.2.2 Secondary Structure

Secondary structure is used to define regions of localised structure, which usually involves between 10 and 20 amino acids.^{3, 8} The structures are controlled by the formation of hydrogen

bonding between the amide functionalities present in the polypeptide backbone. There are three main stable secondary structures: α -helices, β -sheets and β -turns.

1.2.2.1 α -Helices

An α -helix is a structure formed from a single polypeptide chain, which through intra-chain hydrogen bonding form a right handed helix.⁸ The hydrogen bonding exists between the carbonyl oxygen of residue n and the amide nitrogen of residue $n + 4$ (Figure 1.3), creating a turn that contains approximately 3.6 residues.¹⁵

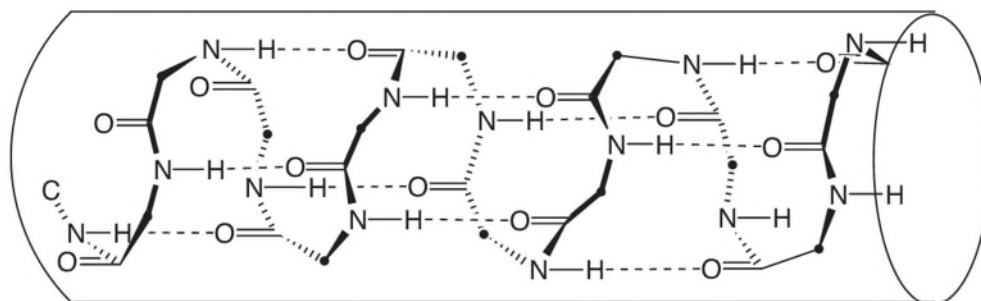


Figure 1.3 Schematic representation of the hydrogen bonding present within an α -helix with the location of R-groups represented by dots. Taken from Bugg.³

The amino acid R groups were found to point outwards from the helical axis and can strongly influence the stability of the α -helix.¹⁶ For example, L-alanine residues are abundant in helical structures as a result of their small uncharged side chain. The presence of residues that possess sterically bulky side chains, such as L-tyrosine and L-asparagine, can destabilise α -helices and so are only typically present in low numbers. Although glycine is a small uncharged amino acid, the high flexibility of the molecule prevents the formation of α -helices.¹⁷ In contrast to the high flexibility of glycine, L-proline residues have a structure that is too rigid making the residue unable to conform to the necessary bond angles required to form an α -helix. Along with the rigid structure of L-proline, the alkylation of the nitrogen atom prevents hydrogen bond formation and therefore L-proline residues are the least abundant residue in α -helices.¹⁷

1.2.2.2 β -Sheets

β -Sheets consist of several β -strands, which are sections of the polypeptide chain, *ca.* 3-10 amino acids in length, in an extended conformation. β -Strands are held together by inter-strand hydrogen bonding between the carbonyl oxygen and amide nitrogen functionalities within the peptide backbone to form β -sheets.⁸ In contrast to the compact structure present in α -helices, the protein strands are almost fully extended when present in β -sheets. Two types of β -sheet exist and are classified dependent upon the direction in which the chains interact: parallel (same N-to-C terminal direction) and anti-parallel (opposite N-to-C terminal direction) (Figure 1.4). The hydrogen bonding within parallel conformations is distorted from the ideal perpendicular arrangement found in anti-parallel β -sheets, thus making parallel β -sheets less stable than the anti-parallel conformers.

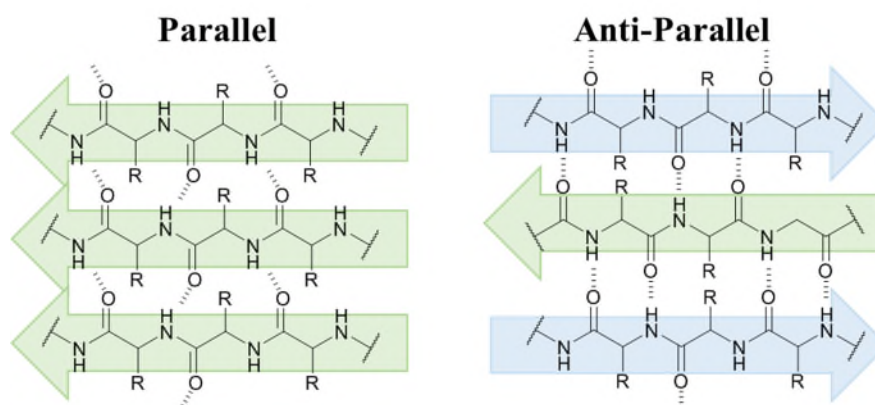


Figure 1.4 Schematic representation of the hydrogen bonding present within parallel and anti-parallel β -Sheets.

β -Sheets can be referred to as pleated structures because of the α -carbon alternating between lying above and below the plane of the β -sheet, which results in the amino acid side chains also alternating direction.¹⁸ This in turn can create amphiphilic structures with hydrophobic residues present only on one side of the sheet, which can aid in the formation of higher order structures due to inter-sheet hydrophobic interactions.¹⁹

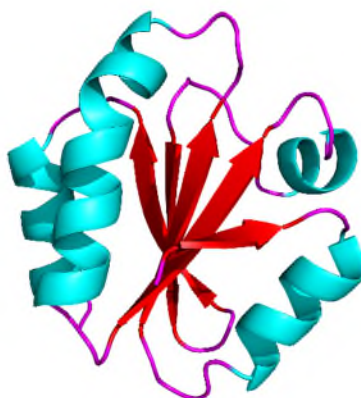


Figure 1.5 Schematic representation of the crystal structure of human thioredoxin (**IERU**) highlighting the twist in the β -sheet shown in red.²⁰ Blue represents α -helix, pink represents random coil and red represents β -sheets. PDB crystal structure references are identified in bold.

Although depicted as planar structures, many β -sheets are twisted as a result of the chirality present in the amino acids.²¹ This twisting is required in order to balance the conformational energies of the amino acid side groups and the strength of the hydrogen bonding. The twisting of β -sheets is present in many proteins such as human thioredoxin, illustrated in Figure 1.5.²⁰

1.2.2.3 β -Turns

Although many types of loops and turns are present within proteins, β -turns are an important class of these structures as they introduce a 180° turn of the peptide chain to facilitate the formation of anti-parallel β -sheets. In order to create this conformation, it is critical that hydrogen bonding is present between the carbonyl oxygen of residue n and the amide nitrogen of residue $n + 3$ (Figure 1.6).³

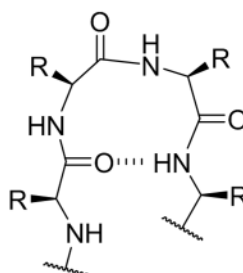


Figure 1.6 General structure of β -turns.

In contrast to the formation of α -helices, glycine and L-proline are frequently found within β -turns.²² With only a proton side chain, glycine has a high flexibility, removing some of the steric hindrance barriers encountered with other, more sterically hindered, amino acids. As a result of its cyclic structure, L-proline is able to induce a sharp turn allowing a 180° bend over the space of only four residues.

1.2.3 Tertiary Structure

The tertiary structure of a protein is the three dimensional structure that forms upon successful folding of a polypeptide chain.⁸ Although residues that are intrinsic to the catalytic function of the active site may not be in close proximity when only considering the primary sequence, the formation of the tertiary structure can bring the residues close in three-dimensional space creating the active site pocket. In comparison to the secondary structures that are stabilised by the formation of hydrogen bonding of the peptide backbone, tertiary structures are formed by the bonding between amino acid side groups. Amino acids contain various functionalities that can interact to form networks of bonds that contribute to the overall tertiary structure including hydrogen bonding, hydrophobic interactions, van der Waals forces, electrostatic interactions, and covalent bonding (Figure 1.7).²³

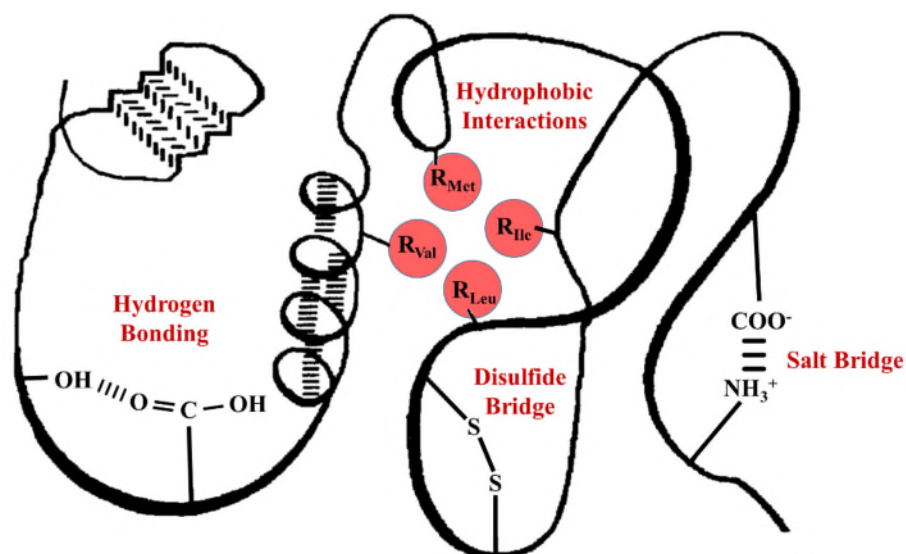


Figure 1.7 Schematic representations of interactions that contribute to the tertiary structure of proteins.
Reproduced from Janecek *et al.*²⁴

The folding of proteins occurs spontaneously and they adopt the most thermodynamically stable conformation referred to as the native state.²⁵ In the 1960s, Levinthal discussed the implausible nature of forming the native structure in the short timescale in which protein folding occurs considering the vast number of possible conformations of a polypeptide chain.²⁶ As a systematic search for the lowest energy conformation would exceed the timescale for protein folding, it was suggested that folding occurs *via* several pathways, including the formation of intra-chain bonding, which remove many possible conformations from the search process.²⁷

Although the pathways for protein folding are not fully understood, it is widely accepted that the energy landscape for protein folding resembles that of a funnel (Figure 1.8).²⁸ At the top of the funnel are conformations of the polypeptide that are typically random coils. As the funnel decreases in energy more complex protein folding is present including secondary and tertiary structures. Leopold *et al.* introduced the concept with the use of computer modelling that the energy landscape of a protein is dependent upon its primary structure.²⁹ It has been hypothesised that the formation of bonding that is present in the native structure lowers the energy of the resulting structure to a greater extent than other possible interactions that could form within the polypeptide chain. Many studies agree with the conclusion that the interaction between a small number of residues generates a nucleation point in which the remainder of the protein rapidly adopts the folding present within the native protein species, which lies at the bottom of the energy funnel.³⁰⁻³²

The energy landscape observed for some proteins can be very simple and only contain one minimum (Figure 1.8a), however for many proteins the landscapes are more complex with routes that can lead to kinetically trapped and misfolded proteins (Figure 1.8b).³³ Chaperone proteins are proteins that assist in the correct folding of macromolecular structures. Chaperone proteins can alleviate the problem of misfolded proteins *in vivo* by binding to a newly synthesised polypeptide

and promoting the formation of the native state.³⁴ Even with the use of chaperones, protein folding is a spontaneous process and therefore folding involving chaperones is referred to as assisted self-assembly.

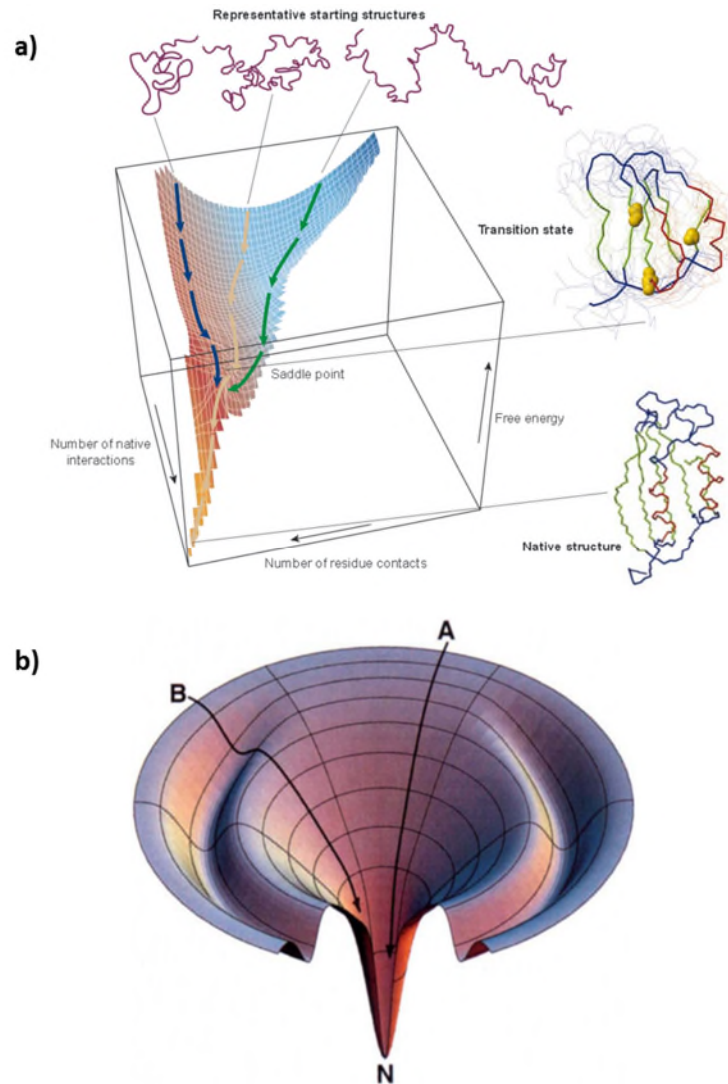


Figure 1.8 Energy landscapes of protein folding. a) Simplified small protein folding showing a single energy minimum. Taken from Dobson.³⁵ b) Simplified energy funnel indicating presence of a local energy minima. Taken from Dill and Chan.³⁶

1.2.4 Quaternary Structure

The highest order of protein structure is the quaternary structure, which is the assembly of multiple pre-folded proteins.³⁷ The final quaternary structure of a protein can be assembled from many identical sub-units or a combination of different protein sub-units. The interactions that

stabilise the formation of these structures are the same as those utilised in the formation of tertiary structures including hydrogen bonding, hydrophobic interactions, van der Waals forces, electrostatic interactions, and covalent bonding. The combinations of multiple protein subunits can reveal functionality that was not present as a single subunit. One common example of a quaternary structure is mammalian haemoglobin, which exists as a tetramer of two unique subunits.³⁸

1.3 Activity of Enzymes

The activity of enzymes can be assessed using a variety of kinetic models, of which the most commonly encountered is the Michaelis-Menten model of kinetics, used to assess the activity of enzymes with a single substrate present.^{39, 40} The model assumes that all species present are diffusion-controlled and the catalytic step in product-formation is irreversible (Equation 1.1).

Equation 1.1 Overall reaction for quasi-steady-state enzyme kinetics used in the Michaelis-Menten model.



E = Enzyme

S = Substrate

ES = Enzyme-Substrate Complex

P = Product

k_1 = Rate of Association

k_2 = Rate of Dissociation

k_{cat} = Rate of Product Formation

The Michaelis-Menten equation (Equation 1.2) was proposed by Michaelis and Menten in 1913 where v is the initial velocity of catalytic reaction, V_{max} is the maximum velocity of the enzyme in a saturated solution of substrate, $[S]$ is the substrate concentration and K_m is the Michaelis constant.^{39, 40} The equation has been derived from a quasi-steady state approximation of the system; this assumes that the enzyme substrate, ES, concentration does not change throughout the

reaction.⁴¹ The Michaelis constant, K_m , is inversely proportional to the affinity of the substrate and is dependent on environmental factors, such as temperature and pH. V_{max} has a concentration dependency and so to eliminate this, the catalytic constant, k_{cat} , can be determined by simply dividing through by the enzyme concentration. k_{cat} is the maximum turnover number of product molecules when the enzyme is in a saturated substrate environment.

Equation 1.2 Michaelis-Menten Equation.

$$v = \frac{V_{max}[S]}{K_m + [S]}$$

This model assumes that the concentration of enzyme, $[E]$, is much less than $[S]$, to ensure this criteria is met assays are performed at low $[E]$.⁴² Another parameter that can be extracted from Michaelis-Menten parameters is the efficiency of the enzyme, which is calculated by k_{cat}/K_m . To allow for simple extraction of parameters using linear regression, a Lineweaver-Burk plot can be employed.⁴³ The plot is a double reciprocal plot of substrate concentration against initial velocity (Figure 1.9). V_{max} is equal to the reciprocal of the y -intercept and can be easily converted into k_{cat} through the division by the enzyme concentration. K_m can either be extracted from the gradient of the plot, as it is equal to K_m/V_{max} , or the x -intercept, as it is the reciprocal of K_m .

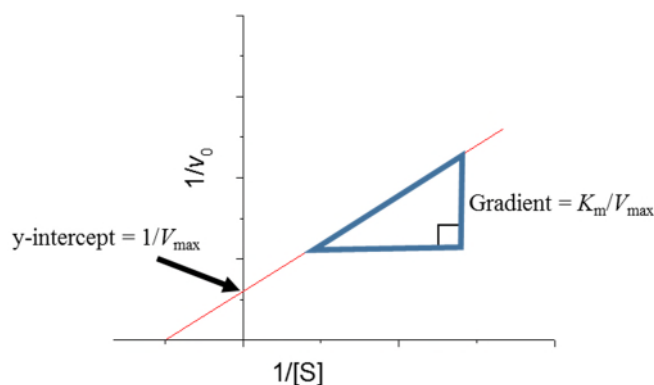


Figure 1.9 Lineweaver-Burk Plot.

1.4 Inhibition of Enzymes

When enzymes are correctly folded, their catalytic abilities are usually higher than comparative synthetic catalysts.¹ Enzymes have been found to catalyse reactions with rate increases of over one million-fold compared with the uncatalysed reaction. However, despite their ability to lower the activating energy in many reactions, they can be susceptible to retardation by both reversible and irreversible routes, known as inhibition.⁴⁴ Inhibitors are species that are able to interact with enzymes or the enzyme-substrate complex formed during catalysis and therefore reduce the efficiency of the enzyme.

1.4.1 Irreversible Inhibition

Irreversible inhibitors form strong interactions with the protein and permanently prevent the formation of product molecules. The most common method of irreversible inhibition is through the alkylation or acylation of amino acids present within the active site of the enzyme.⁴⁵ Many pharmaceutical drugs are irreversible inhibitors that deactivate a target enzyme species within the body and therefore reduce unwanted effects. For example, acetylsalicylic acid, more commonly known as aspirin, is employed to reduce the occurrence of cardiac related incidents.⁴⁶ Aspirin is known to act on the cyclooxygenase enzyme. Cyclooxygenase is an enzyme that catalyses the production of thromboxane A₂, a lipid that is known to induce platelet aggregation, leading to cardiac problems. Aspirin is effective as it can acetylate the L-serine present in the active site of cyclooxygenase and therefore preventing the formation of the thromboxane A₂.⁴⁷

1.4.2 Reversible Inhibition

Reversible inhibitors are bound to the enzyme by non-covalent interactions and can be removed by simple purification methods such as dialysis or filtration. Upon removal of the inhibitor the activity of the enzyme should revert back to the initial activity. Reversible inhibition can be classified into three distinct categories: competitive, uncompetitive and noncompetitive (Figure 1.10).⁸ The categories of inhibition are dependent upon whether the inhibitor (I) interacts with the enzyme (E), the enzyme-substrate complex (ES) or both.

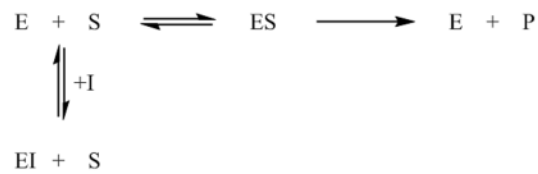
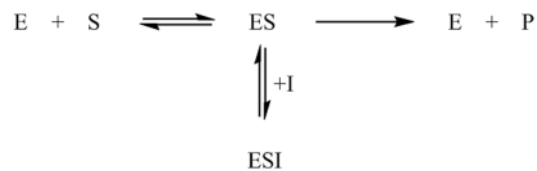
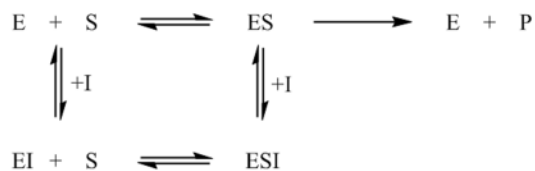
a) Competitive Inhibition**b) Uncompetitive Inhibition****c) Noncompetitive Inhibition**

Figure 1.10 Schematic representations of the three different types of reversible enzyme inhibition.

Competitive inhibitors prevent formation of the enzyme-substrate complex and they are the most common type of inhibitor.¹ There are many methods of competitive inhibition. The main method is reversible binding of an inhibitor to the active site, which prevents the substrate from entering the active site and forming the enzyme-substrate complex. Another major method is through allosteric binding; this is the binding of an inhibitor to a site that is close proximity to the active site, which hinders the substrate's access to the active site.

Uncompetitive and noncompetitive inhibition are more rarely observed in biological systems.⁴⁸ Uncompetitive inhibition is more commonly observed in multi-substrate reactions where the inhibitor only interacts with the enzyme-substrate complex.⁸ Noncompetitive inhibitors tend to be allosteric, i.e. they bind to sites other than the active site within both the enzyme and the enzyme-substrate complex.⁸ The binding of the inhibitor does not affect the ability of the substrate to bind, but prevents the catalytic process from occurring by inducing a conformational change within the enzyme.

The types of inhibition occurring within enzymatic species can be determined by employing Lineweaver-Burk plots (Figure 1.11).⁴³ Lineweaver-Burk plots, as introduced in Section 1.3, are double reciprocal plots derived from a linear derivation of the Michaelis-Menten model of kinetics. As each method of inhibition has characteristic responses to the increase in inhibitor species on the K_m and k_{cat} of the enzyme, these can be clearly identified.⁴⁹ For example, competitive inhibition does not affect the catalytic constant, k_{cat} , but causes increases in K_m and this is indicated in the Lineweaver-Burk plot by a change in gradient yet no change in y -intercept (Figure 1.11a).⁵⁰ In contrast, noncompetitive inhibition maintains K_m but a reduction in k_{cat} can be observed (Figure 1.11c). Uncompetitive inhibition affects both K_m and k_{cat} , however the ratio between the two parameters remains constant and therefore the gradient of the Lineweaver-Burk plot remain constant whilst differences are observed in the x - and y - intercepts (Figure 1.11b).

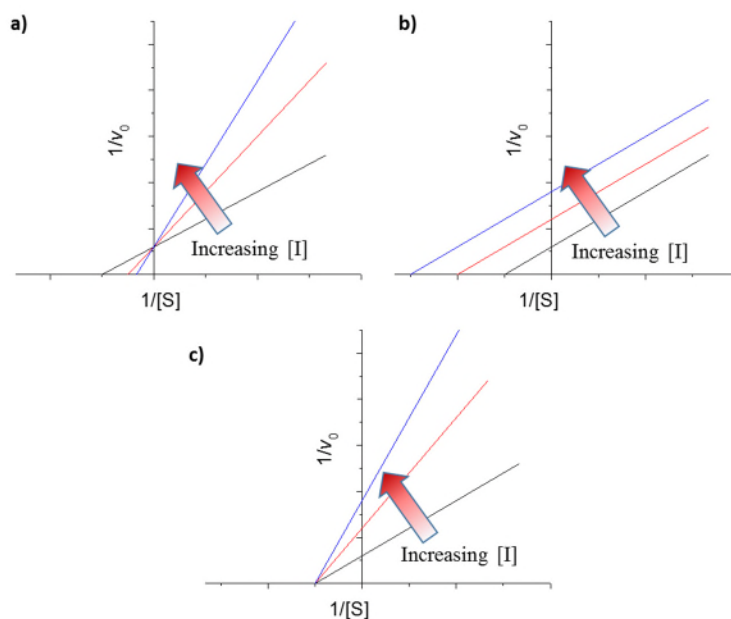


Figure 1.11 Graphical representations of the Lineweaver-Burk plots of the three different types of reversible enzyme inhibition a) competitive c) uncompetitive c) noncompetitive.^{49, 50}

1.5 Denaturation and Inactivation of Proteins

Enzymes are currently used in many industrial application, as a result of their high specificity and catalytic ability, however denaturation and inactivation of proteins and enzymes can occur during

industrial usage. Prevention of inactivation and denaturation of enzymes could improve the efficiency of many industrial processes. Denaturing is the process of unfolding of the protein into a polypeptide chain and therefore induces the loss of the catalytic function. Proteins can be denatured by many external stimuli including heat, solvent, pH and light.⁵¹ The loss of activity is most commonly associated with a disruption of the secondary or tertiary structure of a protein. In the specific case of protease enzymes, there is the additional problem of autolysis; the process of self-digestion.⁵²

Zale and Klibanov highlighted that the denaturing process can be reversible if the external stimuli is removed within a short time frame and no modifications to the polypeptide have occurred.⁵³ However, upon unfolding, the polypeptide chain is more susceptible to undergo alterations to the chemical structure or form inter-protein hydrophobic interactions resulting in aggregation.⁵⁴ These modifications are permanent and lead to the irreversible inactivation of the enzyme (Figure 1.12).

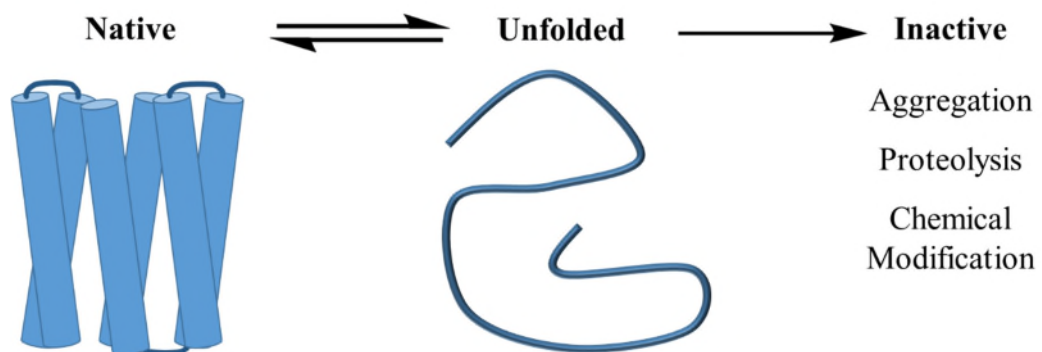


Figure 1.12 Schematic representation of the denaturing process of proteins.

The most common pathway for inactivation of the unfolded protein is aggregation.⁵⁵ Newly exposed hydrophobic segments of the protein can self-assemble into aggregates to minimise unfavourable hydrophobic interactions with the aqueous solvent. The energy required to overcome these interactions and reform the native species is too high and therefore kinetically

trapped aggregates are inactive.⁵⁴ It has also been observed by Parsell and Sauer that unfolded polypeptide chains are more susceptible to proteolysis than their folded analogues.⁵⁶

Elevated temperatures can also cause inactivation. Exposure to increased temperatures can cause L-asparagine and L-glutamine residues to undergo a deamination process resulting in L-aspartic and L-glutamic acid replacements within the primary protein sequence.^{57, 58} These changes in the primary sequence can have significant consequences on the energy landscape and the resulting folding and function of the protein.

The most effective method at investigating the retention of activity when an enzyme is exposed to various stimuli is through enzymatic assays.⁵⁹ With the use of assays, the activity of enzymes at various time points can be determined through spectroscopic methods. The decay in activity of many enzymes has been modelled upon a first-order, or exponential, decay.⁶⁰ This allows simple extraction of an enzymatic half-life by employing a plot of the natural logarithm of residual activity against time and identifying the time at which the residual activity is equal to 0.5.

1.6 Enzyme Stabilisation

Although there are issues with denaturation/loss of activity over time, enzymes are still of significant interest for many industrial applications from fermentation to stain removal to the production of biofuels as they are highly selective and have high activity in aqueous environments.⁶¹⁻⁶³ However, many of these applications require the use of high temperature, organic solvents, and various additives and therefore this limits the use and adaptability of enzymes in such products.⁶⁴ To alleviate these problems, extensive research has been conducted into methods of producing more stable enzymatic species. There are numerous approaches that have been employed to produce more stable enzymes; these include protein engineering, protein immobilisation, introduction of various additives, and protein-polymer conjugates.^{24, 65-67} A brief overview of each approach is given in the following Sections.

1.6.1 Extremophile Enzymes

Nature has many examples of organisms that have adapted to environments that are not typically inhabited due to environmental factors such as a high salt content, exposure to radiation, or extremes of temperature or pH.⁶⁸ The proteins which are synthesised by these organisms are referred to as extremophile proteins and are also tolerant to these extreme conditions. These proteins can therefore be extracted for use as enhanced stability enzymes.⁶⁹ For example, in comparison to proteases found in mammalian species such as α -chymotrypsin (α -CT), which has optimised activity at 37 °C, the protease thermophilic thermitase from extremophile species *Thermoactinomyces vulgaris*, is optimised for catalysis at temperatures up to 70 °C.^{70, 71}

Extremophile enzymes have also been studied in comparison to their mesophilic analogues, which are species that are optimised for moderate environmental conditions. This aids in the further understanding of the interactions that provide the enhanced stability in extreme conditions.^{72, 73} Indeed, Menéndez-Arias and Argos compared the primary sequences and the tertiary structures of six different families of thermophilic enzymes to develop a series of possible criteria for the development of more thermostable enzymes.⁷⁴ Although in later studies suggested that the sample size employed was found to be too small and noted that many thermophilic proteins did not meet the initial criteria set out.⁷⁵ Argos *et al.* performed further experimentation into the types of interactions present within the mesophilic and thermophilic proteins.^{76, 77} They concluded that the increased number of intra-protein hydrogen bonds and salt bridges in the extremophile enzyme, compared to the mesophilic enzyme, correlated with its increased stability at high temperatures.

1.6.2 Protein Engineering

The development of protein engineering technologies allows for the replacement of specific residues within a protein's primary structure.⁷⁸ In combination with the previous studies of extremophilic enzymes, the stability of many enzyme structures have been enhanced through the incorporation of new residues. It is important to consider that the alteration of just one residue within a protein can enhance the stability. For example, subtilisin enzymes contain an

L-methionine residue in close proximity to the active site. This residue readily undergoes an oxidation reaction to form the sulfoxide derivative,⁷⁹ which creates steric hindrance to the active site and lowers the enzyme's ability to perform proteolytic hydrolysis. Hence enzymatic activity decreases over time. The modification of the single L-methionine residue to L-alanine, L-serine or glycine was observed to increase the catalytic ability in oxidative conditions over time.^{80, 81}

Although many alterations to the primary amino acid sequence through protein engineering that are predicted to enhance stability are successful, significant numbers are found after the systematic and time consuming process of screening of numerous modifications that were detrimental to the stability and activity of structures.⁷⁴ Protein modifications tend to rely upon the accuracy of computational modelling of protein structures, which are limited by the energy potential approximations required.⁸² The field of protein engineering through rational design has expanded greatly in recent years, but many examples of proteins stabilised through random mutations cannot be explained by the current models.⁸³

1.6.3 Additives

The use of additives is the most common way to stabilise enzymes due to its simplicity. There are a variety of additives that can improve the stability of an enzyme; these include ligands, salts, polymers and sugars.⁸⁴⁻⁸⁶ Additives can be classified into two categories based upon their characteristics: ionic and osmolytic stabilisers.⁸⁷

Ionic stabilisers have been found to form interactions with the charged surface of the enzyme. The presence of ionic species in a solution can reduce the solubility of hydrophobic groups on a proteins surface and cause the residues to internalise.⁸⁸ In contrast, the presence of ionic salts can increase the solubility of ionisable residues. The combination of the two interactions can result in the protein reducing in size to reduce the unfavourable interactions between hydrophobic residues and the solvent leading to an increase in stability.⁸⁹ Additionally, Obón *et al.* found that a salt's ability to stabilise an enzyme followed the Hofmeister lyotropic series, which is a classification

of an ion's ability to solubilise proteins (Figure 1.13).⁸⁹ Ions that reduce protein solubility were found to aid in enzyme stability greater than those that increase the protein solubility.

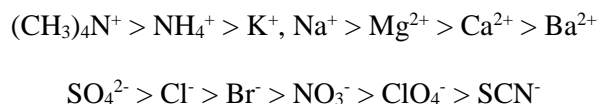


Figure 1.13 Hofmeister lyotropic series.⁸⁹

Osmolytic stabilisers are uncharged species such as sugars and polyols and have also been found to stabilise enzymes towards changes in external stimuli by altering the solvent viscosity and surface tension.⁸⁷ Trehalose, a disaccharide, is an osmolytic stabiliser capable of increasing the catalytic half-life of many enzymes including horseradish peroxidase (HRP) and tyrosinase.^{90, 91} Indeed, Gheibi *et al.* discovered that in addition to an increase in initial activity of mushroom tyrosinase, the addition of trehalose enabled a 3-fold increase in stability at 40 °C.⁹⁰ The limitations of using additives arise due to the high concentrations that are sometimes necessary to provide adequate stabilisation and can interfere with the application's reagents or reaction system.

1.6.4 Polymeric Additives

Although numerous small molecules have been shown to increase both the activity and stability of enzymes, the addition of polymeric species has also been observed to enhance enzymatic stability. Stabilisation of proteins in the presence of polymers is generally attributed to preferential exclusion, surface activity, steric hindrance of protein-protein interactions, or restriction of protein structural movement.⁹² As with small molecule stabilisers, polymeric additives can also be classified as ionic or osmolytic stabilisers.

Ionic polymers can interact with the protein to form complexes that protect the protein from other external interactions such as solvent-protein interactions. An example of an ionic polymer utilised in the stabilisation of enzymes is poly(di(carboxylatophenoxy)phosphazene) (PCPP)

(Figure 1.14). The incubation of PCPP with HRP increases the retention of activity after one hour at 50 °C from 20% to 40% compared with the native species.⁹³

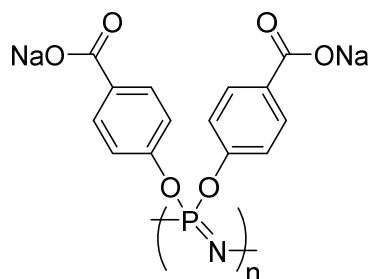


Figure 1.14 Chemical structure of poly(di(carboxylatophenoxy)phosphazene) (PCPP).

The proposed mechanism of PCPP stabilisation includes the formation of a protein-polymer complex through interactions of hydrophobic groups of the polymer with the hydrophobic surface of the protein. Through the use of a turbidimetric method, Marin *et al.* estimated that 440 enzyme molecules were complexed to one 900 kDa polyelectrolyte chain.⁹³

Poly(ethylene glycol) (PEG) is amongst the most common osmolytic polymeric stabiliser employed in the stabilisation of enzymatic species. α -CT has been reported to be stabilised with a 20 kDa PEG species in solutions containing up to 60% v/v ethanol with no loss of activity observed.⁹⁴ The degree of stabilisation provided by PEG was found to be dependent on both concentration and the length of the polymer, with a positive correlation observed for both variables.⁹⁵ However, Yoon and Robyt analysed the stability of ten different enzymes upon incubation with PEG and poly(vinyl alcohol) (PVA) species and discovered that each enzyme had a specific combination of concentration and polymer chain length and functionality to provide maximum stability.⁹⁶

The combination of synthetic polymers and the small molecules reported in the previously in Section 1.6.3, by the immobilisation onto a polymer support have been reported to further enhance stability in comparison to the low molecular species alone. For example, Maynard *et al.* investigated the relative stability of HRP in the presence of trehalose and polymer-bound

trehalose.⁹⁷ Polymers were synthesised from trehalose modified styrenic monomers containing various linkers to the trehalose moiety by free radical polymerisation. HRP was incubated at 70 °C for 30 mins and the resulting enzymatic activity examined as a residual activity percentage. All trehalose based polymers analysed at 80 equivalents polymer to enzyme were found to remain within error of 100% activity, compared to the species with no additive that was observed to decrease to 55% of the initial activity. Although the sample with unbound trehalose was observed to retain a larger percentage of activity than the non-additive sample, with 73% activity, this is a reduction in comparison to the polymeric species. This study indicates the benefit of polymeric stabilisers in comparison to low molecular weight equivalents.

1.6.5 Encapsulation

An alternative method of stabilisation, to prevent interactions with additives that are required for industrial applications but impact the enzyme's stability, is encapsulation within a polymeric shell to form polymeric nanoreactors. The polymeric nanoreactors employed for such reactions are similar in nature to that of cells, with a bilayer membrane that can allow compartmentalisation to occur to prevent undesired interactions between incompatible proteins. Amphiphilic block copolymers can spontaneously self-assemble in a selective solvent into different structures based upon their ratio of hydrophobic-to-hydrophilic segments.⁹⁸ The morphology these polymers adopt is determined by the packing parameter, p , which is related to the volume of the hydrophobic chain, v , the contact area of the hydrophilic segment, a_0 , and the length of the hydrophobic chain, l_c , by the relationship described in Equation 1.3.⁹⁹

Equation 1.3 Packing parameter.⁹⁹

$$p = \frac{v}{a_0 l_c}$$

The formation of spherical micelles is favoured when $p < 1/3$, cylindrical micelles when $1/3 < p < 1/2$, and vesicles when $1/2 < p < 1/3$.⁹⁹ The formation of vesicles creates an aqueous central cavity, the lumen. When assembly occurs in the presence of proteins, species can become

trapped within the lumen.¹⁰⁰ Based upon the polymers employed and the incorporation of pore-forming species into the wall of the vesicle, control over the molecules that are allowed to enter the vesicle can be achieved.^{101, 102} For example, Nardin *et al.* inserted outer membrane protein F (OmpF) into polymeric membranes composed of poly(2-methyl-2-oxazoline) (PMOXA) and poly(dimethylsiloxane) (PDMS).¹⁰³ OmpF is a non-selective transport channel that allows small polar molecules, smaller than 700 Da, to pass through *via* diffusion, whilst not allowing larger molecules to pass across the membrane wall.¹⁰⁴ Nardin *et al.* synthesised ABA triblock copolymers, PMOXA-PDMS-PMOXA, and utilised them to encapsulate β -lactamase with and without the presence of OmpF.¹⁰³ Without the presence of OmpF, the activity of the enzyme was undetectable by spectroscopic methods as the substrate, in the bulk solvent, and the enzyme, trapped within the lumen, were unable to react. Upon the incorporation of OmpF into the membrane, activity was observed and highlighted the theory that the substrate was unable to penetrate the membrane without the presence of pore-like species (Figure 1.15).

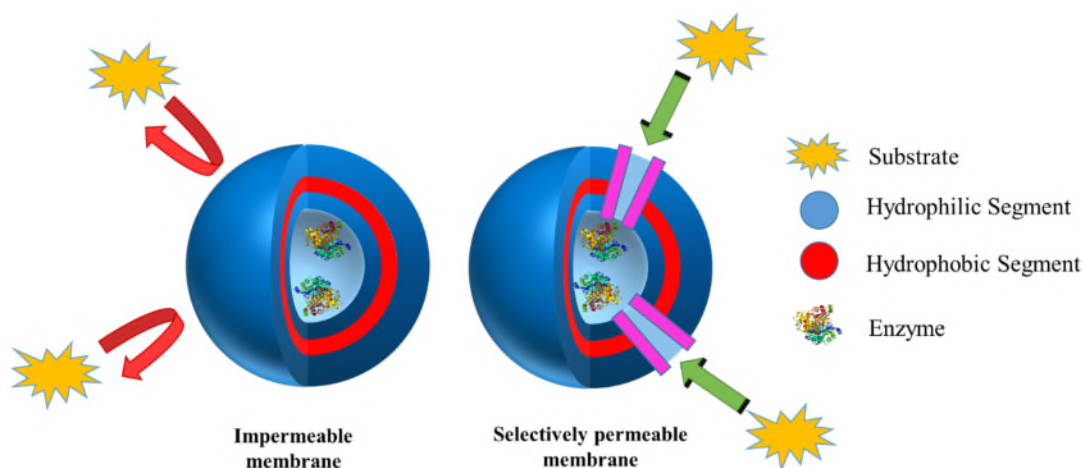


Figure 1.15 Schematic representation of enzyme encapsulation and the effects of selectively permeable membranes.

A combination of these polymeric nanoreactors can create cascade systems that mimic the structure of cells and their organelles.¹⁰⁵ This allows multiple enzymes to exist in solution without protein-protein interactions occurring due to the compartmentalisation of the enzymes. Although

this method can be highly effective at preventing denaturation occurring from additives or other enzymatic species, it does not protect against fluctuations in temperature or autolytic digestion.

1.6.6 Post-translational Protein Modification

All of the methods discussed previously involve the introduction of an additive or modification of the amino acid sequence prior to translation of the protein. As many of the naturally occurring amino acid side chain groups possess functionalities that can be chemically modified using mild conditions, vast research has been conducted into the effects of post-translational modification upon stability.^{24, 65-67} Post-translational modifications include chemical modifications, immobilisations and the synthesis of protein-polymer conjugates.

1.6.6.1 Chemical Modification

Originally chemical modifications were employed to gain information about protein structure and function but the technology has since been utilised to enhance activity and stability of enzymes.¹⁰⁶ Chemical modification strategies aim to increase the stability of enzymes by enhancing the strength of intramolecular bonding.¹⁰⁷ To reduce the potential for loss of activity, the location of the modification needs to be carefully considered as many amino acids are vital for enzymatic functionality. As environmental conditions can also impact upon an enzyme's activity, reaction conditions and reagents also require thoughtful selection. Two methodologies of chemical modification have been highlighted to be effective at inducing higher stabilities within protein species: introducing cross-links and altering the surface charge.¹⁰⁶

Naturally occurring covalent cross-links such as disulfide bonds are commonly present within many native enzymes and provide a significant contribution to the stabilisation of enzymes.¹⁰⁸ Although the introduction of covalent cross-links is thought to destabilise structures with regards to their entropy, the significant increase in enthalpy governs the increase in stability observed in many cases.¹⁰⁹ The introduction of permanent cross-links has been observed to increase protein's stability in regards to catalytic half-life and denaturation temperature. Ryan *et al.* introduced new

permanent cross-linking in HRP by employing bis(*N*-hydroxysuccinimide ester) species with varying core domain functionality.¹¹⁰ Although the specific placement of the cross-linkers was not discussed, inter-protein cross-linking was not observed and only one free L-lysine amino group was found to be present in the final enzymatic species. Catalytic half-life of species modified with suberic acid bis(*N*-hydroxysuccinimide ester) (SA-NHS) were enhanced 6-fold compared with the native species (Figure 1.16). Altering the core domain to an ethylene glycol derivative (EG-NHS) was observed to further enhance stability with an increase of 23-fold, without a substantial decrease in initial activity. The main difference between the two species was the distance the cross-linker could span; SA-NHS only spans 11 Å compared with EG-NHS, which can span 14 Å. This suggests the length of the cross-linker is a key parameter in designing stable cross-linked proteins.

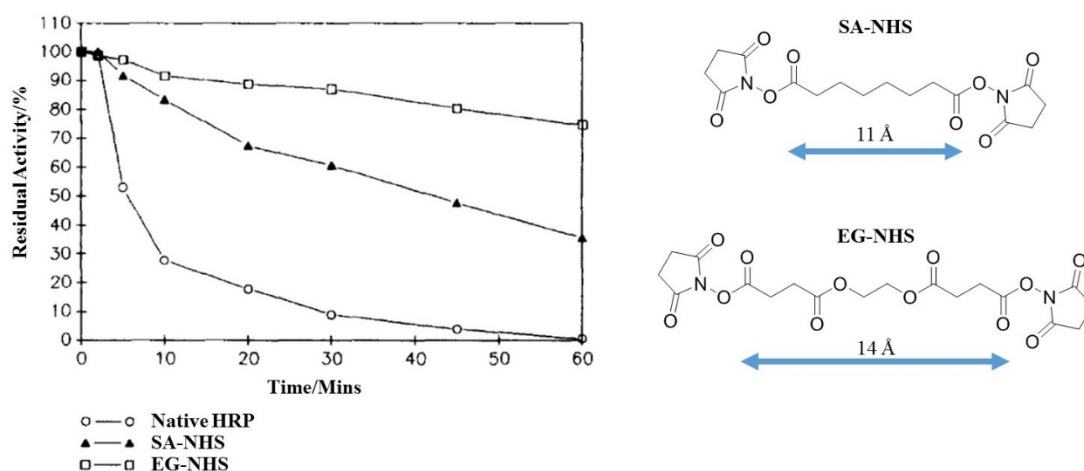


Figure 1.16 Residual activity of HRP with bis(*N*-hydroxysuccinimide ester) cross-linkers. Adapted from Ryan *et al.*¹¹⁰

It has been shown that chemical modification by cross-linking can be combined with protein engineering to generate novel sites in close proximity that can be cross-linked post translation. Indeed, Muheim *et al.* combined the two techniques to generate crosslinking within cytochrome C through chelation of ruthenium ions.¹¹¹ In cytochrome C, the side chains of amino acid residues of 39 and 58 are in close three dimensional proximity and therefore through protein engineering

were both expressed as L-histidine residues to generate the mutant enzyme, H39H58 cytochrome C. The coordination of ruthenium within the mutant species was observed to increase the denaturation temperature from 56.3 °C, observed in the wild type protein, to 72.8 °C. Without the presence of ruthenium, a decrease of 6.7 °C in denaturation temperature was reported in comparison to the wild type enzyme. This supports the theory that the enhancement observed is directly related to the presence of ruthenium cross-linking.

The second type of chemical modification involves the alteration of the surface charge densities, which can be implemented by the introduction of either non-polar or polar residues.¹⁰⁶ The introduction of non-polar residues can enhance the stability of the enzyme by strengthening the hydrophobic interactions found within the tertiary structure of the protein. In contrast, the conversion of residues to contain more hydrophilic or polar species can allow the formation of additional hydrogen bonding interactions and thus enhancing the stability. Additionally, Mozahaev *et al.* hypothesise that the addition of hydrophilic residues can protect hydrophobic segments of the native protein from unfavourable interactions with the surrounding water leading to an increase in stability.¹¹²

The successful stabilisation of many proteins has been achieved by modifying the residues upon the surface of the protein including HRP, trypsin and α -CT.¹¹²⁻¹¹⁴ For example, Melik-Nubarov *et al.* modified varying amounts of the L-lysine residues within α -CT by reductive alkylation (Figure 1.17).¹¹⁴ The resulting alkylated α -CT species all possessed a higher degree of stability than the wild type α -CT. A positive correlation was also observed between the degree of modification and the enhancement of stability.

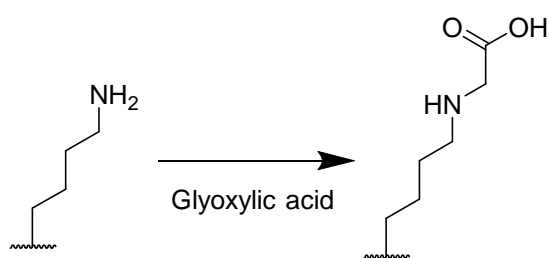


Figure 1.17 Schematic representation of reductive alkylation of L-lysine residues.

1.6.6.2 *Immobilisation*

The process of immobilisation converts enzymes from a soluble species to an insoluble species to increase stability and provide easy purification for industrial processing. In addition to the beneficial properties introduced by chemical modification, immobilisation has the additional advantage of providing the native enzymes with increased rigidity and therefore can withstand harsher conditions before the tertiary structure is affected.¹¹⁵ Enzymes have been immobilised on numerous supports including silica, glycoxy agarose, poly(hydroxyethyl methacrylate) and poly(glycidyl methacrylate).¹¹⁶⁻¹²¹

To allow effective immobilisation of the enzymes, the support must not form unfavourable interactions with the enzyme. The effectiveness of immobilisation on activity and stability can be quantified by two key parameters; immobilisation yield and stability factor. Immobilisation yield is used to quantify the number of enzymes that have been successfully immobilised on to a support; the yield represents the fraction of immobilised enzyme that retains catalytic activity. Stability factor quantifies an enzyme's ability to retain activity in comparison to the native enzyme at various conditions; the factor is calculated by a ratio between the half-life of the native enzyme and the immobilised enzyme.

Enzymes can be immobilised through non-covalent adsorption or the formation of covalent bonds. The most common enzymes employed for non-covalent adsorption immobilisation are lipases as a result of hydrophobic interactions between residues surrounding the active site facilitating the adsorption.^{120, 122} The immobilisation of enzymes can fix the conformation of an

enzyme so it maintains an active conformation.¹²³ Lipases have an inactive conformation in which the active site is shielded by a “lid”; in the presence of hydrophobic droplets the “lid” moves to reveal the active site and possible sites for adsorption.^{124, 125}

Yang *et al.* highlighted that non-covalent attachment methods can enhance stability of lipases to a greater extent than covalent techniques.¹²¹ Indeed, they immobilised *Arthrobacter* lipase on to the surface of glutaraldehyde-modified silica particles using non-covalent and covalent interactions and studied the resulting stability of the lipase (Figure 1.18). Lipase bound by covalent interactions was observed to reduce in activity to 33% of the initial activity when exposed to vinyl acetate at 60 °C for 16 hours. However, lipase that was connected to the silica particles by non-covalent hydrogen bonding was observed to retain 42% of the initial activity. It was hypothesised that the covalent linkages could disrupt the surface charge distribution or the tertiary structure of the protein.

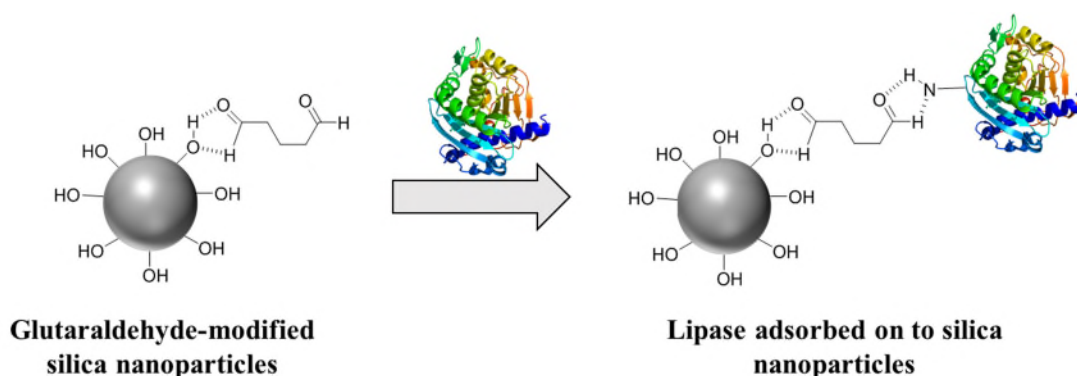


Figure 1.18 Schematic representation of the adsorption of lipase onto glutaraldehyde-modified silica nanoparticles. Reproduced from Jesionowski *et al.*¹²⁰

As the bonds involved in non-covalent immobilisations are mainly weak van der Waals interactions, they are easily disrupted and leaching of enzymes can occur into solution.¹²⁶ As a result of the weak attachment, extensive research has been conducted into immobilisation employing stronger covalent interactions. Although single covalent interactions can provide some stability, multi-point immobilisation, as represented in Figure 1.19, has been observed to be significantly more effective at providing additional stability.¹¹⁵ This is hypothesised to be as a

result of the multi-point attachment causing an increase in rigidity of the enzyme. For example, Fernandez-Lafuente *et al.* covalently attached thermophilic esterase to the surface of glyoxyl agarose gels by both single and multipoint attachment.¹¹⁶ The enzymes were covalently bound to the support through the amine groups from the L-lysine residues on the surface of the esterase. The amine residues react with the glyoxyl groups on the support to form stable amide bonds; the density of glyoxyl groups on the surface was modified to create both single and multi-bound enzymes. The stabilisation factor for the singly immobilised esterase was 550 at pH 5 compared with a stabilisation factor of 30,000 for a multi-point immobilised enzyme, which is over a 50-fold improvement in stability.

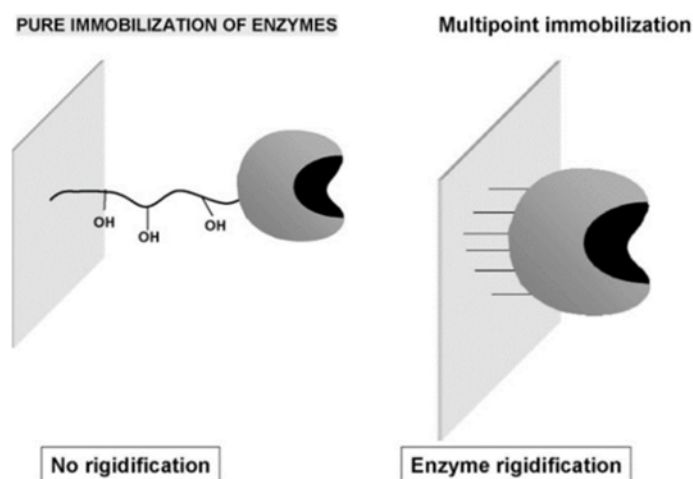


Figure 1.19 Schematic representation of the effect of single point and multipoint immobilisation on enzyme rigidity. Taken from Fernandez-Lafuente *et al.*¹¹⁶

Immobilisation is a technique that is compatible with other stabilisation methods; the production of an enhanced stability enzyme *via* protein engineering or a stable extremophile enzyme can be further stabilised by the immobilisation of the enzyme by multipoint covalent attachment. Indeed, Tardioli *et al.* have successfully immobilised the extremophile enzyme, *Thermoanaerobacter* cyclomaltodextrin glucanotransferase, on to glyoxyl agarose gel;¹¹⁸ the immobilised enzyme exhibits similar activity to that of the free enzyme but has an increase in optimum operating temperature by 10 °C.

1.7 Protein-polymer Conjugates

Although polymers are effective as additives in formulations to stabilise enzymes, the efficiency can be greatly improved when the polymer is covalently conjugated to the enzyme surface. In contrast to immobilisation, protein-polymer conjugates remain soluble in aqueous solutions. The Davis group pioneered the conjugation of synthetic polymers to the surface of proteins with the conjugation of PEG to bovine serum albumin, where they observed the enhanced properties including increased solubility, longer circulation times *in vivo*, and decreased immune response.¹²⁷ Since the initial discovery of protein-polymer conjugates (PPCs) beneficial characteristics, PEG has been bio-conjugated to a variety of biomolecules and furthermore, has also been incorporated into many pharmaceuticals that are both FDA-approved and widely available.¹²⁸⁻¹³²

Following the successful synthesis and beneficial properties of PEGylated proteins, the formation of PPCs has been studied employing numerous polymers and proteins.^{133, 134} PPCs have been shown to provide stability against many external factors and stimuli including pH, temperature and lyophilisation. For example, Depp *et al.* reported an enhancement of catalytic stability of α -CT from 0% to 70% after 48 hours at 37 °C following the formation of a PPC with three grafted poly(*N*-2-hydroxypropylmethylacrylamine) chains.¹³⁵

The formation of a PPC can provide enhanced stability compared to that of an unbound polymeric additive, although the effect can be dependent upon concentration. An example is provided by Mancini *et al.*;¹³⁶ they synthesised PPCs from lysozyme and unbound polymers containing trehalose pendent groups with various molecular weights by reversible addition-fragmentation chain-transfer polymerisation. Lysozyme was examined for stability towards lyophilisation with unbound polymer at concentrations equal to, and 100-fold to, that present within the PPC species. At all molecular weights investigated, PPCs were found to be over 50% more effective at providing stabilisation than the unbound polymer present at the same concentration to the PPC species. However, upon increasing the concentration of the unbound polymer to 100-fold that of

the PPC, both systems were found to be similar in stabilising effect. As a result of the growing interest in the field of PPCs, the subject has been extensively reviewed, most recently by Pelegri-O’Day and Maynard.^{129, 137-141}

1.7.1 Polymerisation Techniques

The development of polymerisation techniques has allowed the scope of possible PPCs to expand greatly with access to a larger number of potential monomers and architectures. The field of PPCs expansion can be linked to the introduction and advances in reversible-deactivation radical polymerisation (RDRP) techniques (Figure 1.20).¹⁴⁰ Compared with other living polymerisation techniques, such as living ionic polymerisation, RDRP can afford similar control over the resulting polymeric species without stringent experimental conditions associated with the other techniques.¹⁴²⁻¹⁴⁴ RDRPs have been adapted to a wide range of reaction conditions including variations in temperature, solvent and monomer species whilst maintaining well-defined structures and control over the molecular weight and composition of the polymer.

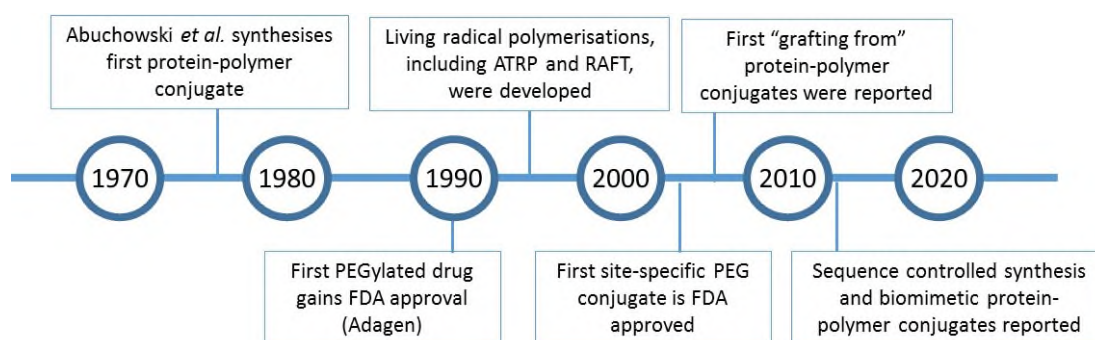


Figure 1.20 Timeline highlighting for advances in protein-polymer conjugates. Reproduced from Pelegri-O’Day *et al.*¹⁴⁰

The most common RDRP techniques employed for the synthesis of PPCs are atom-transfer radical polymerisation (ATRP) and reversible-addition fragmentation chain-transfer (RAFT) polymerisation.¹³⁷ However, there are reports of other polymerisation techniques including ring-opening metathesis polymerisation (ROMP) and ring-opening polymerisations (ROP) achieving successful synthesis of PPC species.¹⁴⁵⁻¹⁴⁷

1.7.1.1 *Atom-Transfer Radical Polymerisation*

ATRP was first demonstrated by both the Sawamoto group and the Matyjaszewski group independently in 1995.^{148, 149} As a result of the potential of the polymerisation technique, ATRP has been reviewed extensively.¹⁵⁰⁻¹⁵² ATRP involves a dormant species with a halide group and a transition metal catalyst capable of accepting the labile halide. The radical species in ATRP is controlled by a reversible redox reaction, which is mediated by a transition metal. Although ATRP is possible with many transition metals including ruthenium,^{148, 153} iron,^{154, 155} molybdenum,^{156, 157} and titanium,¹⁵⁸ copper-catalysed ATRP has dominated this field of research.¹⁵⁹

Many reports have agreed upon an accepted mechanism for ATRP (Figure 1.21).^{149, 159-161} The polymerisation proceeds when the transition metal complex interacts with the dormant species, the organic halide, to generate a radical chain end capable of propagating with monomeric species and an oxidised transition metal complex. This mechanism relies on the equilibrium of the reaction being in favour of the dormant species ($k_{\text{act}} \ll k_{\text{deact}}$) to maintain a low concentration of radicals and therefore minimise termination reactions. Termination reactions can occur through combination of radicals or the abstraction of a hydrogen causing disproportionation. The low concentration of radicals also aids in the control of the narrow molecular distribution associated with RDRP processes.

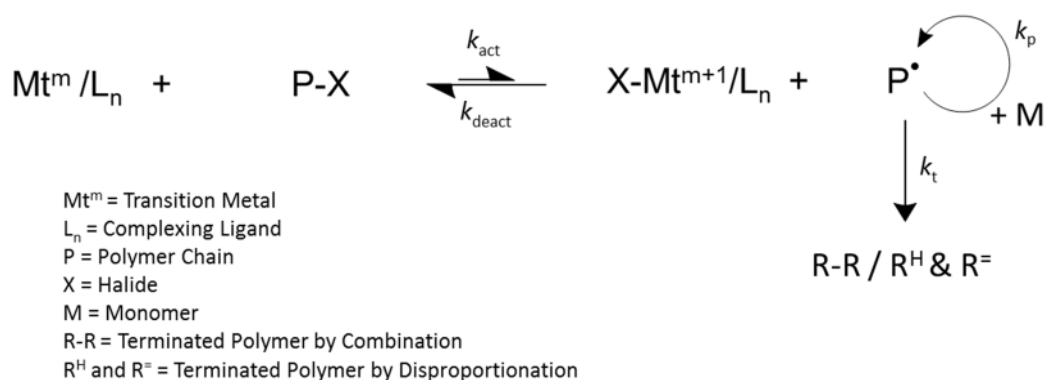


Figure 1.21 Mechanism for ATRP.^{159, 161}

ATRP polymerisation rates are dependent upon the ATRP equilibrium constant, K_{ATRP} , which is defined as the ratio between k_{act} and k_{deact} . K_{ATRP} can be affected by many factors including temperature, solvent, initiator structure, and the metal catalyst/ligand combination.¹⁶²⁻¹⁶⁴ Nitrogen-based ligands have found to be produce successful catalysts for ATRP when combined with transition metals. The number of nitrogen atoms present within the ligand has found to have a significant impact on K_{ATRP} and ligands that have a higher nitrogen content have been found to be more active ATRP catalysts. Additionally, Tang *et al.* have investigated many different nitrogen-based ligands and calculated their K_{ATRP} within a copper catalysed ATRP process (Figure 1.22). This enabled them to draw comparisons based upon not only nitrogen content but also the introduction of branched and cyclic structures within the ligand species.

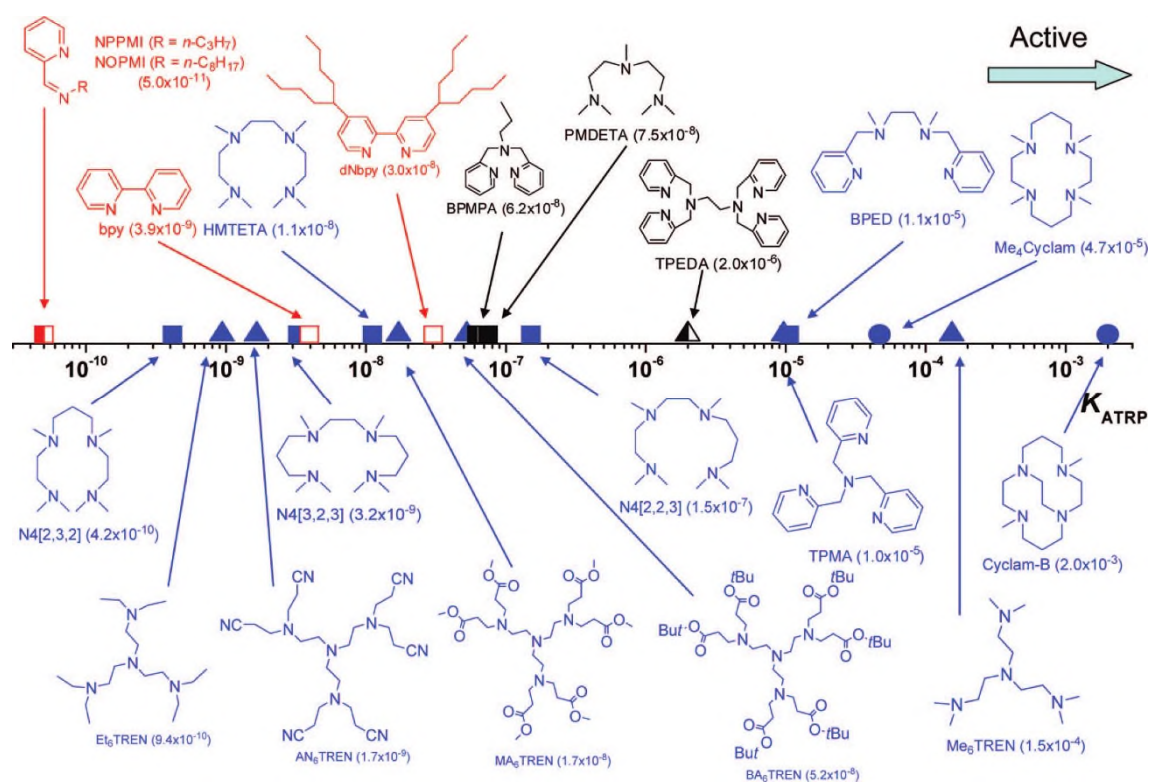


Figure 1.22 ATRP equilibrium constants, K_{ATRP} , for various nitrogen-based ligands with the initiator ethyl α -bromoisobutyrate in the presence of Cu(I)Br in MeCN at 22 °C. Colour key:(red) N2; (black) N3 and N6; (blue) N4. Symbol key: (solid) amine/imine; (open) pyridine; (left-half-solid) mixed; (■) linear; (▲) branched; (●) cyclic. Taken from Tang *et al.*¹⁶⁴

The structure of the initiator also affects K_{ATRP} and therefore also needs careful selection. Indeed, Tang *et al.* thoroughly investigated the use of alkyl halides as initiator species.¹⁶⁴ They found that

bromine-based initiators were more active than their chlorine-based equivalents and concluded that the ability of the halogen atom to act as a leaving group was an important factor in controlling the rate of polymerisation. In addition to the nature of the leaving group, the ability of the initiator to form a stable radical species was essential component to an active ATRP process. For example, tertiary alkyl halides were observed to be on average 30-fold larger than their equivalent secondary halide analogues. The structure of the ATRP initiator can be altered to create different structures including linear, branched, and polymeric stars. The use of trifunctional and tetrafunctional initiator species form star-based polymers upon polymerisation accessing these morphologies without requiring post-polymerisation modification techniques.

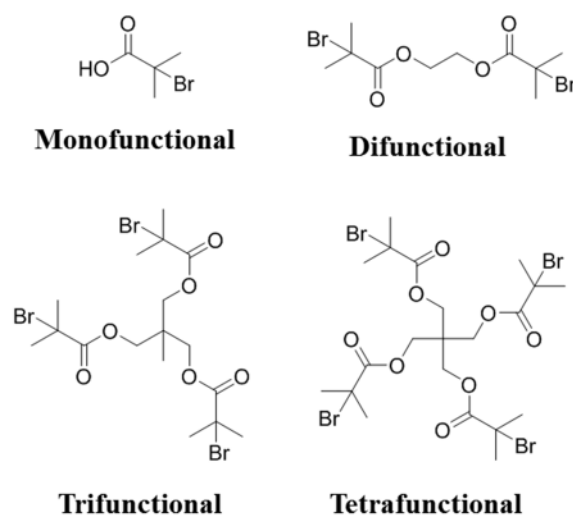


Figure 1.23 Examples of ATRP initiator structures employed to form linear, branched, or polymeric star morphologies.

ATRP has numerous applications due to its simple experimental set up, inexpensive copper catalysts and commercially available ligands and initiators. The technique is also tolerant of many functional groups and so can be applied to a wide range of monomers including acrylates, methacrylates, styrenes, and acrylonitriles.¹⁶⁵ However, one of the main concerns that is raised about the commercialisation of products produced *via* ATRP is the significant presence of the copper metal catalyst, which is required to be removed after the polymerisation.¹⁶⁶ To alleviate these problems, research has been conducted into variants of ATRP that contain lower amounts

of copper including electrochemically mediated ATRP (eATRP),¹⁶⁷ supplemental activator and reducing agent (SARA) ATRP,¹⁶⁸ activators regenerated by electron transfer (ARGET) ATRP,¹⁶⁹ and single electron transfer living radical polymerisation (SET-LRP).¹⁷⁰ Metal-free ATRP was also reported by Treat *et al.*;¹⁷¹ they reported an organic-based photoredox catalyst that was found to catalyse ATRP reactions with activation and deactivation controlled by the presence of light. The resulting polymers had well controlled molecular weights, narrow dispersity and high polymeric chain end fidelity.

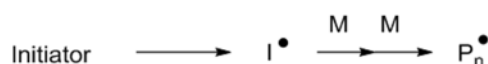
1.7.1.2 Reversible-Addition Fragmentation Chain-Transfer Polymerisation

RAFT polymerisation was first developed by Moad, Rizzardo and Thang in 1998.¹⁷² However, a few months earlier Zard *et al.* introduced the technique of macromolecular design *via* interchange of xanthates (MADIX),^{173, 174} which has since been classified as a sub-type of RAFT polymerisation, which employs xanthates as chain transfer agents (CTAs). RAFT polymerisation techniques are employed as a result of their excellent control over the polymeric architecture and molecular weight distributions. RAFT polymerisation also displays good versatility for a range of solvents and functional monomers.¹⁷⁵ Additionally, RAFT does not use metal complexes, as required for typical ATRP processes, instead requiring the use of a chain transfer agents (CTAs) to mediate the reaction between active (propagating) and stable radical species.

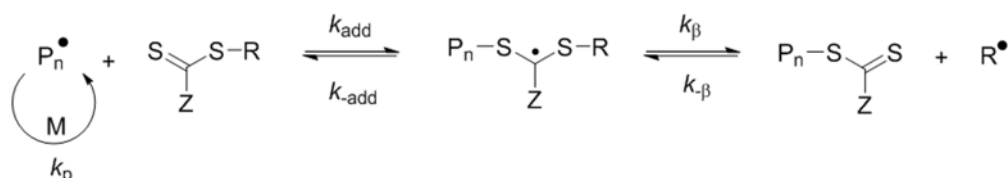
The RAFT mechanism is shown in Figure 1.24.¹⁷⁶ The initiation of the RAFT polymerisation is typically the decomposition of a radical initiator, such as azobisisobutyronitrile (AIBN). The initiator can either be susceptible to thermal decomposition, where temperature is used to initiate the polymerisation, redox reactions, or to photolysis, where a specific wavelength of light is used.¹⁷⁷ The initiator radical reacts with monomer present to form a propagating radical species, which then rapidly adds to the RAFT CTA to stabilise the radical species. The fragmentation of this intermediate can occur reversibly to release either the propagating polymer chain or the reinitiating group (R). Upon fragmentation, the R group is able to initiate polymerisation and form a new propagating polymer chain. Once the reaction contains no free R groups, the system enters

equilibrium between the two propagating polymers. A rapid exchange of dormant and active chains enables all polymer chains to grow at similar rates ensuring a low molecular weight dispersity. Termination reactions can occur through combination and disproportionation, as seen previously with ATRP, though the low concentration of radical species minimises these processes.

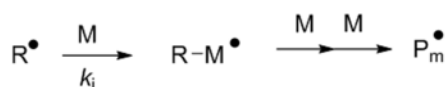
Initiation



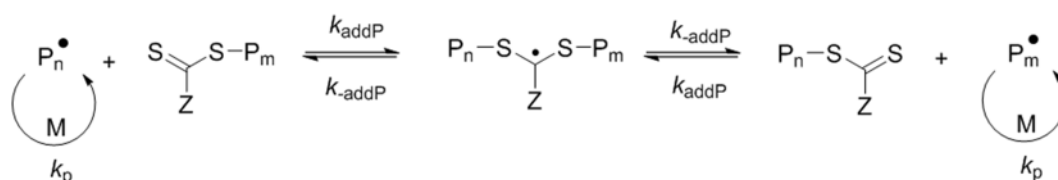
Reversible chain transfer/propagation



Reinitiation



Chain equilibrium/propagation



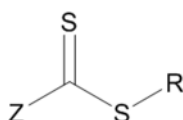
Termination



Figure 1.24 Proposed general mechanism of RAFT/MADIX polymerisation. I = initiator, M = monomer, P = polymer, R and Z = RAFT group functionalities. Reproduced from Moad *et al.*¹⁷⁶

There are a wide variety of RAFT CTA agents available and the selection can significantly affect the ability to synthesise well-defined and well-controlled polymers.^{176, 178} The R and Z groups of the CTA determine the success of the polymerisation. The R group is required to be a good leaving group compared with the propagating polymer chain and is also responsible for the reinitiation

process and so careful selection is required. The nature of the Z group is also important to consider as the group strongly influences the stability of the RAFT CTA. The electron withdrawing or donating properties of the Z group dictate the ability of the CTA to stabilise the propagating radical. Four different groups of RAFT CTA have been reported, identified by the nature of the Z group (Figure 1.25).¹⁷⁸



1. Z = SR, Trithiocarbonate
2. Z = alkyl or aryl, Dithioester
3. Z = NR₂, Dithiocarbamate
4. Z = O-alkyl, Xanthate

R = alkyl or H

Figure 1.25 The generic structure of a RAFT CTA. Taken from Willcock and O'Reilly.¹⁷⁹

Monomers can be classified into two different types, more activated monomers (MAMs) and less activated monomers (LAMs). MAMs, including monomers such as styrenes, acrylates, and methacrylates, require RAFT CTAs with a higher chain transfer constant, i.e. a high rate of chain transfer with respect to the propagating radical, as these monomers form more stable propagating radicals.^{180, 181} In contrast, LAMs, including vinyl acetate and *N*-vinylpyrrolidone, form unstable radical species and therefore it is necessary to employ RAFT CTAs with lower chain transfer constants, such as dithiocarbamates.¹⁸² The selection of both the R and Z group is highly dependent upon the monomer species and extensive research has been conducted to identify compatible pairings of monomers and R and Z groups. Indeed, Moad *et al.* highlighted the preferred R and Z groups for different types of monomer (Figure 1.26).¹⁸²

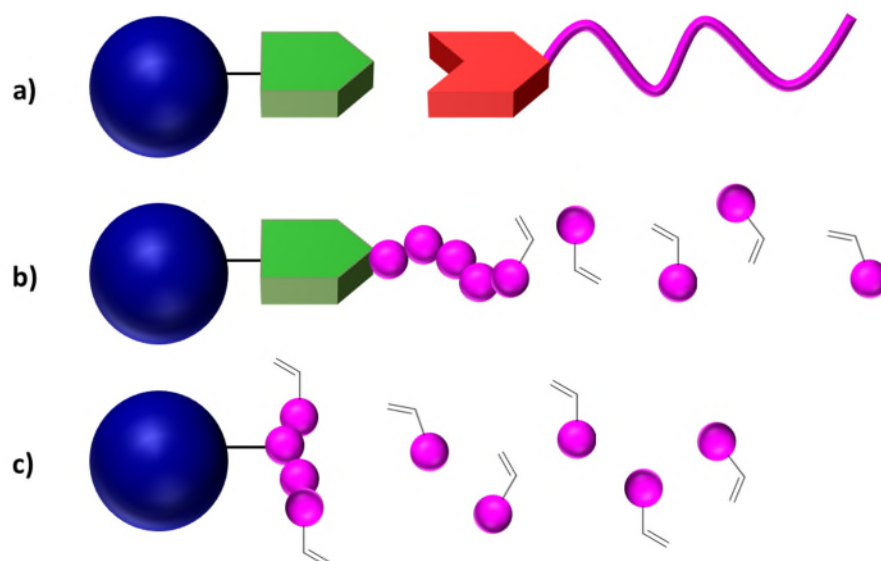


Figure 1.27 Schematic representation of the three main strategies for formation of PPCs: a) “grafting to” b) “grafting from” and c) “grafting through”.

1.7.2.1 “Grafting to”

The “grafting to” approach requires a pre-synthesised polymer chain with a reactive end group, such as an active ester or a disulfide; this allows for reaction with amino acids on the surface in order to form the PPC.^{183, 192-194} The “grafting to” approach is the most commonly used technique as it is possible to make well-defined polymers prior to conjugation, allowing for greater control of the polymeric species.¹⁹⁵ As the polymer is synthesised separately, harsh conditions that may be required during polymerisation do not affect the enzyme, avoiding denaturation during the synthesis.¹⁹⁶

Although the “grafting to” approach is simpler experimentally than “grafting from” or “grafting through” approaches, the products have a large dispersity due to the formation of mono, di, tri and non-conjugated enzymes. Lele *et al.* synthesised PPCs from α -CT and PEG *via* “grafting to” the L-lysine residues on the surface of the α -CT;¹⁹⁷ the MALDI-ToF analysis of the PPCs produced is displayed in Figure 1.28. The spectrum shows the large dispersity and the production of mono, di, and tri-conjugated CTs. In addition, the PPCs synthesised *via* the “grafting to” method often have a lower grafting density than those produced using any other approach owing to the steric hindrance of the polymer chains.¹³⁸ The purification of these “grafting to” reactions

can also be somewhat problematic, as it requires separating out unreacted polymer from the protein-polymer conjugate.

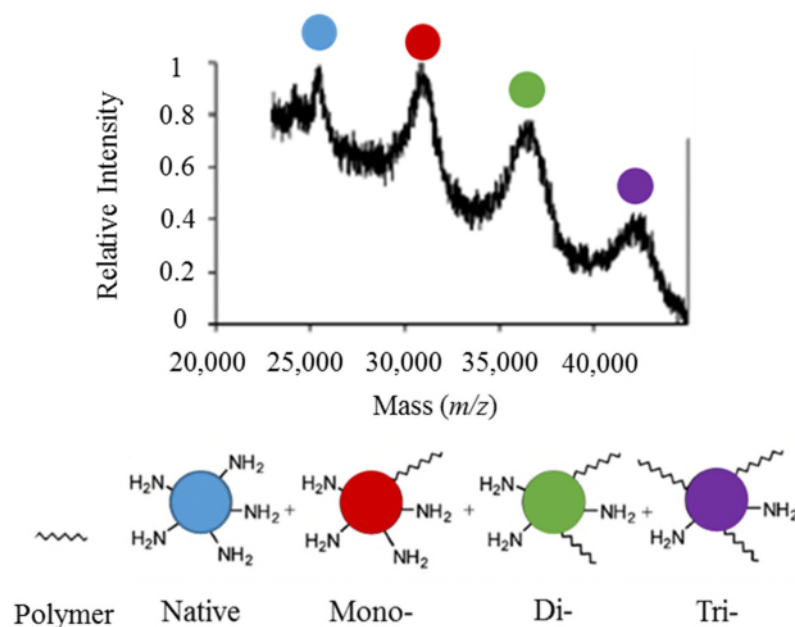


Figure 1.28 MALDI-TOF mass spectrum of α -CT-PEG PPCs synthesised *via* a “grafting to” method. Reproduced from Lele *et al.*¹⁹⁷

1.7.2.2 *In Situ* Formation of Protein-Polymer Conjugates

“Grafting from” and “grafting through” approaches to synthesise PPCs both require an *in situ* polymerisation from the surface of the enzyme. The main feature that distinguishes the two techniques is the functionality that is attached to the surface of the protein. The “grafting from” approach requires an initiator or chain transfer agent to be bound, compared with the “grafting through” approach in which a polymerisable group, for example a vinyl group, is attached to the surface of the protein.^{198, 199} For both of these methodologies, due to the sensitivity of the protein, mild polymerisations conditions need to be utilised to prevent denaturation during polymer synthesis.²⁰⁰ In contrast to the “grafting to” approach that has a major limitation in purification owing to the separation of large polymeric species from the final product, purification of the final PPCs synthesised using “grafting from” and “grafting through” is very simple as it

merely requires the separation of low molecular weight monomeric species or catalysts from the much larger protein-polymer conjugate.

1.7.2.2.1 “Grafting from”

Bontempo *et al.* were among the first to create a protein macro-initiator for use in the synthesis of PPCs *via* a “grafting from” approach.²⁰¹ They exploited the high binding affinity between biotin and streptavidin and successfully attached four biotin-modified ATRP initiators to streptavidin (Figure 1.29). The resulting macro-initiator was employed to grow poly(*N*-isopropylacrylamide) from the surface of the protein.

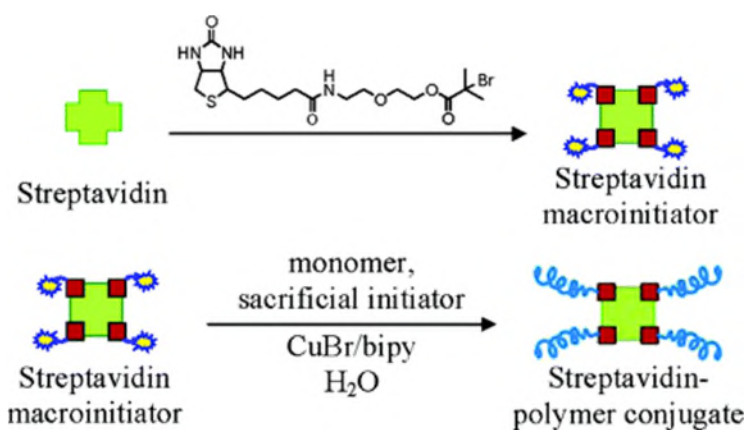


Figure 1.29 Synthesis of a protein macro-initiator for the production of PPCs *via* a “grafting from” approach. Taken from Bontempo *et al.*²⁰¹

Polymers grown from the surface of proteins are difficult to analyse and therefore the use of sacrificial initiators is a common practice when performing ATRP from a surface to enable characterisation of the polymeric species.^{202, 203} Sacrificial initiators are free initiator species incorporated into the reaction to study the polymer species. However, this technique requires the assumption that polymerisations from the surface are occurring at the same rate as the free polymerisation in solution. To alleviate the problems from the use of sacrificial initiators, cleavable linkages have been investigated. Cleavable linkages can be incorporated into the initiator species and can facilitate the removal of the polymers from the protein for post-polymerisation analysis to determine the molecular weight and characteristics of polymers.

For example, Averick *et al.* have successfully attached an ATRP initiator with a cleavable ester linkage (Figure 1.30) to the surface of bovine serum albumin (BSA).²⁰⁰ The BSA macro-initiator was subsequently used to polymerise oligo(ethylene glycol) monomethylether methacrylate (OEGMA) using ATRP. The polymer was then cleaved from the BSA using 5% KOH (w/v) solution through hydrolysis of the ester. In this case, the poly(OEGMA) chains were not affected by the cleavage conditions, but careful consideration is required when selecting reagents for cleavage reactions as to not induce hydrolysis or cause other modifications within the polymer chain.²⁰⁰

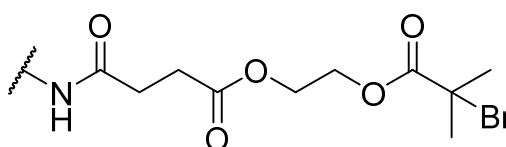


Figure 1.30 Cleavable ATRP initiator employed by Averick *et al.*²⁰⁰

Despite the advantages of the “grafting from” approach, one significant limitation of the technique is the typical initiators and chain transfer agents required for radical polymerisations are insoluble in aqueous conditions. To alleviate this problem, many literature reports indicate the addition of organic solvents to facilitate the conjugation reaction.^{135, 190, 200, 204} However, organic solvents can disrupt the network of bonds that control the tertiary structure of the protein. Indeed, Vinogradov *et al.* found that 20% of the active sites in α -CT were denatured during conjugation to both hydrophobic and hydrophilic substrates when using both DMF-water and ethanol-water mixtures.²⁰⁵

Developments in the synthesis of PPCs has provided two possible solutions to avoid the addition of non-aqueous solvents. The first approach is the development of water soluble initiators, which has been demonstrated by Murata *et al.* and Li *et al.*, synthesising an ATRP initiator and a RAFT CTA, respectively, that can react with primary amine groups present in proteins, through an activated ester, in fully aqueous systems.^{193, 206} The second approach to alleviate this problem can be considered to be a combination of “grafting to” and grafting from”. Falatach *et al.* proposed

an approach to increase the hydrophilicity of the existing initiator species and RAFT CTAs by initially producing short chain oligomers of hydrophilic monomers before conjugation to the protein.²⁰⁷ These oligomers have an increased hydrophilicity and can then be attached to the protein in aqueous environments. The oligomers synthesised are smaller than the polymers typically used in “grafting to” and so steric hindrance is reduced in comparison, resulting in higher grafting densities than those observed in conventional “grafting to” techniques. As block copolymers have successfully been produced from ATRP and RAFT techniques,^{208, 209} this can then be employed to extend the oligomers in a “grafting from” approach.

1.7.2.2.2 “Grafting through”

Similar in nature to “grafting from”, “grafting through” employs an *in situ* polymerisation to form PPC species. The main difference is the moiety attached to the protein is a polymerisable group as opposed to an initiator or CTA. Yan *et al.* employed this approach to synthesise single enzyme nanogels (Figure 1.31).¹⁹⁸ In a two-step process, initially the surface of HRP was chemically modified by acryloylation to provide vinyl groups. The second step was the free-radical polymerisation of acrylamide in the presence of the protein macro-monomer and a crosslinking species. The density of the polymer shell could be increased by performing subsequent polymerisations in the presence of the initial nanogel. The stability of the resulting HRP-nanogels to temperature, methanol, tetrahydrofuran and dioxane was significantly increased compared with free HRP to temperature, methanol, tetrahydrofuran and dioxane. For example, the residual activity of HRP-nanogels after 60 minutes at 65 °C was 90% in comparison to less than 5% for the free enzyme. Additionally, Beloqui *et al.* have stabilised HRP and glucose oxidase using single enzyme nanogels and successfully printed the enzymes to create a two dimensional cascade system.¹⁹⁹

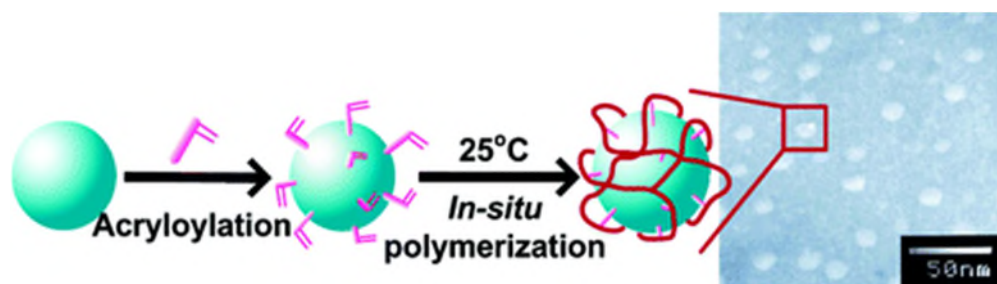


Figure 1.31 Synthesis of single enzyme nanogels *via* the “grafting through” approach. Taken from Yan *et al.*¹⁹⁸

1.7.3 Site-Selectivity

Site-specificity can be an important factor to consider when designing a PPC, as incorrect placement of polymers can block access to an active site or induce unfavourable interactions resulting in aggregation or misfolding of the protein.^{33,35} Single site conjugation can be achieved *via* control over molar ratios but this technique lacks control of the modification location. Site-selectivity can be achieved by the introduction of non-natural groups into the sequence of proteins;²¹⁰ the mutated residues can either provide an initiation point for selective modification or replace a highly reactive residue to allow modification at less reactive sites.²¹¹ For example, Rosendahl *et al.* modified α -interferon (IFN- α) to include a free L-cysteine residue on the protein's surface; it was confirmed by gel electrophoresis that IFN- α was able to undergo mono-site PEGylation without the production of di- or tri- PEGylated products.²¹² In comparison, Yamamoto *et al.* replaced the L-lysine residues in tumor necrosis factor- α with amino acids glycine, L-alanine, L-threonine, and, L-cysteine, so that it retained bioactivity; the replacement allowed the *N*-terminus to be the target of single site PEGylation as the newly introduced amino acids did not contain amine functionalities.²¹³

1.8 Concluding Remarks

In this Chapter, the structures and folding of proteins and enzymes have been discussed, highlighting the interactions present and the spontaneous nature of protein folding. The possible pathways for protein inhibition, denaturation and inactivation have also been introduced to emphasise the unstable nature of protein species and the requirement for enzyme stabilisation technologies. An introduction to the various methodologies for the stabilisation of enzymes has been given with particular attention given to the synthesis of protein-polymer conjugates. From the initial origins and successes of protein-polymer conjugates synthesised *via* PEGylation, the field of protein-polymer conjugates has greatly expanded. The growth of the field has been greatly enhanced by the development of reversible-deactivation radical polymerisations. A review of the potential strategies for the synthesis of protein-polymer conjugates highlighted the effect the synthetic route can have upon the morphology, activity and stability of the resulting conjugate species.

1.9 References

1. T. Bugg, in *Introduction to Enzyme and Coenzyme Chemistry*, Blackwell Publishing Ltd., 2009, pp. 29-50.
2. T. C. Bruice, *Acc. Chem. Res.*, 2002, **35**, 139-148.
3. T. D. H. Bugg, in *Introduction to Enzyme and Coenzyme Chemistry*, John Wiley & Sons, Ltd, 2012, pp. 7-25.
4. M. Hrmova and G. B. Fincher, *Plant Physiol.*, 2001, **125**, 54-57.
5. K. S. Siddiqui and R. Cavicchioli, *Annu. Rev. Biochem.*, 2006, **75**, 403-433.
6. M. Raynal, P. Ballester, A. Vidal-Ferran and P. W. N. M. van Leeuwen, *Chem. Soc. Rev.*, 2014, **43**, 1734-1787.
7. E. Kuah, S. Toh, J. Yee, Q. Ma and Z. Gao, *Chem. Eur. J.*, 2016, **22**, 8404-8430.
8. H. R. Horton, M. Jones, L. A. Moran, R. S. Ochs, D. J. Rawn and K. G. Scrimgeour, *Principles of Biochemistry with Practical Skills in Biology*, Prentice Hall PTR, 2003.
9. J. B. O. Mitchell and J. Smith, *Proteins: Struct., Funct., Bioinf.*, 2003, **50**, 563-571.
10. F. Eisenhaber, B. Persson and P. Argos, *Crit. Rev. Biochem. Mol. Biol.*, 1995, **30**, 1-94.
11. W. H. Zhang, G. Otting and C. J. Jackson, *Curr. Opin. Struct. Biol.*, 2013, **23**, 581-587.
12. T. Hohsaka and M. Sisido, *Curr. Opin. Chem. Biol.*, 2002, **6**, 809-815.
13. A. Deiters, T. A. Cropp, M. Mukherji, J. W. Chin, J. C. Anderson and P. G. Schultz, *J. Am. Chem. Soc.*, 2003, **125**, 11782-11783.
14. E. M. Sletten and C. R. Bertozzi, *Angew. Chem. Int. Ed.*, 2009, **48**, 6974-6998.
15. J. M. Scholtz and R. L. Baldwin, *Annu. Rev. Biophys. Biomol. Struct.*, 1992, **21**, 95-118.
16. S. Kumar and M. Bansal, *Biophys. J.*, 1996, **71**, 1574-1586.
17. R. Aurora, T. P. Creamer, R. Srinivasan and G. D. Rose, *J. Biol. Chem.*, 1997, **272**, 1413-1416.
18. C. L. Nesloney and J. W. Kelly, *Bioorg. Med. Chem.*, 1996, **4**, 739-766.
19. W. Parker and J. J. Stezowski, *Proteins: Struct., Funct., Bioinf.*, 1996, **25**, 253-260.

20. A. Weichsel, J. R. Gasdaska, G. Powis and W. R. Montfort, *Structure*, **4**, 735-751.
21. K. C. Chou and H. A. Scheraga, *Proc. Natl. Acad. Sci. U. S. A.*, 1982, **79**, 7047-7051.
22. H. Fu, G. R. Grimsley, A. Razvi, J. M. Scholtz and C. N. Pace, *Proteins: Struct., Funct., Bioinf.*, 2009, **77**, 491-498.
23. G. D. Rose and R. Wolfenden, *Annu. Rev. Biophys. Biomol. Struct.*, 1993, **22**, 381-415.
24. S. Janeček, *Process Biochem.*, 1993, **28**, 435-445.
25. A. R. Fersht, *Proc. Natl. Acad. Sci. U. S. A.*, 2000, **97**, 1525-1529.
26. C. Levinthal, *J. Chim. Phys. Phys. Chim. Biol.*, 1968, **65**, 44-45.
27. L. Martínez, *J. Chem. Educ.*, 2014, **91**, 1918-1923.
28. K. A. Dill and J. L. MacCallum, *Science*, 2012, **338**, 1042-1046.
29. P. E. Leopold, M. Montal and J. N. Onuchic, *Proc. Natl. Acad. Sci. U. S. A.*, 1992, **89**, 8721-8725.
30. J. N. Onuchic, N. D. Socci, Z. Luthey-Schulten and P. G. Wolynes, *Fold Des.*, 1996, **1**, 441-450.
31. A. R. Fersht, *FEBS Lett.*, 1993, **325**, 5-16.
32. C. M. Dobson, A. Šali and M. Karplus, *Angew. Chem. Int. Ed.*, 1998, **37**, 868-893.
33. A. Smith, *Nature*, 2003, **426**, 883-883.
34. D. Whitley, S. P. Goldberg and W. D. Jordan, *J. Vasc. Surg.*, 1999, **29**, 748-751.
35. C. M. Dobson, *Nature*, 2003, **426**, 884-890.
36. K. A. Dill and H. S. Chan, *Nat. Struct. Mol. Biol.*, 1997, **4**, 10-19.
37. I. M. Klotz, N. R. Langebman and D. W. Dahnall, *Annu. Rev. Biochem.*, 1970, **39**, 25-62.
38. M. Paoli, R. Liddington, J. Tame, A. Wilkinson and G. Dodson, *J. Mol. Biol.*, 1996, **256**, 775-792.
39. L. Michaelis and M. M. L. Menten, *FEBS Lett.*, 2013, **587**, 2712-2720.
40. K. A. Johnson and R. S. Goody, *Biochemistry*, 2011, **50**, 8264-8269.
41. G. E. Briggs and J. B. S. Haldane, *Biochem. J.*, 1925, **19**, 338-339.
42. L. A. Segel and M. Slemrod, *SIAM Rev.*, 1989, **31**, 446-477.
43. H. Lineweaver and D. Burk, *J. Am. Chem. Soc.*, 1934, **56**, 658-666.

44. J. M. Berg, J. L. Tymoczko and L. Stryer, *Biochemistry, Fifth Edition*, W.H. Freeman, 2002.
45. C. González-Bello, *ChemMedChem*, 2016, **11**, 22-30.
46. C. H. Hennekens, M. L. Dyken and V. Fuster, *A Statement for Healthcare Professionals From the American Heart Association*, 1997, **96**, 2751-2753.
47. M. Bala, C. N. Chin, A. T. Logan, T. Amin, L. J. Marnett, O. Boutaud and J. A. Oates, *Biochem. Pharmacol.*, 2008, **75**, 1472-1481.
48. W. W. Cleland, *Biochim. Biophys. Acta*, 1963, **67**, 173-187.
49. A. Cornish-Bowden, *Biochem. J.*, 1974, **137**, 143.
50. M. Dixon, *Biochem. J.*, 1953, **55**, 170.
51. H. Neurath, J. P. Greenstein, F. W. Putnam and J. A. Erickson, *Chem. Rev.*, 1944, **34**, 157-265.
52. G. F. Bickerstaff and H. Zhou, *Anal. Biochem.*, 1993, **210**, 155-158.
53. S. E. Zale and A. M. Klibanov, *Biotechnol. Bioeng.*, 1983, **25**, 2221-2230.
54. A. M. Morris, M. A. Watzky and R. G. Finke, *Biochim. Biophys. Acta*, 2009, **1794**, 375-397.
55. S. S. Deshpande, *Enzyme Immunoassays: From Concept to Product Development*, Springer, 1996.
56. D. A. Parsell and R. T. Sauer, *J. Biol. Chem.*, 1989, **264**, 7590-7595.
57. T. Geiger and S. Clarke, *J. Biol. Chem.*, 1987, **262**, 785-794.
58. N. E. Robinson, *Proc. Natl. Acad. Sci. U. S. A.*, 2002, **99**, 5283-5288.
59. H. Bisswanger, *Perspect. Sci.*, 2014, **1**, 41-55.
60. J. P. Cardoso, *Brit. Polym. J.*, 1986, **18**, 333-339.
61. N. Gurung, S. Ray, S. Bose and V. Rai, *BioMed Res. Int.*, 2013, **2013**, 18.
62. H. S. Olsen and P. Falholt, *J. Surfactants Deterg.*, 1998, **1**, 555-567.
63. H. Pourzolfaghar, F. Abnisa, W. M. A. W. Daud and M. K. Aroua, *Renew. Sustainable Energy Rev*, 2016, **61**, 245-257.
64. A. M. Klibanov, in *Adv. Appl. Microbiol.*, Academic Press, 1983, vol. 29, pp. 1-28.
65. P. V. Iyer and L. Ananthanarayan, *Process Biochem.*, 2008, **43**, 1019-1032.
66. C. Ó'Fágáin, *Biochim. Biophys. Acta*, 1995, **1252**, 1-14.
67. C. Ó'Fágáin, *Enzyme Microb. Technol.*, 2003, **33**, 137-149.

68. L. J. Rothschild and R. L. Mancinelli, *Nature*, 2001, **409**, 1092-1101.
69. A. K. Mandal, W. D. Cheung and J. M. Arguello, *J. Biol. Chem.*, 2002, **277**, 7201-7208.
70. M. Shimomura, M. Ohta, N. Sugiyama, K. Oshima, T. Yamauchi and S. Miyauchi, *Polym. J.*, 1999, **31**, 274-278.
71. C. Vieille and G. J. Zeikus, *Microbiol. Mol. Biol. Rev.*, 2001, **65**, 1-43.
72. A. Szilágyi and P. Závodszky, *Structure*, 2000, **8**, 493-504.
73. M. Tiberti and E. Papaleo, *J. Struct. Biol.*, 2011, **174**, 69-83.
74. L. Menéndez-Arias and P. Argosf, *J. Mol. Biol.*, 1989, **206**, 397-406.
75. G. Bohm and R. Jaenicke, *Int. J. Pept. Protein Res.*, 1994, **43**, 97-106.
76. G. Vogt and P. Argos, *Fold Des.*, 1997, **2**, S40-S46.
77. G. Vogt, S. Woell and P. Argos, *J. Mol. Biol.*, 1997, **269**, 631-643.
78. A. Fersht and G. Winter, *Trends Biochem. Sci.*, **17**, 292-294.
79. C. E. Stauffer and D. Etson, *J. Biol. Chem.*, 1969, **244**, 5333-5338.
80. D. A. Estell, T. P. Graycar and J. A. Wells, *J. Biol. Chem.*, 1985, **260**, 6518-6521.
81. J. A. Wells and D. A. Estell, *Trends Biochem. Sci.*, 1988, **13**, 291-297.
82. L. B. Johnson, L. P. Gintner, S. Park and C. D. Snow, *Protein Eng. Des. Sel.*, 2015, **28**, 259-267.
83. V. G. H. Eijssink, A. Bjørk, S. Gåseidnes, R. Sirevåg, B. Synstad, B. v. d. Burg and G. Vriend, *J. Biotechnol.*, 2004, **113**, 105-120.
84. I. Haque, R. Singh, F. Ahmad and A. A. Moosavi-Movahedi, *FEBS Lett.*, 2005, **579**, 3891-3898.
85. F. Secundo, G. L. Barletta, G. Parini and G. Roda, *J. Mol. Catal. B-Enzym.*, 2012, **84**, 128-131.
86. A. M. Klivanov, *Adv. Appl. Microbiol.*, 1983, **29**, 1-28.
87. C. H. Schein, *Nat. Biotechnol.*, 1990, **8**, 308-317.
88. S. R. Trevino, J. M. Scholtz and C. N. Pace, *J. Mol. Biol.*, 2007, **366**, 449-460.
89. J. M. Obón, A. Manjon and J. L. Iborra, *Enzyme Microb. Technol.*, 1996, **19**, 352-360.
90. N. Gheibi, A. A. Saboury, K. Haghbeen and A. A. Moosavi-Movahedi, *J. Biosci.*, 2006, **31**, 355-362.

91. B. Farzamfar, S. Bayanolhagh, F. Mahboudi and M. Zahrai, *Iran. J. Pharm. Res.*, 2010, **6**, 179-184.
92. R. D. Schmid, in *Advances in Biomedical Engineering*, Springer Berlin Heidelberg, Berlin, Heidelberg, 1979, pp. 41-118.
93. A. Marin, D. P. DeCollibus and A. K. Andrianov, *Biomacromolecules*, 2010, **11**, 2268-2273.
94. L. M. Simon, M. Kotormán, G. Garab and I. Laczkó, *Biochem. Biophys. Res. Commun.*, 2002, **293**, 416-420.
95. D. Combes and P. Monsan, *Ann. N. Y. Acad. Sci.*, 1984, **434**, 061-063.
96. S.-H. Yoon and J. F. Robyt, *Enzyme Microb. Technol.*, 2005, **37**, 556-562.
97. J. Lee, E. W. Lin, U. Y. Lau, J. L. Hedrick, E. Bat and H. D. Maynard, *Biomacromolecules*, 2013, **14**, 2561-2569.
98. D. E. Discher and A. Eisenberg, *Science*, 2002, **297**, 967-973.
99. J. N. Israelachvili, D. J. Mitchell and B. W. Ninham, *J. Chem. Soc., Faraday Trans.*, 1976, **72**, 1525-1568.
100. M. Nallani, S. Benito, O. Onaca, A. Graff, M. Lindemann, M. Winterhalter, W. Meier and U. Schwaneberg, *J. Biotechnol.*, 2006, **123**, 50-59.
101. C. G. Palivan, O. Fischer-Onaca, M. Delcea, F. IteI and W. Meier, *Chem. Soc. Rev.*, 2012, **41**, 2800-2823.
102. A. Ranquin, W. Versées, W. Meier, J. Steyaert and P. Van Gelder, *Nano Lett.*, 2005, **5**, 2220-2224.
103. C. Nardin, J. Widmer, M. Winterhalter and W. Meier, *Eur. Phys. J. E Soft Matter*, 2001, **4**, 403-410.
104. K. Inokuchi, N. Mutoh, S.-i. Matsuyama and S. Mizushima, *Nucleic Acids Res.*, 1982, **10**, 6957-6968.
105. R. J. R. W. Peters, M. Marguet, S. Marais, M. W. Fraaije, J. C. M. van Hest and S. Lecommandoux, *Angew. Chem. Int. Ed.*, 2014, **53**, 146-150.
106. G. E. Means and R. E. Feeney, *Bioconjugate Chem.*, 1990, **1**, 2-12.
107. T. E. Creighton, *Protein Function: A Practical Approach*, IRL Press at Oxford University Press, 1997.
108. A. J. Doig and D. H. Williams, *J. Mol. Biol.*, 1991, **217**, 389-398.
109. S. S. Wong and L. C. Wong, *Enzyme Microb. Technol.*, 1992, **14**, 866-874.

110. O. Ryan, M. R. Smyth and C. Ó'Fágáin, *Enzyme Microb. Technol.*, 1994, **16**, 501-505.
111. A. Muheim, R. J. Todd, D. R. Casimiro, H. B. Gray and F. H. Arnold, *J. Am. Chem. Soc.*, 1993, **115**, 5312-5313.
112. V. V. Mozhaev, V. A. ŠikšNis, N. S. Melik-Nubarov, N. Z. Galkantaite, G. J. Denis, E. P. Butkus, B. Y. Zaslavsky, N. M. Mestechkina and K. Martinek, *Eur. J. Biochem.*, 1988, **173**, 147-154.
113. K. R. Bamdad, B; Naderi-Manesh, H; Sadeghi, M, *EXCLI J.*, 2014, **13**, 611-622.
114. N. S. Melik-Nubarov, V. V. Mozhaev, S. Šikšnis and K. Martinek, *Biotechnol. Lett.*, 1987, **9**, 725-730.
115. C. Mateo, J. M. Palomo, G. Fernandez-Lorente, J. M. Guisan and R. Fernandez-Lafuente, *Enzyme Microb. Technol.*, 2007, **40**, 1451-1463.
116. R. Fernandez-Lafuente, D. A. Cowan and A. N. P. Wood, *Enzyme Microb. Technol.*, 1995, **17**, 366-372.
117. R. M. Blanco and J. M. Guisan, *Enzyme Microb. Technol.*, 1988, **10**, 227-232.
118. P. W. Tardioli, G. M. Zanin and F. F. de Moraes, *Enzyme Microb. Technol.*, 2006, **39**, 1270-1278.
119. S. Akgol, G. Bayramoglu, Y. Kacar, A. Denizli and M. Y. Arica, *Polym. Int.*, 2002, **51**, 1316-1322.
120. T. Jesionowski, J. Zdarta and B. Krajewska, *Adsorption*, 2014, **20**, 801-821.
121. G. Yang, J. Wu, G. Xu and L. Yang, *Colloids Surf., B*, 2010, **78**, 351-356.
122. G. Fernandez-Lorente, Z. Cabrera, C. Godoy, R. Fernandez-Lafuente, J. M. Palomo and J. M. Guisan, *Process Biochem.*, 2008, **43**, 1061-1067.
123. R. Fernandez-Lafuente, P. Armisén, P. Sabuquillo, G. Fernández-Lorente and J. M. Guisán, *Chem. Phys. Lipids*, 1998, **93**, 185-197.
124. A. M. Brzozowski, H. Savage, C. S. Verma, J. P. Turkenburg, D. M. Lawson, A. Svendsen and S. Patkar, *Biochemistry*, 2000, **39**, 15071-15082.
125. A. Idris and A. Bukhari, *Biotechnol. Adv.*, 2012, **30**, 550-563.
126. U. Hanefeld, L. Gardossi and E. Magner, *Chem. Soc. Rev.*, 2009, **38**, 453-468.
127. A. Abuchowski, T. van Es, N. C. Palczuk and F. F. Davis, *J. Biol. Chem.*, 1977, **252**, 3578-3581.

128. J. A. Rodríguez-Martínez, I. Rivera-Rivera, R. J. Solá and K. Griebenow, *Biotechnol. Lett.*, 2009, **31**, 883-887.
129. F. M. Veronese, *Biomaterials*, 2001, **22**, 405-417.
130. J. M. Harris and R. B. Chess, *Nat Rev Drug Discov*, 2003, **2**, 214-221.
131. M. L. Nucci, R. Shorr and A. Abuchowski, *Adv. Drug Delivery Rev.*, 1991, **6**, 133-151.
132. F. Fuertges and A. Abuchowski, *J. Controlled Release*, 1990, **11**, 139-148.
133. M. J. Webber, E. A. Appel, B. Vinciguerra, A. B. Cortinas, L. S. Thapa, S. Jhunjhunwala, L. Isaacs, R. Langer and D. G. Anderson, *Proc. Natl. Acad. Sci. U. S. A.*, 2016, **113**, 14189.
134. B. Jung and P. Theato, in *Bio-synthetic Polymer Conjugates*, Springer Berlin Heidelberg, Berlin, Heidelberg, 2013, pp. 37-70.
135. V. Depp, A. Alikhani, V. Grammer and B. S. Lele, *Acta Biomater.*, 2009, **5**, 560-569.
136. R. J. Mancini, J. Lee and H. D. Maynard, *J. Am. Chem. Soc.*, 2012, **134**, 8474-8479.
137. E. M. Pelegri-O'Day and H. D. Maynard, *Acc. Chem. Res.*, 2016, **49**, 1777-1785.
138. B. S. Sumerlin, *ACS Macro Lett.*, 2012, **1**, 141-145.
139. J. D. Wallat, K. A. Rose and J. K. Pokorski, *Polym. Chem.*, 2014, **5**, 1545-1558.
140. E. M. Pelegri-O'Day, E.-W. Lin and H. D. Maynard, *J. Am. Chem. Soc.*, 2014, **136**, 14323-14332.
141. I. Cobo, M. Li, B. S. Sumerlin and S. Perrier, *Nat. Mater.*, 2015, **14**, 143-159.
142. K. Matyjaszewski and J. Spanswick, *Mater. Today*, 2005, **8**, 26-33.
143. N. V. Tsarevsky, B. S. Sumerlin, P. Vana, Y. Yagci, P. Nesvadba, R. Storey, B. Wayland, A. Goto and G. Moad, *Fundamentals of Controlled/Living Radical Polymerization*, Royal Society of Chemistry, 2012.
144. K. L. Heredia and L. A. University of California, *Synthesis of Polymer Bioconjugates Using Controlled Radical Polymerization*, University of California, Los Angeles, 2008.
145. S. A. Isarov, P. W. Lee and J. K. Pokorski, *Biomacromolecules*, 2016, **17**, 641-648.
146. S. A. Isarov and J. K. Pokorski, *ACS Macro Lett.*, 2015, **4**, 969-973.

147. Z. Liu, C. Dong, X. Wang, H. Wang, W. Li, J. Tan and J. Chang, *ACS Appl. Mater. Interfaces*, 2014, **6**, 2393-2400.
148. M. Kato, M. Kamigaito, M. Sawamoto and T. Higashimura, *Macromolecules*, 1995, **28**, 1721-1723.
149. J. S. Wang and K. Matyjaszewski, *Macromolecules*, 1995, **28**, 7901-7910.
150. K. Matyjaszewski, *Macromolecules*, 2012, **45**, 4015-4039.
151. K. Matyjaszewski, *Isr. J. Chem.*, 2012, **52**, 206-220.
152. D. J. Siegwart, J. K. Oh and K. Matyjaszewski, *Prog. Polym. Sci.*, 2012, **37**, 18-37.
153. F. Simal, A. Demonceau and A. F. Noels, *Angew. Chem. Int. Ed.*, 1999, **38**, 538-540.
154. Y. Kotani, M. Kamigaito and M. Sawamoto, *Macromolecules*, 1999, **32**, 6877-6880.
155. R. K. O'Reilly, V. C. Gibson, A. J. P. White and D. J. Williams, *Polyhedron*, 2004, **23**, 2921-2928.
156. E. Le Grogneec, J. Claverie and R. Poli, *J. Am. Chem. Soc.*, 2001, **123**, 9513-9524.
157. S. Maria, F. Stoffelbach, J. Mata, J.-C. Daran, P. Richard and R. Poli, *J. Am. Chem. Soc.*, 2005, **127**, 5946-5956.
158. Y. A. Kabachii, S. Y. Kochev, L. M. Bronstein, I. B. Blagodatskikh and P. M. Valetsky, *Polym. Bull.*, 2003, **50**, 271-278.
159. K. Matyjaszewski and J. Xia, *Chem. Rev.*, 2001, **101**, 2921-2990.
160. Q. Zhang, P. Wilson, Z. Li, R. McHale, J. Godfrey, A. Anastasaki, C. Waldron and D. M. Haddleton, *J. Am. Chem. Soc.*, 2013, **135**, 7355-7363.
161. Y. Wang, Y. Kwak, J. Buback, M. Buback and K. Matyjaszewski, *ACS Macro Lett.*, 2012, **1**, 1367-1370.
162. W. A. Braunecker, N. V. Tsarevsky, A. Gennaro and K. Matyjaszewski, *Macromolecules*, 2009, **42**, 6348-6360.
163. F. Seeliger and K. Matyjaszewski, *Macromolecules*, 2009, **42**, 6050-6055.
164. W. Tang, Y. Kwak, W. Braunecker, N. V. Tsarevsky, M. L. Coote and K. Matyjaszewski, *J. Am. Chem. Soc.*, 2008, **130**, 10702-10713.
165. D. J. Xuereb and R. Raja, *Catalysis Science & Technology*, 2011, **1**, 517-534.

166. K. Matyjaszewski, T. Pintauer and S. Gaynor, *Macromolecules*, 2000, **33**, 1476-1478.
167. A. J. D. Magenau, N. C. Strandwitz, A. Gennaro and K. Matyjaszewski, *Science*, 2011, **332**, 81.
168. Y. Zhang, Y. Wang, C.-h. Peng, M. Zhong, W. Zhu, D. Konkolewicz and K. Matyjaszewski, *Macromolecules*, 2012, **45**, 78-86.
169. W. Jakubowski and K. Matyjaszewski, *Angew. Chem. Int. Ed.*, 2006, **45**, 4482-4486.
170. C. Waldron, A. Anastasaki, R. McHale, P. Wilson, Z. Li, T. Smith and D. M. Haddleton, *Polym. Chem.*, 2014, **5**, 892-898.
171. N. J. Treat, H. Sprafke, J. W. Kramer, P. G. Clark, B. E. Barton, J. Read de Alaniz, B. P. Fors and C. J. Hawker, *J. Am. Chem. Soc.*, 2014, **136**, 16096-16101.
172. J. Chiefari, Y. K. Chong, F. Ercole, J. Krstina, J. Jeffery, T. P. T. Le, R. T. A. Mayadunne, G. F. Meijs, C. L. Moad, G. Moad, E. Rizzardo and S. H. Thang, *Macromolecules*, 1998, **31**, 5559-5562.
173. S. Z. Zard, *Angew. Chem. Int. Ed.*, 1997, **36**, 672-685.
174. M. Destarac, W. Bzducha, D. Taton, I. Gauthier-Gillaizeau and S. Z. Zard, *Macromol. Rapid Commun.*, 2002, **23**, 1049-1054.
175. C. Barner-Kowollik, *Handbook of RAFT Polymerization*, Wiley, 2008.
176. G. Moad, E. Rizzardo and S. H. Thang, *Aust. J. Chem.*, 2012, **65**, 985-1076.
177. M. Chen, M. Zhong and J. A. Johnson, *Chem. Rev.*, 2016, **116**, 10167-10211.
178. S. Perrier and P. Takolpuckdee, *J. Polym. Sci. Part A: Polym. Chem.*, 2005, **43**, 5347-5393.
179. H. Willcock and R. K. O'Reilly, *Polym. Chem.*, 2010, **1**, 149-157.
180. M. Benaglia, J. Chiefari, Y. K. Chong, G. Moad, E. Rizzardo and S. H. Thang, *J. Am. Chem. Soc.*, 2009, **131**, 6914-6915.
181. G. Moad, E. Rizzardo and S. H. Thang, *Chem. Asian J.*, 2013, **8**, 1634-1644.
182. G. Moad, E. Rizzardo and S. H. Thang, *Polymer*, 2008, **49**, 1079-1131.
183. G. N. Grover and H. D. Maynard, *Curr. Opin. Chem. Biol.*, 2010, **14**, 818-827.
184. Y. Qi and A. Chilkoti, *Polym. Chem.*, 2014, **5**, 266-276.
185. C. T. Walsh, S. Garneau-Tsodikova and G. J. Gatto, *Angew. Chem. Int. Ed.*, 2005, **44**, 7342-7372.

186. B. T. Jung, P., *Bio-synthetic Polymer Conjugates*, Springer Berlin Heidelberg, 2013.
187. J. Hu and W. Sebald, *Int. J. Pharm.*, 2011, **413**, 140-146.
188. P. De, M. Li, S. R. Gondi and B. S. Sumerlin, *J. Am. Chem. Soc.*, 2008, **130**, 11288-11289.
189. C. Boyer, V. Bulmus, J. Q. Liu, T. P. Davis, M. H. Stenzel and C. Barner-Kowollik, *J. Am. Chem. Soc.*, 2007, **129**, 7145-7154.
190. K. L. Heredia, D. Bontempo, T. Ly, J. T. Byers, S. Halstenberg and H. D. Maynard, *J. Am. Chem. Soc.*, 2005, **127**, 16955-16960.
191. D. Moatsou, J. Li, A. Ranji, A. Pitto-Barry, I. Ntai, M. C. Jewett and R. K. O'Reilly, *Bioconjugate Chem.*, 2015, **26**, 1890-1899.
192. N. Vanparijs, S. Maji, B. Louage, L. Voorhaar, D. Laplace, Q. Zhang, Y. Shi, W. E. Hennink, R. Hoogenboom and B. G. De Geest, *Polym. Chem.*, 2015, **6**, 5602-5614.
193. H. Li, M. Li, X. Yu, A. P. Bapat and B. S. Sumerlin, *Polym. Chem.*, 2011, **2**, 1531-1535.
194. H. M. Li, A. P. Bapat, M. Li and B. S. Sumerlin, *Polym. Chem.*, 2011, **2**, 323-327.
195. R. P. Johnson, J. V. John and I. Kim, *Eur. Polym. J.*, 2013, **49**, 2925-2948.
196. R. M. Broyer, G. N. Grover and H. D. Maynard, *Chem. Commun.*, 2011, **47**, 2212-2226.
197. B. S. Lele, H. Murata, K. Matyjaszewski and A. J. Russell, *Biomacromolecules*, 2005, **6**, 3380-3387.
198. M. Yan, J. Ge, Z. Liu and P. Ouyang, *J. Am. Chem. Soc.*, 2006, **128**, 11008-11009.
199. A. Beloqui, S. Baur, V. Trouillet, A. Welle, J. Madsen, M. Bastmeyer and G. Delaittre, *Small*, 2016, **12**, 1716-1722.
200. S. Averick, A. Simakova, S. Park, D. Konkolewicz, A. J. D. Magenau, R. A. Mehl and K. Matyjaszewski, *ACS Macro Lett.*, 2012, **1**, 6-10.
201. D. Bontempo and H. D. Maynard, *J. Am. Chem. Soc.*, 2005, **127**, 6508-6509.
202. K. Matyjaszewski, P. J. Miller, N. Shukla, B. Immaraporn, A. Gelman, B. B. Luokala, T. M. Siclovan, G. Kickelbick, T. Vallant, H. Hoffmann and T. Pakula, *Macromolecules*, 1999, **32**, 8716-8724.

203. R. Mohammadi Sejoubsari, A. P. Martinez, Y. Kutes, Z. Wang, A. V. Dobrynin and D. H. Adamson, *Macromolecules*, 2016, **49**, 2477-2483.
204. B. B. Zhu, D. N. Lu, J. Ge and Z. Liu, *Acta Biomater.*, 2011, **7**, 2131-2138.
205. A. A. Vinogradov, E. V. Kudryashova, V. Y. Grinberg, N. V. Grinberg, T. V. Burova and A. V. Levashov, *Protein Eng.*, 2001, **14**, 683-689.
206. H. Murata, C. S. Cummings, R. R. Koepsel and A. J. Russell, *Biomacromolecules*, 2013, **14**, 1919-1926.
207. R. Falatach, C. McGlone, M. S. Al-Abdul-Wahid, S. Averick, R. C. Page, J. A. Berberich and D. Konkolewicz, *Chem. Commun.*, 2015, **51**, 5343-5346.
208. S. C. Hong, J.-F. Lutz, Y. Inoue, C. Strissel, O. Nuyken and K. Matyjaszewski, *Macromolecules*, 2003, **36**, 1075-1082.
209. D. J. Keddie, *Chem. Soc. Rev.*, 2014, **43**, 496-505.
210. H. Xiao, A. Chatterjee, S.-h. Choi, K. M. Bajjuri, S. C. Sinha and P. G. Schultz, *Angew. Chem. Int. Ed.*, 2013, **52**, 14080-14083.
211. G. G. Kochendoerfer, *Curr. Opin. Chem. Biol.*, 2005, **9**, 555-560.
212. M. S. Rosendahl, D. H. Doherty, D. J. Smith, S. J. Carlson, E. A. Chlipala and G. N. Cox, *Bioconjugate Chem.*, 2005, **16**, 200-207.
213. Y. Yamamoto, Y. Tsutsumi, Y. Yoshioka, T. Nishibata, K. Kobayashi, T. Okamoto, Y. Mukai, T. Shimizu, S. Nakagawa, S. Nagata and T. Mayumi, *Nat. Biotechnol.*, 2003, **21**, 546-552.

2 Synthesis and Characterisation of Site-Selective Protein Macro-Initiators

2.1 Abstract

The work in this Chapter discusses the effect of pH and concentration on the potential site-specific conjugation of an atom transfer radical polymerisation initiator to a model protease enzyme, α -chymotrypsin. The activity and stability of the resulting macro-initiator species was also investigated; a positive correlation was observed between the initiator grafting density and the thermal stability of the enzyme. In all cases, attachment of the initiating molecule onto the α -chymotrypsin was found to not hinder the enzymatic activity of the latter. Both *N*-hydroxysuccinimide esters and aldehyde conjugation-based chemistries were explored as it was found that residual *N*-hydroxysuccinimide can cause inhibition of the α -chymotrypsin activity while aldehydes lack chemical stability in aqueous media and can cause precipitation of the resulting macro-initiator.

2.2 Introduction

2.2.1 Chemical Modification of Proteins

The modification of proteins is a useful tool to alter their natural behaviour and increase their stability, activity, or cellular uptake.¹⁻³ Proteins consist of amino acids that have various functionalities, many of which can be utilised to introduce non-native groups within a protein.⁴ Examples of such chemical modifications include phosphorylation of alcohol-containing amino acids and reaction of active esters with residues containing nucleophilic moieties.^{5,6} Conjugation of small molecules can also occur *via* L-cysteine residues, either in their free thiol form or by breaking their disulfide bonds and reacting them with a small molecule.^{7,8} In a recent example, Robin *et al.* modified the protein salmon calcitonin by bridging the disulfide bond present in the native protein with a dibromomaleimide functionality, creating a dithiomaleimide fluorescent protein conjugate.⁷

As multiple potential conjugation sites are available on every protein, selective chemistries can be employed to direct the modifications to certain types of residues or specific locations within

the primary sequence. Modification reactions must also be conducted in mild conditions, such as aqueous environments and low temperatures, to prevent denaturation of the protein during these synthetic procedures. One way of directing modification sites is to utilise non-natural amino acids that can undergo reactions that are orthogonal to the natural residues.⁹ Deiters *et al.* successfully incorporated non-natural amino acids *via* protein-engineering containing alkyne and azide functionalities into human superoxide dismutase at five different locations within the protein.¹⁰ They were then able to conjugate dyes to the newly introduced residues without modifying any other residues due to the reaction between azide and alkyne functionalities being bioorthogonal to reactions that can take place between the natural residues.¹¹



Figure 2.1 Schematic representation of examples of non-natural amino acids utilised by Deiters *et al.* that can be reacted using biorthogonal chemistries to natural residues.¹⁰

2.2.2 Post-Translational Modification of Proteins

As the introduction of a non-natural amino acid can be time-consuming and low yielding, many post-translational methods exist to modify proteins in a site-selective manner.¹² Proteins that naturally contain a single residue of interest, for example bovine serum albumin (BSA) contains only one free L-cysteine residue that is not participating in disulfide bonds,¹³ can be utilised to create single-site protein modifications. Bontempo *et al.* successfully modified BSA using a disulfide functionalised poly(hydroxyethylmethacrylate) to synthesise a protein-polymer conjugate with a single site graft.¹⁴

When multiple sites of the same residue or functional group are present on the surface of a protein, other chemistries must be employed to target the required site. Schoffelen *et al.* were able to introduce an azide functionality using a diazotransfer reagent, imidazole-1-sulfonyl azide, to a single site within *Candida antarctica* lipase B (CalB). This was achieved by reducing the pH

during the conjugation to 7.0, allowing only the α -amine at the *N*-terminus to react leaving the other amines present in L-lysine residues unreacted.¹⁵

2.2.3 Synthesis of Polymer-Functionalised Proteins

The attachment of polymers to the surface of proteins to form protein-polymer conjugates (PPCs) was first reported by Abuchowski *et al.*, who modified BSA with poly(ethylene glycol) (PEG), where they observed the enhanced properties including increased solubility, longer circulation times *in vivo*, and decreased immune response.¹⁶ Since the initial discovery of PPCs beneficial characteristics, PEG has been bioconjugated to a variety of biomolecules and furthermore, has also been incorporated into many pharmaceuticals that are both FDA-approved and widely available.¹⁷⁻²¹ The field of polymer-functionalised proteins has expanded rapidly with not only the attachment of PEG but many other functional monomers.²²⁻²⁴

Additionally, various routes to generate PPCs have been explored as they can be synthesised not only by covalently attaching a pre-formed polymer but by performing an *in-situ* polymerisation from the surface of a protein. The conjugation of functionalities required for polymerisations from the surface of a protein has been shown in the literature with a variety of species that can facilitate different types of reversible-deactivation radical polymerisation (RDRP) including atom transfer radical polymerisation (ATRP), reversible addition-fragmentation chain transfer (RAFT) and ring-opening metathesis polymerisation (ROMP).²⁴⁻²⁹ The synthesis of ATRP initiator-containing protein macro-initiators is of high interest as the subsequent polymerisation can be performed in an aqueous environment at low temperatures.³⁰⁻³²

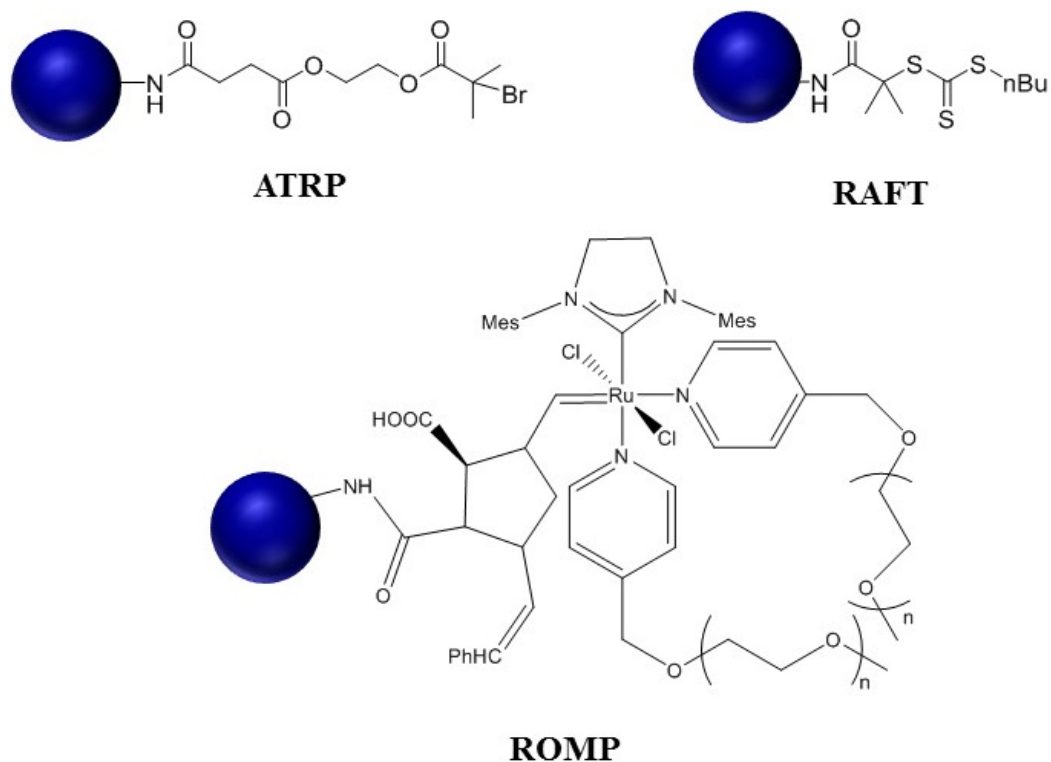


Figure 2.2 Schematic representation of examples of protein macro-initiators utilised in RDRP to form PPCs in literature reports.²⁴⁻²⁶

ATRP initiators with a functional handle that can be used to conjugate them to a protein typically have low water solubility. Many systems require a mixture of water and organic solvents, including dimethyl sulfoxide (DMSO), *N,N*-dimethylformamide (DMF), and dichloromethane, to facilitate a reaction between the initiator and the protein.³³⁻³⁵ The addition of organic solvents can cause denaturation of some enzymatic species as they can disrupt the non-covalent interactions required to form the secondary structure; if the concentration is increased past a certain threshold, it can cause the protein to precipitate.³⁶ Indeed, Wiggers *et al.* found that the addition of only 5% v/v DMSO caused a decrease in the activity of glyceraldehyde-3-phosphate dehydrogenase by 50% thus highlighting the sensitive nature of the exposure of proteins to organic solvents.³⁷ To circumvent solubility and protein denaturing issues, Murata *et al.* developed a novel ATRP initiator that is both water-soluble and can be successfully conjugated to the surface of a

chymotrypsin without the addition of an organic solvent and achieved polymerisations of several monomers including *N,N*-dimethylaminoethyl methacrylate and *N*-isopropylacrylamide.^{38, 39}

2.2.4 Structure and Activation of α -Chymotrypsin

α -Chymotrypsin (α -CT) is a model protease enzyme, which is made up of three separate polypeptide chains that are held together by multiple disulfide bridges, whose stability has been studied in many different conditions including aqueous buffer, human intestinal fluid, and encapsulated in both particles and reverse micelles.^{38, 40-42} α -CT is activated from a zymogen, an inactive enzymatic precursor, chymotrypsinogen.⁴³ As α -CT is secreted by the pancreas in order to aid digestion,⁴⁴ the zymogen allows transport of the enzyme in an inactive form to prevent damage to organs before delivery to the digestive tract. The activation process proceeds *via* two active intermediate species: π -chymotrypsin and δ -chymotrypsin (Figure 2.3). The activation of chymotrypsinogen requires the addition of a second proteolytic enzyme, trypsin.⁴⁵ Trypsin cleaves the peptide bond between Arg15 and Ile16; the cleavage of this bond allows the newly produced *N*-terminus amine group to interact with Glu194 to produce the oxyanion hole required for catalysis to occur.^{46, 47}

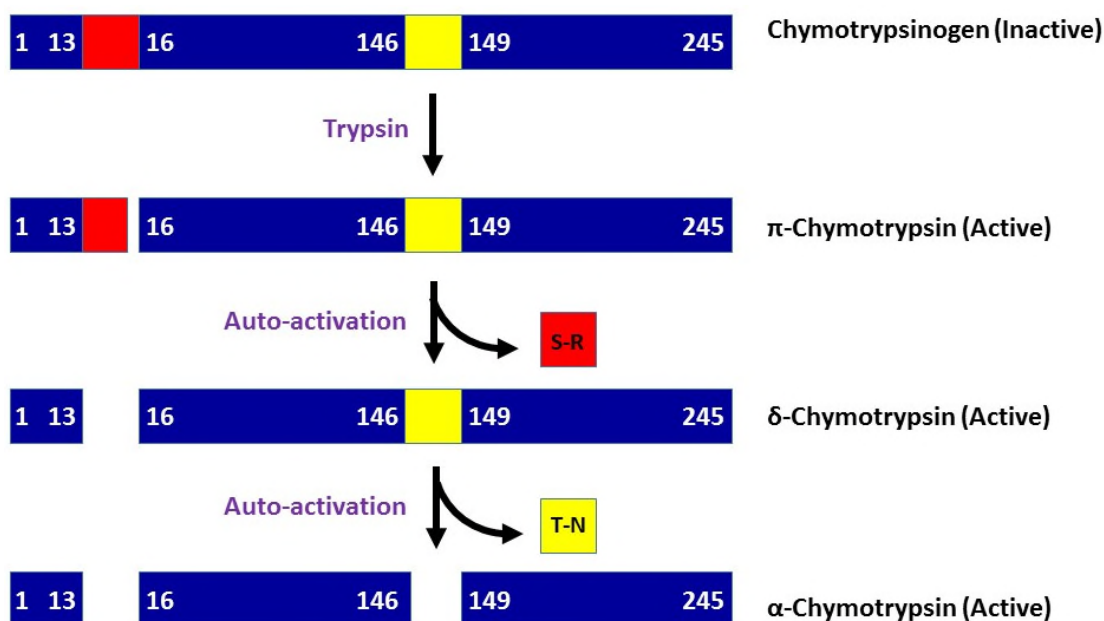
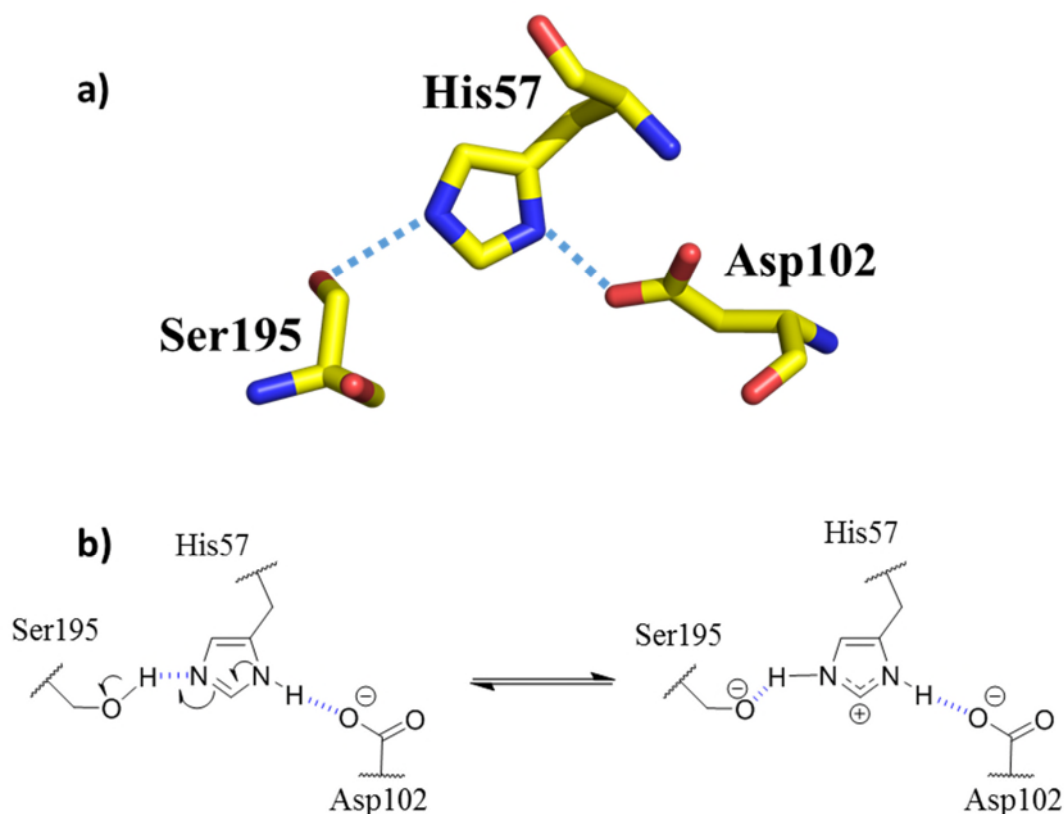


Figure 2.3 Schematic representation of the formation of active α -CT from the inactive zymogen, chymotrypsinogen.

The remaining steps that occur within the activation of α -CT are self-catalysed, or more commonly referred to as auto-activation. π -Chymotrypsin cleaves the bond between Leu13 and Ser14 to release the dipeptide of Ser-Arg and form δ -chymotrypsin. The final process in the activation of chymotrypsinogen is the removal of the dipeptide Thr147-Asn148 to produce species α -CT, which is more stable than either π - or δ -chymotrypsin species.⁴⁸

α -CT is a serine protease, which is a class of enzymes that utilise L-serine as the nucleophilic amino acid within the active site to catalyse the hydrolysis of peptide bonds. α -CT has an active site that consists of three residues, referred to as a catalytic triad, consisting of Ser195, His57, and Asp102 (Figure 2.4).⁴⁹ Enzymes are selective catalysts and certain proteases will only cleave bonds at specific locations within a primary sequence, the selectivity of serine proteases is based on the composition of the S1 pocket., α -CT selectively cleaves peptide bonds next to aromatic residues such as L-phenylalanine, L-tyrosine, and L-tryptophan due to the hydrophobic S1 pocket.^{50, 51}

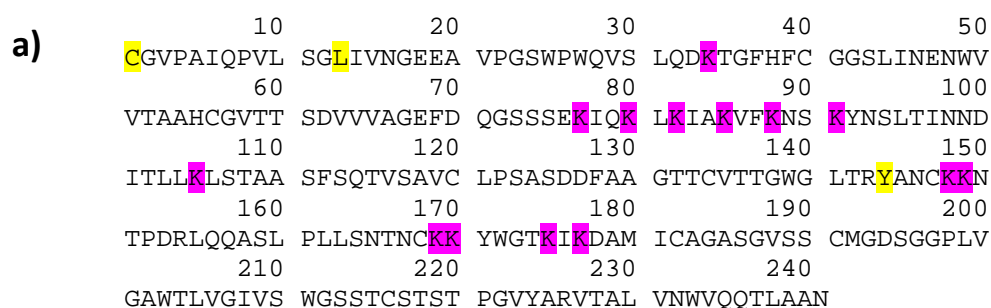


Although much research has already been conducted in the area of post-translational protein modification and synthesis of PPCs, there is still scope for further investigation. Site-specific chemistries tend to only be applicable to certain residues within particular proteins, however this work aims to investigate attachment behaviour and initiator grafting densities and their effect on enzymatic properties with more general chemistries that can direct conjugation by altering environmental factors including concentration and pH.

2.3 Results and Discussion

2.3.1 Conjugation of Initiator to Chymotrypsin

As α -CT has many sites that could be modified to create a protein macro-initiator, this work focuses on the reaction of primary amines, which are located within both the L-lysine residues and the *N*-termini of α -CT. α -CT contains 14 L-lysine residues and 3 *N*-termini; Figure 2.5 highlights the locations of these residues. It is therefore concluded that the potential sites for modification are spread evenly across the surface of the enzyme.



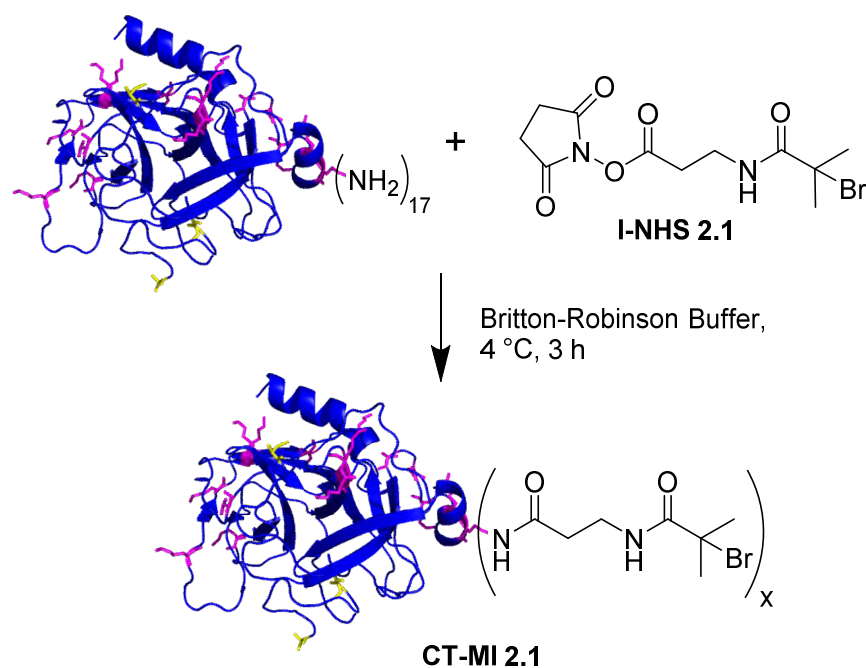
b)



Figure 2.5 a) Primary structure and b) crystal structure (**4CHA**)⁴⁹ of α -CT. L-Lysine residues have been highlighted in pink and the three *N*-termini highlighted in yellow. PDB crystal structure references are identified in bold.

The aim of this study was to investigate effects of grafting density upon both macro-initiators and PPCs and although there are different techniques to synthesise PPCs, to achieve the higher

grafting densities required for this study a “grafting from” approach, which involves an *in situ* polymerisation from the surface of a protein, has been investigated. To allow the production of PPCs *via* a “grafting from” approach, an initiator or chain transfer agent is required to be conjugated to the surface of the protein. To facilitate the reaction between an ATRP initiator species and the α -CT amine residues, active ester chemistry was initially utilised. Murata *et al.* have developed an ATRP initiator (**I-NHS 2.1**, Scheme 2.1) that is fully water-soluble and has an active ester functionality, based upon *N*-hydroxysuccinimide (NHS), that is able to couple with the available amine residues on the surface of α -CT.^{38, 52} In order to establish the conjugation efficiency between initiator and α -CT, **I-NHS 2.1** was dissolved in Britton-Robinson buffer at pH 8.0 using an excess of initiator per amine (3.3 equivalents) and allowed to react with α -CT at 4 °C.⁵³



Scheme 2.1 Schematic representation of primary amines on the α -CT reacting with an NHS active ester, **I-NHS 2.1**, to form **CT-MI 2.1**.

Confirmation of the successful conjugation was achieved by ^1H nuclear magnetic resonance (NMR) spectroscopy and matrix-assisted laser desorption/ionisation time-of-flight (MALDI-ToF) mass spectrometry (Figure 2.6 and Figure 2.7, respectively). In the ^1H NMR

spectrum, the appearance of an additional peak at 1.5 ppm was attributed to the methyl groups the initiator species present in the purified product, however due to the accuracy of the integration of the protein backbone, ^1H NMR spectroscopy cannot quantify the attachment. Furthermore, the native enzyme was found to contain an impurity, a singlet shown highlighted in yellow at 3.0 ppm, which is removed by the conjugation of the initiator process, most likely during the dialysis and ultrafiltration of the newly formed **CT-MI 2.1** product.

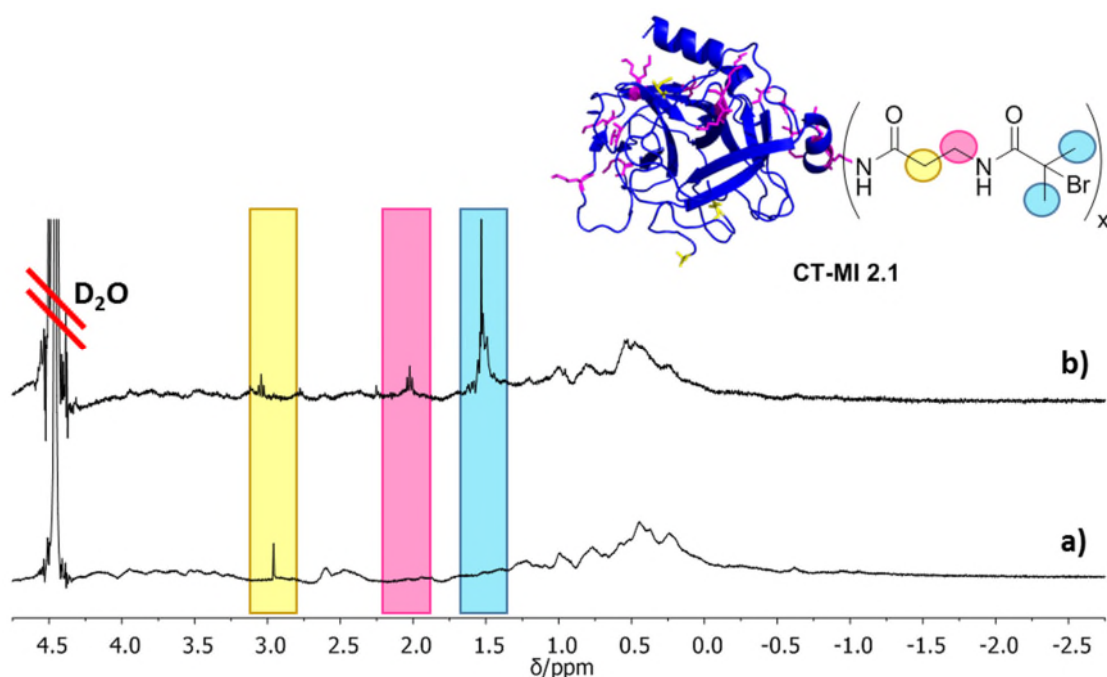


Figure 2.6 ^1H NMR spectra of a) native $\alpha\text{-CT}$ and b) $\alpha\text{-CT}$ macro-initiator species (**CT-MI 2.1**) synthesised using 3.3 eq. of initiator per amine at pH 8.0, in D_2O at 400 MHz. The yellow region highlights the disappearance of an impurity at 3.0 ppm and the blue region highlights the appearance of **I-NHS 2.1** peaks at 1.5 ppm.

MALDI-ToF MS analysis was used to quantify the number of initiators that were bound to $\alpha\text{-CT}$ based on the difference in the molar mass of the detected species before and after the conjugation reaction. When using 3.3 equivalents of **I-NHS 2.1** per amine (*i.e.* 56.1 equivalents per $\alpha\text{-CT}$) and conducting the conjugation reaction at pH 8.0, there was a molar mass difference of 2.9 kDa between native and macro-initiator species. This difference corresponds to an average of 13 ± 3 units covalently bound to the surface of $\alpha\text{-CT}$.

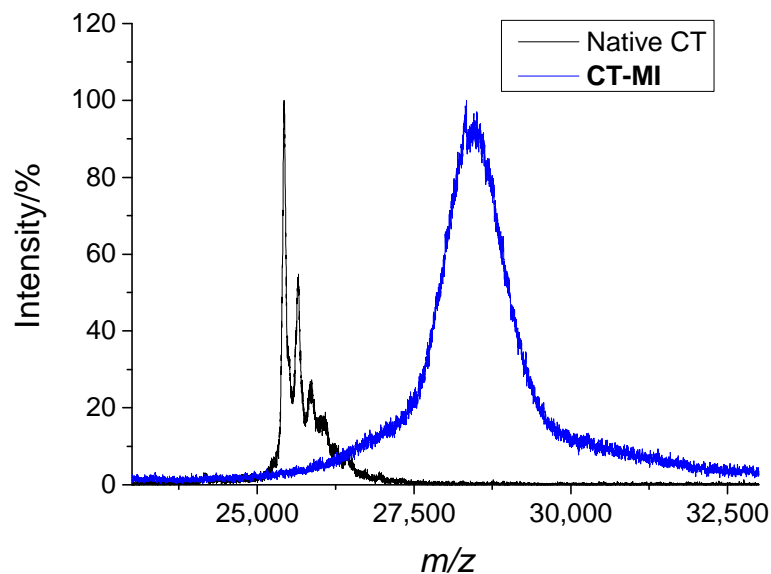


Figure 2.7. MALDI-ToF mass spectra for α -CT and **CT-MI 2.1** recorded using a positive linear mode.

To obtain macro-initiators of varying initiator grafting density, it was hypothesised that it would be possible to sample a one-pot reaction to obtain a gradient of grafting density over time. In order to establish the reaction kinetics, the conjugation between **I-NHS 2.1** and α -CT was studied over time by extracting samples from the reaction and analysing them by MALDI-ToF MS (Figure 2.8). Although MALDI-ToF mass spectrometry is not typically employed as quantitative analytical technique,^{54,55} when samples are similar in nature, a degree of quantitative analysis can be performed.⁵⁶ This assumption is utilised when fitting the spectra to a Gaussian distribution and extracting the average number of initiators attached to the protein species and the respective error.

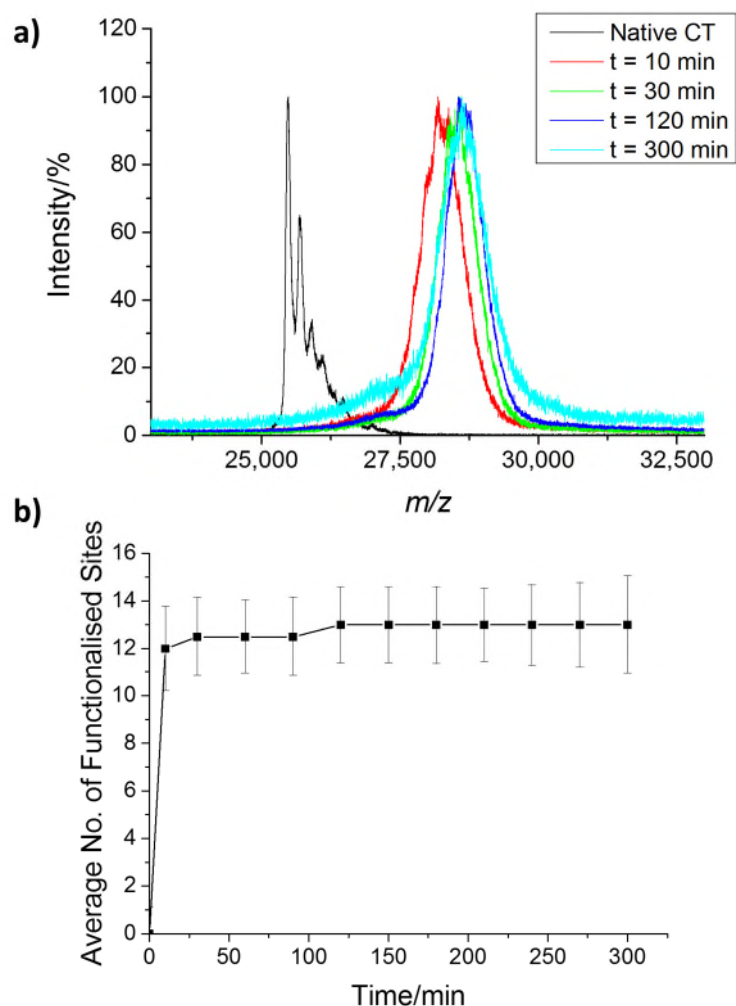


Figure 2.8. a) MALDI-ToF mass spectra and b) Average number of functionalised sites as determined by MALDI-ToF of α -CT at various time intervals after the addition of **I-NHS 2.1**. Error bars are displayed as the standard deviation of the distribution based on the assumption of a Gaussian fit of the MALDI-ToF mass spectra.

The reaction was found to proceed rapidly with 12 sites out of the 17 sites available being modified within 10 minutes. Due to the speed of the reaction, it is not possible to create α -CT with different initiator grafting densities by sampling the reaction with the current conditions.

2.3.2 pH and Concentration Profile of **CT-MI 2.1** Conjugation

It has been previously shown by Liu *et al.* that it is possible to control the number of conjugated sites on α -CT by altering the concentration of the initiator species, who further reported that the modifications on α -CT occurred randomly with no site specificity.⁵⁷ In contrast, Schoffelen *et al.*

were able to synthesise azide-containing proteins using a diazotransfer reagent and control the number and location of the species introduced with the pH of the reaction.¹⁵ Considering these two studies and as a consequence of the nucleophilicity of the reaction between the active ester and the targeted amines, it is postulated that altering the pH at which conjugation occurs will afford control to the α -CT modifications.

To ascertain whether the conjugation to α -CT was dependent upon the pH of the system, CT-MI 2.1s were synthesised using a moderate excess (3.3 equivalents) of I-NHS 2.1 per amine at varying pH values, using Britton-Robinson buffer. The efficiency of the conjugation reaction was assessed after 3 hours using MALDI-ToF mass spectrometry (Figure 2.9 and Table 2.1).

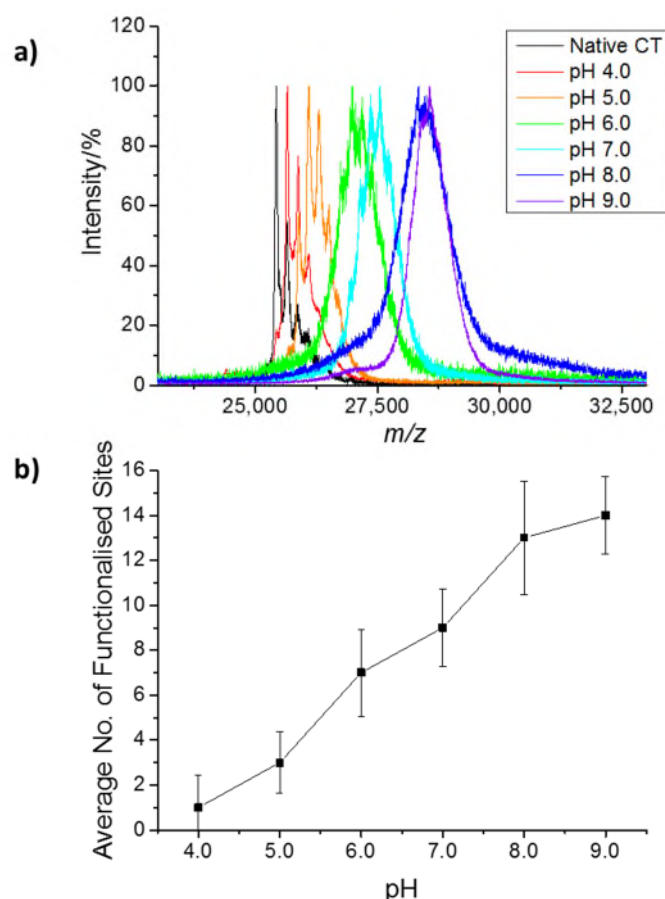


Figure 2.9 a) MALDI-ToF mass spectra of CT-MI 2.1 species synthesised using 3.3 equivalents of I-NHS 2.1 per amine at varying pH values b) Average number of functionalised sites as determined by MALDI-ToF of α -CT at various pH values after the addition of I-NHS 2.1. Error bars are displayed as the standard deviation of the distribution based on the assumption of a Gaussian fit of the MALDI-ToF mass spectra.

Table 2.1 Average degree of attachment of **I-NHS 2.1** initiator for **CT-MI 2.1** species synthesised at varying pH values of initiator as determined by MALDI-ToF analysis. Errors are reported as the standard deviation of the distribution based on the assumption of a Gaussian fit of the MALDI-ToF mass spectra.

	pH at which conjugation occurred					
	4.0	5.0	6.0	7.0	8.0	9.0
Average number of sites functionalised	1 ± 1	3 ± 1	7 ± 2	9 ± 2	13 ± 3	14 ± 2

When conjugating at a pH value of 4.0 only one site was found to be functionalised compared to fourteen sites that were reacted with the active ester at pH 9.0. This observation can be explained by the relative pK_a values of the L-lysine residues within α -CT confirming the stipulation that the nucleophilic reaction between **I-NHS 2.1** and α -CT is pH-dependent.⁵⁸ When the L-lysine residues are above their pK_a and therefore deprotonated, the reaction with the active ester is promoted. The ϵ -amino groups on L-lysine residues have been found to have a higher average pK_a than observed in α -amino groups present at the *N*-termini,⁵⁹ as highlighted by Magni *et al.*, who utilised the lower pK_a of the α -amino group to selectively modify biotin-tumor necrosis factor at pH 5.8. This indicates that conducting conjugations at pH 4.0 has allowed site specific modification of one of the *N*-termini.⁶⁰

In addition to the single site modification at pH 4.0, it was also observed that the number of functionalised sites increased as the pH of the reaction was increased, generating **CT-MI 2.1** species with an average of 1, 3, 7, 9, 13, and 14 initiators attached. Furthermore, as the pH of the conjugation is increased, the degree of functionalisation increases with a relatively linear progression. This introduces the potential of estimating, or possibly targeting, the degree of modification of α -CT by controlling the pH of the conjugation reaction.

Another variable that was hypothesised to have an impact upon the number of sites conjugated was the concentration of initiator species present. In addition to altering the pH that the conjugation occurs, the concentration of the active ester species **I-NHS 2.1** was also varied (Table

2.2 and Figure 2.10), from 0.5 to 6.6 equivalents per amine at pH values 4.0, 6.0, and 8.0. Characterization by MALDI-ToF MS analysis confirmed that attachment occurred in all samples.

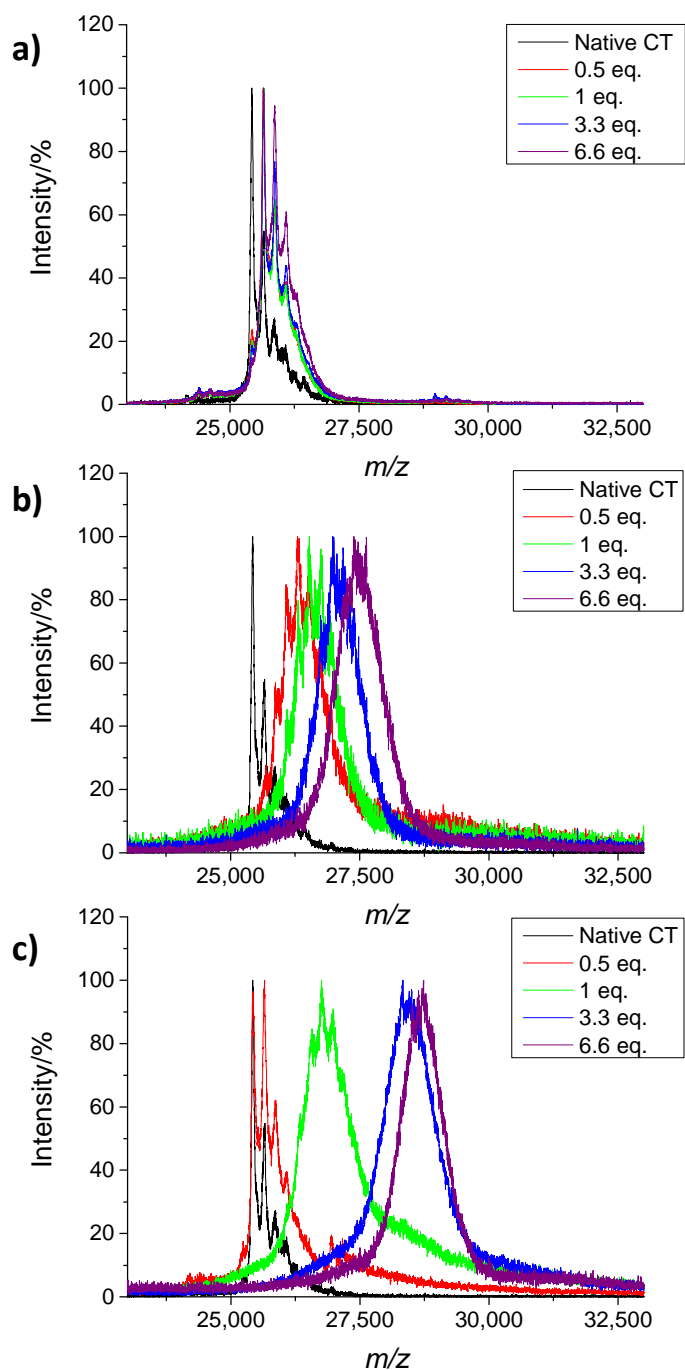


Figure 2.10 MALDI-ToF mass spectra of CT-MI 2.1 species formed at varying concentrations of I-NHS 2.1 when the conjugation reaction was carried out at a) pH 4.0, b) pH 6.0, and c) pH 8.0.

When conjugation was conducted at pH 4.0, the resulting **CT-MI 2.1** species all were found to have a molar mass of 25.7 kDa, an increase of 0.2 kDa compared with native α -CT. This increase indicates that only a single modification site was achieved in this species. Therefore this result indicates that the modification at pH 4.0 is concentration-independent and only one site is nucleophilic enough under these conditions to undergo successful conjugation. In addition to the single addition, the distribution in the MALDI-ToF spectra was found to be narrow compared to samples where the conjugation reaction was carried out at pH 6 or 8, signifying the low dispersity of the number of initiator molecules attached.

Contrary to the observed single-site conjugation obtained at pH 4.0, **CT-MI 2.1s** synthesised at pH 6.0 show an increase in the number of attachments of the initiator upon increasing its concentration. Similarly, conducting the conjugation reaction at pH 8.0 resulted in a similar concentration dependence as at pH 6.0. Moreover, in comparison to reactions occurring at pH 6.0, pH 8.0 conjugations were found to reach much higher degrees of modification (up to 14 initiator units). The overall trend with the observed data is that an increase in pH leads to an increase in sites conjugates, however, when conjugating using 0.5 equivalents of initiator per amine, the obtained average degree of attachment at pH 8.0 was lower than pH 6.0. This was possibly due to changes in the overall tertiary structure of α -CT that take place within the protein once it reaches its point of ionisation (pI). Furthermore, it is also observed that the distribution of the **CT-MI 2.1s** produced at a higher pH have an increased dispersity in comparison to their counterparts synthesised at lower pH values.

Table 2.2. Average degree of attachment of I-NHS 2.1 initiator for CT-MI 2.1 species synthesised at varying pH values and concentrations of initiator as determined by MALDI-ToF analysis. Errors are reported as the standard deviation of the distribution based on the assumption of a Gaussian fit of the MALDI-ToF mass spectra.

	Equivalents of Initiator Added per Amine			
	0.5	1	3.3	6.6
pH 4.0	1 ± 1	1 ± 1	1 ± 1	1 ± 1
pH 6.0	4 ± 2	5 ± 2	7 ± 2	9 ± 2
pH 8.0	<1 ± 2	6 ± 3	13 ± 3	14 ± 2

By utilising activated ester chemistry, the synthesis of α -CT with a tuneable initiator grafting density has been achieved. The initiator grafting density has been shown to be altered not only through variations in concentration but also the pH at which the reaction is conducted effectively affects the reactivity of the primary amines.

2.3.3 Continuous Formation of Intermediates

The samples analysed in the previous Section 2.3.2 were all prepared separately and so the aim of the subsequent work was to be able to design a system in which all the macro-initiators with varying initiator grafting densities were synthesised in a single continuous fashion. The conditions used were identical to those previously described but with the samples being exposed to conjugation conditions for one hour and then the pH increased by 2 units. Samples were taken for MALDI-ToF MS analysis before each pH change and the results are summarised in Figure 2.11 and Table 2.3.

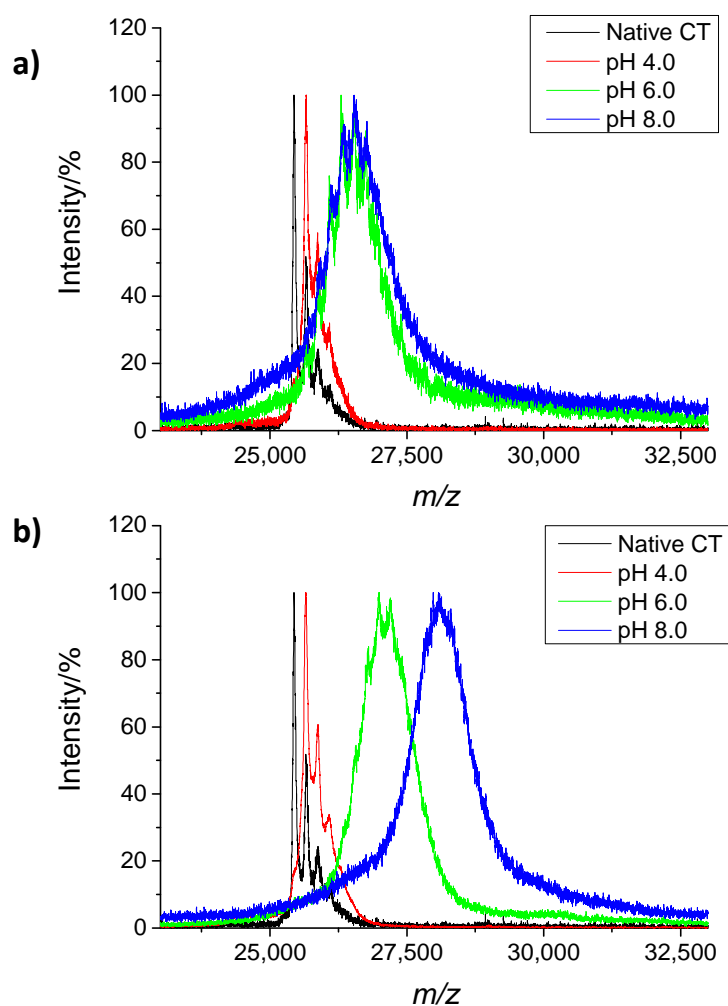


Figure 2.11 MALDI-TOF mass spectra of **CT-MI 2.1** species formed in a continuous manner using a) 1 equivalent and b) 3.3 equivalents of initiator of **I-NHS 2.1** per amine.

Table 2.3 Average degree of attachment of the initiator species onto α -CT forming **CT-MI 2.1** in a single continuous manner with varying concentrations of initiator and solution pH, as determined by MALDI-ToF MS analysis. Errors are reported as the standard deviation of the distribution based on the assumption of a Gaussian fit of the MALDI-ToF mass spectra.

	Equivalents of Initiator Added per Amine			
	0.5	1	3.3	6.6
pH 4.0	1 \pm 1	1 \pm 1	1 \pm 1	1 \pm 1
pH 6.0	2 \pm 2	5 \pm 2	7 \pm 2	9 \pm 3
pH 8.0	3 \pm 2	5 \pm 3	12 \pm 3	13 \pm 3

At pH 4.0, the conjugation reaction results in a macro-initiator species with one modification, confirming that at this pH, only one amine group is nucleophilic enough to promote the reaction with the active ester. When the pH of the reaction is increased to pH 6.0, the number of initiator molecules attached to the α -CT species increases. It is noteworthy that a concentration dependence can be observed with the higher active ester concentrations producing **CT-MI 2.1s** with a higher initiator grafting density.

When the reaction pH was further increased to pH 8.0, the reactions that contained 3.3 and 6.6 equivalents of initiator per amine resulted in a higher degree of modification. The reaction that employed 1 equivalent of initiator per amine remained at 5 initiator units conjugated to the MI species. This observation was also seen in the separate systems reported previously. This result indicates that the maximum conjugation that can be reached using 1 equivalent of initiator per amine is achieved at pH 6.0. This can be compared with the conditions using 3.3 equivalents of initiator per amine that required a higher pH to achieve maximum conjugation. Although the control of number of modified sites can be controlled, it was also observed that, just as in the prior system, as the pH increases, the dispersity of conjugation sites modified increases.

The results from the continuous system correlate strongly with the results observed in the separate systems. The ability to increase conjugation by altering the pH can facilitate a simple one-pot system to synthesise multiple modified α -CT with varying conjugation sites on their surface.

2.3.4 Locating Modified Sites in CT-MI 2.1 Species

The previous Section described the ability to produce macro-initiator species with a variety of initiator grafting densities but the location of these sites is still an unknown. The distribution of these modified residues could be either in a site-selective or random fashion and investigating the possible locations could provide an insight as to whether the reaction could be targeted at certain locations. There are many factors that can affect the microenvironment of L-lysine residues. Two

of the main environmental factors are the hydrophobicity and acidity of the neighbouring residues, as highlighted in Figure 2.12 and Figure 2.13, respectively.

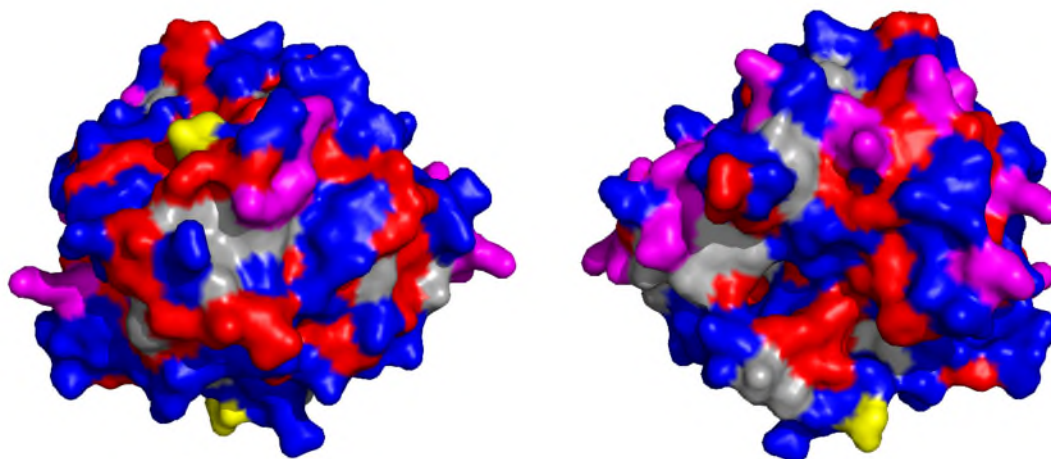


Figure 2.12 Crystal structure of α -CT(4CHA)⁴⁹ highlighting the positions of L-lysine residues with respect to hydrophobic and hydrophilic residues. L-Lysine residues have been highlighted in pink, N-termini in yellow, hydrophobic residues (Ala, Gly, Val, Leu, Ile, Met, and Phe) are shown in red and hydrophilic residues (Arg, His, Glu, Asp, Asn, Gln, Thr, Ser and Cys) in blue.

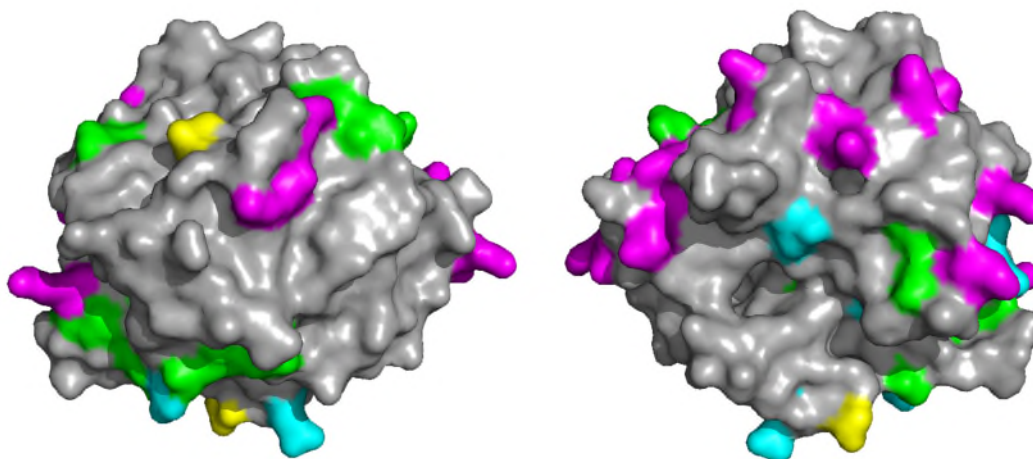


Figure 2.13 Crystal structure of α -CT (4CHA)⁴⁹ highlighting position of L-lysine residues with respect to acidic and basic residues. L-Lysine residues have been highlighted in pink, N-termini in yellow, acidic residues (Asp and Glu) are shown in green and basic residues (Arg and His) in cyan.

The pK_a of the L-lysine residues of chymotrypsin is dependent on neighbouring residues both in the sequence and in the three-dimensional structure. To this end, the DEPTH server was utilised

to predict the pK_a values of the ionisable groups of the enzyme based on the microenvironment in which the residue is found.⁶¹ The parameters used to describe the environment include:

- Depth of main-chain atoms
- Depth of polar side-chain atoms
- Number of hydrogen bonds involving the ionisable groups
- The electrostatic energy of the interaction between the ionisable groups and their environments
- Percentage of the side-chain surface area that is solvent-accessible

α -CT was submitted to the DEPTH server in the monomeric form of the crystal structure of 4CHA (Figure 2.14).⁴⁹ The predicted values for the pK_a of α -CT indicate that residues 84, 90, 107 and 169 are most probable to react during conjugation, as they will become deprotonated at a lower pH than the other amine functionalities and facilitate the nucleophilic reaction. Despite being a powerful tool for the calculation of the pK_a of L-lysine residues, DEPTH is limited by its inability to compute the estimated pK_a values of the three *N*-termini. Previous work from Grimsley *et al.* surveyed over 75 proteins with a wide variety of functionality, including lysozyme, RNase, and insulin, and observed that the pK_a of the *N*-termini is lower than that of the L-lysine residues, with average values of 7.7 ± 0.5 and 10.5 ± 1.1 , respectively, suggesting that the *N*-termini will be the groups most likely to react.⁶²

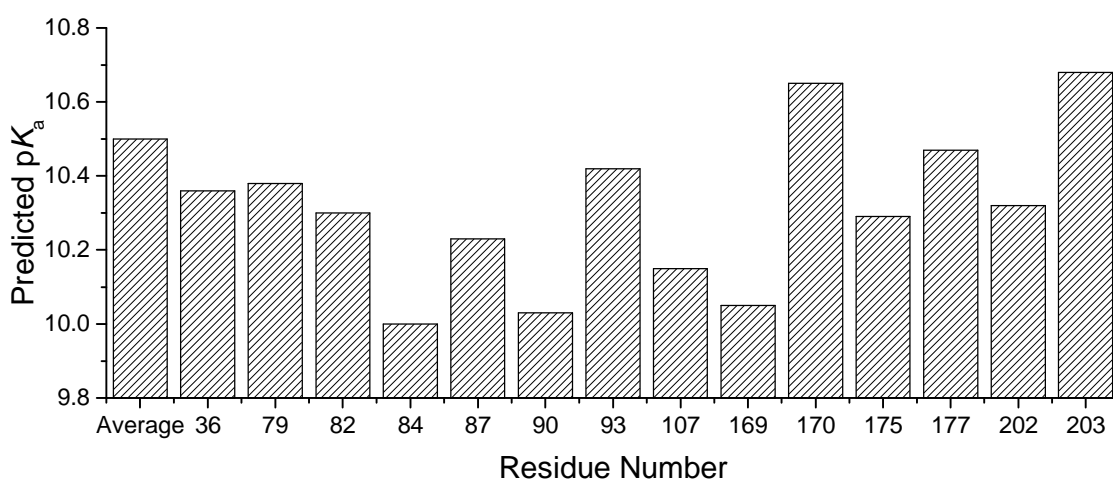


Figure 2.14 Predicted pK_a values of amine groups in L-lysine residues within α -CT compared with the average pK_a of L-lysine at 10.5. All values have been calculated by the DEPTH server.⁶¹

To gain experimental data on the location of these sites, the previously discussed reactions were repeated replacing the initiator molecule with fluorescent and UV active tags. Upon tryptic digestion, fragments that contain these residues were anticipated to be highlighted by fluorescence or UV-Vis spectroscopy. In order to establish good representation of the reaction occurring with the **I-NHS 2.1** system, an NHS activated ester-functional dye was chosen. Fluorescein is highly fluorescent in water and has been used as a fluorescent tag in many biological applications,⁶³ while its carboxyl derivative can be easily converted into an NHS activated ester (5(6)-carboxyfluorescein *N*-hydroxysuccinimide ester, **FAM-NHS**) for the aforementioned conjugation purposes (Figure 2.15).

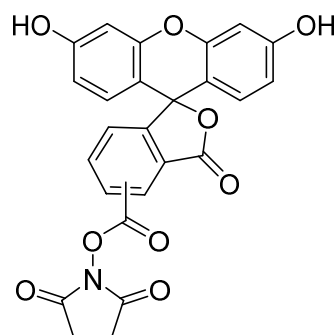


Figure 2.15 Chemical Structure of **FAM-NHS** used in the experiments conducted aiming to locate modification sites within α -CT.

Using the same conjugation conditions, **FAM-NHS** was reacted with α -CT to form **CT-FAM**. Similarly to the characterization carried out for the **CT-MI 2.1** species, MALDI-ToF mass spectroscopy was employed to determine the average amount of conjugated dye moieties per α -CT. Figure 2.16 shows that the number of attached species is much lower than what was observed with **I-NHS 2.1** under similar reaction conditions. It is possible that a high degree of modification was prevented as a result of fluorescein being more sterically bulky than the initiator species. Furthermore, as fluorescein is a highly conjugated molecule and can experience π - π stacking, the location of the conjugation sites may be influenced by this interaction that is not present in the previous system containing **I-NHS 2.1**.

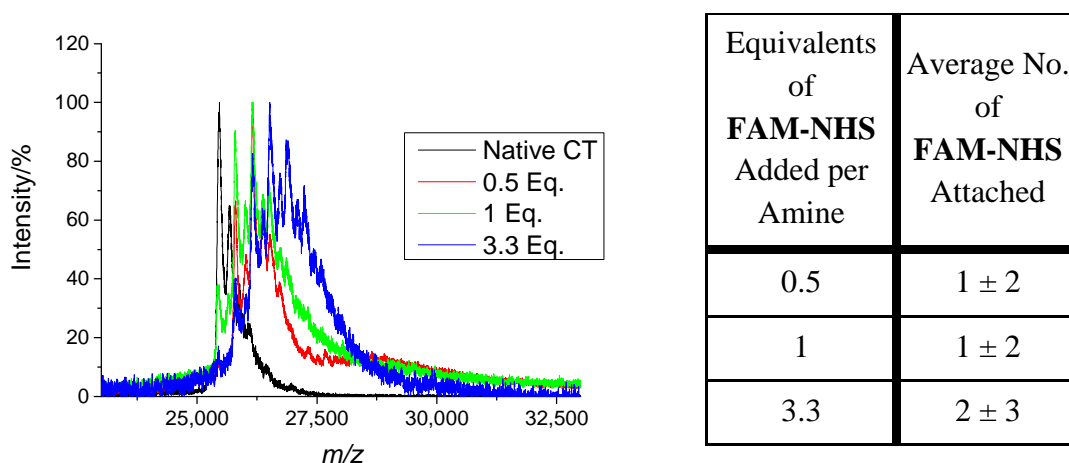


Figure 2.16 MALDI-ToF mass spectra of **CT-FAM** species synthesised at pH 8.0 at varying concentrations of **FAM-NHS**. Errors are reported as the standard deviation of the distribution based on the assumption of a Gaussian fit of the MALDI-ToF mass spectra.

To avoid steric constraints preventing conjugation, attachment of chain transfer agents (CTAs), which can be used to synthesise polymers using RAFT polymerization were investigated. There are four main classes of RAFT CTAs: dithiobenzoates, trithiocarbonates, dithiocarbamates, and xanthates.⁶⁴⁻⁶⁶ Due to the conjugation reaction occurring in aqueous solution, a trithiocarbonate species was chosen to prevent its degradation or hydrolysis in water⁶⁷ As previously attempted with **FAM-NHS**, the same conditions and conjugation chemistries will be used to attach 2-(ethylthiolythio)-2-methyl propionic acid NHS ester (**CTA-NHS 2.1**, Figure 2.17), to the

surface of α -CT to order to aid in locating of modification sites in **CT-MI 2.1**. In addition to containing a useful functionality for the synthesis of PPCs by RAFT polymerisation, **CTA-NHS 2.1** gratifyingly provides a UV handle that, upon tryptic digestion, can aid in identification of peptides that contain the modified residues.⁶⁸ Li *et al.* have used a similar species and were successful in conjugating two initiator units to the surface of lysozyme.³⁴

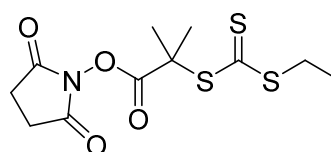


Figure 2.17 Chemical structure of **CTA-NHS 2.1** used in the attempt to locate the conjugation sites within α -CT.

Conjugation reactions of α -CT and **CTA-NHS 2.1** were performed using the same conditions as previously used for **I-NHS 2.1** and the resulting **CT-CTA** products were analysed using MALDI-ToF mass spectroscopy to determine if a similar conjugation profile was observed for the two species.

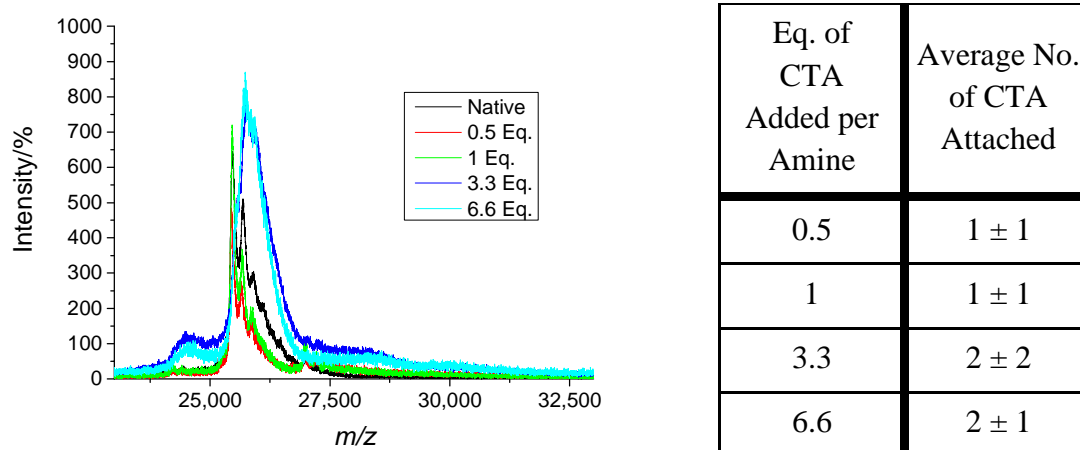
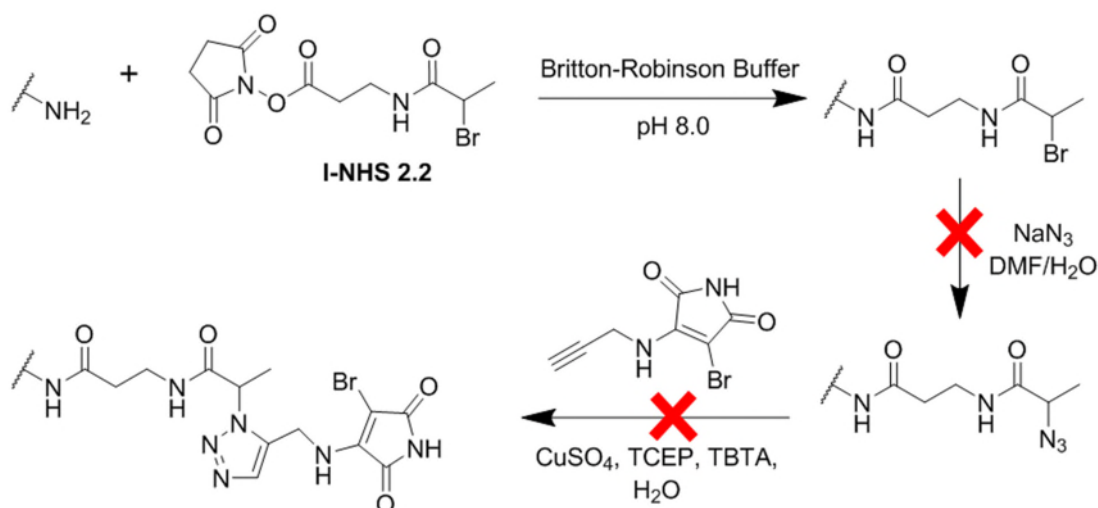


Figure 2.18 MALDI-ToF mass spectra of **CT-CTA** species synthesised at pH 8.0 at varying concentrations of **CTA-NHS 2.1**. Errors are reported as the standard deviation of the distribution based on the assumption of a Gaussian fit of the MALDI-ToF mass spectra.

MALDI-ToF MS analysis showed that conjugations performed at pH 8.0 resulted in minimal attachment of **CTA-NHS 2.1** onto the α -CT. Considering the solubility of the CTA, it was

postulated that the lower degree of modification seen in this experiment is a result of the RAFT CTA being water soluble at basic pH but more hydrophobic than **I-NHS 2.1**.

Although the same synthetic procedure was followed, the observed conjugation efficiency profiles exhibited by **I-NHS 2.1**, carboxyfluorescein and **CTA-NHS 2.1** do not show comparable ratios of attachment and therefore studying these species does not help in locating the modified residues of **CT-MI 2.1**. Due to the limitations from the dye species, the assumption was made that the small molecule that is conjugated must be similar in nature to **I-NHS 2.1**. The new route devised utilises the secondary bromide analogue of **I-NHS 2.1** (Scheme 2.2, **I-NHS 2.2**) and relies on conversion of the initiator to an azide prior to performing a copper-catalysed Huisgen cycloaddition “click” reaction with an alkyne aminobromomaleimide (ABM).⁶⁹ An alkyne ABM was chosen as the clickable fluorescent group as it is much smaller than most fluorescent groups and exhibits high fluorescence quantum yields.⁷⁰ Azidation and “click” reactions are useful tools in biochemistry as proteins do not naturally contain azides or alkynes in their structures and so any labelling occurring is not from natural residues but from modified groups.^{11, 71}



Scheme 2.2 Schematic representation of the attachment of **I-NHS 2.2** to α -CT and intended subsequent modification to azide and “click” of fluorescent ABM tag. TCEP = (tris(2-carboxyethyl)phosphine), TBTA = tris[(1-benzyl-1H-1,2,3-triazol-4-yl)methyl]amine.

Gratifyingly, when conjugation reactions were performed at pH 4.0 and pH 8.0 with **I-NHS 2.2**, the MALDI-ToF spectra showed the same degree of modification as when the tertiary bromide

analogue **I-NHS 2.1** was used (Table 2.4). Based on the great resemblance of the two molecules and the identical experimental conditions employed in both cases, it is hypothesised that the sites of modification within α -CT are the same for both macro-initiators species.

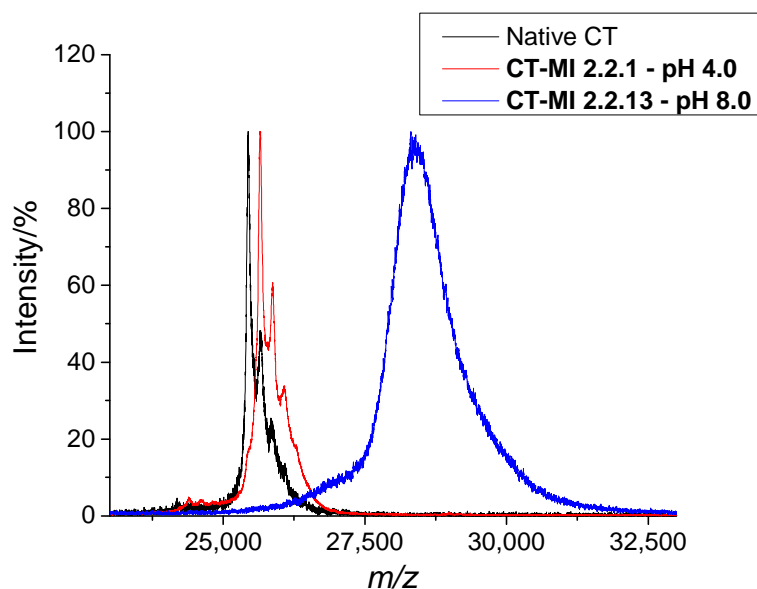


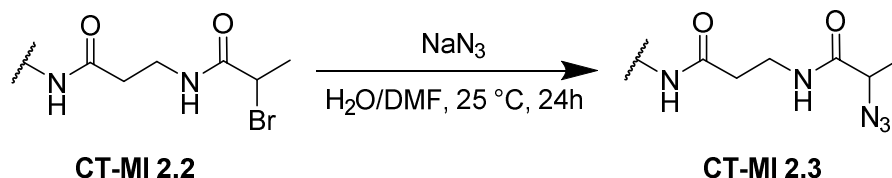
Figure 2.19 MALDI-ToF mass spectra of α -CT-MI 2.2 species synthesised at varying pH values using 3.3 equivalents of **I-NHS 2.2** per amine.

Table 2.4. Comparison of average degree of attachment of 3.3 equivalents of **I-NHS 2.1/2.2** initiator at varying pH values as determined by MALDI-ToF analysis. Errors are reported as the standard deviation of the distribution based on the assumption of a Gaussian fit of the MALDI-ToF mass spectra.

	Initiator Added	
	I-NHS 2.1	I-NHS 2.2
pH 4.0	1 \pm 1	1 \pm 1
pH 8.0	13 \pm 3	13 \pm 3

Following the successful attachment of **I-NHS 2.2** to α -CT, the modification of the bromide groups *via* reaction with sodium azide was carried out in order to obtain an azide-functional α -CT, **CT-MI 2.3**. The azidation was initially trialled in DMF but α -CT, and subsequently the α -CT macro-initiator modified at 13 sites with **I-NHS 2.2** (**CT-MI 2.2.13**), was found to be insoluble

in the pure solvent. To increase the solubility of the enzyme, water was added to the reaction; the final solvent was 50% v/v water and 50% v/v DMF.



Scheme 2.3 Schematic representation of the post-conjugation modification reaction of the secondary bromide to azide.

The macro-initiator, **CT-MI 2.3**, was purified by ultrafiltration to ensure removal excess sodium azide and the purified **CT-MI 2.3** species was analysed by MALDI-ToF mass spectroscopy (Figure 2.18) and Fourier transform infrared spectroscopy (FTIR) spectroscopy (Figure 2.21). The FTIR spectra shows the appearance of a small peak at 2160-2120 cm^{-1} , the region of the azide stretch, which attributed to the successful conversion of the bromide to an azide. The low intensity of the observed signal was attributed to the fact that as the enzyme is a large molecule (over 25 kDa), signals from other bonds saturate the spectrum.

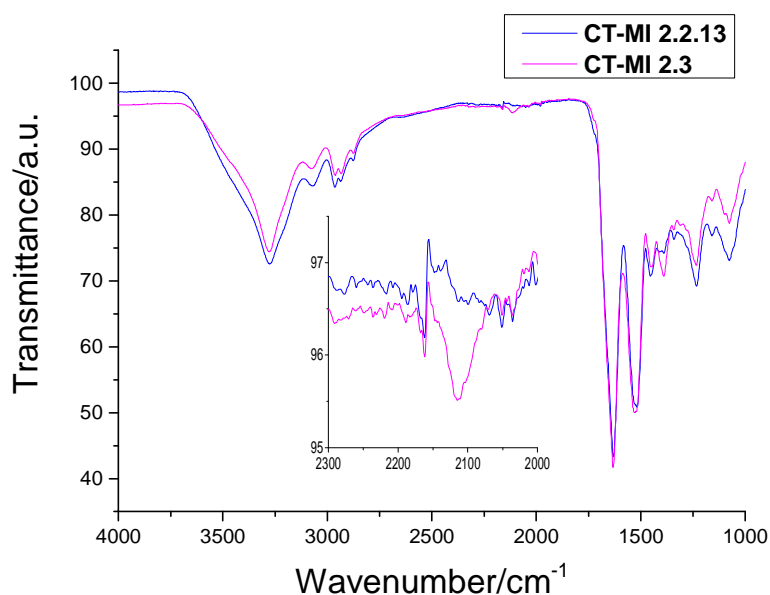


Figure 2.20 FTIR spectra of **CT-MI** before (**2.2.13**) and after azidation (**2.3**). Inset shows an enlargement of the region from 2300 to 2000 cm^{-1} .

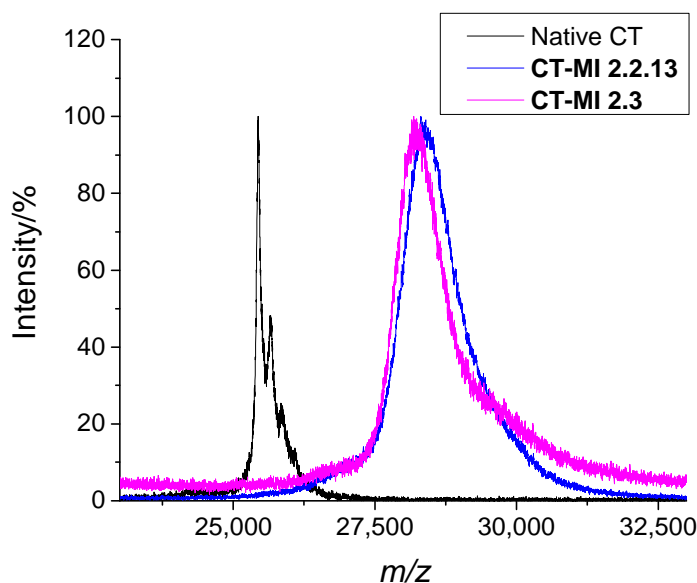


Figure 2.21 MALDI-ToF mass spectra of **CT-MI 2.2** species before and after azidation.

MALDI-ToF mass spectroscopy of the azidation product revealed a decrease of the molar mass by 0.1 kDa. This decrease was attributed to the successful azidation of only three bromide units. Despite the moderate success of the proposed method, the incomplete azidation of the bromines renders it ineffective as further steps are highly dependent on the presence of an azide on every functionalized residue. While optimization of the reaction would likely achieve complete azidation, the following pathway (*vide infra*) was being simultaneously pursued and owing to its obtained results, no further optimization of the azidation reaction was carried out.

As methods that further modify the enzyme have been unsuccessful, the macro-initiator species conjugated with **I-NHS 2.1** were subjected to a tryptic digestion followed by liquid chromatography–mass spectrometry (LC-MS) analysis (Figure 2.22). To investigate if **CT-MI 2.1** species formed at varying pH were observed to have different conjugation tendencies, the three species underwent this process were native α -CT and α -CT with 1 and 10 modification sites (**CT-MI 2.1.1** and **CT-MI 2.1.10**, respectively). Trypsin is known to cleave at L-arginine and L-lysine residues; however, as the L-lysine residues have been modified it is anticipated that an increase in missed cleavage sites with an increase in conjugation would be observed.^{72, 73}

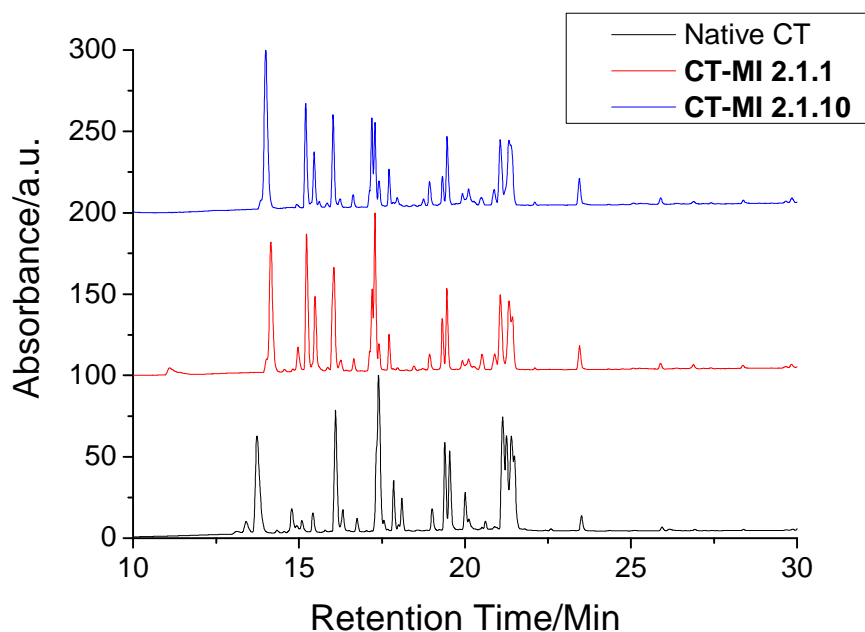


Figure 2.22 LC-MS chromatograms obtained from the tryptic digestion of α -CT and the **CT-MI** species **CT-MI 2.1.1** and **CT-MI 2.1.10**, recorded at $\lambda = 280$ nm.

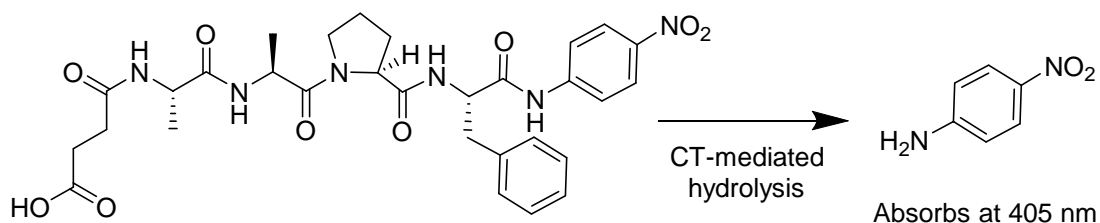
The three samples show different LC profiles, for example an increase in intensity of the peaks at 15 minutes in the **CT-MI 2.1** samples compared to the native one is observed. Although the LC results show that there are differences between the three protein species, the MS analysis was unable to locate any fragments from the native sample that correspond to α -CT. It is hypothesised that as α -CT is a protease itself, fragments from multiple digestions, namely α -CT to α -CT, trypsin to α -CT, and α -CT to trypsin are observed instead. Trypsin to trypsin digestion is not expected as MSgrade trypsin was used, which has been chemically modified to prevent autolysis.⁷⁴ As the fragments cannot be identified in the native enzyme, the assignment of modification sites cannot be carried out.

Although the initial aim was to be able to control the grafting behaviours of ATRP-initiating groups onto the surface of α -CT, it is apparent that many factors affect the efficiency of the grafting reaction and identification of the modifications sites is challenging due to the autolytic tendency of α -CT. To this extent, a further study would be required to evaluate these factors

utilizing proteins with less complex function to determine a connection between pK_a of the L-lysines, pH of conjugation and the location of the modification site.

2.3.5 Activity of α -CT Macro-Initiator Species

Any modifications to enzymes have the potential to affect their catalytic activity.^{4, 75, 76} A common method to examine the activity of protease enzymes is an assay that cleaves a short peptide (Suc-AAPF) from *p*-nitroaniline (*p*NA), which can be detected spectroscopically *via* an increase of absorption at $\lambda = 405$ nm (Scheme 2.4).⁷⁷



Scheme 2.4 Schematic representation of the *p*NA assay for proteases.

The retention of the catalytic activity of α -CT and **CT-MI 2.1.10**, was examined by the *p*NA assay (Figure 2.23).

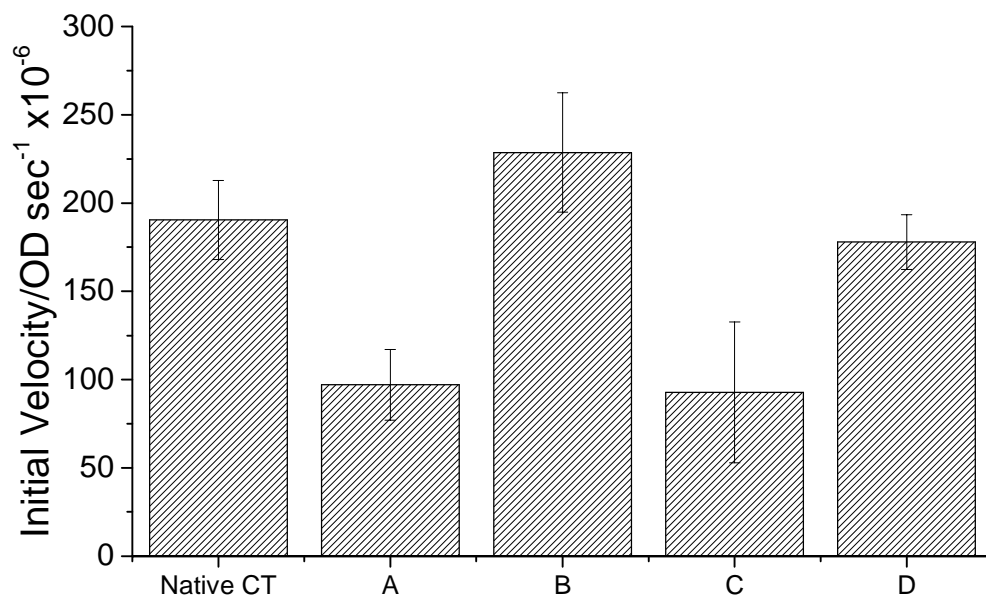


Figure 2.23 Initial velocity of α -CT-catalysed hydrolysis upon exposure to varying conditions. A - purified by dialysis, B - exposed to reaction conditions, C - exposed to NHS and dialysis, D - purified by ultrafiltration. Each data point is based on the average of four repeats of *p*NA assay with standard deviation displayed as error.

The activity of **CT-MI 2.1.10** was found to be significantly reduced in comparison to the native species. Further experiments were conducted to examine whether this decrease was a consequence of the reaction conditions employed, the formation of small molecule by-products, or the conjugation of the initiator molecules. Initially, α -CT was exposed to reaction conditions identical to those employed during the conjugation reaction, however without the addition of the initiator, while in a second experiment α -CT was incubated with the by-product of the conjugation reaction, NHS. α -CT that had been exposed to reaction conditions was found to maintain the initial activity shown by the native enzyme; however, α -CT that had been incubated with NHS showed a significant decrease in initial velocity suggesting that the small molecule NHS inhibits the α -CT activity. Indeed, after purification of the mixture by ultrafiltration to remove the NHS, the activity of the final **CT-MI 2.1.10** species was found to be within error of the native enzyme. This suggests that the inhibition caused by NHS is most likely a reversible process.

As introduced in Chapter 1, Section 1.3, the Michaelis-Menten model of enzyme kinetics is the most common model for the analysis of enzyme activity in the presence of a single substrate. The catalytic activities of α -CT, **CT-MI 2.1.1**, and **CT-MI 2.1.10** were analysed using the *p*NA assay with Michaelis-Menten parameters extracted from the hydrolysis data by employing Lineweaver-Burk plots (Table 2.5).

Table 2.5 Michaelis-Menten Parameters of α -CT, **CT-MI 2.1.1**, and **CT-MI 2.1.10** based on the *p*NA assay.

Sample	$K_m/\mu\text{M}$	$k_{\text{cat}}/\text{sec}^{-1}$	$k_{\text{cat}}/K_m/\text{sec}^{-1} \mu\text{M}^{-1}$
Native α -CT	105 ± 6	14.6 ± 0.7	0.14 ± 0.01
CT-MI 2.1.1	107 ± 10	14.5 ± 1.0	0.14 ± 0.02
CT-MI 2.1.10	105 ± 3	15.5 ± 0.4	0.15 ± 0.01

By comparing the three samples tested, all parameters are within error of each other suggesting that the catalytic ability of α -CT was not compromised by attaching small molecules or as a result of the reaction conditions that they have been exposed to.

2.3.6 Stability of α -CT Macro-Initiator Species

As the results from the activity studies show that there has been no significant impact on the activity of the **CT-MI 2.1** species, the stability of these enzymes was also investigated. There are many different factors that can be studied with regards to stability, however this Section will focus on thermal, autolytic, and protective stability.

2.3.6.1 Thermal Stability

The catalytic activity of α -CT and **CT-MI** with 1, 5 and 10 initiator units covalently bonded to the surface of α -CT (**CT-MI 2.1.1**, **2.1.5** and **2.1.10** respectively) was monitored over time at 40 °C (Figure 2.24) using the *p*NA assay. The residual activity was calculated as a ratio of initial rates of hydrolysis at given incubation time over the initial activity.

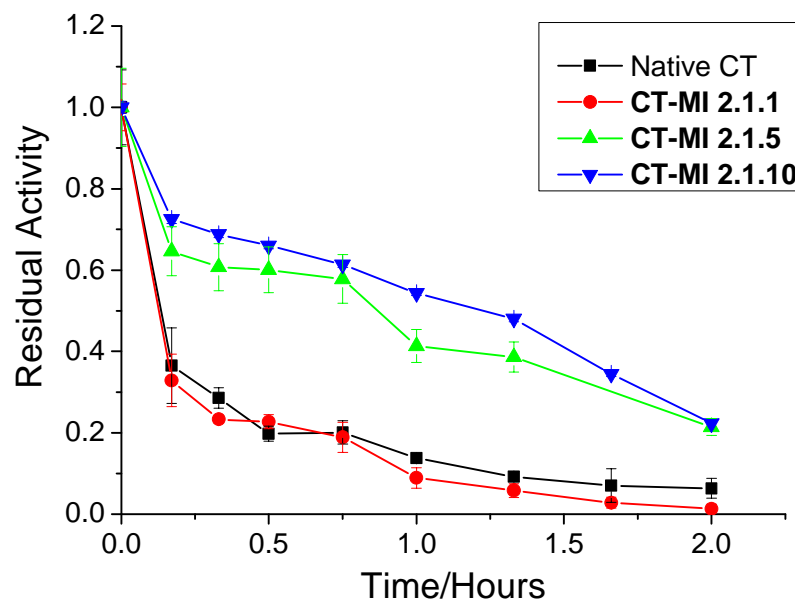


Figure 2.24 Thermal stability profiles of α -CT and **CT-MI 2.1** species at pH 8.0, 40 °C. Each data point is based on the average of four repeats of pNA assay with standard deviation displayed as error. Initial catalytic velocity at $t = x$ is divided by their relative initial catalytic velocity at $t = 0$ to calculate residual activity.

The decays of the activity of the native α -CT and **CT-MI 2.1.1** are very similar and appear to have the same degradation profile. The samples with higher initiator densities, however, showed a clear increase in stability compared to the native α -CT.

To allow these stability profiles to be quantitatively compared, their half-lives were extracted from a linear plot of the natural logarithm of residual activity against time (Figure 2.25); all stability profiles were assumed to be based on an exponential decay. Although no difference can be observed between α -CT and **CT-MI 2.1.1**, the half-life of the **CT-MI 2.1.10** species is a factor of six larger than that of the native species. The addition of 5 initiator units also shows a significant increase in half-life in comparison to the native enzyme.

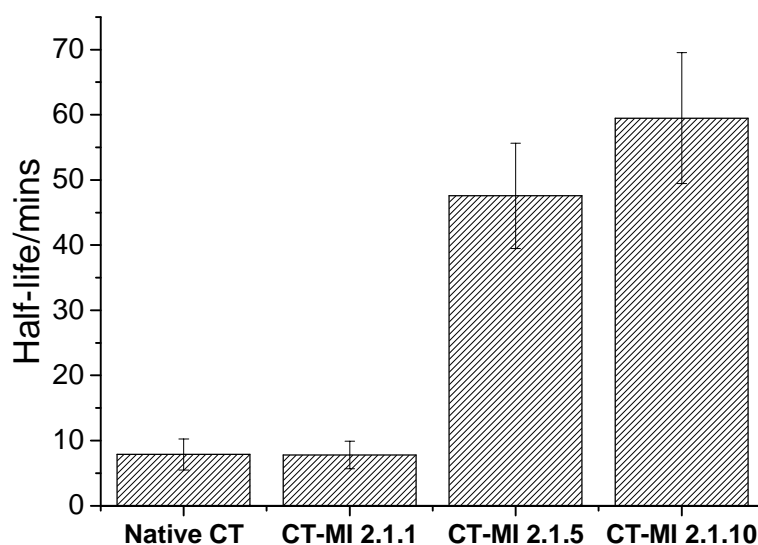


Figure 2.25 Activity half-life at 40 °C for α -CT and **CT-MI 2.1** species extracted from the linear regression of $\ln(\text{residual activity})$ against time.

One factor that is hypothesised to have an impact on the stability of these enzymes is the surface charge.⁵⁹ As the modification is reducing the number of potential ionisable groups from the system, it could lead to a different overall or localised charge. The zeta potential of all α -CT samples was investigated in water (Figure 2.26).

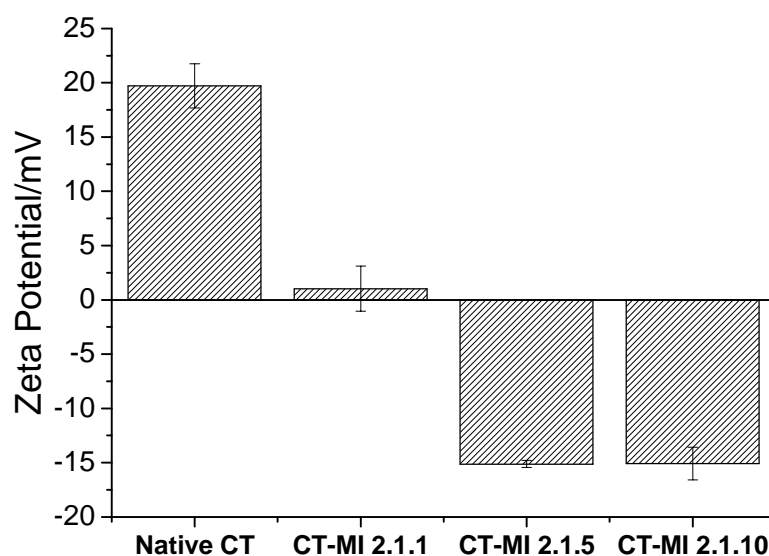


Figure 2.26 Zeta potential values of α -CT and **CT-MI 2.1** species in water.

The zeta potential of the native α -CT shows a positive overall surface charge while as more modifications are introduced (**CT-MI 2.1.1-CT-MI 2.1.10**) the zeta potential decreases, showing a neutral species upon conjugation of one initiator and then negatively charged species for five and ten initiator additions. The zeta potential results show a negative correlation to the stability results obtained, as the negatively charged species exhibited a significantly increased activity half-life at 40 °C.

Another method of determining thermal stability is to investigate the melting temperature (T_m) of the protein. This is achieved by performing a thermal shift assay (Figure 2.27) where the protein is heated in the presence of a dye that becomes fluorescent upon binding.^{78, 79} When unbound the chosen dye, SYPRO orange, is quenched by the aqueous environment however upon melting the hydrophobic surfaces of the protein are exposed, allowing SYPRO orange to bind, excluding water, creating an increase in observed fluorescence.⁸⁰

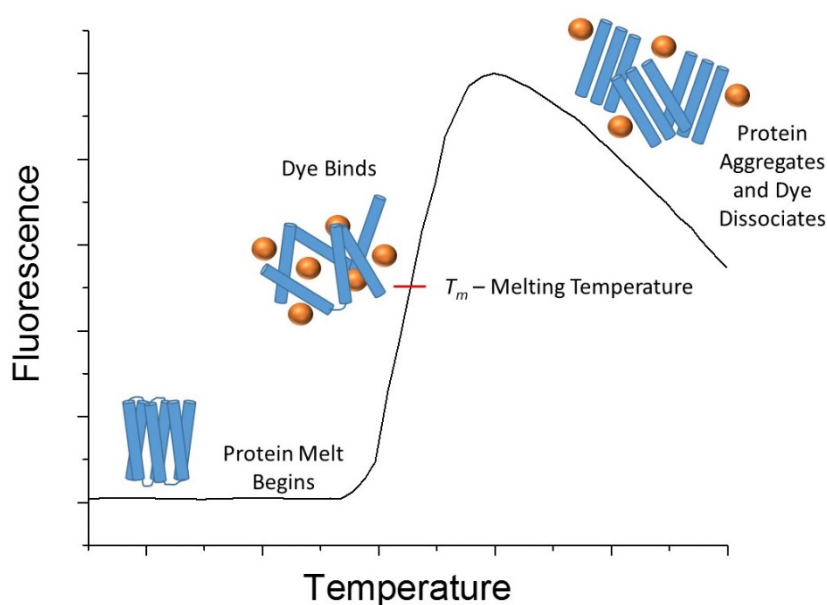


Figure 2.27 Schematic representation of dye-protein binding during thermal shift assays.

To ensure the accuracy of the thermal shift assay, α -CT was analysed by both thermal shift assay and differential scanning calorimetry (DSC) (Figure 2.28).

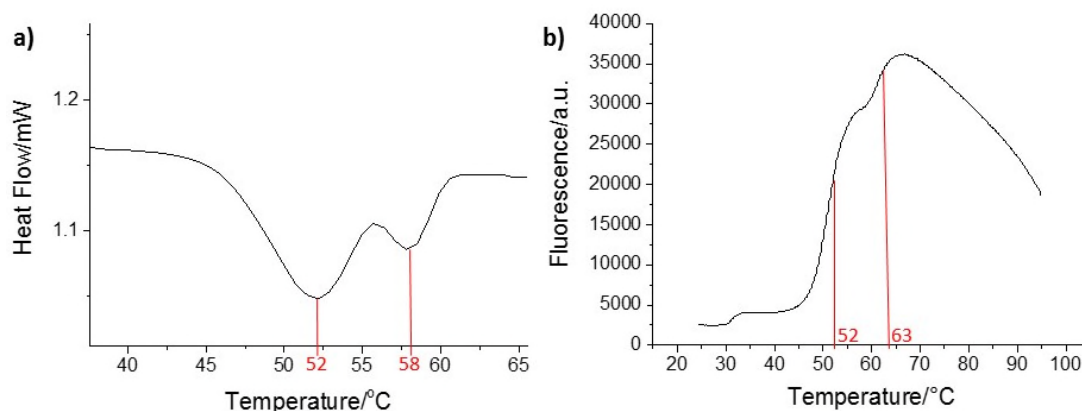


Figure 2.28 T_m of native α -CT by a) DSC, 50 mg/mL in water, 1 °C/min ramp rate and b) thermal shift assay, 5 mg/mL in water with SYPRO orange, excitation $\lambda = 492$ nm, emission $\lambda = 610$ nm.

The values obtained from both techniques show the same T_m for the primary melt at 52 °C, which is in agreement with literature findings.⁸¹ Furthermore, it was found that α -CT has both a primary and secondary melt which can be explained by the existence of different regions or substructures of the protein undergoing melting at different temperatures. As there is variation in T_m for the secondary melt from 58 to 63 °C, the primary melt will be used as the point of comparison for all α -CT species.

The thermal shift assay has been chosen as the primary method of analysis over DSC due to the less sample volume required for each test; DSC requires >10 mg per test and the response observed is small compared to the thermal shift assay which uses 1 mg per test and exhibits a much larger response. T_m measurements were conducted for all **CT-MI 2.1** species (Figure 2.29).

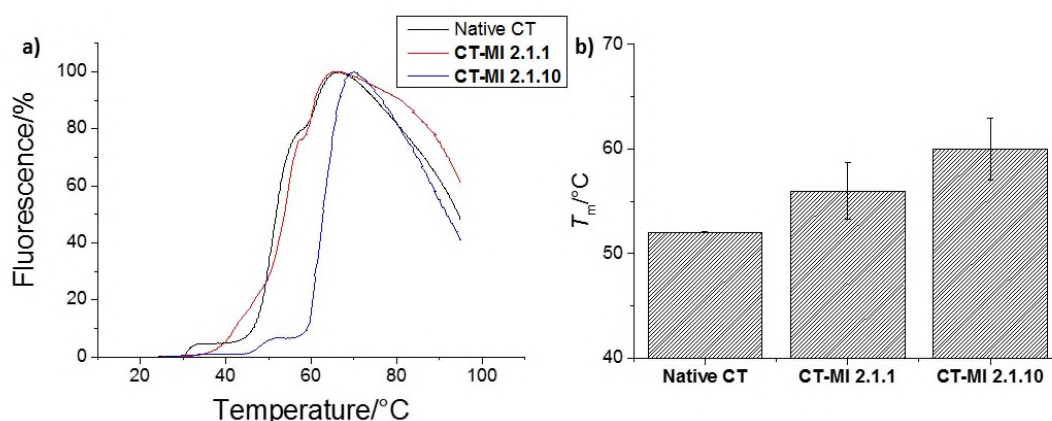


Figure 2.29 a) Thermal shift assay profile of native α -CT and initiator-functionalized α -CT, 5 mg/mL in water with SYPRO orange, excitation $\lambda = 492$ nm, emission $\lambda = 610$ nm and b) graph displaying T_m of α -CT and **CT-MI 2.1** species. Values are obtained from triplicate repeats and error is displayed as standard deviation.

The T_m was shown to increase with the addition of initiator units whereby an increase of 8 °C was seen with the addition of 10 initiator units. This result correlates with the earlier stability study at 40 °C for the **CT-MI 2.1.10** species however the **CT-MI 2.1.1** species exhibited an increase in T_m but no improvement in catalytic stability. It is also observed that **CT-MI 2.1.10** only has one melt peak as opposed to the primary and secondary melts seen by both native α -CT and **CT-MI 2.1.1**. These changes could be attributed to changes in the electrostatic interaction between positively charged L-lysine residues and the remaining protein structure.⁸²

From the observed changes in both catalytic stability and T_m , it is concluded that altering the surface chemistry of α -CT by attaching **I-NHS 2.1** increases the thermal stability of the enzyme. It is hypothesised that altering the charge of the surface of α -CT is one of the causes of the observed effects.

2.3.6.2 *Autolytic Stability*

As the enzyme α -CT is a protease, there is a possibility of the newly formed peptide bond between **I-NHS 2.1** and α -CT being cleaved from the protein in an autolytic process. **CT-MI 2.1.10** was studied both in aqueous solution and solid form at 4 °C and 25 °C for signs of cleavage of the initiator residue (Figure 2.30).

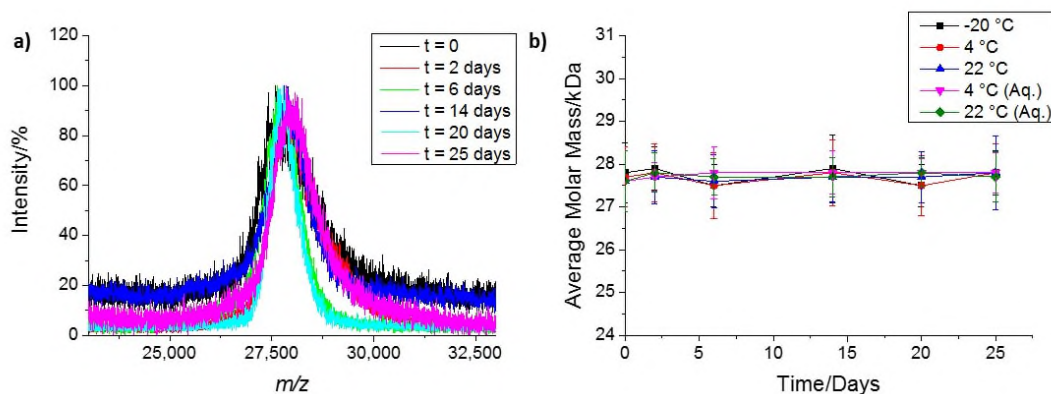


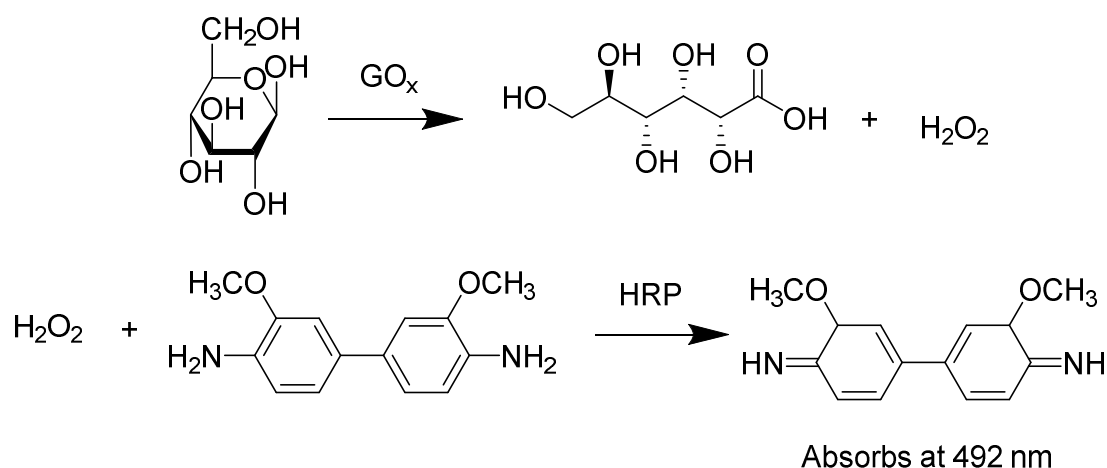
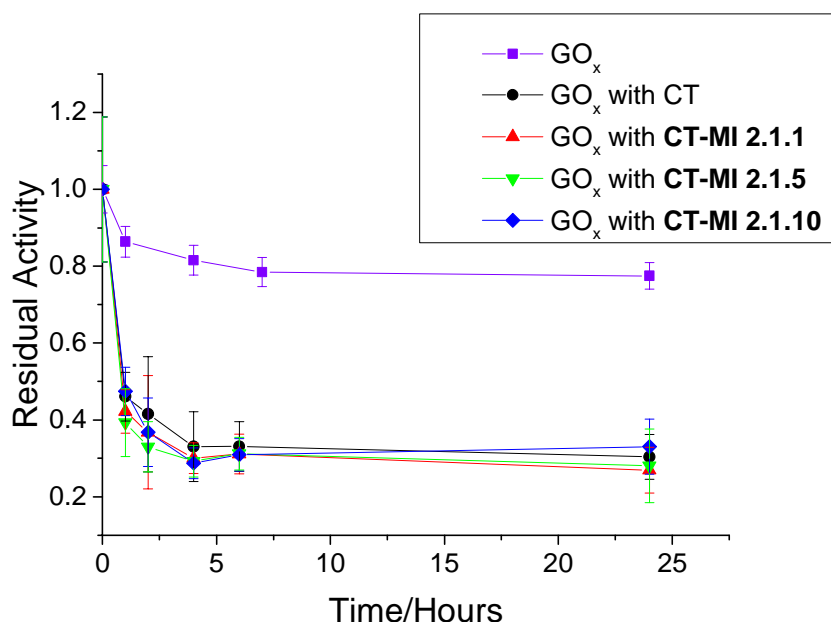
Figure 2.30 a) MALDI-ToF mass spectra of **CT-MI 2.1.10** stored in solution at RT at various time points b) Average molar masses as determined by MALDI-ToF spectroscopy of **CT-MI 2.1.10** at various time intervals in various storage conditions. Errors bars are displayed as the standard deviation of the distribution based on the assumption of a Gaussian fit of the MALDI-ToF mass spectra.

No reduction in mass by MALDI-ToF mass spectroscopy was observed in any samples within 25 days suggesting the sample is stable to autolysis. The lack of autolytic activity shown by **CT-MI 2.1.10** allows stable storage of these compounds and it is hypothesised that cleavage of a polymeric species synthesised from **CT-MI 2.1.10** would be unlikely.

2.3.6.3 *Secondary Enzyme Stability*

The final form of stability that was explored for these macro-initiators was secondary enzyme stability. This form of stability examines the ability of the protease enzyme to digest a secondary enzyme species in solution and the impact upon the catalytic activity of the secondary enzyme. Glucose oxidase (GO_x) was utilised as the secondary enzyme as the stability of this enzyme is relatively high for over 24 hours, allowing discrete stability curves with and without the presence of protease species.⁸³

GO_x activity is assessed using the *o*-dianisidine that proceeds by the production of hydrogen peroxide and with the aid of horseradish peroxidase (HRP) *via* a two-step reaction with glucose as the initial substrate (Figure 2.31). α -CT and **CT-MI 2.1** species were incubated with GO_x at 30 °C for 24 hours with aliquots tested for GO_x activity (Figure 2.32).

Figure 2.31 Schematic representation of the *o*-dianisidine assay for glucose oxidase.Figure 2.32 Stability profiles of GO_x incubated with α -CT and CT-MI species at various time intervals at pH 5.0, 30 °C. Each data point is based on the average of four repeats of *o*-dianisidine assay with standard deviation displayed as error.

α -CT alone was shown to have no catalytic effect on the *o*-dianisidine assay used to assess GO_x activity. Native GO_x showed a 20% decrease in activity over 24 hours without addition of any protease species. Upon the addition of α -CT or CT-MI 2.1 species, the activity of GO_x decreased to 30% within 4 hours. This suggests that the conjugation of any number of initiators does not have an impact on the ability of the protease to digest other proteins in solution.

2.3.7 Other Methods of Conjugation to α -CT

As described previously, NHS can have a detrimental effect on the enzymatic activity of α -CT (Section 2.3.5). Due to the presence of the inhibiting small molecule by-product that is formed in the production of the NHS active ester macro-initiator, other methods of conjugation were investigated.

Based on its water stability and ability to react with an amine without producing any by-products, **I-BA 2.1** was synthesised. **I-BA 2.1** was based on a similar molecule, originally synthesised by Hoshi *et al.*, which was utilised to synthesise poly(sulfobetaine methacrylate) from the surface of silicon oxide surfaces.⁸⁴ Although Hoshi *et al.* did not perform the conjugation reaction in aqueous systems, it was hypothesised that the short ethylene glycol linker present in **I-BA 2.1** would aid in water solubility.

As imine formation in aqueous environments is unstable due to hydrolysis, to ensure that the benzaldehyde initiator would undergo reaction with an amine, benzylamine was combined with **I-BA 2.1** in dichloromethane. ¹H NMR spectroscopy was used to analyse the formation of the imine product (Figure 2.34).

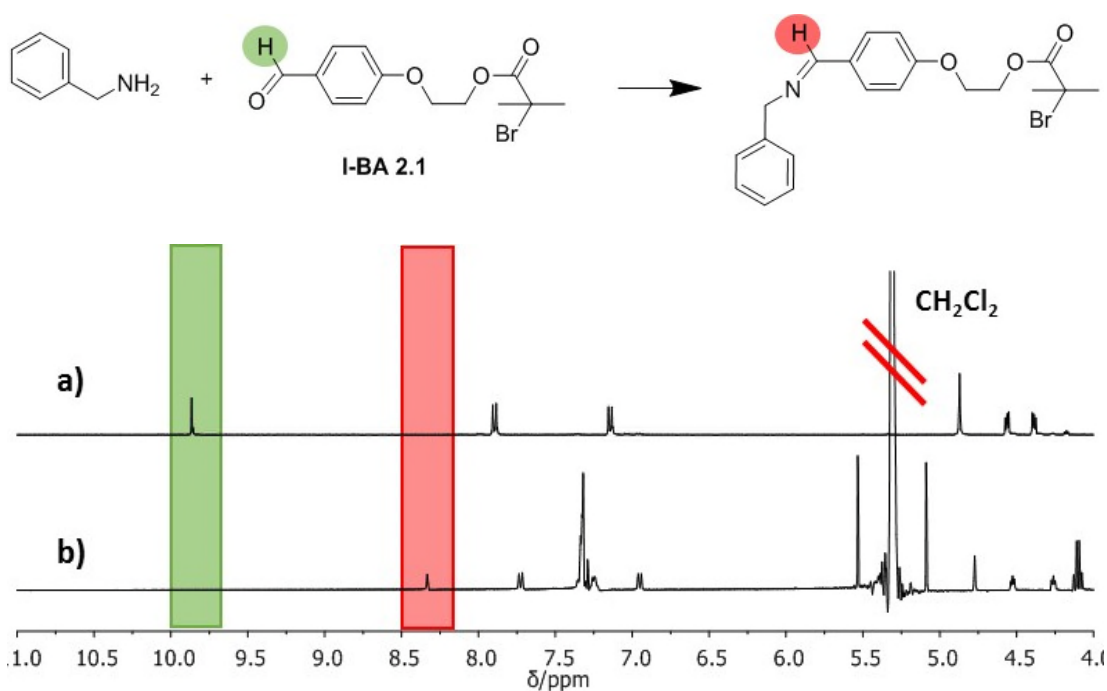
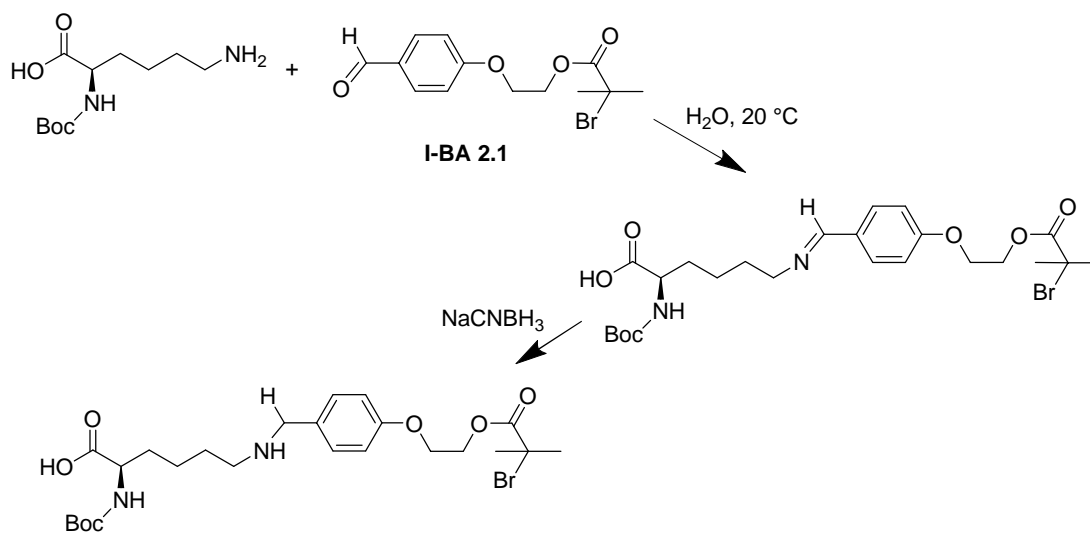


Figure 2.33. ¹H NMR spectra of a) **I-BA 2.1** and b) Imine formation reaction between benzylamine and **I-BA 2.1** in dichloromethane. ¹H NMR solvent: CDCl₃, 400 MHz. Green highlights aldehyde peak disappearance and red highlights the appearance of imine peak.

The formation was confirmed based on the shifting of the phenyl proton peaks from 7.1 and 7.9 ppm to 6.9 and 7.7 ppm respectively, the disappearance of the aldehyde proton peak at 9.8 ppm, and the appearance of the imine proton peak at 8.3 ppm. Although the imine is shown to form in dichloromethane, imines are prone to hydrolysis in water and do not form under aqueous conditions with more appropriate analogues of the model system.

For preliminary reactions, a small molecule analogue (Boc- L-Lysine) was used to represent the protein L-lysine residues to help to ascertain reaction conditions for conjugation. As the reaction between an aldehyde and primary amines forms an imine that is unstable in the presence of water, a reducing agent is required to irreversibly form the secondary amine product (Scheme 2.5).



Scheme 2.5 Schematic for the formation of secondary amine, from **I-BA 2.1**, sodium cyanoborohydride and L-lysine residues.

The product was characterised by ¹H NMR spectroscopy whereby the appearance of peaks attributed to the phenyl protons of the secondary amine product at 6.75 and 7.30 ppm suggests the successful formation of the product, with the reaction proceeding to 25% conversion over 18 hours (Figure 2.34). A second addition of sodium cyanoborohydride was introduced to attempt to increase the conversion to product; this was found not to force the reaction to proceed further but to stay constant at 25% conversion.

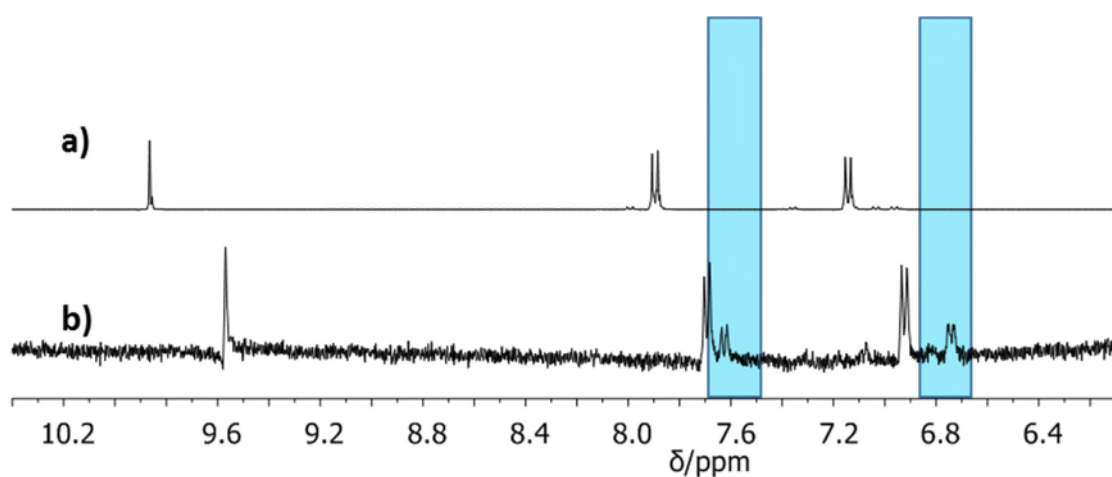


Figure 2.34. ¹H NMR spectra of a) **I-BA 2.1** and b) secondary amine formation reaction between Boc-Lys and **I-BA 2.1** with single addition of sodium cyanoborohydride (10 eq.) MeOD, 400 MHz. Blue highlights formation of product species at 7.65 and 6.75 ppm.

For the reaction to occur, the addition of a reducing agent is required. As such, it was important to confirm that addition of sodium cyanoborohydride does not affect the activity of α -CT. The samples were incubated at 3 °C with either 18.2 M Ω cm water, 10 equivalents of sodium cyanoborohydride or 3.3 equivalents of NHS per amine for 18 hours before dialysis to remove impurities. The samples were analysed using a pNA assay (Figure 2.35).

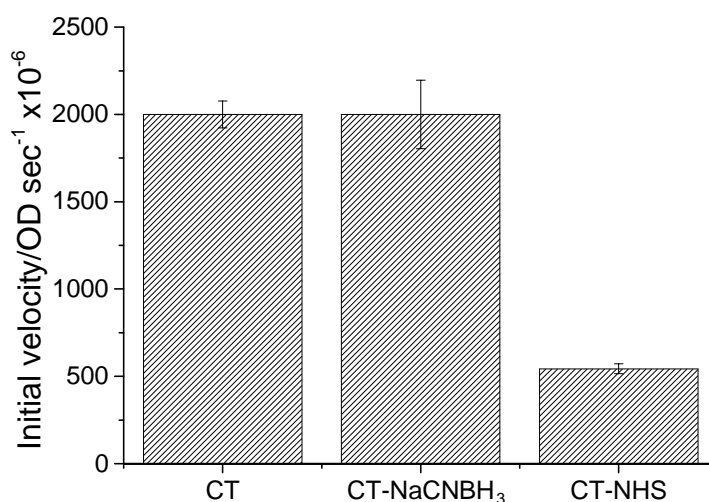


Figure 2.35. Initial hydrolysis rate of α -CT after with incubation at 3 °C, (CT) in water, (CT-NaCNBH₃) with sodium cyanoborohydride (10 eq.), (CT-NHS) with NHS (6.6 eq.). Each data point is based on the average of four repeats of pNA assay with standard deviation displayed as error.

Sodium cyanoborohydride appears to have no impact on the enzymatic activity of α -CT, with the results within error of the sample of α -CT that was only exposed to 18.2 M Ω cm water. This compares to the sample that was exposed to NHS that shows a decrease of 75% activity after purification by dialysis.

Due to the successful attachment of **I-BA 2.1** to a small molecule analogue and the compatibility of the enzyme with sodium cyanoborohydride, studies were conducted to analyse the conjugation between **I-BA 2.1** and α -CT. In an attempt to control the degree of modification, the concentration of sodium cyanoborohydride was varied and conjugation was quantified using MALDI-ToF MS (Figure 2.36).

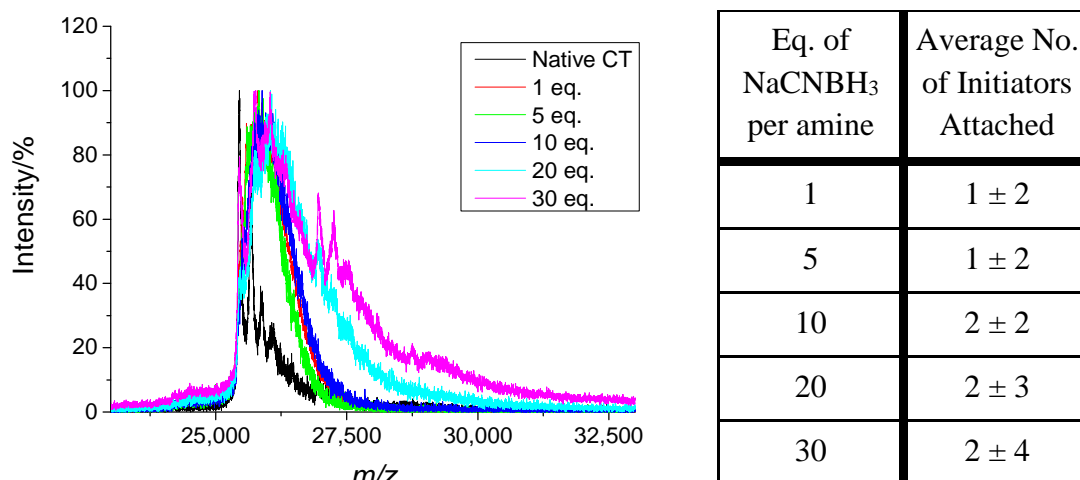


Figure 2.36. MALDI-ToF mass spectra of CT-MI-BA species synthesised at pH 8.0, 10 eq. of I-BA 2.1 and varying concentrations of NaCNBH₃. Errors are reported as the standard deviation of the distribution based on the assumption of a Gaussian fit of the MALDI-ToF mass spectra.

Successful conjugation was observed in all samples with an average of between 1 and 2 units becoming covalently bound dependent upon concentration of NaCNBH₃. When the concentration of NaCNBH₃ was increased to 30 equivalents there was a small population of α -CT found to contain 5 initiator units on average leading to a broadening of the spectrum and suggesting that higher functionalisation is possible under optimised conditions. Although successful conjugation was achieved in all cases, during the reaction the macro-initiators that conjugated greater than one initiator precipitated out of solution which was also hypothesised to be the cause of the low degree of functionalisation. Due to the insolubility of the macro-initiators formed using in I-BA 2.1, a new, more hydrophilic aldehyde initiator would have to be synthesised for this route to be utilised to form macro-initiators with higher initiator densities.

2.4 Conclusions

To conclude, the conjugation of a small molecule ATRP initiator to L-lysine residues on the surface on a protein was able to be tuned with pH of the reaction and concentration of initiator. This system can be adapted to a continuous process to allow the production of initiators with varying grafting density from a one-pot experiment. Although various methods were attempted, the location of the modification sites could not pinpointed. It was also not possible to conclude

whether the initiators that were synthesised were site-specific at varying pH or underwent random conjugation due to the autolytic behaviour exhibited by α -CT.

As the macro-initiators formed, NHS was found to be produced as a by-product of the conjugation reaction. The small molecule NHS was found to inhibit the catalytic ability of α -CT, however the impurity could be removed by purification using ultrafiltration. All **CT-MI 2.1** species were found to have the same kinetic parameters as the native protein after purification. Although the activity was not altered by the introduction of initiator molecules, the thermal stability of macro-initiators with greater than five initiators covalently bound showed a significant increase in activity half-life. The half-life of **CT-MI 2.1** has a negative correlation with the surface charge as species that were negatively charged showed increased stability in comparison to neutral and positively charged enzymes. Even though **CT-MI 2.1s** show a higher degree of thermal stability, the modifications do not provide protection for a secondary enzyme in solution.

Other conjugation methods were investigated to prevent inhibiting by-products being formed during synthesis. Benzaldehyde-based initiators produced no side products when reacting with L-lysine residues on the surface of the protein but they require the use of a coupling agent to reduce the imine formed in water and prevent reversible coupling occurring. The reducing agent, sodium cyanoborohydride, did not appear to have a negative effect on the enzymatic activity of α -CT and could be utilised to control the degree of conjugation by simply altering the concentration. Nonetheless, due to the hydrophobic nature of benzaldehyde, the macro-initiator species formed were no longer soluble in water and formed a precipitate. As a consequence of the precipitation of **CT-MI-BA** in aqueous solution, this chemistry was deemed unsuitable for the project because of the need to synthesise PPCs in a fully aqueous systems.

2.5 Experimental

2.5.1 Materials

All chemicals were obtained from Sigma-Aldrich and used without further purification unless stated otherwise. Ultrafiltration membranes with a 5 kDa MWCO were supplied by Amicon. SYPRO orange was supplied as a 5,000× concentrate in DMSO from Thermo Fisher. CTA-NHS 2.1 (2-(ethylthiolythio)-2-methyl propionic acid NHS ester) was synthesised by a previous group member, Sean Flynn.

2.5.2 Instrumentation

2.5.2.1 *¹H Nuclear Magnetic Resonance (NMR) and ¹³C NMR Spectroscopy*

¹H NMR spectra were recorded on a Bruker DPX-300 or DPX-400 spectrometer at 300 MHz and 400 MHz, respectively with MeOD, D₂O, or CDCl₃ as the solvent. The chemical shifts of protons were quoted relative to tetramethylsilane (TMS) at $\delta = 0$ ppm when using CDCl₃, or relative to residual solvent protons when using MeOD (¹H: $\delta = 3.31$ ppm) and D₂O (¹H: $\delta = 4.79$ ppm). ¹³C NMR spectra were recorded on a Bruker DPX-300 or DPX-400 spectrometer at 75 MHz and 100 MHz, respectively with MeOD, D₂O, or CDCl₃ as the solvent. The chemical shifts of carbons were quoted relative to solvent carbons when using MeOD (¹³C: $\delta = 49.3$ ppm) and CDCl₃ (¹³C: $\delta = 77.0$ ppm).

2.5.2.2 *Matrix-Assisted Laser Desorption/Ionization Time-of-Flight (MALDI-ToF) Mass Spectrometry*

MALDI-ToF mass spectrometry was conducted on a Bruker Autoflex MALDI ToF/ToF spectrometer. The acceleration voltage was 20 kV in a positive linear mode. Protein solution (1.0-2.0 mg/mL) was mixed with an equal volume of matrix (0.5 mL of water, 0.5 mL of acetonitrile, 2 μ L of trifluoroacetic acid, and 8 mg of 4-hydroxy-3,5-dimethoxycinnamic acid), and 2 μ L of the resulting mixture was spotted on the target plate. Samples were calibrated against

native α -CT. Number of sites conjugated and associated errors were extracted from a Gaussian fit of the MALDI-ToF mass spectra.

2.5.2.3 *Fourier Transform Infrared (FTIR) Spectroscopy*

FTIR spectroscopy was carried out using a Perkin Elmer Spectrum 100 FTIR spectrometer. 16 scans from 600 to 4000 cm^{-1} were taken, and the spectra were corrected for background absorbance.

2.5.2.4 *Liquid Chromatography–Mass Spectrometry (LC-MS)*

20 μL of digest solutions were injected through a reverse phase column (Zorbax C18, size 46 x 150 mm, particle size 5 μm) connected to an Agilent 1100 HPLC. The outflow was routed to a Bruker High Capacity Trap (HCT) + ion trap mass spectrometer with an electrospray source, operating in positive ion mode. A 5 min isocratic elution (95:5 solvent A/solvent B) was followed by gradient elution to 0:100 solvent A/solvent B over 25 min. Solvents A and B were water (0.1% v/v HCOOH) and methanol (0.1% HCOOH), respectively.

2.5.2.5 *Ultraviolet-Visible (UV-Vis) Spectroscopy*

UV-Vis spectroscopy was conducted on a FLUOstar OPTIMA multi-well microplate reader. 96-well polystyrene plates were used with an excitation filter of $\lambda = 405 \text{ nm}$, unless otherwise stated. Data was analysed using MARS v3.01 software.

2.5.2.6 *Zeta Potential*

Zeta potential measurements were carried out using a Malvern Zetasizer Nano. The zeta potential values of enzymes in water were obtained by measuring the electrophoretic movement of the enzymes under an applied electric field at 25 $^{\circ}\text{C}$. All determinations were repeated 5 times. Zeta potentials were all carried out by Miss Maria Inam.

2.5.2.7 *Thermal Shift Assay*

Thermal shift assay measurements were conducted on an Agilent MX3005P rtPCR with an excitation filter of $\lambda = 492 \text{ nm}$ and an emission filter of $\lambda = 610 \text{ nm}$ used unless otherwise stated.

10 μL of enzyme (50 mg/mL) was added to 90 μL of SYPRO orange solution (12.5 x conc.). Heating ramps were performed at a rate of 1 $^{\circ}\text{C min}^{-1}$.

2.5.2.8 Differential Scanning Calorimetry (DSC)

DSC was carried out on each sample (2 -10 mg) in an aluminium sample holder where an empty holder was used as the reference. Changes in heat flow were recorded between 0 $^{\circ}\text{C}$ and 100 $^{\circ}\text{C}$ with a scan rate of 5 $^{\circ}\text{C min}^{-1}$, under a nitrogen stream (50 mL min^{-1}). The instrument was calibrated using indium metal standards supplied by Mettler Toledo and the data was analysed using STARe software package (version 9.30). DSC analysis was carried out by Mr Jon Husband.

2.5.3 Software

All protein crystal structure images were produced using The PyMOL Graphics System, Version 1.3, Schrödinger LLC.

2.5.4 Enzyme Kinetic Studies

2.5.4.1 pNA Protease Assay

To assess initial hydrolysis rate, 20 μL of enzyme (2 $\mu\text{g/mL}$ protein concentration) was added to 160 μL of 50 mM Tris-HCl buffer (pH 8). 20 μL of *N*-succinyl-Ala-Ala-Pro-Phe-*p*-nitroanilide in methanol at 1 mM was added to the enzyme solution. The initial rate of hydrolysis of the peptide substrate was monitored by recording the increase in absorption at $\lambda = 405 \text{ nm}$ at 25 $^{\circ}\text{C}$. Background hydrolysis was subtracted to give initial rates of hydrolysis.

2.5.4.2 α -CT Stability Assays

Native α -CT and α -CT-conjugates (2 $\mu\text{g/mL}$) were incubated in 50 mM of Tris buffer at pH 8.0 at 40 $^{\circ}\text{C}$. The assay was performed immediately after the aliquot had been taken to prevent samples degrading over time. The residual activity was calculated as a ratio of initial rates of hydrolysis, calculated as described above, for a given incubation time over the initial activity. Activity half-lives were extracted from a linear plot of the natural logarithm of residual activity against time; all stability profiles were assumed to be based on an exponential decay.

2.5.4.3 Michaelis-Menten Kinetics and Parameters

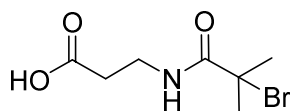
Michaelis-Menten parameters were established by performing the pNA protease assay (see Section 2.5.4.1) with varying *N*-succinyl-Ala-Ala-Pro-Phe *p*-nitroanilide substrate concentrations. A range of *N*-succinyl-Ala-Ala-Pro-Phe *p*-nitroanilide solutions were prepared by diluting with methanol to 10, 5, 2, 1, 0.5, 0.2 mM solutions; the initial hydrolysis rate was recorded as before. MARS data analysis software was used to extract values of K_m , k_{cat} and k_{cat}/K_m from a plot of substrate concentration against initial hydrolysis rate.^{85, 86}

2.5.4.4 Glucose Oxidase Stability Assays

Native α -CT and α -CT-conjugates (5 mg/mL) were incubated with glucose oxidase (GO_x) (0.5 units/mL) in 50 mM sodium acetate buffer at pH 5.0 at 30 °C. Aliquots (50 μ L) were collected and the activity assay was performed immediately. The residual activity of GO_x was calculated as a ratio of initial rates of activity at given incubation time over the initial activity. To assess initial activity rate a 10 μ L of GO_x (0.5 units/mL) was added to 190 μ L of a solution of glucose (1.72% w/v), *o*-dianisidine (0.17 mM) and horseradish peroxidase (PO_x) (3 Purpogallin units/mL). The initial rate of oxidation of *o*-dianisidine was monitored by recording the increase in absorption at $\lambda = 492$ nm at 25 °C. Background hydrolysis was subtracted to give initial rates of hydrolysis. PO_x was used in a large excess and stored in aliquots at -20 °C to ensure that this is not the limiting factor in enzyme kinetics.

2.5.5 Synthesis of I-NHS 2.1

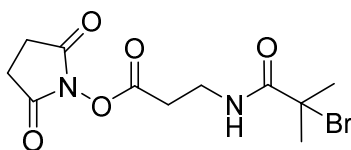
2.5.5.1 Synthesis of 3-(2-Bromo-2-methylpropionylamino)propionic acid



Synthesis previously reported by Murata *et al.*³⁸ A mixture of 2-bromo-2-methylpropionyl bromide (3.1 mL, 25 mmol) and dichloromethane (12 mL) was slowly added to a solution of β -alanine (2.23 g, 25 mmol) and sodium hydrogen carbonate (5.25 g, 62 mmol) in deionised water

(50 mL) at 0 °C, and then the mixture was stirred at room temperature for 2 h. The aqueous phase was washed with dichloromethane (25 mL × 3) and adjusted to pH 2 with 1.0 M HCl. The product was extracted with ethyl acetate (20 mL × 6) and the organic phase was dried with MgSO₄, filtered, and evaporated under vacuum. 3-(2-Bromo-2-methylpropionylamino)propionic acid was isolated by recrystallisation from a mixture of diethyl ether and *n*-hexane (1/9 volume ratio). The product was isolated in a 65% yield. ¹H NMR (300 MHz, CDCl₃): δ (ppm) 7.23 (broad s, 1H, CH₂NHC=O), 3.56 (td, 2H, ³J_{H-H} = 6.1 Hz, CH₂CH₂NHC=O), 2.65 (t, 2H, ³J_{H-H} = 6.0 Hz, HOOCCH₂CH₂NH), 1.95 (s, 6H, NHC=OC(CH₃)₂Br). ¹³C NMR (100 MHz, CDCl₃): δ (ppm) 177.6, 172.5, 62.3, 35.6, 32.4, 30.5. ESI-MS (*m/z*): [M+Na]⁺ calcd. for C₇H₁₂BrNO₃: 259.9892; found: 259.9894.

2.5.5.2 Synthesis of 2,5-Dioxo-1-pyrrolidinyl 3-(2-bromo-2-methylpropionylamino)propionate (**1-NHS 2.1**)



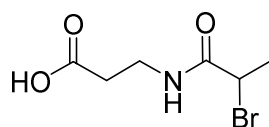
Synthesis previously reported by Murata *et al.*³⁸ *N,N'*-Diisopropylcarbodiimide (0.86 mL, 6 mmol) was slowly added to a solution of 3-(2-bromo-2-methylpropionylamino)propionic acid (1.2 g, 5 mmol), and *N*-hydroxysuccinimide (0.625 g, 6 mmol) in dichloromethane (50 mL) at 0 °C. The mixture was stirred at room temperature for 4 h. After filtering out the precipitated urea, the solution was evaporated to remove the solvent. The product was purified by recrystallisation from 2-propanol. Product isolation was achieved with an 83% yield. ¹H NMR (300 MHz, CDCl₃): δ (ppm) 7.18 (broad s, 1H, CH₂NHC=O), 3.68 (td, 2H, ³J_{H-H} = 5.8 Hz, CH₂CH₂NHC=O), 2.91-2.84 (m, 6H, O=CCH₂CH₂NH and ONC=OCH₂CH₂C=O), 1.95 (s, 6H, NHC=OC(CH₃)₂Br). ¹³C NMR (100 MHz, CDCl₃): δ (ppm) 179.3, 177.6, 172.5, 62.3, 35.9, 32.2, 31.3, 25.6. ESI-MS (*m/z*): [M+Na]⁺ calcd. for C₁₁H₁₅BrN₂O₅: 357.0092; found: 357.0055.

2.5.6 Typical Synthesis of a α -CT Macro-Initiator (CT-MI)

α -CT (1.0 g, 0.56 mmol of amine groups) was dissolved in Britton-Robinson buffer (250 mL) at 0 °C. After the addition **I-NHS 2.1** (619 mg, 1.85 mmol), the solution was stirred at 3 °C for 3 h. The α -CT macro-initiator was purified by ultrafiltration using a Millipore stirred filtration cell and a 5 kDa MWCO membrane against deionised water, and isolated by lyophilisation.

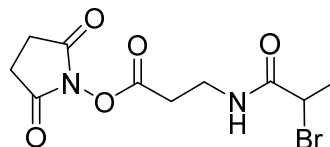
2.5.7 Synthesis of I-NHS 2.2

2.5.7.1 Synthesis of 3-(2-Bromo-propionylamino)propionic acid



Synthesis adapted from Murata *et al.*³⁸ A mixture of 2-bromo-2-propionyl bromide (2.6 mL, 25 mmol) and dichloromethane (12 mL) was slowly added to a solution of β -alanine (2.23 g, 25 mmol) and sodium hydrogen carbonate (5.25 g, 62 mmol) in deionised water (50 mL) at 0 °C. The mixture was stirred at room temperature for 2 h before the aqueous phase was washed with dichloromethane (25 mL \times 3) and adjusted to pH 2 with 1.0 M HCl. The product was extracted with ethyl acetate (20 mL \times 6), and the organic phase was dried with MgSO₄, filtered, and evaporated under vacuum. 3-(2-Bromo-propionylamino)propionic acid was isolated by recrystallisation from a mixture of diethyl ether and *n*-hexane (1/9 volume ratio). The product was isolated with a 76% yield. ¹H NMR (300 MHz, CDCl₃): δ (ppm) 6.93 (broad s, 1H, CH₂NHC=O), 4.31 (quart, 1H, ³J_{H-H} = 6.9 Hz, C=OCHBrCH₃), 3.50 (td, 2H, ³J_{H-H} = 5.7 Hz, CH₂CH₂NHC=O), 2.58 (t, 2H, ³J_{H-H} = 5.6 Hz, HOOCCH₂CH₂NH), 1.79 (d, 3H, ³J_{H-H} = 7.0 Hz, NHC=OCH₃Br). ¹³C NMR (75 MHz, CDCl₃): δ (ppm) 177.5, 175.1, 44.8, 35.3, 33.4, 23.1. ESI-MS (*m/z*): [M+Na]⁺ calcd. for C₆H₁₀BrNO₃: 245.9692; found: 245.9687.

2.5.7.2 Synthesis of 2,5-Dioxo-1-pyrrolidiny 3-(2-bromo-propionylamino)propionate
(I-NHS 2.2)



Synthesis adapted from Murata *et al.*³⁸ *N,N'*-Diisopropylcarbodiimide (0.86 mL, 6 mmol) was slowly added to a solution of 3-(2-bromo-propionylamino)propionic acid (1.2 g, 5 mmol), and *N*-hydroxysuccinimide (0.625 g, 6 mmol) in dichloromethane (50 mL) at 0 °C. The mixture was stirred at room temperature for 4 h. After filtering out the precipitated urea, the solution was evaporated to remove the solvent. The product was purified by recrystallisation from 2-propanol. Product isolation was achieved with a 69% yield. ¹H NMR (300 MHz, CDCl₃): δ (ppm) 6.93 (broad s, 1H, CH₂NHC=O), 4.34 (quart, 1H, ³J_{H-H} = 7.1 Hz, C=OCHBrCH₃), 3.63 (td, 2H, ³J_{H-H} 5.8 Hz, CH₂CH₂NHC=O), 2.84-2.79 (m, 6H, O=CCH₂CH₂NH and ONC=OCH₂CH₂C=O), 1.79 (d, 3H, ³J_{H-H} = 7.0 Hz, NHC=OCCCH₃Br). ¹³C NMR (75 MHz, CDCl₃): δ (ppm) 177.5, 169.5, 167.3, 44.2, 35.6, 33.4, 25.4, 22.7. ESI-MS (*m/z*): [M+Na]⁺ calcd. for C₁₀H₁₃BrN₂O₅: 342.9892; found: 342.9899.

2.5.8 Azidation of CT-MI-NHS 2.2.13 (CT-MI 2.3)

CT-MI-NHS 2.2.13 (10 mg, 0.0036 mmol of bromide groups) was dissolved in a DMF/water (50:50 v/v) solution (2 mL). NaN₃ (5 mg, 0.07 mmol) was added to the mixture before being stirred at room temperature for 48 hours. Excess NaN₃ and DMF were removed by dialysis and ultrafiltration using a Millipore stirred filtration cell and a 5 kDa MWCO membrane against deionised water, before isolation of the product **CT-MI 2.3** by lyophilisation. The production of the enzyme-azide conjugate was confirmed by FTIR and MALDI-ToF analysis.

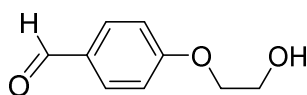
2.5.9 Typical Tryptic Digestion of Proteins

A solution of 100 mM DL-1,4-Dithiothreitol (5 μL, 0.5 μmol) was added to a solution of α-CT (0.1 mg, 0.004 μmol) in 100 mM ammonium bicarbonate solution (50 μL) and heated at 60 °C

for 15 minutes. The mixture was cooled and a solution of 200 mM iodoacetamide (5 μL , 1.0 μmol) was added and allowed to react in the dark for 30 minutes. A solution of Trypsin (10 μL , 0.5 $\mu\text{g}/\mu\text{L}$, 0.0002 μmol) was added to the solution and heated at 37 $^{\circ}\text{C}$ for 8 h. The sample was spin-filtered with a 10 kDa MWCO filter to remove any undigested protein fragments and then submitted directly to LC-MS for analysis without any further purification.

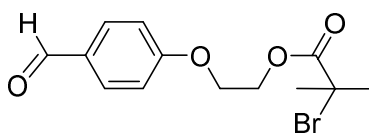
2.5.10 Synthesis of I-BA 2.1

2.5.10.1 Synthesis of 4-(2-Hydroxyethoxy)-benzaldehyde



Synthesis adapted from Liu *et al.*⁸⁷ *p*-Hydroxybenzaldehyde (3.05 g, 20 mmol), 2-bromoethanol (2.22 mL, 30 mmol), and NaOH (1.2 g, 30 mmol) were stirred in deionised water (20 mL) under reflux for 18 h. The solution was cooled to room temperature and extracted with dichloromethane (10 mL x 6). The organic phase was washed with 10% w/v NaOH solution (10 mL x 3), dried with MgSO₄, and filtered. The solvent was removed under vacuum to leave a viscous yellow liquid. Product isolation was achieved with an 87% yield. ¹H NMR (400 MHz, CDCl₃): δ (ppm) 9.85 (s, 1H, **HC=O**), 7.79-7.83 (m, 2H, ArH), 6.98-7.02 (m, 2H, ArH), 4.17 (t, 2H, ³*J*_{H-H} = 4.9 Hz, ArO**CH**₂CH₂OH), 4.01 (t, 2H, ³*J*_{H-H} = 4.9 Hz, ArOCH₂**CH**₂OH) and 3.04 (s, 1H, ArOCH₂CH₂**OH**). ¹³C NMR (100 MHz, CDCl₃): δ (ppm) 191.2, 163.8, 130.4, 129.9, 114.8, 67.7, 60.9. ESI-MS (*m/z*): [2M+Na]⁺ calcd. for C₉H₁₀O₃: 355.1092; found: 355.0716.

2.5.10.2 Synthesis of 2-(4-Formyl-phenoxy)ethyl 2-bromo-2-methylpropanoate



Synthesis adapted from Hoshi *et al.*⁸⁴ A solution of 4-(2-hydroxyethoxy)-benzaldehyde (0.5 g, 3 mmol) and triethylamine (0.5 mL, 3.6 mmol) in anhydrous dichloromethane (5 mL) was slowly

added to 2-bromo-2-methylpropionyl bromide (0.37 mL, 3 mmol) whilst stirring at 0 °C. After 10 minutes the solution was allowed to warm to room temperature, and stirred for a further 16 h. The resultant solution was washed with water (5 mL x 2), 1N HCl (5 mL x 2), NaHCO₃ solution (5 mL x 2) and brine (5 mL x 2). The organic phase was dried over MgSO₄ and the solvent removed *in vacuo* to yield a pale yellow oil. Product isolation of **I-BA 2.1** was achieved with a 69% yield. ¹H NMR (400 MHz, CDCl₃): δ (ppm) 9.90 (s, 1H, **HC=O**), 7.84-7.86 (m, 2H, ArH), 7.02-7.04 (m, 2H, ArH), 4.56 (t, 2H, ³J_{H-H} = 4.9 Hz, ArO**CH**₂CH₂O), 4.32 (t, 2H, ³J_{H-H} = 4.9 Hz, ArO**CH**₂CH₂O) and 1.94 (s, 6H, C=OC(**CH**₃)₂Br). ¹³C NMR (100 MHz, CDCl₃): δ (ppm) 190.8, 171.6, 163.4, 132.0, 128.3, 114.8, 65.8, 63.8, 55.4, 30.7. ESI-MS (*m/z*): [M+15]⁺ calcd. for C₁₃H₁₅BrO₄: 329.0273; found: 329.0445. [M+15]⁺ observed due to reaction occurring with methanol in ESI-MS.⁸⁸

2.5.11 Typical Synthesis of **CT-MI-BA**

α-CT (5 mg, 0.0028 mmol of amine groups) was dissolved in deionised water at 0 °C. After addition of **I-BA 2.1** (20 mg, 0.084 mmol) and sodium cyanoborohydride (1.5 mg, 0.0028 mmol), the mixture was stirred at 3 °C for 3 h and the α-CT-initiator conjugate was purified by dialysis using a 3.5 kDa molecular weight cut-off dialysis tube in deionised water at 3 °C for 24 h, and then isolated by lyophilisation. The production of the enzyme-initiator conjugate was confirmed MALDI-ToF analysis.

2.6 References

1. R. Fernandez-Lafuente, D. A. Cowan and A. N. P. Wood, *Enzyme Microb. Technol.*, 1995, **17**, 366-372.
2. L. L. Chen, A. D. Frankel, J. L. Harder, S. Fawell, J. Barsoum and B. Pepinsky, *Anal. Biochem.*, 1995, **227**, 168-175.
3. C. Mateo, J. M. Palomo, G. Fernandez-Lorente, J. M. Guisan and R. Fernandez-Lafuente, *Enzyme Microb. Technol.*, 2007, **40**, 1451-1463.
4. C. T. Walsh, S. Garneau-Tsodikova and G. J. Gatto, *Angew. Chem. Int. Ed.*, 2005, **44**, 7342-7372.
5. A. J. King, H. Sun, B. Diaz, D. Barnard, W. Miao, S. Bagrodia and M. S. Marshall, *Nature*, 1998, **396**, 180-183.
6. S. Kalkhof and A. Sinz, *Anal. Bioanal. Chem.*, 2008, **392**, 305-312.
7. M. P. Robin, P. Wilson, A. B. Mabire, J. K. Kiviaho, J. E. Raymond, D. M. Haddleton and R. K. O'Reilly, *J. Am. Chem. Soc.*, 2013, **135**, 2875-2878.
8. J. M. Chalker, G. J. L. Bernardes, Y. A. Lin and B. G. Davis, *Chem. Asian J.*, 2009, **4**, 630-640.
9. J. Xie and P. G. Schultz, *Nat. Rev. Mol. Cell Biol.*, 2006, **7**, 775-782.
10. A. Deiters, T. A. Cropp, M. Mukherji, J. W. Chin, J. C. Anderson and P. G. Schultz, *J. Am. Chem. Soc.*, 2003, **125**, 11782-11783.
11. E. M. Sletten and C. R. Bertozzi, *Angew. Chem. Int. Ed.*, 2009, **48**, 6974-6998.
12. N. Krall, F. P. da Cruz, O. Boutureira and G. J. L. Bernardes, *Nature Chem.*, 2016, **8**, 103-113.
13. I. Rombouts, B. Lagrain, K. A. Scherf, M. A. Lambrecht, P. Koehler and J. A. Delcour, *Sci. Rep.*, 2015, **5**, 12210.
14. D. Bontempo, K. L. Heredia, B. A. Fish and H. D. Maynard, *J. Am. Chem. Soc.*, 2004, **126**, 15372-15373.
15. S. Schoffelen, M. B. van Eldijk, B. Rooijackers, R. Raijmakers, A. J. R. Heck and J. C. M. van Hest, *Chem. Sci.*, 2011, **2**, 701-705.
16. A. Abuchowski, T. van Es, N. C. Palczuk and F. F. Davis, *J. Biol. Chem.*, 1977, **252**, 3578-3581.
17. J. A. Rodríguez-Martínez, I. Rivera-Rivera, R. J. Solá and K. Griebenow, *Biotechnol. Lett.*, 2009, **31**, 883-887.

18. F. M. Veronese, *Biomaterials*, 2001, **22**, 405-417.
19. J. M. Harris and R. B. Chess, *Nat Rev Drug Discov*, 2003, **2**, 214-221.
20. M. L. Nucci, R. Shorr and A. Abuchowski, *Adv. Drug Delivery Rev.*, 1991, **6**, 133-151.
21. F. Fuertges and A. Abuchowski, *J. Controlled Release*, 1990, **11**, 139-148.
22. R. J. Mancini, J. Lee and H. D. Maynard, *J. Am. Chem. Soc.*, 2012, **134**, 8474-8479.
23. T. Shimoboji, Z. Ding, P. S. Stayton and A. S. Hoffman, *Bioconjugate Chem.*, 2001, **12**, 314-319.
24. H. M. Li, A. P. Bapat, M. Li and B. S. Sumerlin, *Polym. Chem.*, 2011, **2**, 323-327.
25. V. Depp, A. Alikhani, V. Grammer and B. S. Lele, *Acta Biomater.*, 2009, **5**, 560-569.
26. S. A. Isarov and J. K. Pokorski, *ACS Macro Lett.*, 2015, **4**, 969-973.
27. B. S. Sumerlin, *ACS Macro Lett.*, 2012, **1**, 141-145.
28. N. Vanparijs, R. De Coen, D. Laplace, B. Louage, S. Maji, L. Lybaert, R. Hoogenboom and B. G. De Geest, *Chem. Commun.*, 2015, **51**, 13972-13975.
29. B. B. Zhu, D. N. Lu, J. Ge and Z. Liu, *Acta Biomater.*, 2011, **7**, 2131-2138.
30. S. Averick, A. Simakova, S. Park, D. Konkolewicz, A. J. D. Magenau, R. A. Mehl and K. Matyjaszewski, *ACS Macro Lett.*, 2012, **1**, 6-10.
31. W. A. Braunecker, N. V. Tsarevsky, A. Gennaro and K. Matyjaszewski, *Macromolecules*, 2009, **42**, 6348-6360.
32. M. Fantin, A. A. Isse, A. Gennaro and K. Matyjaszewski, *Macromolecules*, 2015, **48**, 6862-6875.
33. B. S. Lele, H. Murata, K. Matyjaszewski and A. J. Russell, *Biomacromolecules*, 2005, **6**, 3380-3387.
34. H. Li, M. Li, X. Yu, A. P. Bapat and B. S. Sumerlin, *Polym. Chem.*, 2011, **2**, 1531-1535.
35. J. Liu, V. Bulmus, D. L. Herlambang, C. Barner-Kowollik, M. H. Stenzel and T. P. Davis, *Angew. Chem. Int. Ed.*, 2007, **46**, 3099-3103.
36. J. T. Chin, S. L. Wheeler and A. M. Klibanov, *Biotechnol. Bioeng.*, 1994, **44**, 140-145.

37. H. J. Wiggers, J. Cheleski, A. Zottis, G. Oliva, A. D. Andricopulo and C. A. Montanari, *Anal. Biochem.*, 2007, **370**, 107-114.
38. H. Murata, C. S. Cummings, R. R. Koepsel and A. J. Russell, *Biomacromolecules*, 2013, **14**, 1919-1926.
39. C. Cummings, H. Murata, R. Koepsel and A. J. Russell, *Biomacromolecules*, 2014, **15**, 763-771.
40. M. L. M. Serralheiro and J. M. S. Cabral, *Biocatal. Biotransform.*, 1999, **17**, 3-19.
41. I. J. Castellanos, G. Flores and K. Griebenow, *J. Pharm. Sci.*, 2006, **95**, 849-858.
42. A. Wohlman, B. L. Kabacoff and S. Avakian, *Exp. Biol. Med.*, 1962, **109**, 26-28.
43. W. J. Dreyer and H. Neurath, *J. Biol. Chem.*, 1955, **217**, 527-540.
44. P. E. Wilcox, in *Methods Enzymol.*, Academic Press, 1970, vol. 19, pp. 64-108.
45. M. Kunitz and J. H. Northrop, *J. Gen. Physiol*, 1935, **18**, 433-458.
46. J. H. Wang, *Proc. Natl. Acad. Sci. U. S. A.*, 1970, **66**, 874-881.
47. J. J. Birktoft, J. Kraut and S. T. Freer, *Biochemistry*, 1976, **15**, 4481-4485.
48. J. Kraut, H. T. Wright, M. Kellerman and S. T. Freer, *Proc. Natl. Acad. Sci. U. S. A.*, 1967, **58**, 304-311.
49. H. Tsukada and D. M. Blow, *J. Mol. Biol.*, 1985, **184**, 703-711.
50. L. Hedstrom, L. Szilagyí and W. Rutter, *Science*, 1992, **255**, 1249-1253.
51. G. H. Cohen, E. W. Silverton and D. R. Davies, *J. Mol. Biol.*, 1981, **148**, 449-479.
52. C. Cummings, H. Murata, R. Koepsel and A. J. Russell, *Biomaterials*, 2013, **34**, 7437-7443.
53. H. T. S. Britton and R. A. Robinson, *J. Chem. Soc.*, 1931, 1456-1462.
54. E. Szájli, T. Fehér and K. F. Medzihradzsky, *Mol. Cell. Proteomics*, 2008, **7**, 2410-2418.
55. M. W. Duncan, H. Roder and S. W. Hunsucker, *Briefings in Functional Genomics*, 2008, **7**, 355-370.
56. M. Bucknall, K. Y. C. Fung and M. W. Duncan, *J. Am. Soc. Mass Spectrom.*, 2002, **13**, 1015-1027.
57. M. Liu, P. Tirino, M. Radivojevic, D. J. Phillips, M. I. Gibson, J.-C. Leroux and M. A. Gauthier, *Adv. Funct. Mater.*, 2013, **23**, 2007-2015.
58. F. H. Westheimer and D. E. Schmidt, *Biochemistry*, 1971, **10**, 1249-1253.

59. C. N. Pace, G. R. Grimsley and J. M. Scholtz, *J. Biol. Chem.*, 2009, **284**, 13285-13289.
60. F. Magni, F. Curnis, L. Marazzini, R. Colombo, A. Sacchi, A. Corti and M. G. Kienle, *Anal. Biochem.*, 2001, **298**, 181-188.
61. K. P. Tan, T. B. Nguyen, S. Patel, R. Varadarajan and M. S. Madhusudhan, *Nucleic Acids Res.*, 2013, **41**, W314-W321.
62. G. R. Grimsley, J. M. Scholtz and C. N. Pace, *Protein Sci.*, 2009, **18**, 247-251.
63. M. Brinkley, *Bioconjugate Chem.*, 1992, **3**, 2-13.
64. G. Moad, E. Rizzardo and S. H. Thang, *Polymer*, 2008, **49**, 1079-1131.
65. G. Moad, E. Rizzardo and S. H. Thang, *Chem. Asian J.*, 2013, **8**, 1634-1644.
66. M. Benaglia, J. Chiefari, Y. K. Chong, G. Moad, E. Rizzardo and S. H. Thang, *J. Am. Chem. Soc.*, 2009, **131**, 6914-6915.
67. D. B. Thomas, A. J. Convertine, R. D. Hester, A. B. Lowe and C. L. McCormick, *Macromolecules*, 2004, **37**, 1735-1741.
68. H. Willcock and R. K. O'Reilly, *Polym. Chem.*, 2010, **1**, 149-157.
69. H. C. Kolb, M. G. Finn and K. B. Sharpless, *Angew. Chem. Int. Ed.*, 2001, **40**, 2004-2021.
70. A. B. Mabire, M. P. Robin, W.-D. Quan, H. Willcock, V. G. Stavros and R. K. O'Reilly, *Chem. Commun.*, 2015, **51**, 9733-9736.
71. J. C. Jewett and C. R. Bertozzi, *Chem. Soc. Rev.*, 2010, **39**, 1272-1279.
72. J. V. Olsen, S.-E. Ong and M. Mann, *Mol. Cell. Proteomics*, 2004, **3**, 608-614.
73. C. M. Smith, P. R. Gafken, Z. Zhang, D. E. Gottschling, J. B. Smith and D. L. Smith, *Anal. Biochem.*, 2003, **316**, 23-33.
74. E. J. Finehout, J. R. Cantor and K. H. Lee, *Proteomics*, 2005, **5**, 2319-2321.
75. P. Tae Gwan and A. S. Hoffman, *J. Biomater. Sci., Polym. Ed.*, 1993, **4**, 493-504.
76. K. Velonia, A. E. Rowan and R. J. M. Nolte, *J. Am. Chem. Soc.*, 2002, **124**, 4224-4225.
77. E. G. DelMar, C. Largman, J. W. Brodrick and M. C. Geokas, *Anal. Biochem.*, 1979, **99**, 316-320.
78. G. V. Semisotnov, N. A. Rodionova, O. I. Razgulyaev, V. N. Uversky, A. F. Gripas and R. I. Gilmanshin, *Biopolymers*, 1991, **31**, 119-128.

79. M. W. Pantoliano, E. C. Petrella, J. D. Kwasnoski, V. S. Lobanov, J. Myslik, E. Graf, T. Carver, E. Asel, B. A. Springer, P. Lane and F. R. Salemme, *J. Biomol. Screen.*, 2001, **6**, 429-440.
80. M.-C. Lo, A. Aulabaugh, G. Jin, R. Cowling, J. Bard, M. Malamas and G. Ellestad, *Anal. Biochem.*, 2004, **332**, 153-159.
81. T. Tretyakova, M. Shushanyan, T. Partskhaladze, M. Makharadze, R. van Eldik and D. E. Khoshtariya, *Biophys. Chem.*, 2013, **175–176**, 17-27.
82. S. S. Strickler, A. V. Gribenko, A. V. Gribenko, T. R. Keiffer, J. Tomlinson, T. Reihle, V. V. Loladze and G. I. Makhatadze, *Biochemistry*, 2006, **45**, 2761-2766.
83. G. Ozyilmaz, S. S. Tukel and O. Alptekin, *J. Mol. Catal. B: Enzym.*, 2005, **35**, 154-160.
84. Y. Hoshi, Y. Xu and C. K. Ober, *Polymer*, 2013, **54**, 1762-1767.
85. H. Lineweaver and D. Burk, *J. Am. Chem. Soc.*, 1934, **56**, 658-666.
86. L. Michaelis and M. M. L. Menten, *FEBS Lett.*, 2013, **587**, 2712-2720.
87. J. Liu, P.-Y. Gu, N.-J. Li, L.-H. Wang, C.-Y. Zhang, Q.-F. Xu and J.-M. Lu, *J. Appl. Polym. Sci.*, 2013, **129**, 2913-2921.
88. L. Wang, Y. Chai, P. Tu, C. Sun and Y. Pan, *J. Mass Spectrom.*, 2011, **46**, 1203-1210.

3 Effects of Polymeric Grafting Density on the Stabilisation of α -Chymotrypsin

3.1 Abstract

In this Chapter, the synthesis and characterisation of protein-polymer conjugates using a “grafting from” approach was demonstrated. α -chymotrypsin macro-initiators were synthesised as described in Chapter 2 to allow, *via* atom-transfer radical polymerisation of hydrophilic monomers, the production of protein-polymer conjugates with varying polymeric grafting densities and molecular weights. The protein-polymer conjugates were characterised with the aid of poly(acrylamide) gel electrophoresis and ultraviolet-visible spectroscopy to confirm successful synthesis. With the aim of providing enhancement to stability without hindering the initial activity, the resulting protein-polymer conjugates were studied for differences in their initial activity and thermal stability. Aiming towards creating a one-pot system that contains multiple enzymes that are catalytically stable, the conjugates were also assessed for their ability to be incubated with a secondary enzyme.

3.2 Introduction

Enzymes are biological catalysts that can promote a wide variety of reactions in nature. Although enzymes are typically stable in their natural environments, when exposed to many external stimuli enzymes can rapidly lose catalytic ability. As discussed in Chapter 1, there are numerous different approaches that are able to increase the stability of enzymes including immobilisation, addition of various additives, and introduction of non-natural modifications. Although polymers are effective as additives to stabilise enzymes, the efficiency can be greatly improved when the polymer is covalently conjugated to the enzyme surface.¹⁻³ Protein-polymer conjugates (PPCs) have been shown to exhibit better stability against many external stimuli including pH, temperature and lyophilisation compared to the corresponding native enzyme.⁴⁻⁶

Synthesis of PPCs can cause alterations to the secondary and tertiary structure of the enzyme; this can lead to alterations to both the activity and stability of the enzyme. There are examples of the conjugation of polymers providing enhancement in stability yet causing a detrimental reduction

in the initial catalytic activity.⁷ Indeed, Velonia *et al.* synthesised PPCs from lipase B;⁸ the specific attachment of poly(polyethylene glycol acrylate) (PPEGA) to the enzyme was achieved by functionalising the single disulfide bridge (Cys293-Cys311). This conjugation resulted in a 60% reduction in initial enzymatic activity.

The positive or negative impact of the attachment of polymers to initial activity does not have a direct correlation to the effect on the enzyme's stability.⁹⁻¹² The attachment of polymers to the globular protein surface can cause a decrease in initial activity but an increase in overall stability; Luo *et al.* found that Glucose oxidase (GO_x) modified with PPEGA had a reduced initial activity of 60% compared to the native GO_x .¹² Figure 3.1 shows that although the initial enzymatic activity is reduced, the activity of the PPC after three hours is enhanced by a factor of four compared to native GO_x .

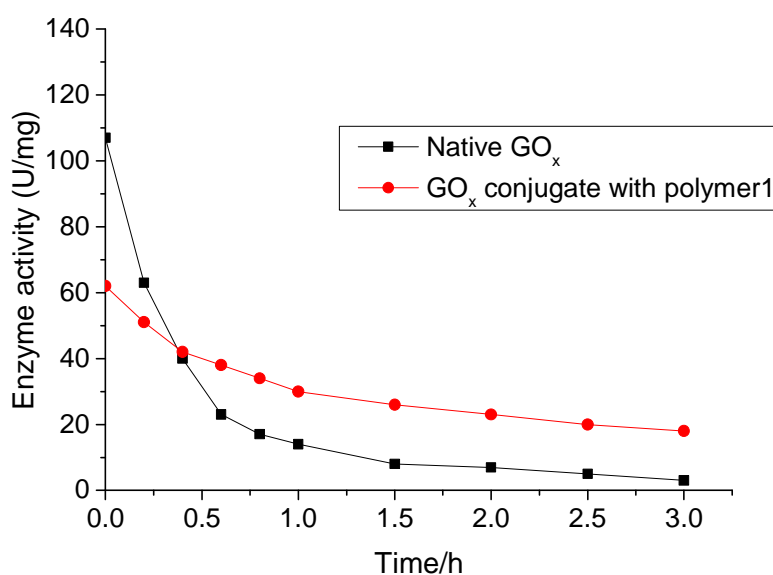


Figure 3.1 Thermal stability of native and modified Glucose oxidase (GO_x) with PPEGA incubated at 70 °C. Reproduced from Luo *et al.*¹²

As introduced in Chapter 1, Section 1.7.2, there are three different synthetic routes for the synthesis of PPCs: “Grafting to”, “grafting from”, and “grafting through”. The limitations of polymeric grafting density experienced by Lele *et al.* highlighted the requirement to employ a

“grafting from” technique to allow the study of polymeric grafting density within PPC species.¹¹ The research into the “grafting from” approach has grown greatly in recent years due to the development of reversible deactivation radical polymerisations (RDRP) including atom-transfer radical polymerisation (ATRP),¹³⁻¹⁵ nitroxide-mediated radical polymerisation (NMP),^{16, 17} and reversible addition-fragmentation chain-transfer (RAFT).¹⁸⁻²⁰ Some of these polymerisations have been adapted to enable the synthesis of polymers in mild conditions allowing for the retention of protein activity.²¹ Further research into ring opening metathesis polymerisation (ROMP) has led to the production of PPCs *via* this polymerisation process,²² which leads to the possibility of using chemistries exploited by Moatsou *et al.* to generate PPCs with defined sequence control and single monomer additions.^{23, 24}

As the attachment of polymers to the surface of α -CT can greatly improve the thermal stability and using the activated ester chemistry that was explored in the previous Chapter to create α -CT with varying initiator grafting densities, it is aimed to investigate the effect of polymeric grafting density on the stability of α -CT.

3.3 Results and Discussion

3.3.1 Synthesis and Characterisation of CT-PGMA PPCs

To evaluate the effects of polymeric grafting density upon the stability and activity of α -CT, five different PPCs were designed (Table 3.1 and Figure 3.2). α -CT PPCs with grafted poly(glycerol methacrylate) (PGMA), **CT-PGMAs**, were designed with the aim to assess whether the polymeric grafting density or overall molecular weight had a more substantial impact upon enzymatic stabilisation. Glycerol methacrylate (GMA) was chosen as the appropriate monomer for this study as it is hydrophilic and has been found to have no response towards pH or temperature changes in the conditions planned to be used that could affect stabilisation.^{25,26} It has also been reported by Lee *et al.* that trehalose, an alcohol-rich disaccharide, has been found to significantly increase enzymatic stability, therefore in addition to the primary aim, the investigation of such an effect will be explored in a non-saccharide monomer containing multiple alcohol units.^{5,27}

Table 3.1. Targeted molecular weights and grafting densities of **CT-PGMA** PPCs.

PPC	Target Polymer M_w /kDa	Average number of polymers attached	Target overall PPC M_w /kDa
CT-PGMA 3.1.5	5	1	30
CT-PGMA 3.1.25	25	1	50
CT-PGMA 3.1.50	50	1	75
CT-PGMA 3.5.5	5	5	50
CT-PGMA 3.10.5	5	10	75

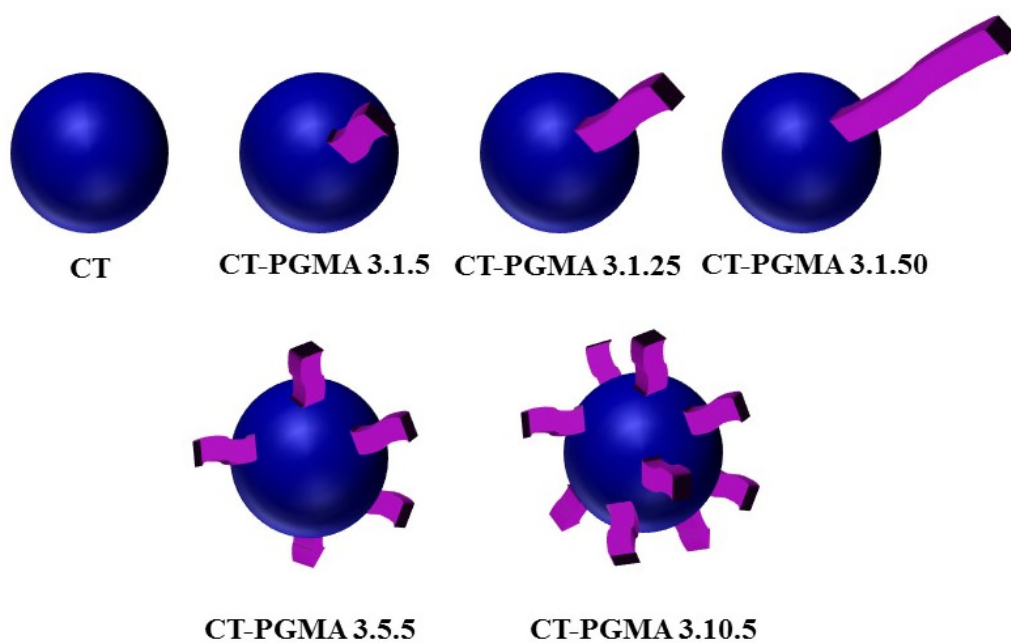


Figure 3.2 Schematic representation of targeted **CT-PGMA** structures.

To generate these **CT-PGMAs** with varying polymeric grafting densities, α -CT macro-initiators synthesised in Chapter 2 with 1, 5, and 10 initiators, **CT-MI 2.1.1**, **CT-MI 2.1.5**, **CT-MI 2.1.10** were utilised. The **CT-PGMA** species were synthesised by polymerising GMA from the surface of **CT-MI 2.1** in aqueous conditions at low temperature using ATRP reagents, copper(I) bromide and 1,1,4,7,10,10-hexamethyltriethylenetetramine (HMTETA).

to incorporate sacrificial initiator to allow the formation of free polymer and facilitate simple analysis of the grafted species.^{28, 29} This analysis assumes the formation of free polymers is equivalent to that of the polymer attached to the surface. To confirm the synthesis of the polymer is occurring from the surface of the enzyme, the addition of 2 equivalents of sacrificial initiator per **CT-MI 2.1**, **I-NHS 2.1**, was utilised to investigate the formation of free polymer alongside the formation of **CT-PGMA 3.10.5**.

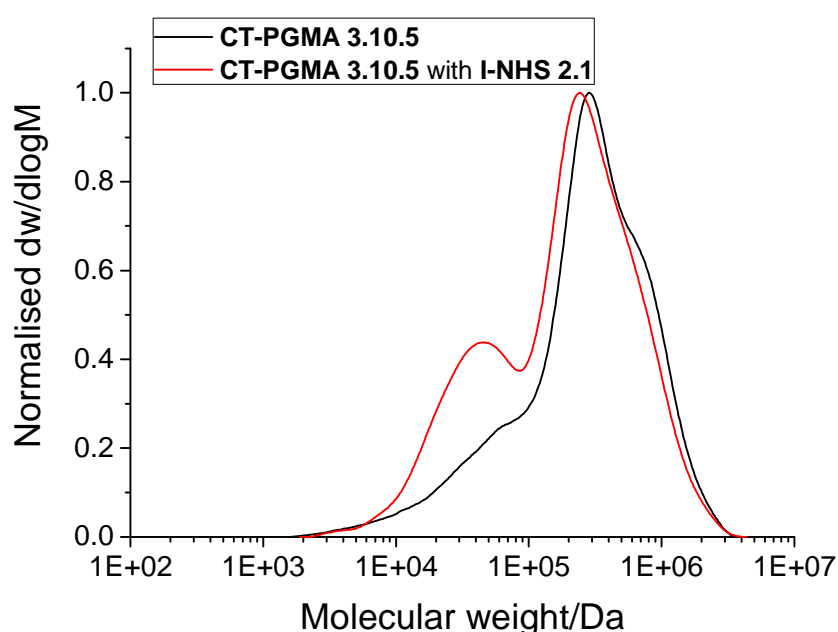
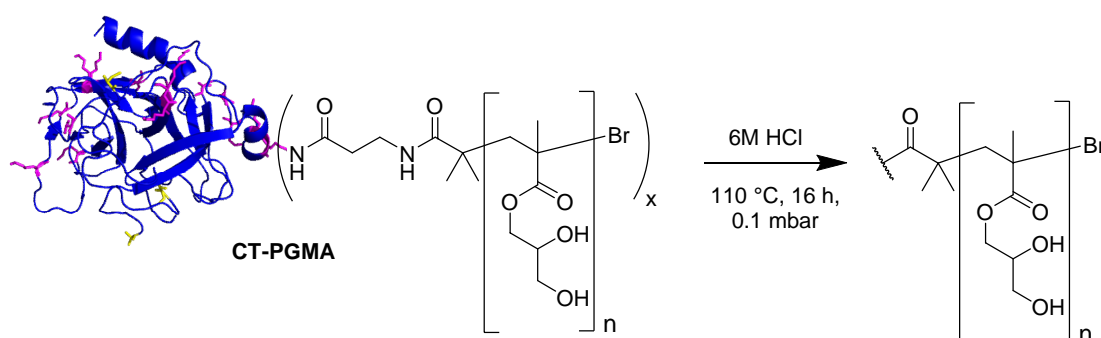


Figure 3.3 Molecular weight distributions of **CT-PGMA 3.10.5** with and without the presence of 2 equivalents of **I-NHS 2.1** obtained by SEC in DMF.

The PPC that was synthesised in the presence of sacrificial initiator produces a bimodal SEC trace with the smaller peak having a molecular weight of approximately ten times smaller than the primary peak. As **CT-PGMA 3.10.5** has been designed to have ten polymers grafted to the surface, this suggests that the free and grafted polymers are similar in nature. Noteworthy, is the presence of a low molecular weight shoulder in the **CT-PGMA 3.10.5** species synthesised without the addition of sacrificial initiator. This suggests there was a small percentage of free initiator present within **CT-MI 2.1.10**, which was not removed during the purification *via* ultrafiltration of the protein macro-initiator, described in Chapter 2.

Although this technique was useful for the analysis of the formation of PPCs, it could only be used with PPCs of high polymeric grafting densities due to a lack of solubility in DMF of native α -CT and PPCs with only a single-site polymeric graft. To enable the analysis of PPCs with low solubility in DMF and allow analysis of the polymeric species alone, the PPCs were subjected to conditions in an attempt to cleave the polymer from the surface of the protein using an acidic hydrolysis (Scheme 3.2).



Scheme 3.2 Schematic representation of acidic hydrolysis of a PPC

Although this technique has been used to analyse other polymers such as poly(dimethylaminoethyl methacrylate) (PDMAEMA),^{30, 31} it was required to establish if PGMA would be stable to the harsh acidic hydrolysis conditions necessary for successful cleavage. A polymer of GMA, **PGMA 3.1**, was synthesised using identical synthetic conditions to **CT-PGMAs** from **I-NHS 2.1** and then subjected to the acid hydrolysis and subsequently analysed by SEC (Figure 3.4 and Table 3.2). Acidic hydrolysis conditions, which are typically used to analyse amino acid composition of proteins, have been utilised to ensure full hydrolysis of the protein species.³²

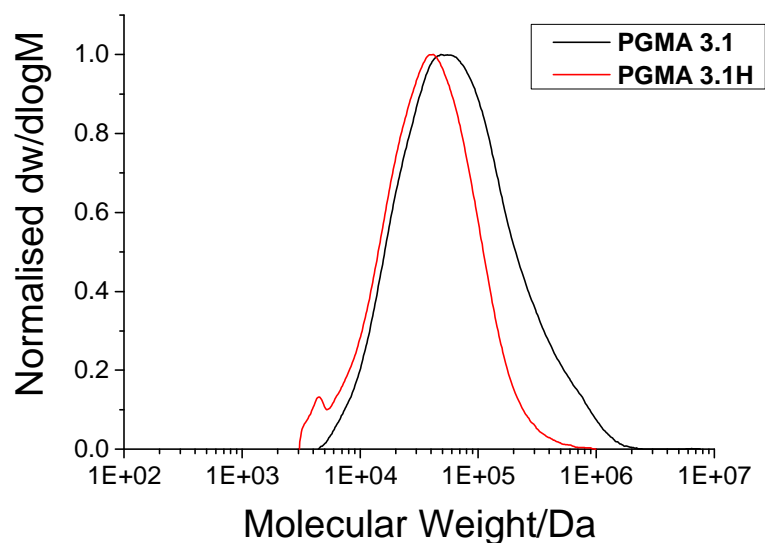


Figure 3.4 Molecular weight distributions of **PGMA 3.1** before and after (**PGMA 3.1H**) obtained by SEC in DMF.

Table 3.2 Molecular weights and dispersities for **PGMA 3.1** before and after hydrolysis (determined by SEC in DMF against poly(methyl methacrylate) standards).

Polymer	M_n /kDa	M_w /kDa	D_M
PGMA 3.1	38.4	116.9	3.04
PGMA 3.1H	23.7	53.5	2.26

PGMA 3.1 undergoes a reduction in M_n from 38.4 to 23.7 kDa during hydrolysis and it is hypothesised that this is a consequence of the hydrolysis of the ester bond connecting the glycerol functionality to the polymeric backbone. As the hydrolysis was found to cause changes in the observed molecular weight, acid hydrolysis followed by SEC analysis is not an appropriate technique for the analysis of **CT-PGMA**s.

Due to the issues of solubility and instability to cleavage conditions, SEC of both intact and hydrolysed PPCs is not a viable method for successful characterisations of **CT-PGMA** species and as such, other methods of characterisation were investigated.

3.3.1.2 *Ultraviolet-Visible (UV-Vis) Characterisation*

As most native proteins have a well-established molar extinction coefficient,³³ this can be utilised to calculate a weight percentage of protein within the PPC and subsequently extrapolate a PPC molecular weight. The extinction coefficient of a protein is most commonly defined at $\lambda = 280$ nm, where the intensity of absorption is based upon the aromatic residues, L-tryptophan, L-tyrosine, and L-phenylalanine, and as these residues are unchanged during the formation of **CT-PGMA**, this should allow for the percentage protein in the conjugate to be calculated based upon this absorption. Therefore, by employing UV-Vis spectroscopy and utilising the Beer-Lambert law (Equation 3.1), the percentage protein can be calculated using Equation 3.2 and further molecular weights of PPCs can be extracted by using Equation 3.3. All synthesised **CT-PGMA** PPCs were characterised using this method (Table 3.3).

Equation 3.1 Beer-Lambert law.

$$A = \epsilon cl$$

A = absorbance, ϵ = molar absorption coefficient, $\text{L mol}^{-1} \text{cm}^{-1}$,
 c = concentration, mol, l = path length, cm

Equation 3.2 Calculation for percentage protein from UV-Vis spectroscopy at $\lambda = 280$ nm.

$$\frac{\text{Mass of protein by absorption at 280 nm}}{\text{Mass of PPC}} \times 100 = \% \text{ protein}$$

Equation 3.3 Calculation for molecular weight of PPCs from percentage protein.

$$\frac{\text{Molar mass of native enzyme}}{\% \text{ protein}} \times 100 = \text{Molecular Weight of PPC}$$

Table 3.3 Percentage protein and molecular weights of **CT-PGMA** PPCs extracted from the intensity of absorbance at $\lambda = 280$ nm.

PPCs	Blank-Corrected Absorbance at $\lambda = 280$ nm	Concentration of PPC /mg/mL	Percentage Protein /%	PPC M_w /kDa	Target PPC M_w /kDa
CT-PGMA 3.1.5	0.569	0.48	96	26.5	30
CT-PGMA 3.1.25	0.394	0.30	81	31.2	50
CT-PGMA 3.1.50	0.054	0.18	20	124.6	75
CT-PGMA 3.5.5	0.151	0.25	41	62.4	50
CT-PGMA 3.10.5	0.496	1.10	36	70.8	75

From the UV-Vis analysis, it confirms that all species underwent polymerisation and formed **CT-PGMA** protein-polymer conjugates. It is apparent that **CT-PGMA 3.1.5** and **3.1.25** have a lower molecular weight than initially targeted, it is hypothesised that this may be due to low efficiencies of amide-based initiators that have been reported to cause poor control over the synthesis of polymers using an ATRP approach.³⁴⁻³⁶ It was also postulated that the copper has the potential to bind to the diol within the monomer species, further reducing polymerisation efficiency. **CT-PGMA 3.1.50** was found to have a greater M_w than the targeted 75 kDa by 50 kDa, resulting in a conjugate species of 125 kDa. Overall this characterisation technique has proven that successful polymerisation has occurred and a range of PPCs have been synthesised to be further investigated for enhanced catalytic properties.

3.3.1.3 *Poly(acrylamide) Gel Electrophoresis (PAGE) Characterisation*

The final technique employed to characterise the **CT-PGMA** species, which is the method most commonly used to analyse PPCs in literature, was SDS-PAGE. Gel electrophoresis separates proteins based on their electrophoretic mobility, and as SDS is incorporated to ensure the protein is in both a non-folded and negatively charged form, this electrophoretic mobility is directly

related to the molecular weight of the protein. Although SDS is able to disrupt ionic and hydrogen bonding interactions within proteins, disulfide bridges tend to be unaffected by exposure to SDS. Native α -CT was initially investigated using a 15% poly(acrylamide) gel and visualised with Coomassie Brilliant blue dye (Figure 3.5).

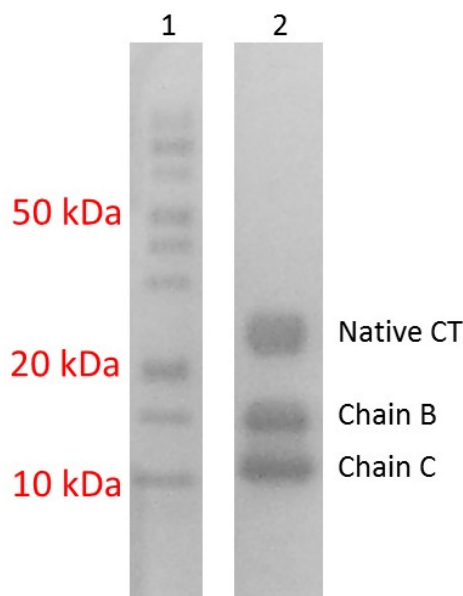


Figure 3.5 SDS-PAGE gel of Native α -CT visualised by Coomassie Brilliant Blue.
Lane 1: Protein ladder, lane 2: Native α -CT.

Upon analysis of native α -CT using SDS-PAGE analysis, three distinct bands were observed in the SDS-PAGE gel. This is not unexpected as native α -CT is comprised of three separate polypeptide chains connected by disulfide bridges. The sample preparation for SDS-PAGE involved heating samples to 80 °C, which provided enough energy to cause some of these bridges to break. However, the molecular weights of these bands, approximated from the calibration protein ladder, have allowed the assignment of bands at 15 and 10 kDa to the chains B and C respectively. Chain A is noticeably absent from the SDS-PAGE analysis; this is due to the chain A consisting of only 13 residues and having a molecular weight of approximately 1 kDa, which is outside the molecular weight range of the gel. As a consequence of the band splitting observed from native α -CT, only the band that corresponds to the entire protein at 25 kDa will be employed to assess the alterations in molecular weight of the final PPCs.

To allow the separation of a larger range of molecular weights with both PPC species and native proteins able to be separated within one gel, 4-20% gradient poly(acrylamide) gels were employed for further SDS-PAGE analysis of all **CT-PGMA** species (Figure 3.6). Densitometric analysis was performed on the subsequent gels to determine both molecular weights and dispersities (Table 3.4).

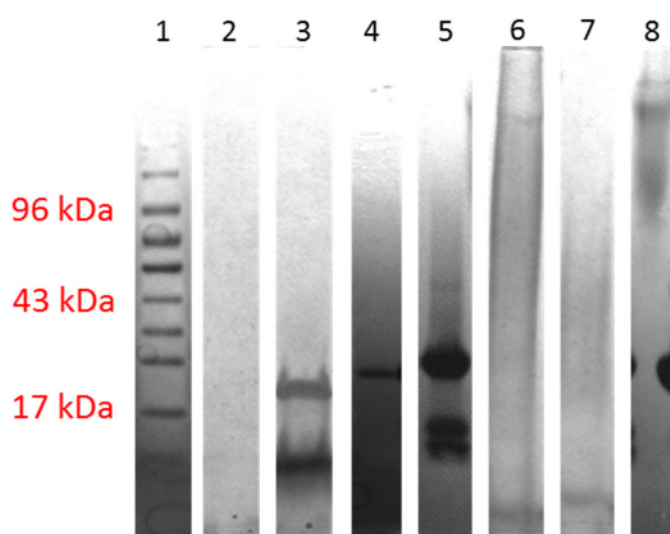


Figure 3.6 SDS-PAGE gel of **CT-PGMAs** visualised by Coomassie Brilliant Blue. Lane 1: Protein ladder, lane 2: **PGMA 3.1**, lane 3: Native α -CT, lane 4: **CT-PGMA 3.1.5**, lane 5: **CT-PGMA 3.1.25**, lane 6: **CT-PGMA 3.1.50**, lane 7: **CT-PGMA 3.5.5**, lane 8: **CT-PGMA 3.10.5**. Samples were run on various PAGE gels.

Table 3.4. Extracted molecular weights and dispersities of native α -CT and **CT-PGMAs** from densitometric analysis of SDS-PAGE gel using ImageJ.

Polymer	M_n /kDa	M_w /kDa	D_M
Native α -CT	22.2	24.8	1.12
CT-PGMA 3.1.5	27.3	27.4	1.00
CT-PGMA 3.1.25	28.8	40.6	1.41
CT-PGMA 3.1.50	108.9	157.0	1.44
CT-PGMA 3.5.5	47.7	60.5	1.27
CT-PGMA 3.10.5	173.4	195.7	1.13

Firstly, the control polymer **PGMA 3.1** was found to not be stained by the dye utilised to visualise the proteins and conjugates. Thus it is assumed that any changes seen in molecular weight can be attributed to the formation of PPC species. It is also important to note that the starting molecular weight of native α -CT from this technique is slightly reduced compared to the value obtained from matrix-assisted laser desorption/ionisation time-of-flight (MALDI-ToF) mass spectrometry and literature mass values.³⁷

However, upon analysis of the five PPCs, all species were found to have an increased molecular weight in comparison to native α -CT. As a result of the dispersity of the initiator species grafted on to the surface, as discussed in Chapter 2, and the dispersity introduced by the ATRP process, all PPC species are observed as a broad band in the PAGE gel. As such, M_n and M_w values can be extracted from the densitometric analysis to aid in the quantification of molecular weight and dispersity.

Although the extracted values correlate with the targeted results, it is apparent that PPCs with a targeted high molecular weight appear larger than expected using the SDS-PAGE analysis. For example, **CT-PGMA 3.10.5** was targeted to have a molecular weight of 75 kDa and was found to have a molecular weight of 70.8 kDa using UV-Vis spectroscopy yet SDS-PAGE analysis observed a conjugate of 195.7 kDa. As the final calibration point on the protein ladder is 170 kDa, sizes above this are out of the calibration and it is hypothesised that due to the large size of the PPCs and the gradient gel chosen, the PPCs do not show enough separation at the higher molecular weights to calculate molecular weight of the PPCs to a high level of accuracy.

Another consideration when utilising SDS-PAGE is whether the grafted polymer affects the electrophoretic mobility and therefore if the proteins used to calibrate the PPCs are an appropriate representation. SDS-PAGE analysis relies upon the sample preparation imparting a negative charge onto the protein backbone allowing the species to be attracted to the positive anode. This ionic effect induces a movement of the species through the poly(acrylamide) gel and allows

separation to occur based on molecular weight. Alterations to size-to-charge ratios, such as the introduction of polymeric species, can cause variations in the distance travelled within the gel compared with to the protein standards used for calibration.

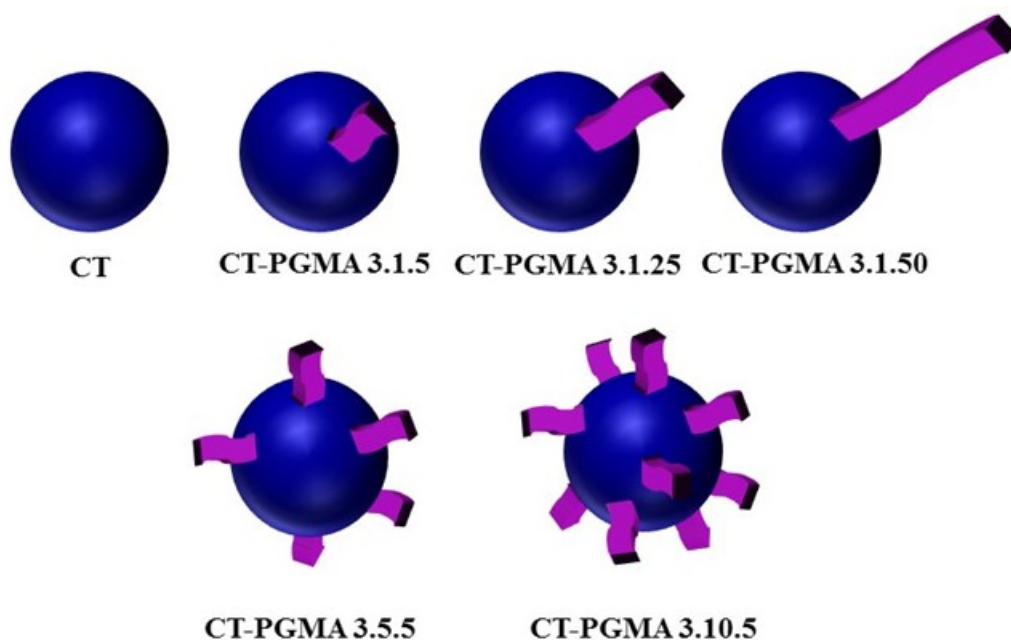
The SDS-PAGE technique has confirmed the results observed from UV-Vis spectroscopy that successful polymerisation has occurred and a range of PPCs have been synthesised. However the absolute values obtained, particularly for conjugate species with a large polymer-to-protein ratio, may not be as accurate as other techniques as polymer attachment is most likely to have altered the surface charge ratio and affected how the PPCs interact within the SDS-PAGE gel.

*3.3.1.4 Summary of Characterisation of **CT-PGMA** PPCs*

The most successful techniques that were used to characterise the **CT-PGMA** PPCs were UV-Vis spectroscopy and SDS-PAGE analysis. A summary of the five PPCs synthesised, **CT-PGMAs**, with characterisation data is shown in Table 3.5.

Table 3.5. Summary **CT-PGMA**s with UV-Vis spectroscopy and SDS-PAGE characterisation.

PPCs	Target PPC M_w /kDa	PPC M_w /kDa (UV-Vis)	PPC M_w /kDa (SDS-PAGE)
CT-PGMA 3.1.5	30	26.5	27.3
CT-PGMA 3.1.25	50	31.2	40.6
CT-PGMA 3.1.50	75	124.6	157.0
CT-PGMA 3.5.5	50	62.4	60.6
CT-PGMA 3.10.5	75	70.8	195.7



Despite all of the protein-polymer conjugates that were synthesised not being in their desired target molecular weight range, it is apparent that PPCs have been synthesised with a range of molecular weights and grafting densities to help identify correlations between these variables. Following the successful synthesis and characterisation of these **CT-PGMA** species, all PPCs were then examined for any variations in stability and activity compared to the native enzyme.

3.3.2 Activity of CT-PGMA PPCs3.3.2.1 Batch-to-Batch α -CT Variation

As the main aim of this study is to investigate the effects of polymeric species on the stability of enzymes, it is important to establish if the batches of native enzymes possess the same initial activity and stability prior to modifications. Before analysing any variations between **CT-PGMA** and the native species, it was important to ascertain if any discrepancies exist between different batches of α -CT purchased on different occasions. To this end, Michaelis-Menten parameters were extracted using the same method and protocol as in the previous Chapter from the *p*-nitroaniline (*p*NA) peptide hydrolysis assay for both batches of α -CT which were used in this Chapter (Table 3.6).

Table 3.6 Michaelis-Menten Parameters of batches of α -CT based on the *p*NA assay.

Sample	$K_m/\mu\text{M}$	$k_{\text{cat}}/\text{sec}^{-1}$	$k_{\text{cat}}/K_m/\text{sec}^{-1} \mu\text{M}^{-1}$
α -CT Batch 1	105 ± 6	14.6 ± 0.7	0.14 ± 0.01
α -CT Batch 2	64 ± 4	12.8 ± 2.0	0.20 ± 0.03

Is it evident from the Michaelis-Menten parameters that the two batches vary significantly in all extracted variables. Thus, it is apparent that parameters of **CT-PGMAs** are required to be compared with the corresponding batch of α -CT as opposed to directly with each other. To establish if there are also variations in the catalytic half-lives between batches of α -CT, both batches of α -CT utilised within this Chapter were dissolved in Britton-Robinson buffer at pH 8.0 and incubated at 40 °C with the *p*NA assay performed on aliquots;³⁸ residual activities were plotted against time and half-lives extracted by assuming an exponential decay (Figure 3.7).

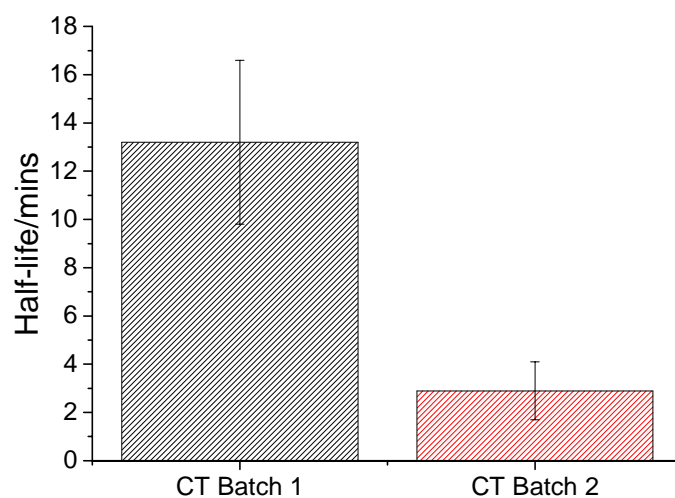


Figure 3.7 Activity half-lives of native α -CT batches at 40 °C based on *p*NA assay extracted from the linear regression of $\ln(\text{residual activity})$ against time.

The half-life for batch one is a factor of four larger than that of batch two. Due to the differences observed, a normalisation factor will be applied to any further half-life results and as such will be reported as a factor of half-life increase to negate any influence of the initial native α -CT batch half-life on the comparison of data points.

The two batches of native α -CT were analysed by multiple methods to determine the origin of the differences in activity and stability. Firstly, to ensure that there was no alteration to the overall mass of α -CT, both batches of native α -CT were analysed using matrix-assisted laser desorption/ionisation time-of-flight (MALDI-ToF) mass spectrometry (Figure 3.8).

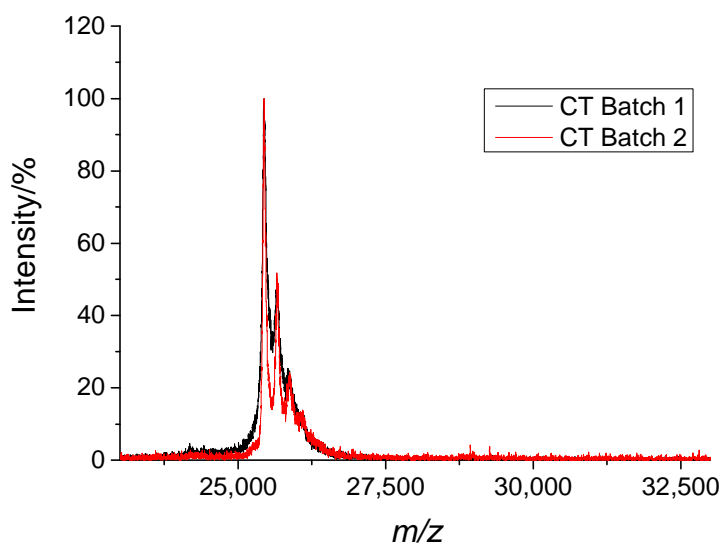


Figure 3.8 MALDI-ToF mass spectra for α -CT batch one and two recorded using a positive linear mode.

The two spectra from MALDI-ToF MS superimpose with a high degree of accuracy and suggest that there is no alteration in overall mass between the two batches. It is hypothesised that any variations in properties are either due to a change in secondary or tertiary structure or as a consequence of additives to the system.

To assess the tertiary structure of α -CT, dynamic light scattering (DLS) was employed to investigate how the batches of α -CT behave in solution (Figure 3.9). DLS allows the determination of the hydrodynamic radius of the α -CT species and can be used to confirm uniformity and size of the two batches of α -CT.

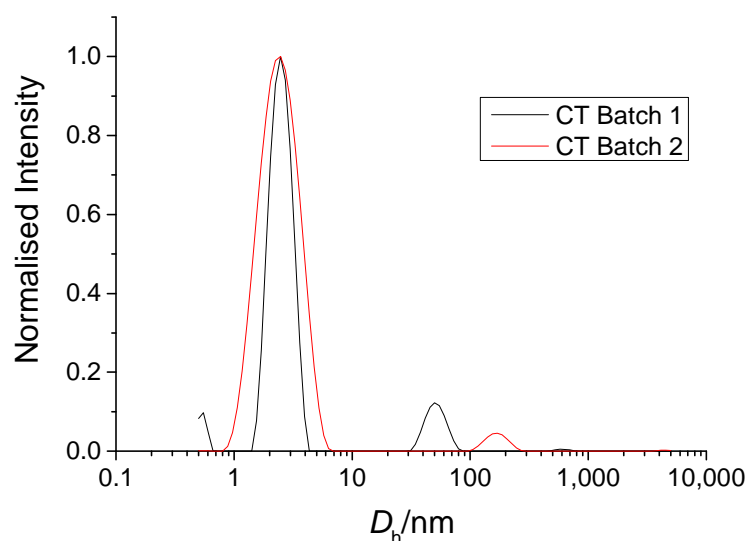


Figure 3.9 Size distributions averaged by intensity for α -CT batch one and two in water at 25 °C.

DLS analysis shows that the same overall average size for both batches of α -CT, however it is evident that the size distribution of batch two is larger than that of batch one. Although there are differences in the size distribution, there is no significant differences in the observed size.

To assess if there are any changes in the secondary structure of the α -CT batches, the circular dichroism (CD) spectra of the two batches were collected. CD is a technique that utilises circularly polarised light to analyse the folding of proteins and more specifically secondary structures within protein species including α -helices, β -sheets, β -turns, and random coils.³⁹ Far-UV CD spectra were recorded for the two batches of native α -CT (Figure 3.10).

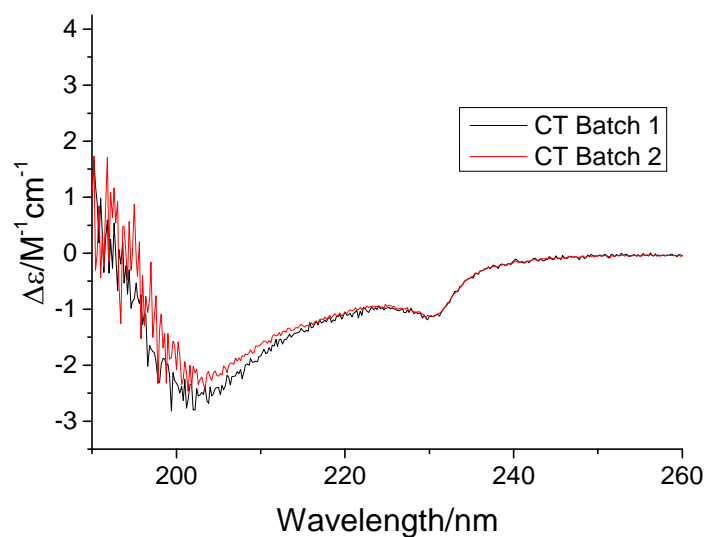


Figure 3.10 Far-UV CD spectra of native α -CT batch 1 and 2 run at 20 °C.

The spectra for the two batches of native α -CT maintain a very similar spectral profiles between 220 and 260 nm indicating similar protein folding for both batches. Below 220 nm there is a slight deviation, which potentially suggests a reduction in number of alpha helices present in batch two of α -CT.⁴⁰ However, although this reduction in response can be observed, due to the increase in signal-to-noise ratio as the wavelength decreases, it is not possible to draw reliable conclusions from this region of the spectra.

As no significant differences have been observed from the previous techniques discussed, the investigation was focused on additives that may be present in the batches of α -CT. α -CT is supplied as a greater than 85% lyophilised powder, and therefore it is clear that there are other compounds present within the composition of the native α -CT. Conductivity can be strongly affected by alterations in composition owing to an increase or decrease of salts or charges species that could be included in the α -CT composition. Therefore samples of the two batches of α -CT batch were dissolved in water at 1 mg/mL and the conductivity of the resulting solution was recorded (Table 3.7).

Table 3.7 Conductivity of batches of α -CT dissolved in water at 1 mg/mL and 20 °C.

Polymer	Conductivity (ρ) /mS cm ⁻¹
α -CT Batch 1	31
α -CT Batch 2	5

The conductivity of the second batch is a factor of six smaller than the conductivity shown by the first batch. The conductivity is most likely affected by the salt content of the supplied batches and it has been reported in the literature that the concentration of additives such as salt can have a significant effect on both catalytic activity and stability of enzymes.^{41, 42} It is hypothesised that the presence of varying levels of urea could also affect the conductivity in this manner, and can be added to proteins to add stability during lyophilisation.

Although it may be possible to purify the α -CT upon arrival, due to the lack of information about the species that could be included in the composition of the supplied α -CT, it is concluded from the analysis of the two batches of α -CT that normalisation of both activity and stability will have to be performed on the PPCs in accordance with their corresponding batch of native α -CT to allow comparisons between batches of PPCs synthesised.

3.3.2.2 *Michaelis-Menten of CT-PGMA PPCs*

As discussed in Chapter 2, a Michaelis-Menten model of kinetics is one of the most commonly used models to assess the activity of enzymes in presence of a single substrate.^{43, 44} This model was used to assess the effect of polymeric attachment on the catalytic ability of **CT-PGMA** PPCs by analysing a series of *p*NA assays with Michaelis-Menten parameters being extracted from the hydrolysis data by employing Lineweaver-Burk plots (Table 3.8).

Table 3.8 Michaelis-Menten Parameters of **CT-PGMA** PPCs based on the *p*NA assay.

Sample	$K_m/\mu\text{M}$	$k_{\text{cat}}/\text{sec}^{-1}$	$k_{\text{cat}}/K_m/\text{sec}^{-1} \mu\text{M}^{-1}$
Native α -CT Batch 1	105 ± 6	14.6 ± 0.7	0.14 ± 0.01
CT-PGMA 3.1.5	130 ± 18	14.8 ± 1.6	0.11 ± 0.02
CT-PGMA 3.1.25	164 ± 28	19.5 ± 2.8	0.12 ± 0.03
CT-PGMA 3.10.5	178 ± 27	18.6 ± 2.5	0.10 ± 0.02
Native α -CT Batch 2	64 ± 4	12.8 ± 2.0	0.20 ± 0.03
CT-PGMA 3.1.50	102 ± 18	15.3 ± 1.4	0.13 ± 0.01
CT-PGMA 3.5.5	99 ± 9	13.0 ± 0.8	0.13 ± 0.01

Given the discussion in the previous Section, PPCs have been separated by the batch of α -CT from which they were synthesised. All **CT-PGMA** species show an increase in K_m in comparison to their respective native α -CT, this suggests competitive inhibition is occurring.⁴⁵⁻⁴⁷ Competitive inhibition takes place when another molecule is binding to the enzyme, which prevents the substrate from binding to the enzyme at the same time; in this particular system it is hypothesised that the polymeric chains are preventing the substrate molecule from entering the active site. Figure 3.11 was plotted to explore the relationship between overall PPC molecular weight and the increase in K_m .

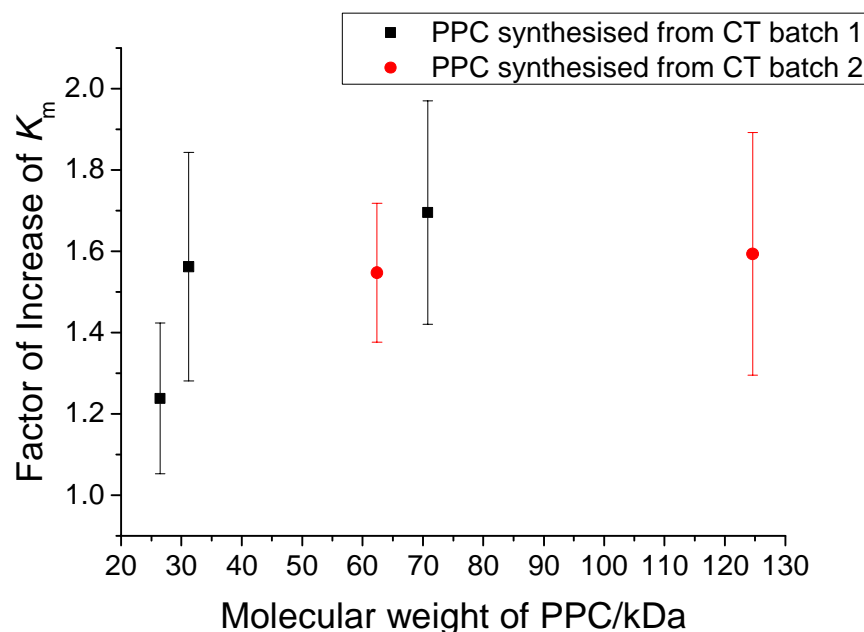


Figure 3.11 Relationship between K_m and the molecular weight of PPC as determined by UV-Vis spectroscopy.

The PPC with a single 1 kDa polymer attached, **CT-PGMA 3.1.5**, has the smallest increase in K_m in comparison to the other PPCs, but nevertheless an increase in K_m is observed, which suggests that the singly modified polymer location is close in proximity to the active site. As the single site modification is predicted to be found at one of the three *N*-termini, the location of these residues were examined with respect to the active site (Figure 3.12). Based on the increase in K_m , it is hypothesised that the *N*-terminus located at residue 144 is the most likely location of the polymeric species owing to its close proximity to the active site. The factor of increase of K_m for the PPCs with molecular weights above 30 kDa are all within error of each other, showing no further increase is observed with higher grafting density or increased molecular weight of the polymer.

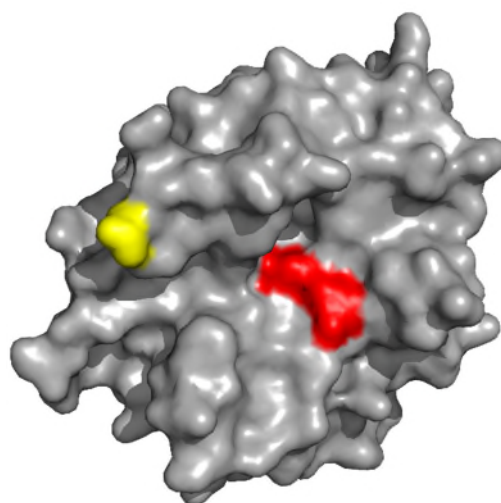


Figure 3.12 Crystal structure of α -CT (4CHA)³⁷ highlighting the location of the active site and the relative position of the *N*-terminus. Residues within the active site have been highlighted in red, *N*-terminus in yellow.

Although an increase in K_m is observed when at least one polymer is conjugated, the catalytic constant, k_{cat} , was found to either remain constant or increase slightly in comparison to the native species. There is no obvious trend between either molecular weight or grafting density that accounts for the variations observed in k_{cat} . Furthermore, despite the variations in k_{cat} and K_m , the overall efficiency remains above 65% for all PPC in comparison to the native protein values.

Despite observing competitive inhibition occurring with the attachment of the polymeric species, there is minimal effect on the overall catalytic ability, k_{cat} , of the enzyme suggesting the activity of α -CT is stable to the polymerisation conditions. As most systems require a balance of stability and activity, the decrease in catalytic efficiency of α -CT in the **CT-PGMA** species is not detrimental if this leads to an increase in stability.

3.3.3 Stability of CT-PGMA PPCs

3.3.3.1 Thermal Stability of α -CT and PGMA

Numerous polymers have been reported in the literature to provide stabilisation to enzymes as non-covalently bound additives rather than of attached to the surface of an enzyme.^{5, 48} Furthermore, the stabilisation of enzyme species has been found to be tuneable with both a

dependence on molecular weight and concentration of the polymeric species.⁴⁹ Indeed Marin *et al.* found that by increasing the concentration of poly[di(carboxylatophenoxy)phosphazene] disodium salt from 0.2 to 1.0 mg/mL, the enzymatic stability of horseradish peroxidase was increased by 10%.⁴⁹ In order to confirm whether unbound PGMA has any effect on the stabilisation of α -CT, four PGMA polymers were synthesised, aiming at different molecular weights, using identical ATRP conditions as the ones utilised to produce the **CT-PGMA** PPCs. The resulting polymers, **PGMA 3.2-3.5**, were subsequently analysed by SEC (Figure 3.13 and Table 3.9).

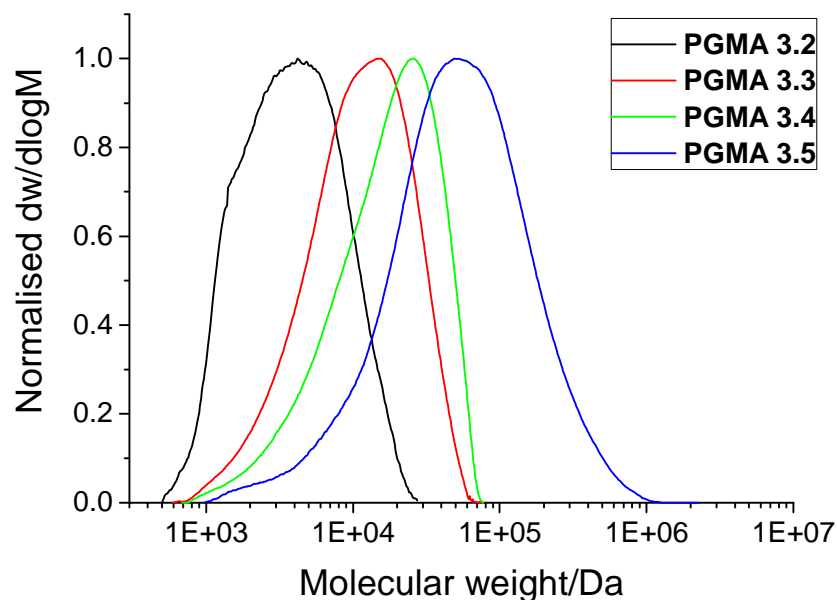


Figure 3.13 Molecular weight distributions of **PGMA 3.1-3.5** obtained by SEC in DMF.

Table 3.9 Molecular weights and dispersities for **PGMA 3.2-3.5** (determined by SEC in DMF against poly(methyl methacrylate) standards).

Polymer	M_n /kDa	M_w /kDa	D_M
PGMA 3.2	2.8	4.7	1.69
PGMA 3.3	6.2	14.1	2.28
PGMA 3.4	10.6	21.0	1.98
PGMA 3.5	24.6	81.2	3.29

Overall four polymers were synthesised with a range of molecular weights varying from 3 to 25 kDa. In all cases, the molecular weight distributions observed are relatively large for an RDRP process where dispersity is typically less than 1.2.⁵⁰ It is hypothesised that, due to the polymerisation conditions having been optimised for the synthesis of PPCs, the differences could be attributed to the variations in localised concentration of the initiator species. Indeed, the initiator used to synthesise PGMA species is unbound and therefore relies on Brownian motion and diffusion to maintain an even dispersion of initiators throughout the reaction solution. In contrast to the PPC synthesis, where the macro-initiator restricts the free movement of the initiators, producing microenvironments rich in initiating sites. Consequently, this has the ability to alter the ratios of catalyst, monomer, and initiator present in the microenvironment compared to that of the free solution creating discrepancies in the reaction kinetics and therefore leading to an increase of dispersities.

Aiming towards identifying whether a relationship exists between the thermal stability of α -CT and the concentration or molecular weight of PGMA, solutions of α -CT and **PGMA 3.2-3.5** in Britton-Robinson buffer at pH 8.0 were incubated at 40 °C with the *p*NA assay performed on solution aliquots and recorded as a ratio of the initial activity (Figure 3.14). Concentrations are reported as equivalents per enzyme to allow comparison to the corresponding **CT-PGMA** species, *i.e.* 17 equivalents per enzyme corresponds a PPC with 17 polymers conjugated to its surface. The stability tests for **PGMA 3.2-3.5** were conducted using 85 equivalents per α -CT, which is significantly larger than the number of polymer chains grafted to the surface of α -CT for the synthesis of the PPCs to ensure any stabilisation effect could be detected.

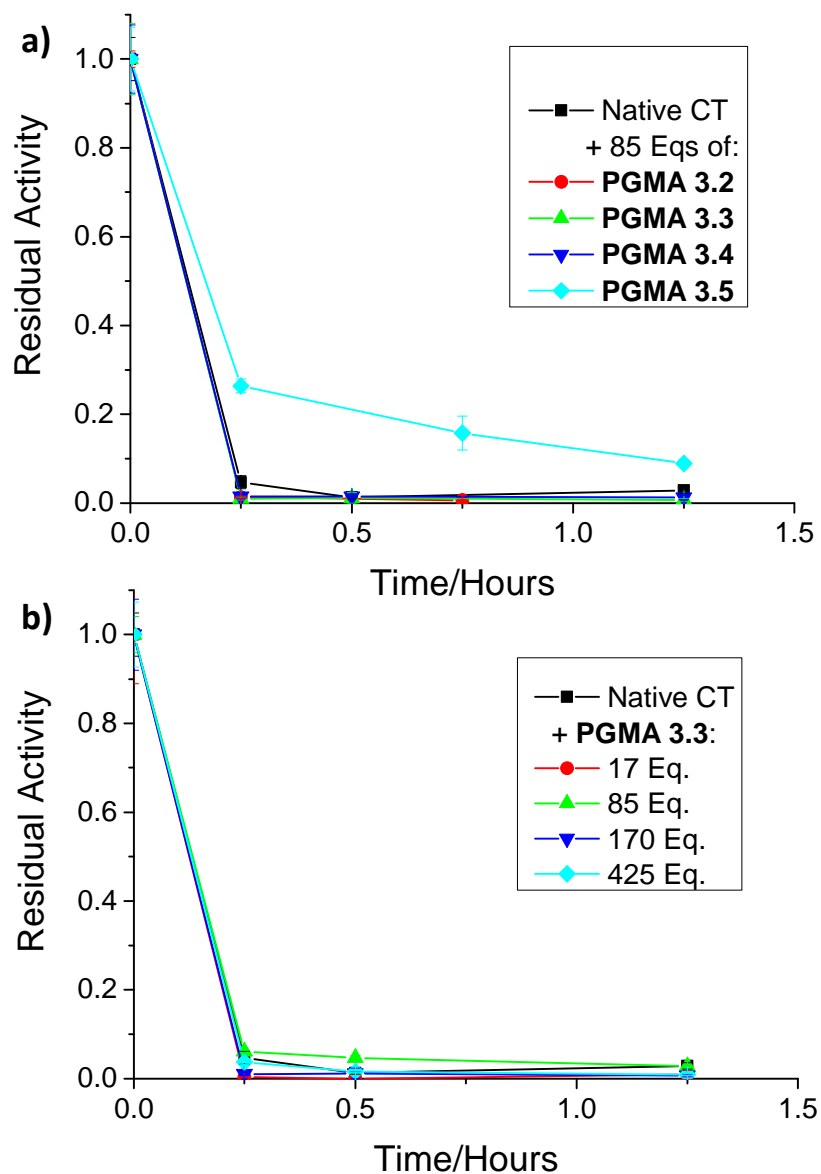


Figure 3.14 Thermal stability profiles of α -CT incubated with **PGMA 3.2-3.5** at pH 8.0, 40 °C. a) α -CT and **PGMA 3.2-3.5** at 85 equivalents per α -CT b) α -CT and **PGMA 3.3** at varying concentrations. Each data point is based on the average of four repeats of *p*NHA assay with standard deviation displayed as error.

All experiments were performed with the same batch of α -CT, hence the results were not normalised to account for discrepancies in batch-to-batch variations. When altering the molecular weight of PGMA from 2 kDa to 10 kDa, **PGMA 3.2-3.4**, no change in stability is observed in comparison to the native enzyme, even though a large excess of PGMA had been employed. Although a small increase in stability is observed for α -CT that was incubated with **PGMA 3.5**,

which has a M_n of 25 kDa, the half-life of α -CT was shown to increase from 7.2 to 10.1 minutes, which is only a small effect.

Although minimal enhancement in stability was observed from **PGMA 3.2-3.5**, the stability of α -CT was further examined under varying concentrations of **PGMA 3.3**, which has a M_n of 5 kDa and is comparable in molecular weight to the polymers attached to conjugates **CT-PGMA 3.1.5**, **3.5.5**, and **3.10.5**. In all cases of α -CT incubation with **PGMA 3.3**, no increase in stability was observed.

In conclusion, there was no increase in stability of α -CT when incubated with PGMA of a molecular weight less than or equal to 10 kDa. These results will be compared to any enhancements observed upon synthesising the corresponding protein-polymer conjugate species.

3.3.3.2 *Thermal Stability of CT-PGMA PPCs*

As the incubation of free polymer and α -CT showed no substantial increase in stability, **CT-PGMA** PPCs were used to explore if the covalent attachment of polymers could impart a higher degree of stability to α -CT. The PPCs were also examined to investigate whether a correlation was present between the stability of α -CT and the polymeric grafting density or overall PPC molecular weight. To facilitate this assessment, solutions of **CT-PGMA** PPCs in Britton-Robinson buffer at pH 8.0 were incubated at 40 °C and activity assessed with the *p*NA assay at frequent time intervals; residual activities were plotted against time and half-lives extracted by assuming an exponential decay and subsequently normalised by the half-life of the corresponding batch of α -CT (Figure 3.15).

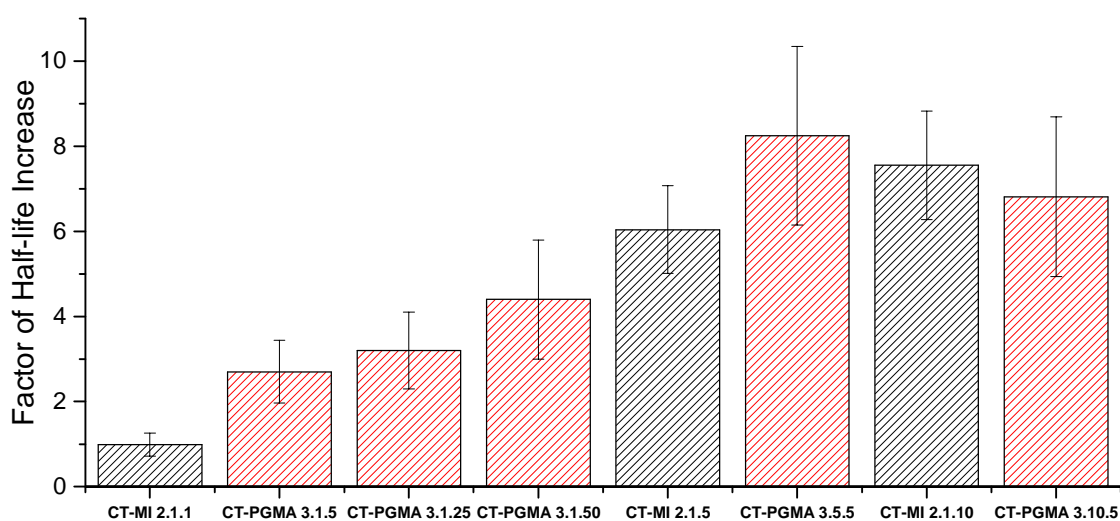


Figure 3.15 Factor of half-life increase for **CT-MI 2.1.X** and **CT-PGMA** PPC species at 40 °C and pH 8.0 extracted from the linear regression of $\ln(\text{residual activity})$ against time and normalised to the corresponding batch of α -CT.

Compared to the unconjugated polymer and enzyme samples examined in the previous Section 3.3.3.1, all PPCs showed an increase in the overall catalytic half-life. For example, **CT-PGMA 3.10.5**, which exhibits an increase in half-life with a factor of 6.8 compared to native α -CT, can be directly compared to **PGMA 3.3**, as the molecular weight of the polymer species is similar. **PGMA 3.3** was found to have no increase in half-life at concentrations more than ten-fold higher than the one that would be present in the PPCs.

As reported in the previous Chapter, the α -CT macro-initiator with one initiator bound, **CT-MI 2.1.1**, was found to not have an increase in stability compared to with the native enzyme. However, in the case of the singly grafted PPCs, there is an observed trend between the increase in the molecular weight of polymer from 2 kDa to 100 kDa, **CT-PGMA 3.1.X**, and the resulting increase in stability, with the factor of half-life increase being enhanced from 2.7 to 4.4. Previous theories suggest a singly grafted polymer has the ability to wrap around the protein enhancing the stability,⁵¹⁻⁵³ it is hypothesised that the increase in stability with increasing polymer length is related to polymers ability to encapsulate the enzyme and provide an effective shell to shield the protein from possible interactions with the surrounding solvent.

Similar to the increase in half-life observed between **CT-MI 2.1** species, **CT-PGMA** PPCs with multiple polymers conjugated to their surface, **CT-PGMA 3.5.5** and **3.10.5**, exhibit improved stability compared with their singly grafted analogues. This suggests that grafting density of the α -CT PPCs has a more significant impact upon the stability of α -CT in comparison to the overall molecular weight of the PPCs. It is hypothesised that a plausible explanation of this phenomenon is the ability of the polymer to form a barrier preventing the solvent interaction with the protein (Figure 3.16). Due to the increased surface coverage, PPCs with a higher grafting density can provide a higher degree of protection. However, it is important to note that **CT-PGMA 3.10.5** was found to have a similar stability to that of the corresponding **CT-MI 2.1** species, which suggests that the stability may be also induced by a protection of the charged residues on the proteins surface from the surrounding environment.

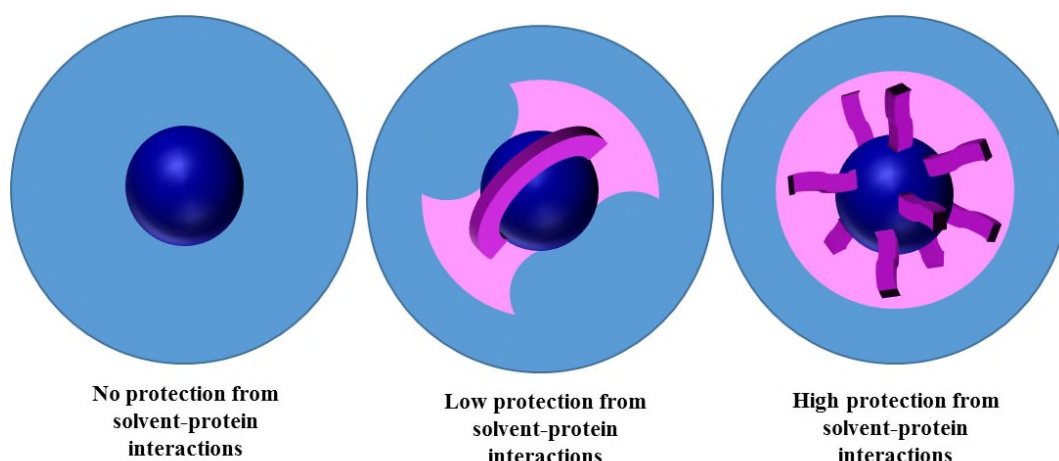


Figure 3.16 Schematic representation of the ability of polymers to prevent solvent-protein interactions based on the effect of increasing grafting density.

Although the catalytic half-life was found to be unchanged between the macro-initiator and PPC with 10 grafting sites, **CT-MI 2.1.10** and **CT-PGMA 3.10.5** respectively, further investigation was undertaken to evaluate if any other properties had been affected by the introduction of the polymer. To this end, thermal shift assays using SYPRO orange were conducted for α -CT, **CT-MI 2.1.10** and the corresponding PPC **CT-PGMA 3.10.5** to establish their melting temperature (T_m) (Figure 3.17). As explained in Chapter 2, as the protein melts and exposes

hydrophobic regions, the SYPRO orange dye can bind allowing an increase in the observed fluorescence indicating the T_m of the protein.

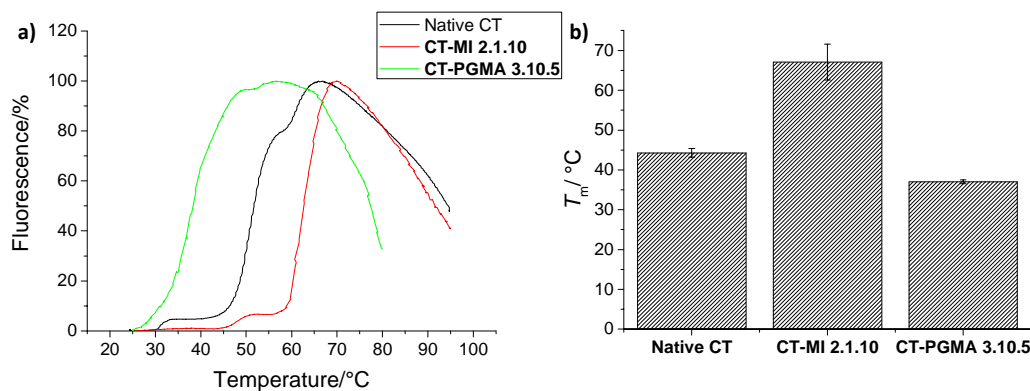


Figure 3.17 a) Thermal shift assay profile of native α -CT, **CT-MI 2.1.10**, and **CT-PGMA 3.10.5**, 5 mg/mL in water with SYPRO orange, excitation $\lambda = 492$ nm, emission $\lambda = 610$ nm and b) graph displaying half-lives of α -CT **CT-MI 2.1.10**, and **CT-PGMA 3.10.5** species. Values are obtained from triplicate repeats and error is displayed as standard deviation.

The thermal shift assay found that there was a significant reduction in the T_m of the **CT-PGMA 3.10.5** species, not only in comparison to **CT-MI 2.1.10** but also in relation to the native enzyme. Noteworthy is the fact that the stability studies previously discussed were conducted at 40 °C, which was found to be 3 °C higher than the melting temperature of **CT-PGMA 3.10.5**. This implies that during the stability studies, both native and **CT-PGMA 3.10.5** were in a conformation that exposes the hydrophobic regions of the enzyme, which may compromise some of the results.

Although the melting temperature of **CT-PGMA 3.10.5** was lower than native α -CT, this induced a higher catalytic stability within the protein and therefore, the influence of temperature on the tertiary structure and the folding of PPCs was studied. CD is typically a useful tool in analysing the tertiary structure of proteins, however the CD spectra of native α -CT was found not to contain many characteristic features that could be tracked through temperature variations. As such the structural differences of α -CT and **CT-PGMA** were investigated by employing small-angle X-ray scattering (SAXS) techniques (Figure 3.17).

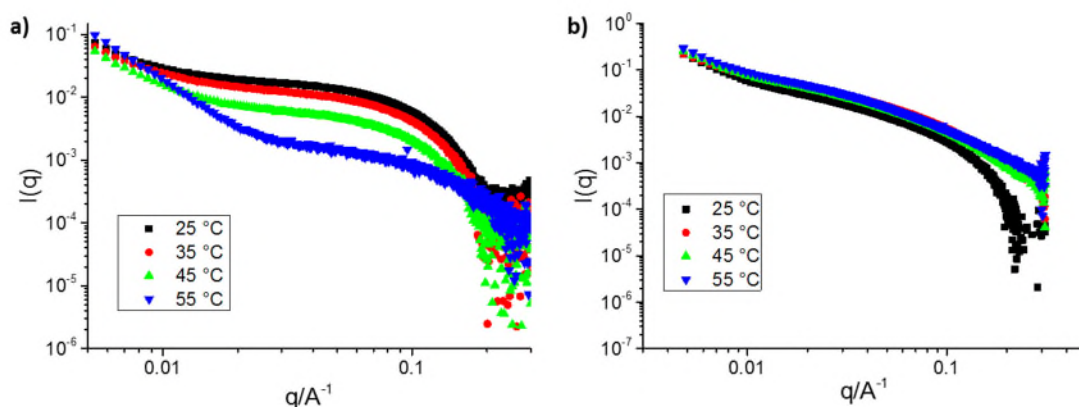


Figure 3.18 Scattering profiles of a) α -CT and b) **CT-PGMA 3.10.5** of $I(q)$ plotted against q at varying temperatures.

The scattering profiles were observed to contain variations as the temperature is increased for both α -CT and **CT-PGMA 3.10.5**. For examples, the decrease in scattering intensity when q tends towards zero indicates a decrease in concentration with an increase of temperature. Furthermore, a great change of profile is observed for the 55 °C sample, which strongly indicated a change in morphology in solution at this temperature, such as aggregation or denaturation. The changes found are more pronounced in α -CT compared to that of **CT-PGMA 3.10.5**, which is most likely due to the higher protein content of the samples, 100 wt.% and 35 wt.% respectively. It is therefore hypothesised the PGMA polymeric species dominates the scattering profile and hence little information can be extracted from the PPC SAXS data.

To allow a comparison between protein species, Kratky plots ($q^2I(q)$ vs q) for α -CT and **CT-PGMA 3.10.5** at varying temperatures were derived, from the SAXS raw data, in order to further analyse the PPC morphology. Such plots are often used to emphasise the differences between compact objects such as globular, structured proteins and that of a random chain, such as an unfolded protein.^{54, 55} Bell-shaped curves are obtained in the case of compact structures whereas a plateau is found for the random chain phase, and depending on the local rigidity of the chain, an increase in slope as q increases may also be observed.

However, Kratky plots cannot be used to compare scattering profiles of objects of different sizes such as native α -CT and **CT-PGMA 3.10.5**. Hence, a dimensionless Kratky plot was employed to avoid this limitation. The intensity, $I(q)$, is normalized to the forward scattering intensity $I(0)$, which allows comparison of samples of different molecular weights as $I(0)$ is proportional to the molecular weight. Additionally, q is normalized to the radius of gyration of the protein, which makes the angular scale independent of the protein size.⁵⁶ However, due to the aggregation observed in the scattering profile of α -CT, the R_g could only be successfully calculated for regions of the protein that were still folded causing the data to be skewed in favour of the folded protein. As a result of this, a standard Kratky plot was employed to analyse native α -CT whilst a dimensionless Kratky plot was utilised for **CT-PGMA 3.10.5** (Figure 3.19);

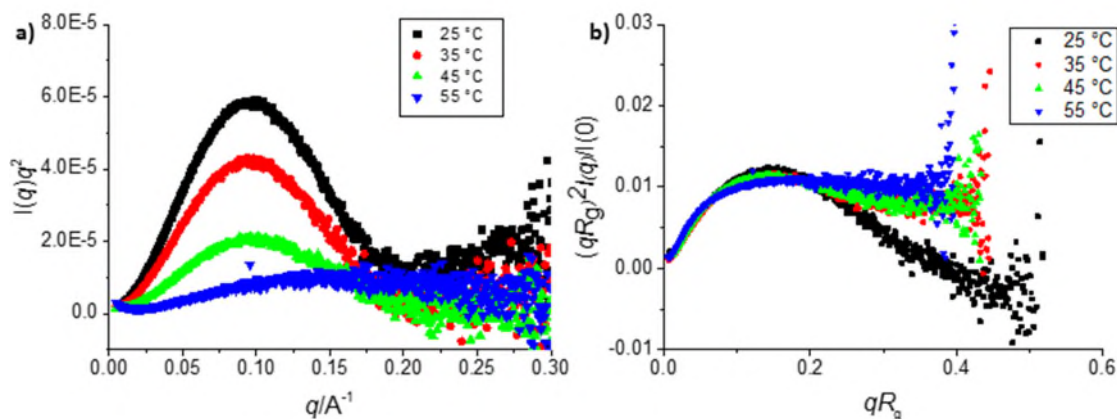


Figure 3.19 of a) Kratky plots of α -CT of $q^2 I(q)$ plotted against q and b) dimensionless Kratky plots of **CT-PGMA 3.10.5** of $(R_g q)^2 I(q)/I(0)$ plotted against $R_g q$ at varying temperatures.

Native α -CT at 25 °C plots show a symmetrical bell-shaped curve as well as a horizontal asymptote at high q values, characteristic of a folded protein. Additionally, the analysis of the dimensionless Kratky plot of **CT-PGMA 3.10.5** indicated that the structured domains of α -CT are unaltered as the bell-shape is still present.

Although a folded structure was observed for both species at 25 °C as the temperature was elevated from 25-55 °C, the disappearance of the bell-shape was observed in all cases. Furthermore, it was evident at temperatures as low as 35 °C that the loss of the folded structure

had started to occur. From the SAXS analysis, there is evidence that the PPC gradually loses its shape upon heating. Whilst it is expected that the polymer would allow longer retention of the folded structure owing to the improved catalytic stability in comparison to native α -CT, both species undergo shape changes in similar temperature ranges.

Despite observing a decrease in the T_m and no improvement upon tertiary structure retention from SAXS analysis of **CT-PGMA 3.10.5**, the catalytic half-life of all PPCs synthesised, **CT-PGMA** PPCs, is increased in comparison to that of native α -CT. Additionally it was found that PPCs with a high polymeric grafting density exhibit longer half-lives, although the enhanced half-lives appear to correlate with the stability of the corresponding macro-initiator. This has led to the hypothesis that the stability is proportional to the ability of the polymer or initiator to exclude interactions between charged residues and the surrounding environment.

3.3.3.3 *Secondary Enzyme Stability of CT-MI and CT-PGMA PPCs*

As the ultimate aim of this study is to be able to store multiple enzymes for long periods of time in one solution, the ability of a protease enzyme, such as α -CT, to digest a secondary enzyme species in solution is an important factor to investigate. It is also imperative to consider if the conjugation of only the protease enzyme within a solution of multiple enzymes, as opposed to modifying each individual enzyme, can provide the additional stability desired to all enzymes in solution. This is particularly important if protease PPCs are carried forward for use in an industrial application, as a reduction in the number of synthetic processes required would overall generate a more cost-effective product.

As in the previous Chapter glucose oxidase (GO_x) was utilised as the secondary enzyme because of its reported high stability over 24 hours.⁵⁷ To be able to assess the ability of the protease to digest proteins, α -CT, **CT-MI 2.1.10**, and **CT-PGMA 3.10.5** species were incubated with GO_x at 30 °C for 24 hours with aliquots removed and tested for GO_x activity using the *o*-dianisidine assay (Figure 3.20). **CT-PGMA 3.10.5** was chosen for this study because of its high catalytic

stability and owing to its high degree of polymeric grafting density is most likely to protect the secondary enzyme, GO_x , against digestion.

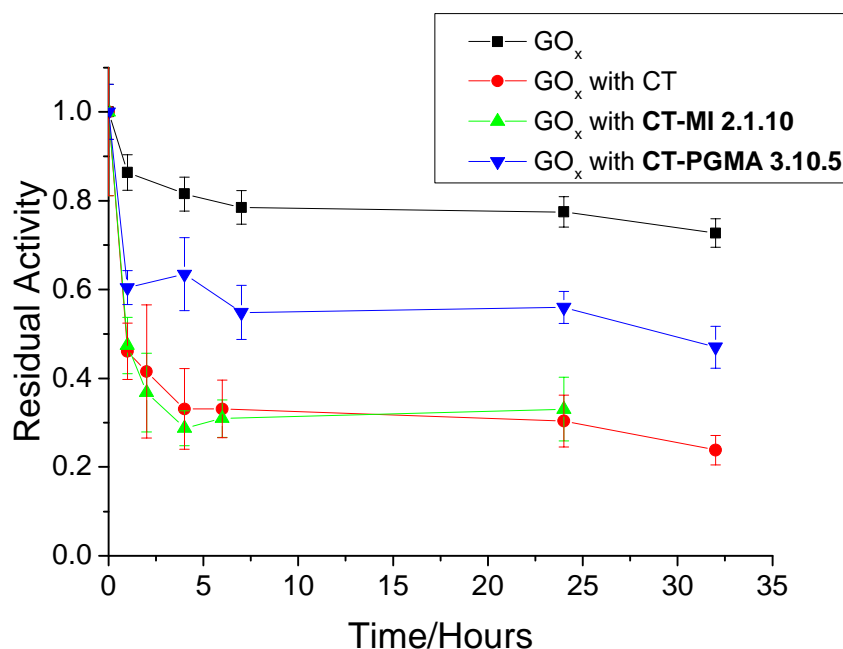


Figure 3.20 Stability profiles of GO_x incubated with α -CT, CT-MI 2.1.10, and CT-PGMA 3.10.5 at various time intervals at pH 5.0, 30 °C. Each data point is based on the average of four repeats of *o*-dianisidine assay with standard deviation displayed as error.

Although α -CT has a short half-life, the CT species were all incubated at a high protein concentration of 5 mg/mL to ensure that even as proteolytic activity is depleted, the solution would contain an active protease species. Undiluted samples of the stability tests were examined after 24 hours for protease activity using the *p*NA assay and were found to have an initial velocity that was too high to be recorded confirming proteolytic activity was still viable over the time scale of the experiment.

Upon the addition of any CT species, the activity of GO_x was observed to have a sharp initial decrease, which is most likely explained by the activity of the protease species being at its highest during the first hour of the experiment. However, this reasoning would suggest, due to the CT-MI 2.1.10 and CT-PGMA 3.10.5 PPC having a longer catalytic half-lives than that of native α -CT, GO_x activity should continue to decrease rapidly over the subsequent time points.

Despite this expectation, this was not observed and therefore the exponential decay behaviour is not directly linked to the relative activity of the protease.

It was found that after 24 hours of incubation, the activity of GO_x with native α -CT had reduced to 30% of the initial activity and no improvement was found by the addition of 10 initiators to α -CT, **CT-MI 2.1.10**. However, **CT-PGMA 3.10.5**, which has 10 PGMA polymers conjugated to the surface of α -CT, is only observed to decrease the GO_x activity to 56% of the initial activity. As there is some reduction in activity observed in the case of native GO_x to 80%, **CT-PGMA 3.10.5**, in comparison to native α -CT and **CT-MI 2.1.10**, was found to have a 72% increase in stabilisation of the secondary enzyme.

Though no increase was observed in GO_x stability upon the addition of initiators to α -CT, **CT-MI 2.1.10**, the growth of polymers from this macro-initiator to synthesise a PPC, **CT-PGMA 3.10.5**, shows a substantial increase in secondary enzyme activity which was inferred to relate to its improved stability. This suggests that the PGMA polymers can allow small molecules, such as the substrate for the *p*NA assay, to access the active site of α -CT but prevent larger peptides and proteins, including GO_x , entering the active site and losing activity due to digestion.

3.4 Conclusions

To conclude, PPCs of PGMA were successfully synthesised by ATRP from the surface of α -CT. Although the synthesis was successful, not all of the conjugates possessed the desired architectures, most likely due to poor initiation of the amide initiator in aqueous environments. As the conversion of the polymerisations could not be monitored by 1H NMR spectroscopy or GC, the characterisation methods that were observed to be best suited to analyse to composition of the final PPCs were densitometric analysis of SDS-PAGE and extraction of percentage protein from UV-Vis spectroscopy at $\lambda = 280$ nm. Despite the problems that were experienced in

batch-to-batch variations of both activity and stability, these limitations were overcome by the normalisation of data to the corresponding batch of native α -CT.

The subsequent analysis of the **CT-PGMA** PPCs revealed that, despite the competitive inhibition observed in the initial activity, all PPCs showed an improvement in catalytic stability at 40 °C. It was also observed that the grafting density of **CT-PGMA** PPCs was more influential on the catalytic stability than the overall molecular weight of the conjugate. It was postulated that the observed increase was related to the polymers ability to shield the protein residues from experiencing interactions with the surrounding environment. This suggests the most effective conjugate for enhanced thermal stability possesses a high polymeric grafting density. Although an increase was observed in catalytic stability, no enhancement was observed in either the T_m or retention of tertiary structure from SAXS analysis of **CT-PGMA 3.10.5**.

Despite only observing a retention of catalytic stability in comparison to the corresponding macro-initiator, **CT-PGMA 3.10.5** was found to allow the stability of a secondary enzyme to remain higher than both the native enzyme or the respective macro-initiator. It is hypothesised that the polymers perform molecular sieving to prevent larger substrates such as proteins reaching the active site but allows smaller molecules such as peptides through. This allows for a high enzymatic activity to be maintained for both enzymes in solution.

3.5 Experimental

3.5.1 Materials

All chemicals were obtained from Sigma-Aldrich and used without further purification unless stated otherwise. Ultrafiltration membranes were supplied by Amicon at 5 kDa MWCO. SYPRO orange was supplied as a 5,000x concentrate in DMSO from Thermo Fisher. SDS-PAGE gradient gels were purchased from Biorad.

3.5.2 Instrumentation

3.5.2.1 *¹H Nuclear Magnetic Resonance (NMR) and ¹³C NMR Spectroscopy*

¹H NMR spectra were recorded on a Bruker DPX-300 or DPX-400 spectrometer at 300 MHz and 400 MHz, respectively with MeOD, D₂O, or CDCl₃ as the solvent. The chemical shifts of protons were quoted relative to tetramethylsilane (TMS) at $\delta = 0$ ppm when using CDCl₃, or relative to residual solvent protons when using MeOD (¹H: $\delta = 3.31$ ppm) and D₂O (¹H: $\delta = 4.79$ ppm). ¹³C NMR spectra were recorded on a Bruker DPX-300 or DPX-400 spectrometer at 75 MHz and 100 MHz, respectively with MeOD, D₂O, or CDCl₃ as the solvent. The chemical shifts of carbons were quoted relative to solvent carbons when using MeOD (¹³C: $\delta = 49.3$ ppm) and CDCl₃ (¹³C: $\delta = 77.0$ ppm).

3.5.2.2 *Size Exclusion Chromatography (SEC)*

SEC was carried out using an Agilent390-MDS Multi detector suite fitted with an RI and a UV detector, and viscometer, and equipped with a guard column (VarianPLGel) and two PLGel mixed D columns. The mobile phase was DMF with 5mM NH₄BF₄ with a flow rate of 1.0 mL min⁻¹. Data was analysed using Cirrus v3.3 with calibration curves produced using Varian Polymer laboratories linear poly(methyl methacrylate) (PMMA) standards.

3.5.2.3 *Ultraviolet-Visible (UV-Vis) Spectroscopy*

UV-Vis spectroscopy for the determination of protein concentrations were conducted on a Perkin Elmer Lambda 35 UV/Vis spectrometer recording absorbance at $\lambda = 280$ nm. Utilising the

Beer-Lambert law and the molar extinction coefficient for α -CT of 50,585 L mol⁻¹ cm⁻¹, percentage protein and the theoretical molecular weights were extracted. UV-Vis spectroscopy for kinetic measurements was conducted on a FLUOstar OPTIMA multi-well microplate reader. 96-well polystyrene plates were used with an excitation filter of $\lambda = 405$ nm, unless otherwise stated. Data was analysed using MARS v3.01 software.

3.5.2.4 Sodium Dodecyl Sulfate Poly(acrylamide) Gel Electrophoresis (SDS-PAGE)

SDS-PAGE gel analysis was carried out using 4-12 % BioRad SDS-PAGE gels. Gels were run at a constant voltage, 150 V, for 60 minutes and subsequently stained with Coomassie Brilliant Blue. Samples were prepared by heating protein solutions combined with loading buffer in a 1:1 ratio for 5 minutes at 80 °C. Densitometric analysis was performed on the resulting gels using ImageJ software and determining the grayscale profile of the lane length.

3.5.2.5 Matrix-Assisted Laser Desorption/Ionization Time-of-Flight (MALDI-ToF) Mass Spectrometry

MALDI-ToF mass spectrometry was conducted on a Bruker Autoflex MALDI ToF/ToF spectrometer. The acceleration voltage was 20 kV in a positive linear mode. Protein solution (1.0-2.0 mg/mL) was mixed with an equal volume of matrix (0.5 mL of water, 0.5 mL of acetonitrile, 2 μ L of trifluoroacetic acid, and 8 mg of 4-hydroxy-3,5-dimethoxycinnamic acid), and 2 μ L of the resulting mixture was spotted on the target plate. Samples were calibrated against native α -CT. Number of sites conjugated and associated errors were extracted from a Gaussian fit of the MALDI-ToF mass spectra.

3.5.2.6 Dynamic Light Scattering (DLS)

DLS measurements were conducted on a Malvern Zetasizer Nano ZS instrument equipped with a 4 mW He-Ne 633 nm laser module and a detector at 173°. Samples were prepared at 1 mg/mL in water and filtered using a 0.22 μ m nylon filter prior to analysis. All experiments were run in triplicate with twelve acquisitions per repeat.

3.5.2.7 *Circular Dichroism (CD)*

All CD Spectra were recorded on a J-720 CD spectrometer in 1 mM pH 8.0 Tris-HCl using a quartz cuvette with a path length of 0.1 cm. All experiments were run in triplicate with three acquisitions per repeat and recorded at 20 nm min⁻¹.

3.5.2.8 *Conductivity*

Conductivity was assessed by measuring the resistance of the system and subsequently calculating by utilising Pouillet's law. Conductivity measurements were all carried out by Dr Wen Dong Quan.

3.5.2.9 *Thermal Shift Assay*

Thermal shift assay measurements were conducted on an Agilent MX3005P rtPCR with an excitation filter of $\lambda = 492$ nm and an emission filter of $\lambda = 610$ nm used unless otherwise stated. 10 μ L of enzyme (50 mg/mL) was added to 90 μ L of SYPRO orange solution (12.5x conc.). Heating ramps were performed at a rate of 1 °C min⁻¹.

3.5.2.10 *Small Angle X-Ray Scattering (SAXS)*

SAXS measurements were conducted using the beamline at the Australian Synchrotron facility. The samples were prepared in Tris-HCl pH 8.0 buffer and were run using 1.5 mm diameter quartz capillaries, which could be temperature regulated *via* a water bath to provide variable temperature measurements. The measurements were collected at an energy of 11 keV and at a sample to detector distance of 3.414 m to give a q range of 0.005 to 0.3 Å⁻¹, where q is the scattering vector and is related to the scattering angle (2θ) and the photon wavelength (λ) by Equation 3.4.

Equation 3.4 Relation of scattering angle, θ , to scattering vector, q .

$$q = \frac{4\pi\sin(\theta)}{\lambda}$$

All patterns were normalised to fixed transmitted flux using a quantitative beam stop detector. The scattering from a blank was measured in the same location as sample collection and was

subtracted for each measurement. The two-dimensional SAXS images were converted in one-dimensional SAXS profile ($I(q)$ versus q) by circular averaging, where $I(q)$ is the scattering intensity. ScatterBrain and Igor software were used to plot and analyse data.^{58,59} R_g and $I(0)$ values were determined using the Guinier-Porod fit from the NIST SANS analysis package.⁶⁰⁻⁶³ All SAXS measurements and subsequent data fitting was performed by Dr Anaís Pitto-Barry.

3.5.3 Enzyme Kinetic Studies

3.5.3.1 pNA Protease Assay

To assess initial hydrolysis rate, 20 μ L of enzyme (2 μ g/mL protein concentration) was added to 160 μ L 50 mM Tris-HCl buffer (pH 8). 20 μ L of *N*-succinyl-Ala-Ala-Pro-Phe-*p*-nitroanilide in methanol, at 1 mM, was added to the enzyme solution. The initial rate of hydrolysis of the peptide substrate was monitored by recording the increase in absorption at $\lambda = 405$ nm at 25 °C. Background hydrolysis was subtracted to give initial rates of hydrolysis.

3.5.3.2 α -CT Stability Assays

Enzyme species (2 μ g/mL protein concentration) were incubated in 50 mM Tris-HCl buffer at pH 8.0. For samples incubated at 40 °C, the assay was performed immediately after the aliquot had been taken to prevent samples degrading over time. For samples incubated at 4 °C or 20 °C, the samples were stored at -20 °C until the 28th day study was completed. The residual activity was calculated as a ratio of initial rates of hydrolysis, calculated as described above, at given incubation time over the initial activity. Activity half-lives were extracted from a linear plot of the natural logarithm of residual activity against time; all stability profiles were assumed to be based on an exponential decay. Half-life values were subsequently normalised to factor of half-life increase by dividing by the half-life of the corresponding batch of α -CT to alleviate issues of batch-to-batch variations.

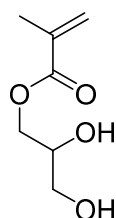
3.5.3.3 Michaelis-Menten Kinetics and Parameters

Michaelis-Menten parameters were established by performing the *p*NA protease assay (see Section 3.5.3.1) with varying *N*-succinyl-Ala-Ala-Pro-Phe *p*-nitroanilide substrate concentrations. A range of *N*-succinyl-Ala-Ala-Pro-Phe *p*-nitroanilide solutions were prepared by diluting with methanol to 10, 5, 2, 1, 0.5, 0.2 mM solutions; the initial hydrolysis rate was recorded as before. MARS data analysis software was used to extract values of K_m , k_{cat} and k_{cat}/K_m from a plot of the reciprocal of substrate concentration against the reciprocal of initial hydrolysis rate.

3.5.3.4 Glucose Oxidase Stability Assays

Native α -CT and α -CT-PPCs (5 mg/mL protein concentration) were incubated with glucose oxidase (GO_x) (0.5 units/mL) in 50 mM sodium acetate buffer at pH 5.0 at 30 °C. Aliquots (50 μ L) were collected and the activity assay was performed immediately. The residual activity of GO_x was calculated as a ratio of initial rates of activity at given incubation time over the initial activity. To assess initial activity rate a 10 μ L of GO_x (0.5 units/mL) was added to 190 μ L of a solution of glucose (1.72% w/v), *o*-dianisidine (0.17 mM) and horseradish peroxidase (PO_x) (3 Purpogallin units/mL). The initial rate of oxidation of *o*-dianisidine was monitored by recording the increase in absorption at $\lambda = 492$ nm at 25 °C. Background hydrolysis was subtracted to give initial rates of hydrolysis. PO_x was used in a large excess and stored in aliquots at -20 °C to ensure that this is not the limiting factor in enzyme kinetics.

3.5.4 Synthesis of Glycerol Methacrylate (GMA)



Synthesis previously reported by Ratcliffe *et al.*⁶⁴ Glycidyl methacrylate was passed over basic alumina before use. A solution of glycidyl methacrylate (3 mL) in deionised water (27 mL) was

refluxed at 80 °C for 9 hrs. The monomer was synthesised with a 99% yield; the product was not isolated from the reaction solution but used for polymerisations with no further processing or purification. ^1H NMR: (300 MHz, MeOD): δ (ppm) 6.01 (s, 1H, $\text{CH}_3\text{C}=\text{CHH}$), 5.59 (s, 1H, $\text{CH}_3\text{C}=\text{CHH}$), 4.00-4.15 (m, 2H, OCOCH_2), 3.87 (quin, $^3J_{\text{H-H}} = 5.3$ Hz, 1H, $\text{OCOCH}_2\text{CHOH}$), 3.46-3.58 (m, 2H, CH_2OH) and 1.78 (s, 3H, $\text{CH}_3\text{C}=\text{CH}_2$). ^{13}C NMR (75 MHz, MeOD): δ (ppm) 169.5, 135.7, 127.0, 75.7, 69.5, 62.3, 17.4. ESI-MS (m/z): $[\text{M}+\text{Na}]^+$ calcd. for $\text{C}_7\text{H}_{12}\text{O}_4$: 183.0592; found: 183.0964.

3.5.5 Typical Polymerisation of GMA to Synthesise α -CT-PPCs

A solution of GMA (10% v/v) (1040 μL , 0.8 mmol), and **CT-MI 2.1.10** (20 mg, 0.0092 mmol of initiator groups) in deionised water (7 mL) was sealed and bubbled with nitrogen in an ice bath for 20 min. A deoxygenated catalyst solutions of HMTETA (10 μL , 0.04 mmol) and Cu(I)Br (5 mg, 0.04 mmol) in deionised water (3 mL) was then added to the conjugation reactor under nitrogen bubbling. The mixture was sealed and stirred for 18 h at 4 °C. **CT-PGMA** conjugate was isolated by ultrafiltration using a Millipore stirred filtration cell and a 5 kDa MWCO membrane against deionised water and then lyophilised. The production of the PPC, **CT-PGMA**, was confirmed by UV-Vis spectroscopy and SDS-PAGE analysis.

3.5.6 Typical Polymerisation of GMA to Synthesise **PGMA**

A solution of GMA (10% v/v) (5.2 mL, 4 mmol), and **I-NHS 2.1** (11 mg, 0.046 mmol of initiator groups) in deionised water (7 mL) was sealed and bubbled with nitrogen in an ice bath for 20 min. Deoxygenated catalyst solutions of HMTETA (55 μL , 0.04 mmol) and Cu(I)Br (29 mg, 0.04 mmol) in deionised water (3 mL) was then added to the conjugation reactor under nitrogen bubbling. The mixture was sealed and stirred for 18 h at 4 °C. PGMA was isolated by dialysis with a 3.5 kDa molecular weight cut off dialysis tube in deionised water and then lyophilised. **PGMA** species were analysed by SEC in DMF.

3.5.7 Typical Hydrolysis of CT-PGMA/PGMA

PGMA (10 mg) was dissolved in 6 M HCl aq. (2 mL) in a hydrolysis tube. After three freeze-pump-thaw cycles, the hydrolysis was performed at 110 °C for 24 h at 0.1 mbar. The resulting polymer was isolated by dialysis using a 3.5 kDa molecular weight cut off dialysis tube in deionised water and subsequently lyophilised. The polymer was characterised using SEC in DMF.

3.6 References

1. M. Fernandez, M. L. Villalonga, A. Fragoso, R. Cao and R. Villalonga, *Enzyme Microb. Tech.*, 2004, **34**, 78-82.
2. G. N. Grover and H. D. Maynard, *Curr. Opin. Chem. Biol.*, 2010, **14**, 818-827.
3. E. M. Pelegri-O'Day and H. D. Maynard, *Acc. Chem. Res.*, 2016, **49**, 1777-1785.
4. C. Cummings, H. Murata, R. Koepsel and A. J. Russell, *Biomacromolecules*, 2014, **15**, 763-771.
5. J. Lee, E. W. Lin, U. Y. Lau, J. L. Hedrick, E. Bat and H. D. Maynard, *Biomacromolecules*, 2013, **14**, 2561-2569.
6. P. De, M. Li, S. R. Gondi and B. S. Sumerlin, *J. Am. Chem. Soc.*, 2008, **130**, 11288-11289.
7. P. Tae Gwan and A. S. Hoffman, *J. Biomater. Sci., Polym. Ed.*, 1993, **4**, 493-504.
8. K. Velonia, A. E. Rowan and R. J. M. Nolte, *J. Am. Chem. Soc.*, 2002, **124**, 4224-4225.
9. V. Depp, A. Alikhani, V. Grammer and B. S. Lele, *Acta Biomater.*, 2009, **5**, 560-569.
10. H. H. Liu, J. Z. Zhang, X. Luo, N. Kong, L. Cui and J. Q. Liu, *Eur. Polym. J.*, 2013, **49**, 2949-2960.
11. B. S. Lele, H. Murata, K. Matyjaszewski and A. J. Russell, *Biomacromolecules*, 2005, **6**, 3380-3387.
12. X. Luo, J. Q. Liu, G. Z. Liu, R. Wang, Z. Liu and A. H. Li, *J. Polym. Sci. Pol. Chem.*, 2012, **50**, 2786-2793.
13. W. A. Braunecker and K. Matyjaszewski, *Prog. Polym. Sci.*, 2007, **32**, 93-146.
14. M. Fantin, A. A. Isse, A. Gennaro and K. Matyjaszewski, *Macromolecules*, 2015, **48**, 6862-6875.
15. W. Tang, Y. Kwak, W. Braunecker, N. V. Tsarevsky, M. L. Coote and K. Matyjaszewski, *J. Am. Chem. Soc.*, 2008, **130**, 10702-10713.
16. R. B. Grubbs, *Polym. Rev.*, 2011, **51**, 104-137.
17. C. J. Hawker, G. G. Barclay and J. Dao, *J. Am. Chem. Soc.*, 1996, **118**, 11467-11471.
18. M. Benaglia, J. Chiefari, Y. K. Chong, G. Moad, E. Rizzardo and S. H. Thang, *J. Am. Chem. Soc.*, 2009, **131**, 6914-6915.

19. G. Moad, E. Rizzardo and S. H. Thang, *Polymer*, 2008, **49**, 1079-1131.
20. G. Moad, E. Rizzardo and S. H. Thang, *Chem. Asian J.*, 2013, **8**, 1634-1644.
21. S. Averick, A. Simakova, S. Park, D. Konkolewicz, A. J. D. Magenau, R. A. Mehl and K. Matyjaszewski, *ACS Macro Lett.*, 2012, **1**, 6-10.
22. S. A. Isarov and J. K. Pokorski, *ACS Macro Lett.*, 2015, **4**, 969-973.
23. D. Moatsou, C. F. Hansell and R. K. O'Reilly, *Chem. Sci.*, 2014, **5**, 2246-2250.
24. D. Moatsou, A. Nagarkar, A. F. M. Kilbinger and R. K. O'Reilly, *J. Polym. Sci. Part A: Polym. Chem.*, 2016, **54**, 1236-1242.
25. P. Soulonganga, C. Marion, F. Huber and P. Gerardin, *J. Appl. Polym. Sci.*, 2003, **88**, 743-749.
26. V. J. Cunningham, A. M. Alswieleh, K. L. Thompson, M. Williams, G. J. Leggett, S. P. Armes and O. M. Musa, *Macromolecules*, 2014, **47**, 5613-5623.
27. R. J. Mancini, J. Lee and H. D. Maynard, *J. Am. Chem. Soc.*, 2012, **134**, 8474-8479.
28. K. Matyjaszewski, P. J. Miller, N. Shukla, B. Immaraporn, A. Gelman, B. B. Luokala, T. M. Siclovan, G. Kickelbick, T. Vallant, H. Hoffmann and T. Pakula, *Macromolecules*, 1999, **32**, 8716-8724.
29. R. Mohammadi Sejoubsari, A. P. Martinez, Y. Kutes, Z. Wang, A. V. Dobrynin and D. H. Adamson, *Macromolecules*, 2016, **49**, 2477-2483.
30. P. van de Wetering, N. J. Zuidam, M. J. van Steenberg, O. van der Houwen, W. J. M. Underberg and W. E. Hennink, *Macromolecules*, 1998, **31**, 8063-8068.
31. H. Murata, C. S. Cummings, R. R. Koepsel and A. J. Russell, *Biomacromolecules*, 2013, **14**, 1919-1926.
32. E. L. Smith and A. Stockell, *J. Biol. Chem.*, 1954, **207**, 501-514.
33. S. C. Gill and P. H. von Hippel, *Anal. Biochem.*, 1989, **182**, 319-326.
34. Y. Li, Y. Tang, R. Narain, A. L. Lewis and S. P. Armes, *Langmuir*, 2005, **21**, 9946-9954.
35. M. Senoo, Y. Kotani, M. Kamigaito and M. Sawamoto, *Macromolecules*, 1999, **32**, 8005-8009.
36. M. Teodorescu and K. Matyjaszewski, *Macromol. Rapid Commun.*, 2000, **21**, 190-194.
37. H. Tsukada and D. M. Blow, *J. Mol. Biol.*, 1985, **184**, 703-711.

38. H. T. S. Britton and R. A. Robinson, *J. Chem. Soc.*, 1931, 1456-1462.
39. N. J. Greenfield, *Nat. Protocols*, 2007, **1**, 2876-2890.
40. N. Sreerama, S. Y. U. Venyaminov and R. W. Woody, *Protein Sci.*, 1999, **8**, 370-380.
41. Y. L. Khmel'nitsky, S. H. Welch, D. S. Clark and J. S. Dordick, *J. Am. Chem. Soc.*, 1994, **116**, 2647-2648.
42. J. M. Obón, A. Manjon and J. L. Iborra, *Enzyme Microb. Technol.*, 1996, **19**, 352-360.
43. L. Michaelis and M. M. L. Menten, *FEBS Lett.*, 2013, **587**, 2712-2720.
44. K. A. Johnson and R. S. Goody, *Biochemistry*, 2011, **50**, 8264-8269.
45. C. P. Woodbury, *Biochemistry for the Pharmaceutical Sciences*, Jones & Bartlett Learning, 2011.
46. J. M. Berg, J. L. Tymoczko and L. Stryer, *Biochemistry, Fifth Edition*, W.H. Freeman, 2002.
47. W. W. Cleland, *Biochim. Biophys. Acta*, 1963, **67**, 173-187.
48. E.-H. Lee, T. Tsujimoto, H. Uyama, M.-H. Sung, K. Kim and S. Kuramitsu, *Polymer*, 2010, **42**, 818-822.
49. A. Marin, D. P. DeCollibus and A. K. Andrianov, *Biomacromolecules*, 2010, **11**, 2268-2273.
50. M. H. Stenzel and C. Barner-Kowollik, *Mater. Horiz.*, 2016.
51. D. Moatsou, J. Li, A. Ranji, A. Pitto-Barry, I. Ntai, M. C. Jewett and R. K. O'Reilly, *Bioconjugate Chem.*, 2015, **26**, 1890-1899.
52. C. Le Cœur, S. Combet, G. Carrot, P. Busch, J. Teixeira and S. Longeville, *Langmuir*, 2015, **31**, 8402-8410.
53. E. P. DeBenedictis, E. Hamed and S. Ketten, *ACS Nano*, 2016, **10**, 2259-2267.
54. C. N. Lam, D. Chang, M. Wang, W.-R. Chen and B. D. Olsen, *J. Polym. Sci. Part A: Polym. Chem.*, 2016, **54**, 292-302.
55. D. Durand, C. Vivès, D. Cannella, J. Pérez, E. Pebay-Peyroula, P. Vachette and F. Fieschi, *J. Struct. Biol.*, 2010, **169**, 45-53.
56. R.-B. Veronique and D. Dominique, *Curr. Protein Pept. Sci.*, 2012, **13**, 55-75.
57. G. Ozyilmaz, S. S. Tukul and O. Alptekin, *J. Mol. Catal. B: Enzym.*, 2005, **35**, 154-160.

58. S. T. Mudie, *Australian Synchrotron*, 2013.
59. S. Kline, *J. Appl. Crystallogr.*, 2006, **39**, 895-900.
60. A. Guinier and G. Fournet, *Small-angle scattering of X-rays*, Wiley, 1955.
61. O. Glatter and O. Kratky, *Small Angle X-ray Scattering*, Academic Press, 1982.
62. R. J. Roe, *Methods of X-ray and Neutron Scattering in Polymer Science*, Oxford University Press, 2000.
63. P. Bartlett and R. H. Ottewill, *J. Chem. Phys.*, 1992, **96**, 3306-3318.
64. L. P. D. Ratcliffe, A. J. Ryan and S. P. Armes, *Macromolecules*, 2013, **46**, 769-777.

4 The Effect of Grafted Polymer Functionality upon the Stability of α -Chymotrypsin

4.1 Abstract

In this Chapter, the synthesis of protein-polymer conjugates utilising various polymeric functionalities and architectures was demonstrated. Polymers of hydroxypropyl methacrylate and oligo(ethylene glycol) methacrylate of varying pendant chain lengths were synthesised from the surface of a model protease enzyme, α -chymotrypsin, utilising the atom-transfer radical polymerisation technique discussed in Chapter 3. The initial activity and thermal stability were studied of the resulting protein-polymer conjugates and compared with the glycerol methacrylate analogues previously examined in Chapter 3, Section 3.3.3.

4.2 Introduction

Synthetic polymers can possess numerous functionalities that influence their properties e.g. charge density, presence of reactive groups, and responsive transitions.¹⁻³ Furthermore, these functionalities can be imparted either by polymerisation of the corresponding monomer or by synthesising a scaffold polymer and subsequently employing post-polymerisation modification chemistries.^{4,5} Post-polymerisation techniques allow for direct comparison between polymeric species as they originate from the same scaffold. However, altering the functionality of protein-polymer conjugates (PPCs) *via* this methodology is challenging as a result of the conditions required to modify the scaffold tending to require reagents, solvents, or temperatures that have the potential to denature enzymatic species.^{6,7}

Various research efforts focus on the effect that polymer functional groups have on enzymes. In a prominent such example, the Maynard group has conducted research on the incorporation of trehalose into polymers and their subsequent effect on proteins.^{8,9} To enable this, they synthesised a new monomer by modifying a styrenic derivative with a trehalose substituent (Figure 4.1).

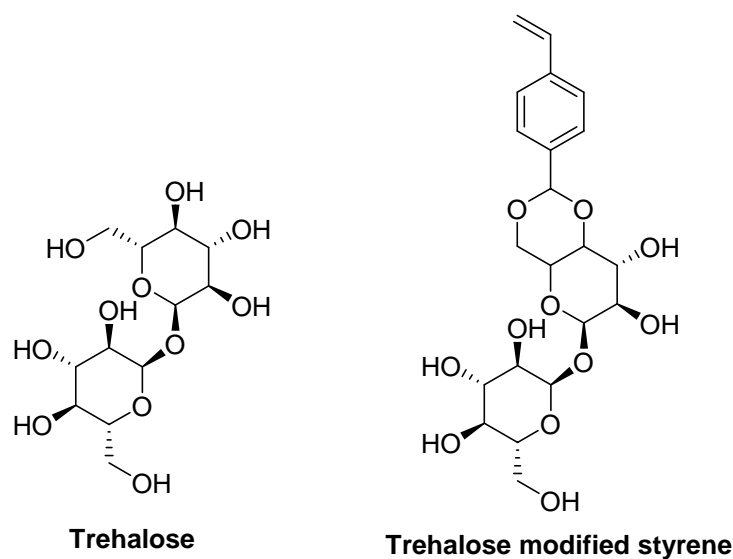


Figure 4.1 Chemical structures of trehalose and a trehalose-modified styrenic monomer utilised by Mancini *et al.*⁹

Although trehalose, a disaccharide, has previously been reported to stabilise proteins against heat and lyophilisation, the polymer-bound trehalose further improved the stability of a protein under these conditions.⁸ Moreover, when the trehalose polymeric species was conjugated to lysozyme, the resulting PPC was shown to be more resistant than the non-conjugated polymeric form against lyophilisation.⁹

As well as being employed to enhance stability, polymeric functionality has also been utilised to induce selectivity, which can depend on the characteristics of the substrate such as electrostatic charge, or environmental factors such as pH or temperature. Indeed, Murata *et al.* utilised the positively charged polymeric species poly(2-(dimethylethylammonium)ethyl methacrylate), which was conjugated to α -chymotrypsin (α -CT) to selectively catalyse negatively charged substrates (Figure 4.2).¹⁰ The electrostatic repulsions between the grafted polymers and the substrate species prevented the positively charged substrate from entering the active site and form the enzyme-substrate complex.

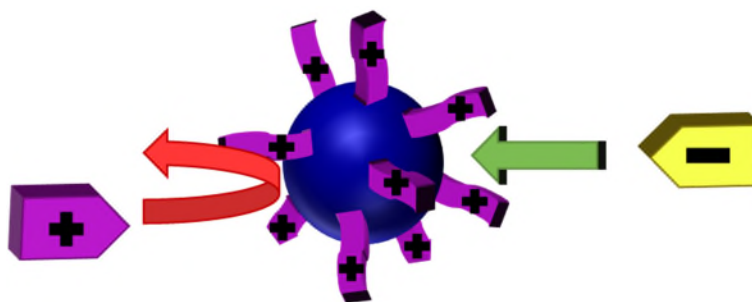


Figure 4.2 Schematic representation of the effect of charged grafted polymers on the substrate affinity and selectivity observed by Murata *et al.*¹⁰

Another method for synthesising selective PPCs is by employing responsive polymers, which can prevent access to the active site under environmental conditions in which the reaction is not desired to occur.¹¹ Polymers have been observed to have a response to many external stimuli including temperature, pH and light.¹²⁻¹⁴ One important class of such polymers is thermoresponsive polymers that undergo globule-to-random coil morphology change upon changing the solution temperature.¹⁵ Thermoresponsive polymers can be separated into two different types: Polymers with a lower critical solution temperature (LCST) and polymers with an upper critical solution temperature (UCST). LCST polymers are soluble below their transition temperature and as the temperature increases to a critical point, their hydrophilicity rapidly decreases and the chains become insoluble and collapse. In contrast, UCST polymers show the reverse behaviour; they are insoluble at low temperatures and become soluble above a critical temperature. However, this transition is typically reported as a “cloud” point, as the transition depends on concentration, amongst other things. As such, a phase diagram can be employed to extract the LCST/UCST as the curve minimum or maximum respectively (Figure 4.3).¹⁵

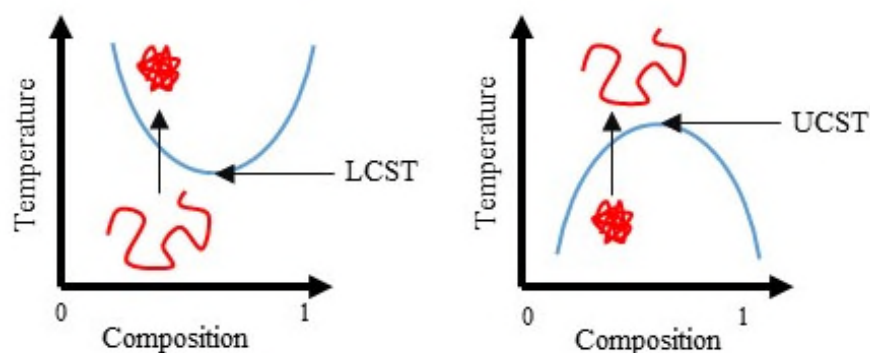


Figure 4.3 Schematic representation of the phase diagrams associated with the LCST and UCST transitions observed within thermoresponsive polymer solutions. Reproduced from Phillips *et al.*¹⁵

Numerous polymers have been found to exhibit thermoresponsive properties including poly(oligo(ethylene glycol)methacrylate) (POEGMA),¹⁶ poly(*N*-isopropylacrylamide) (PNIPAm),^{17, 18} poly(*N*-vinylpiperidone) (PNVP),¹⁹ poly(*N,N*-diethylacrylamide) (PDEAAm),²⁰ and poly(sulfobetaines).²¹ Amongst them, PNIPAm has been studied in great detail as a consequence of its sharp LCST transition occurring at approximately 32 °C, which is close to physiological temperatures leading to possible *in vivo* applications.^{22, 23} Since protein stability is largely influenced by temperature, the low temperature transition exhibited by PNIPAm is a beneficial property. Extensive research has been conducted by the Hoffman group into the conjugation of PNIPAm to the surface of various proteins and its subsequent implications to enzymatic properties.^{11, 24-29} They reported that the binding of biotin to a protein, streptavidin, was only viable when the grafted PNIPAm was in the hydrated non-collapsed form while upon collapsing the binding could not occur as the polymer hindered access to the binding site (Figure 4.4).²⁸

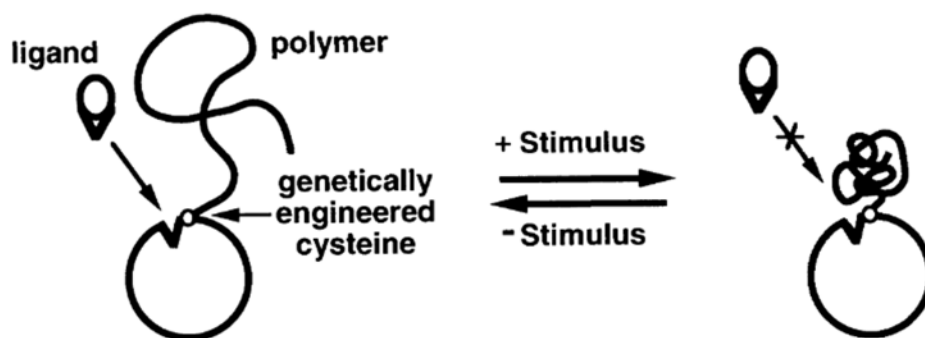


Figure 4.4 Schematic representation of responsive polymer species preventing access to the active site by undergoing a transition from Stayton *et al.*²⁸

As reversible deactivation radical polymerisation (RDRP) techniques allow the synthesis of block copolymers with varying functionalities,^{30, 31} further research has been conducted to explore the combination of UCST and LCST functionalities within a protein-conjugated polymer.³²⁻³⁴ Indeed, Cummings *et al.* synthesised block copolymers of sulfobetaine methacrylamide (SBAm), which exhibits a UCST in water, and NIPAm from the surface of α -CT.³⁵ Moreover, they observed three different enzymatic catalysis kinetics profiles that were hypothesised to be related to the morphologies adopted by the grafted polymers as a result of the corresponding LCST and UCST transitions (Figure 4.5).

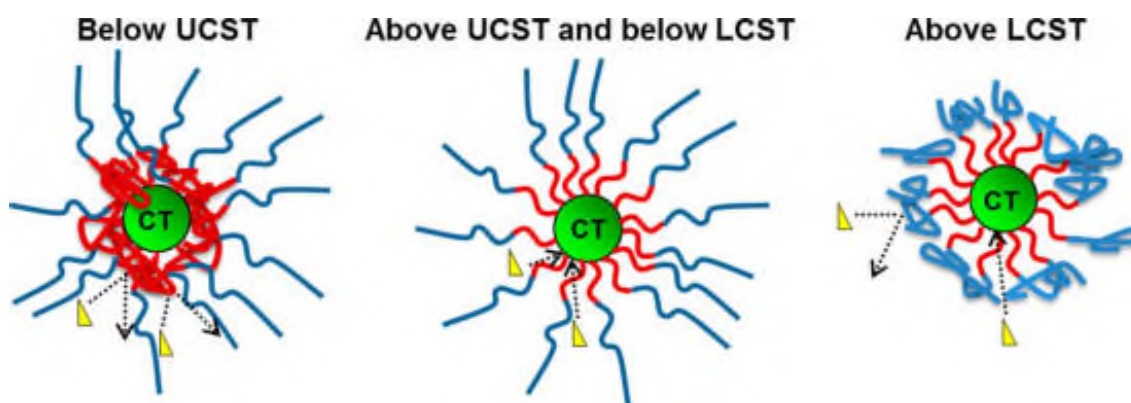


Figure 4.5 Schematic representation of the effect of combining UCST and LCST monomers to generate diblock polymers grafted to a protein from Cummings *et al.*³⁵

It was postulated that at temperatures below the UCST of PSBAm, the core block collapsed and prevented all substrate from accessing the active site. In contrast, when the PPC is exposed to temperatures above the LCST of PNIPAm, the corona block collapsed and was only able to

prevent a percentage of substrate molecules from accessing the active site. Nevertheless, the effect was not as prominent as in the case of the collapsed core polymer as a result of the collapsed corona forming a less dense layer. However, in the window between the two transitions, the substrate had unhindered access to the active site and therefore the highest rate of catalysis was observed. As such, this gives the potential for tuneable catalytic systems to be synthesised and thus to be activated at certain environmental conditions such as pH, temperature, or light intensity.

Although many polymer functionalities have been employed in the synthesis of protein-polymer conjugates, very few are directly compared based upon their functionality. Many literature studies report the effect of grafted polymers upon their activity, but many do not explore the effect on the resulting enzymatic stability over time. As such, this work aims to identify whether the polymer functionality has a direct impact upon the observed enhancement of stability of the protein-polymer conjugate species.

4.3 Results and Discussion

4.3.1 Comparison of Hydrophilic Polymers

Following from the enhanced stability of **CT-PGMA** species in Chapter 3, Section 3.3.3, further investigation was conducted into the role of the monomer on enzyme stability. Aiming towards identifying whether the structure, functionality, or hydrophilicity of GMA enables the enhanced properties that were observed, another monomer was selected to allow the comparison of properties exhibited by the resulting PPCs. PGMA did not exhibit thermal, light, or pH-responsive properties during the test conditions used in Section 3.3.3 and to allow a direct comparison, polymers that are reported as stimuli-responsive were omitted from the selection. Hence, the monomer *N*-(2-hydroxypropyl)methacrylamide (HPMA) was chosen as it is hydrophilic, and non-stimuli-responsive, but also has the additional benefit of being biocompatible and non-immunogenic. Indeed, PHPMA has been used in many biological applications including micellar drug delivery,³⁶ polymer-drug conjugates,^{37, 38} and as a blood plasma expander.³⁹

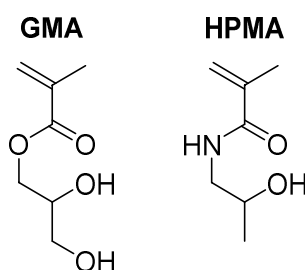


Figure 4.6 Chemical structures of GMA and HPMA.

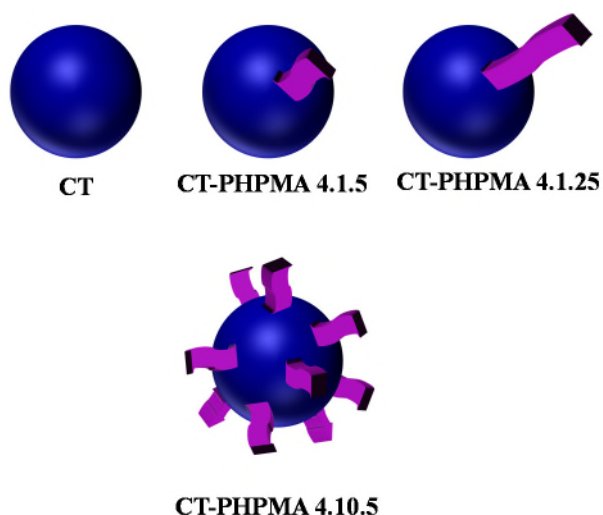
4.3.1.1 Synthesis and Characterisation of CT-PHPMA PPCs

In an attempt to make α -CT-PPCs from HPMA, which would be comparable to the **CT-PGMA** PPCs synthesised in the previous Chapter, the same PHPMA molecular weights were targeted as those of PGMA in conjugates **CT-PGMA 3.1.5**, **3.1.25**, and **3.10.5** (Table 4.1). Although only three PPCs were targeted in this study in comparison to the five conjugates of PGMA analysed in Chapter 3, the three designed PPCs include species of varying polymer

molecular weights and polymeric grafting densities to explore the effects of these variables upon the stability of α -CT.

Table 4.1. Targeted molecular weights and grafting densities of **CT-PHPMA** PPCs.

PPC	Target Polymer M_w /kDa	Average number of polymers attached	Target PPC M_w /kDa
CT-PHPMA 4.1.5	5	1	30
CT-PHPMA 4.1.25	25	1	50
CT-PHPMA 4.10.5	5	10	75



To generate **CT-PHPMA**s with the targeted polymeric grafting densities and molecular weights listed above, α -CT macro-initiators synthesised in Chapter 2 with 1 and 10 initiators conjugated to the surface of α -CT, **CT-MI 2.1.1** and **CT-MI 2.1.10** respectively, were utilised. **CT-PHPMA** PPCs were synthesised by polymerising HPMA from the surface of **CT-MI 2.1** using the copper catalysed ATRP conditions stated previously for the synthesis of **CT-PGMA** PPCs. Utilising the most effective methods found previously in Section 3.3.1, analysis of the resulting **CT-PHPMA** PPCs was performed by UV-Vis spectroscopy and sodium dodecyl sulfate poly(acrylamide) gel electrophoresis (SDS-PAGE) analysis (Figure 4.7).

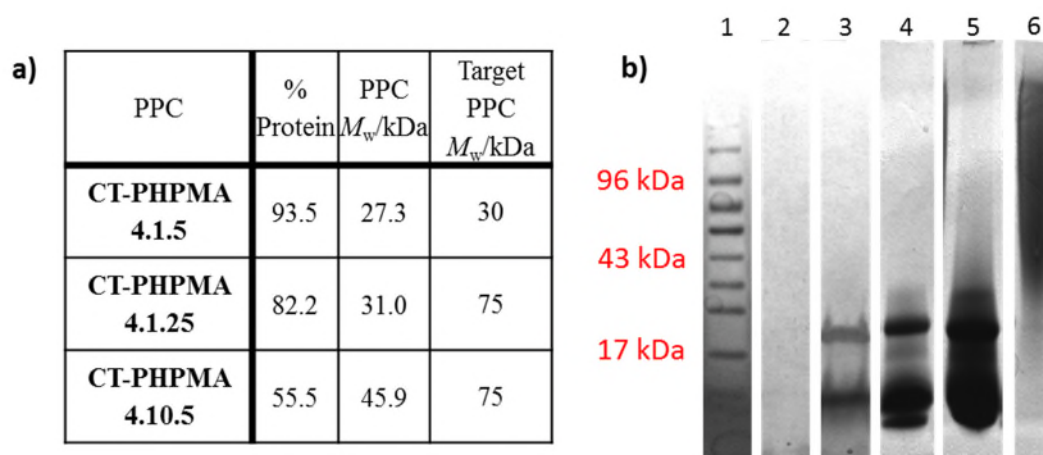


Figure 4.7 a) Weight percentage protein and molecular weights of **CT-PHPMA** PPCs extracted from absorbance at $\lambda = 280$ nm b) SDS-PAGE gel of **CT-PHPMA** PPCs visualised by Coomassie Brilliant Blue. Lane 1: Ladder, lane 2: **PHPMA**, lane 3: Native α -CT, lane 4: **CT-PHPMA 4.1.5**, lane 5: **CT-PHPMA 4.1.25**, lane 6: **CT-PHPMA 4.10.5**.

Both methods, UV-Vis and SDS-PAGE, confirmed an increase in molecular weight and therefore successful synthesis of **CT-PHPMA** in all three samples. As seen previously with **CT-PGMA** PPCs, **CT-PHPMA** PPCs were all smaller than targeted as a consequence of reduced initiator efficiencies. Along with the previously concluded reduced efficiencies as a result of an amide initiator, there are literature reports discussing the lack of control of the polymerization in the ATRP of acrylamides and methacrylamides.⁴⁰ Indeed, Teodorescu *et al.* reported that lower ATRP equilibrium constants were observed for HPMA and *N,N*-dimethylacrylamide (DMA) using ligands commonly employed in ATRP than those observed for styrenic or methacrylate monomers.^{41,42} Rademacher *et al.* were able to confirm the loss of the halogen chain-end during polymerisation of DMA *via* mass spectrometry.⁴³ It was hypothesised that the copper ions have the ability to complex with the amide functionality, and therefore the deactivation process is slowed, making the polymerisation uncontrolled.⁴⁰

To analyse differences between the PGMA and PHPMA conjugates, the three **CT-PHPMA** PPCs synthesised were compared to the corresponding **CT-PGMA** PPCs, as shown in Table 4.2.

Table 4.2. Summary **CT-PGMA** PPC and **CT-PHPMA** PPC characterisation with UV-Vis spectroscopy and SDS-PAGE analysis.

PPC	Target PPC M_w /kDa	PPC M_w /kDa (UV-Vis)	PPC M_w /kDa (SDS-PAGE)
CT-PGMA 3.1.5	30	26.5	27.3
CT-PHPMA 4.1.5	30	27.3	26.5
CT-PGMA 3.1.25	50	31.2	40.6
CT-PHPMA 4.1.25	50	31.0	37.9
CT-PGMA 3.10.5	75	70.8	195.7
CT-PHPMA 4.10.5	75	45.9	109.4

Despite **CT-HPMA** PPCs having a lower molecular weight than initially targeted when analysed by UV-Vis spectroscopy and SDS-PAGE analysis, **CT-PHPMA 4.1.5** and **4.1.25** are of comparable molecular weights to those of **CT-PGMA 3.1.5** and **3.1.25**. Although **CT-PGMA 3.10.5** and **CT-PHPMA 4.10.5** showed larger variations in molecular weight, **CT-PHPMA 4.10.5** had 10 conjugates polymers of approximately 2 kDa which was a good analogue to compare with **CT-PHPMA 4.1.5**, which had 1 covalently attached polymer of *ca.* 2 kDa. As there is strong correlation in the characterisation results between the PPCs synthesised from α -CT and both HPMA and GMA, **CT-PHPMA** PPCs were carried forward and analysed for variations in activity and stability.

4.3.1.2 *Activity of CT-PHPMA PPCs*

To assess the effect of polymeric attachment on the catalytic ability, the Michaelis-Menten parameters were extracted for **CT-PHPMA** PPCs by carrying out the *p*-nitroaniline (*p*NA) assay and employing Lineweaver-Burk plots (Table 4.3) as described in Section 2.3.5. All **CT-PHPMA** species were synthesised from the same batch of α -CT and therefore only one set of α -CT parameters is listed.

Table 4.3 Michaelis-Menten Parameters of α -CT and **CT-PHPMA** PPCs based on the *p*NA assay.

Sample	$K_m/\mu\text{M}$	$k_{\text{cat}}/\text{sec}^{-1}$	$k_{\text{cat}}/K_m/\text{sec}^{-1} \mu\text{M}^{-1}$
Native α -CT Batch 2	64 ± 4	12.8 ± 2.0	0.20 ± 0.03
CT-PHPMA 4.1.5	98 ± 4	10.0 ± 0.4	0.10 ± 0.01
CT-PHPMA 4.1.25	69 ± 8	10.0 ± 1.0	0.14 ± 0.02
CT-PHPMA 4.10.5	85 ± 8	10.8 ± 1.0	0.13 ± 0.02

As was previously observed with **CT-PGMA** species, in all cases for **CT-PHPMA** the K_m was found to increase from that of the native α -CT. However, unlike with PPCs composed of PGMA, there appears to be no obvious trend in the increase of K_m based on either the grafting density or overall molecular weight of the **CT-PHPMA** species. Although an increase in K_m is observed, the catalytic constant, k_{cat} , was found to decrease slightly for all **CT-PHPMA** samples in comparison to the native α -CT. An average reduction of 20% in k_{cat} is observed, but as the PPCs require a balance between stability and activity, the decrease was not deemed detrimental to the viability of the **CT-PHPMA** PPCs.

Overall in comparison to the **CT-PGMA** analogues, PPCs composed of PHPMA showed a similar increase in K_m suggesting competitive inhibition is occurring between polymers and substrate. However, **CT-PHPMA**s were observed to have a slight reduction in catalytic ability in comparison to their corresponding **CT-PGMA** species which exhibited no decrease in k_{cat} . It is postulated that as α -CT is a protease enzyme, which possesses an active site designed to interact and form weak bonding with peptide substrates, the presence of the amide bond within HPMA could interact with the active site and therefore lower the catalytic efficiency of the enzyme.

4.3.1.3 *Stability of CT-PHPMA PPCs*

4.3.1.3.1 *Thermal Storage Stability of CT-PHPMA PPCs*

To ascertain whether the stability trends that were observed for α -CT PPCs synthesised with GMA are mirrored by the **CT-PHPMA** PPCs, solutions of **CT-PHPMA 4.1.5**, **4.1.25**, and **4.10.5** were

incubated at 40 °C, pH 8.0 and analysed using the *p*NA assay at frequent time intervals. Subsequently, residual activities were plotted against time and half-lives extracted by assuming an exponential decay and due to batch-to-batch variations within α -CT, normalised by the half-life of the corresponding batch of α -CT (Figure 4.8) as described in Section 3.3.2.1.

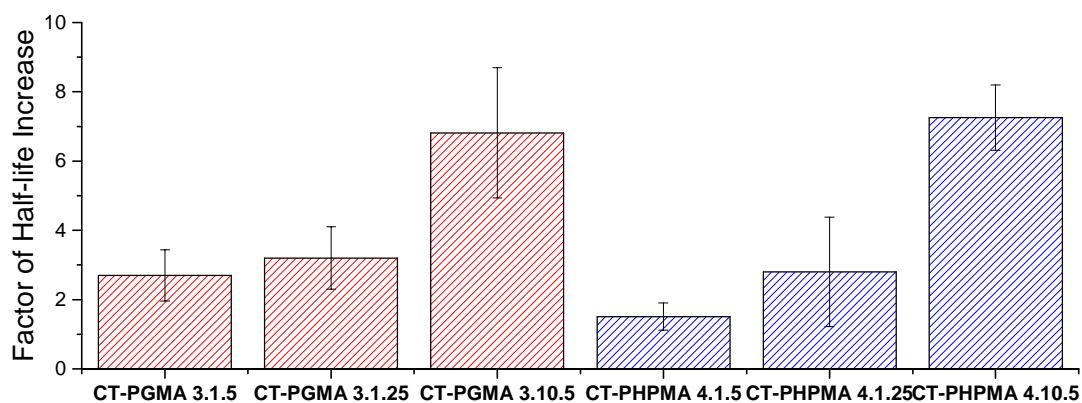


Figure 4.8 Factor of activity half-life increase compared to α -CT for **CT-PGMA** PPCs and **CT-PHPMA** PPCs at 40 °C and pH 8.0 extracted from the linear regression of $\ln(\text{residual activity})$ against time.

As a result of increasing the grafting density from 1 to 10 polymers, **CT-PHPMA** is shown to increase in stability over time by a factor of four and therefore it is clear from the analysis that the same overall trend with respect to grafting density is present in PPCs synthesised with either HPMA or GMA. Likewise, for both sets of PPCs, when examining the stability of singly grafted species, as the molecular weight of the polymer increases, the stability was also found to increase. Additionally, these results support the previous hypothesis that the role of the polymers in stabilising the enzyme is to prevent solvent-protein interactions from occurring.

Although there are similarities between the two sets of PPCs, it is apparent there are some variations. While the overall molecular weights of **CT-PHPMA 4.1.5** and **4.1.25** are comparable to those of **CT-PGMA 3.1.5** and **3.1.25**, the stability increase from the native α -CT of the HPMA PPCs is reduced in comparison to the GMA PPCs. For example, although they are observed to have very similar overall molecular weights, **CT-PGMA 3.1.5** and **CT-PHPMA 4.1.5** were

found to have slightly different enhancements to stability, by a factor of 2.7 and 1.5, respectively, which were confirmed to be statistical significant results with 95% confidence based upon a *t*-test.

In contrast to the singly grafted species, **CT-PHPMA 4.10.5** is smaller in size in comparison to **CT-PGMA 3.10.5**, with 10 polymers of 2 kDa grafted compared to 4.5 kDa respectively, yet the stability of the two species is comparable. Furthermore, it has been postulated that once the polymer molecular weight reaches a certain size threshold to prevent solvent-protein interactions from occurring enhanced stability will be observed. Further increase in molecular weight past this threshold will not provide any additional stability.

Aiming towards storage of enzymes in solution at ambient or low temperatures, stability experiments were performed on α -CT, **CT-PGMA 3.10.5**, and **CT-PHPMA 4.10.5** at 4 °C and 20 °C and compared to the results obtained at 40 °C. These two PPCs were chosen as they displayed a substantial increase in half-life in the accelerated studies.

In order to be able to compare the samples with a high degree of accuracy, all time points analysed were required to be tested with the same substrate solution to prevent variations in substrate concentration and therefore activity levels. One limitation of this requirement is that the substrate hydrolyses naturally overtime in methanol, and so to alleviate this problem aliquots were taken at various time points and stored at -20 °C for the entire stability study of 28 days. Subsequently all samples were defrosted and analysed at the same time using the *p*NA assay. As a consequence of the methodology employed, it was imperative to determine if there were variations in initial velocity of hydrolysis of α -CT, **CT-PGMA 3.10.5**, and **CT-PHPMA 4.10.5** in solution before and after storage at -20 °C.

Figure 4.9 reveals that all samples have undergone some reduction in activity from the prolonged storage at -20 °C. The most noticeable change in activity is the significant reduction for the native α -CT, as the initial velocity decreases from 642 to 31×10^{-6} OD sec⁻¹. It is apparent that the stability of both PPCs examined, **CT-PGMA 3.10.5** and **CT-PHPMA 4.10.5**, at -20 °C is

improved in comparison to the native enzyme. Moreover, the stability of **CT-PGMA 3.10.5** is substantially increased compared to that of **CT-PHPMA 4.10.5**, as the reduction of initial velocity is 20% compared to 60% respectively.

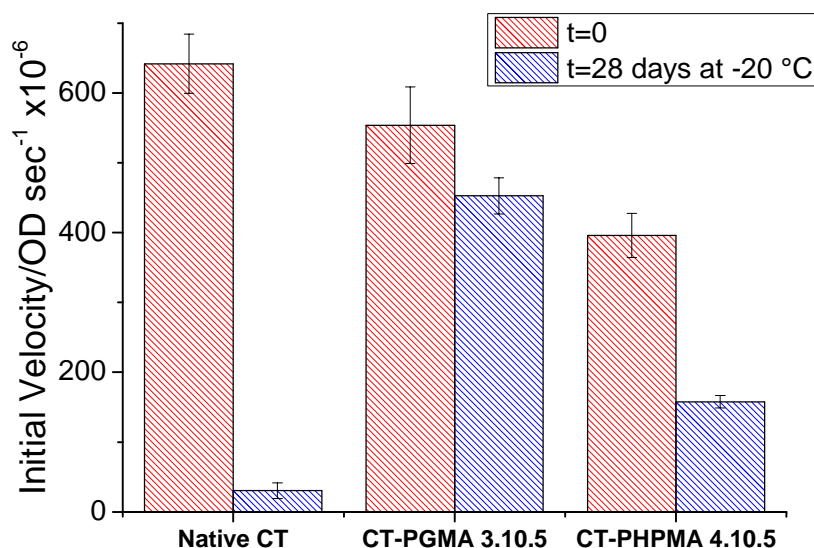


Figure 4.9 Initial velocity of α -CT, **CT-PGMA 3.10.5**, and **CT-PHPMA 4.10.5** species at t = 0, before and after storage at -20 °C, at pH 8.0. Each data point is based on the average of four repeats of pNA assay with standard deviation displayed as error.

There are several factors to consider in an attempt to explain the reasoning behind these differences. Firstly, it is important to consider **CT-PHPMA 4.10.5** is of a lower molecular weight than **CT-PGMA 3.10.5**, with the grafted polymers being approximately half the molecular weight. Although the differences in molecular weight were not observed to impact the catalytic stability at 40 °C, it is hypothesised that as the solution freezes, the effectiveness of the polymer to shield interactions between the protein and the solvent are reduced, therefore reducing the overall stability.

Another factor that is important to consider is the presence of multiple alcohol groups within the polymer structures. Lee *et al.* have previously found that trehalose, a disaccharide with multiple alcohol groups, stabilises proteins from conditions such as lyophilisation and heat.^{8,9} From this

study, it is hypothesised that as a consequence of the diol present in GMA, it enables the formation of more stabilising interactions with **CT-PGMA 3.10.5** and therefore leads to have higher degree of activity retention compared to the HPMA analogue.

Despite the reduction in activity observed from the storage of the $t = 0$ samples, the stability profiles for α -CT, **CT-PGMA 3.10.5**, and **CT-PHPMA 4.10.5** were investigated at 4 °C and 20 °C (Figure 4.10) using the previously described methodology. The data has not been normalised to residual activity to highlight the variations in activity observed by the three PPC species.

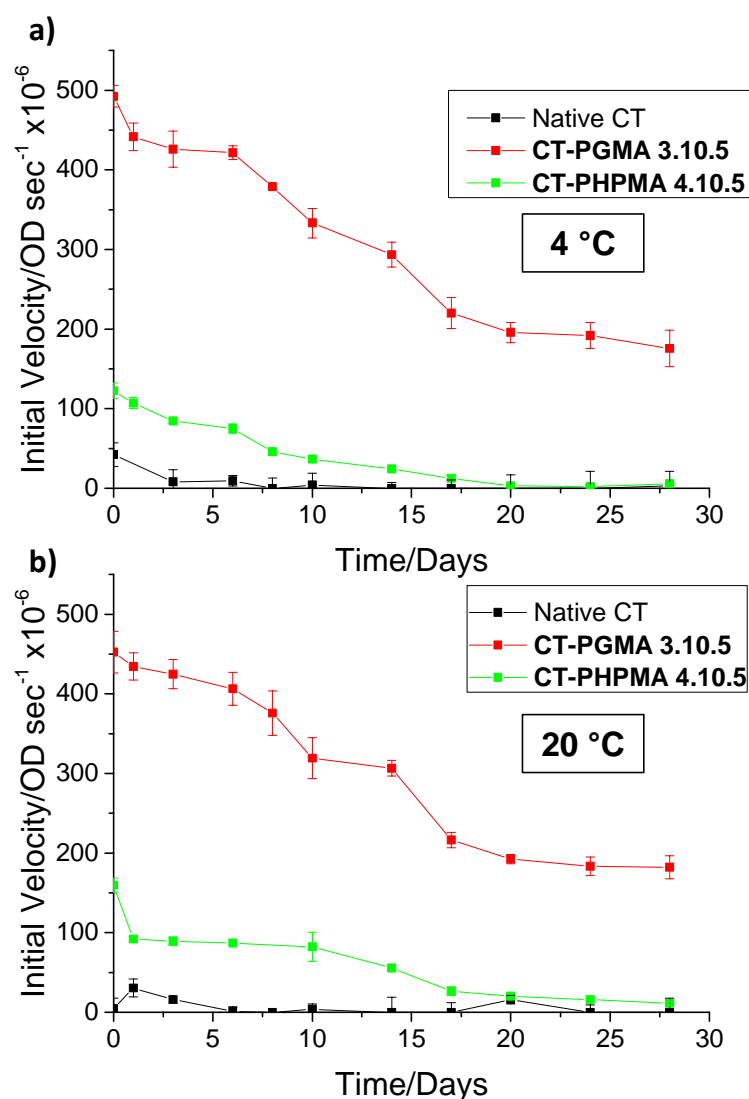


Figure 4.10 Stability profiles of α -CT, CT-PGMA 3.10.5 and CT-PHPMA 4.10.5 species at pH 8.0 incubated at a) 4 °C and b) 20 °C. Each data point is based on the average of four repeats of *p*NA assay with standard deviation displayed as error.

As a consequence of the detrimental reduction in α -CT activity upon storage at -20 °C, an accurate half-life could not be extracted from the data. Despite the inability to calculate a half-life, the data does confirm that both PPCs, CT-PGMA 3.10.5 and CT-PHPMA 4.10.5, were more stable to the testing conditions than native enzyme. From the stability profiles, it appears that there is not a significant change between the stability of the PPCs at 4 °C and 20 °C but to allow for a direct comparison of PPCs at varying storage temperatures, half-lives were extracted by assuming an exponential decay (Figure 4.11).

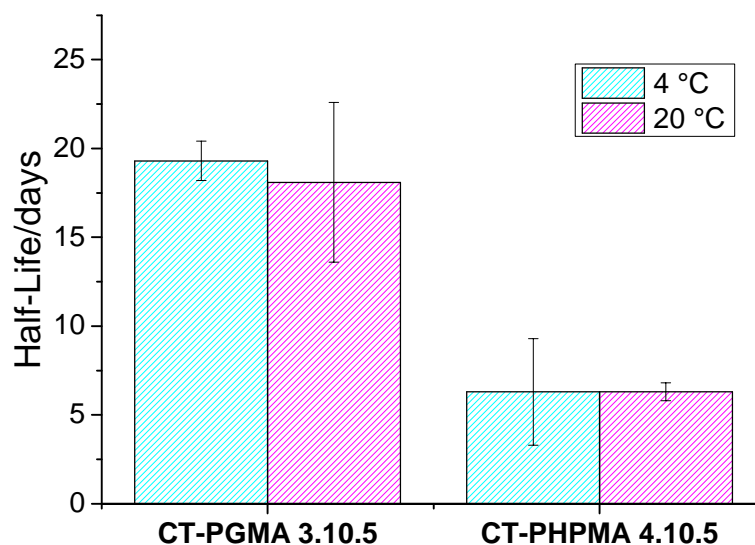


Figure 4.11 Factor of activity half-life increase for **CT-PGMA 3.10.5** and **CT-PHPMA 4.10.5** species at 4 °C and 20 °C, pH 8.0 extracted from the linear regression of $\ln(\text{residual activity})$ against time.

In spite of the varying storage temperatures, the observed half-lives for the both PPCs appears to be independent of temperature. These results suggest that **CT-PGMA 3.10.5** has a half-life that is a factor of three larger than **CT-PHPMA 4.10.5**. Although these results appear to be positive in favour of **CT-PGMA 3.10.5** species, the differences observed between the two species could be triggered either from the initial test storage conditions or from the requirement that samples were stored at -20 °C for up to 28 days prior to analysis. The half-lives of α -CT, **CT-PGMA 3.10.5**, and **CT-PHPMA 4.10.5** at varying storage temperatures have been summarised to allow comparison between the species (Table 4.4).

Table 4.4 Summary of catalytic half-lives for α -CT, **CT-PGMA 3.10.5**, and **CT-PHPMA 4.10.5** at 4 °C, 20 °C, and 40 °C. Half-lives at 40 °C have been normalised to a native α -CT half-life of 13.2 minutes.

	4 °C/days	20 °C/days	40 °C /mins
Native α -CT	-	-	13.2 ± 3.4
CT-PGMA 3.10.5	19.3 ± 1.1	18.1 ± 4.5	89.9 ± 9.1
CT-HPMA 4.10.5	6.3 ± 3.0	6.3 ± 0.5	95.8 ± 12.4

From the observed half-lives, it is concluded that **CT-PGMA 3.10.5** is the most stable over the three temperature studies. Although comparable half-lives were observed for **CT-PGMA 3.10.5** and **CT-PHPMA 4.10.5** at 40 °C, **CT-PGMA 3.10.5** was found to exhibit higher stability in comparison the PHPMA analogue when stored at ambient and low temperatures. However, it is potentially a result of the freezing process required during the testing protocol as opposed to the initial storage temperature.

4.3.1.3.2 T_m of CT-PHPMA PPCs

In addition to comparing the catalytic stability of PGMA and PHPMA PPCs, the melting temperature, T_m , of the conjugates was investigated in order to establish if different polymers could influence the overall melting temperature. T_m of the protein species can be extracted by conducting thermal shift assays, which analyse the fluorescence at increasing temperature.⁴⁴⁻⁴⁶ Upon protein melting, the hydrophobic regions of the protein become exposed and allow the binding of a dye species. The typically employed dye is SYPRO orange, which upon binding excludes water and increases in fluorescence enabling the melt to be identified. To this end, thermal shift assays using SYPRO orange, as described previously in Section 2.3.6.1, were performed on α -CT, **CT-PGMA 3.10.5**, and **CT-PHPMA 4.10.5** to determine T_m values (Figure 4.12).

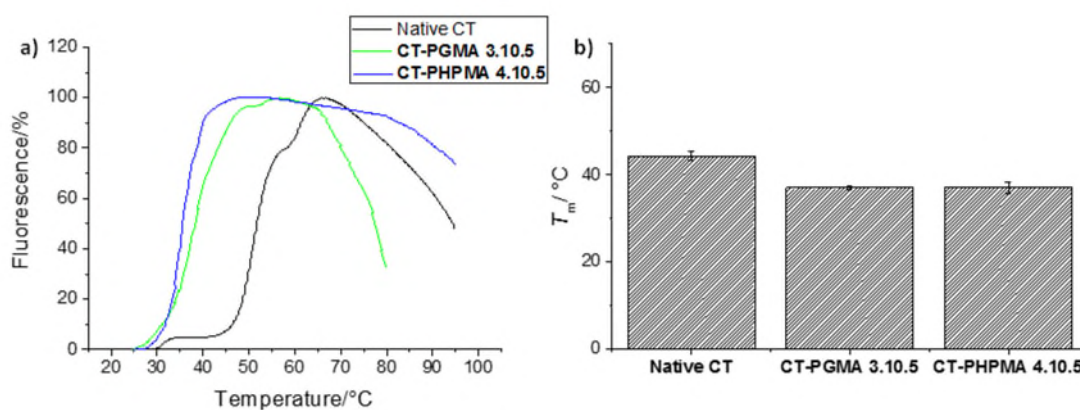


Figure 4.12 a) Thermal shift assay profile of native α -CT, **CT-PGMA 3.10.5**, and **CT-PHPMA 4.10.5**, at 5 mg/mL in water with SYPRO orange, excitation $\lambda = 492$ nm, emission $\lambda = 610$ nm and b) graph displaying the half-lives of α -CT, **CT-PGMA 3.10.5**, and **CT-PHPMA 4.10.5** species. Values are obtained from triplicate repeats and error is displayed as standard deviation.

Despite observing differences in the catalytic stability, no significant variation in T_m was observed between **CT-PGMA 3.10.5** and **CT-PHPMA 4.10.5**. Both PPCs were found to have a reduction of 5 °C from the native α -CT. It should also be noted that the T_m for both of the PPCs examined using the thermal shift assay is below 40 °C, which is the temperature that the raised temperature stability tests are conducted. The reduction in T_m suggests a disruption of the intra-protein bonding yet a higher catalytic half-life was observed.

4.3.1.3.3 Secondary Enzyme Stability of CT-PHPMA and CT-GMA PPCs

Following the successful results, reported in Section 3.3.3.3, for the protection of GO_x in the presence of **CT-PGMA 3.10.5** in comparison to native α -CT, it was desired to compare these results to the PHPMA analogue, **CT-PHPMA 4.10.5**. To be able to assess any variations in protective ability, α -CT, **CT-PGMA 3.10.5**, and **CT-PHPMA 4.10.5** species were incubated with GO_x at 30 °C for 32 hours with aliquots tested for GO_x activity using the *o*-dianisidine assay (Figure 4.13).

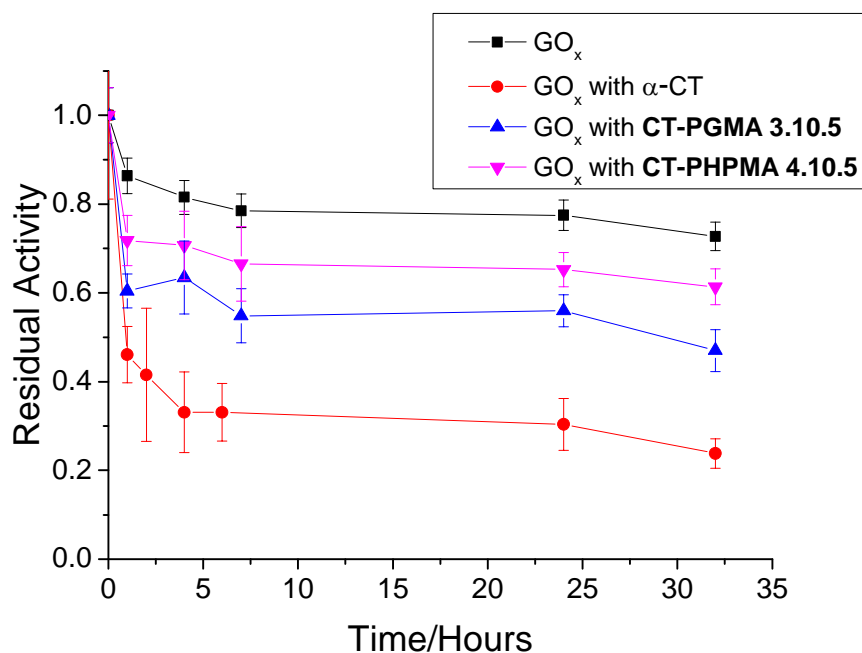


Figure 4.13 Stability profiles of GO_x incubated with α -CT, CT-PGMA 3.10.5, and CT-PHPMA 4.10.5 at various time intervals at pH 5.0, 30 °C. Each data point is based on the average of four repeats of *o*-dianisidine assay with standard deviation displayed as error.

As observed previously in Chapter 2, the addition of any α -CT species caused the activity of GO_x to undergo a sharp initial decrease, however the decrease observed in samples containing PPCs is reduced in comparison to that of native α -CT. Despite the initial decrease in GO_x activity, CT-PHPMA 4.10.5 is able to maintain 65% of the activity of GO_x in comparison to 56% when GO_x was incubated with CT-PGMA 3.10.5. Although this could be a consequence of the slight reduction in catalytic ability observed from the initial conjugate, due to the high concentrations (5 mg/mL) of protease enzyme, it is assumed that the variations observed are a result of the difference in polymer functionality. It is hypothesised that as a consequence of its amide functionality, PHPMA has the possibility of interacting with the active site of α -CT and therefore providing a secondary substrate for α -CT. This would therefore generate a system with competitive inhibition between GO_x and PHPMA digestion, allowing a higher retention in GO_x activity.

From these results, although **CT-PGMA 3.10.5** can retain proteolytic activity for a longer time, **CT-PHPMA 4.10.5** was found to allow high retention of activity for a secondary enzyme in solution, possibly by providing an alternative substrate for the active site of α -CT.

4.3.2 Comparison of Linear and Comb-Like Polymers

Furthering the investigation of the role of the polymer in stabilising α -CT, the architecture of the monomer species was deemed an important property to explore. Both PGMA and PHPMA are polymers with short pendant groups and so polymers that possess a comb-like structure were chosen to investigate in a comparative study. As a consequence of polyethylene glycol (PEG) being the most commonly utilised polymer in the synthesis of PPC species, the methacrylate analogue of PEG was identified as viable option due to the comb-like architecture of the resulting polymer and its high degree of biocompatibility.⁴⁷ As such, oligo(ethylene glycol) methacrylate (OEGMA) was chosen as a suitable monomer as a result of its hydrophilic nature, primary alcohol end group, and potential for variable pendant chain length. Additionally, POEGMA can be synthesised directly, without the need for post-polymerisation modifications.⁴⁸

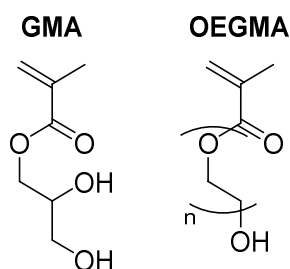


Figure 4.14 Chemical structure comparison of GMA to OEGMA.

Lui *et al.* have previously found that POEGMA attached to the surface of α -CT exhibited a range of architectures dependent upon various factors including comb-length and grafting density of the polymer.⁴⁹ The architectures of the polymer species were found to influence the access to the active site and the level of molecular sieving that was observed. From this report, OEGMA with a M_n of 360 g mol⁻¹ (OEGMA₃₆₀) was chosen as the initial monomer to investigate; OEGMA₃₆₀

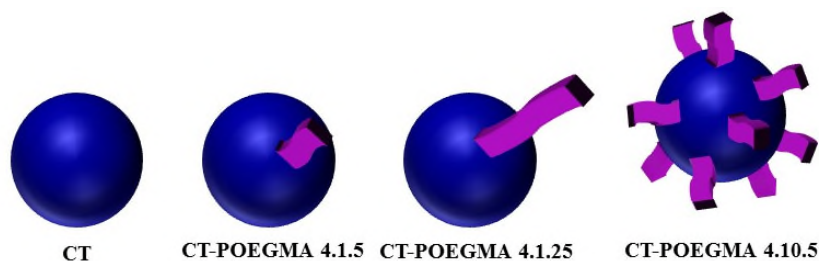
has a pendant group size that was predicted to not completely prevent access to the active site but to provide a degree of molecular sieving.

4.3.2.1 *Synthesis and Characterisation of CT-POEGMA PPCs*

Aiming towards the synthesis of PPCs comparable to those of PGMA, **CT-POEGMA** PPCs were synthesised by polymerising OEGMA₃₆₀ from the surface of the corresponding **CT-MI 2.1** using the conditions stated previously for the synthesis of **CT-PGMA** and **CT-PHPMA** PPCs (Section 3.3.1 and 4.3.1.1). Analysis of the resulting **CT-POEGMA** PPCs was conducted by UV-Vis spectroscopy and SDS-PAGE analysis and summarised in Table 4.5 with the corresponding **CT-PGMA** PPC for comparison.

Table 4.5. Summary of **CT-PGMA** PPCs and **CT-POEGMA** PPCs with characterisation data from UV-Vis spectroscopy and SDS-PAGE analysis.

PPC	Target PPC M_w /kDa	PPC M_w /kDa (UV-Vis)	PPC M_w /kDa (SDS-PAGE)
CT-PGMA 3.1.5	30	26.5	27.3
CT-POEGMA 4.1.5	30	26.5	29.1
CT-PGMA 3.1.25	50	31.2	40.6
CT-POEGMA 4.1.25	50	56.6	54.3
CT-PGMA 3.10.5	75	70.8	195.7
CT-POEGMA 4.10.5	75	81.0	144.5



In all cases, both analytical methods, UV-Vis and SDS-PAGE, confirm the successful synthesis of **CT-POEGMA** conjugates. Furthermore, good correlation was observed between **CT-PGMA**

and **CT-POEGMA** PPCs and therefore all conjugates were utilised in the assessment of variations in activity and stability between linear and comb-like polymer morphologies.

4.3.2.2 *Activity of CT-POEGMA PPCs*

To establish if any variations in initial activity were present between PPC species, Michaelis-Menten parameters were extracted for **CT-POEGMA** conjugates by employing Lineweaver-Burk plots from the analysis of the pNA assay (Table 4.3). Only one set of α -CT parameters are listed as **CT-POEGMA 4.1.5**, **4.1.25**, and **4.10.5** were synthesised from the same batch of α -CT.

Table 4.6 Michaelis-Menten Parameters of α -CT and **CT-POEGMA** PPCs based on the pNA assay.

Sample	$K_m/\mu\text{M}$	$k_{\text{cat}}/\text{sec}^{-1}$	$k_{\text{cat}}/K_m/\text{sec}^{-1} \mu\text{M}^{-1}$
Native α -CT Batch 1	105 ± 6	14.6 ± 0.7	0.14 ± 0.01
CT-POEGMA 4.1.5	174 ± 16	8.0 ± 0.6	0.05 ± 0.01
CT-POEGMA 4.1.25	121 ± 7	9.4 ± 0.4	0.08 ± 0.01
CT-POEGMA 4.10.5	108 ± 4	8.3 ± 0.2	0.08 ± 0.01

Although the **CT-PGMA** species were observed in Section 3.3.2.2 to undergo a competitive inhibition process, as K_m was observed to increase whilst maintaining k_{cat} , **CT-POEGMA** PPCs were observed to undergo different inhibition processes. In all cases for **CT-POEGMA**, the k_{cat} was found to decrease. **CT-POEGMA 4.1.25** and **4.10.5** were observed to either maintain or undergo a minimal increase in K_m but exhibit a significant decrease in k_{cat} , it is suggested that they are inhibited by a non-competitive mechanism. This type of inhibition does not affect the binding of substrate but prevents the catalytic process occurring. However, it is hypothesised that the reduction in catalytic constant observed could be due to the polymeric species preventing the assay product leaving the active site and therefore leading to a slower detection of the product.

CT-POEGMA 4.1.5 was found to have both an increase in K_m and also a decrease in k_{cat} . It is hypothesised that the short polymeric species is of an appropriate length to hinder access to the

active site by potentially binding itself but also to prevent substrate that has been hydrolysed from leaving the active site into free solution. Overall in comparison to the **CT-PGMA** analogues, **CT-POEGMA** PPCs showed a reduction catalytic ability and the total catalytic efficiency.

4.3.2.3 *Stability of CT-POEGMA PPCs*

Despite the observed decrease in catalytic ability, the stability of **CT-POEGMA** PPCs was assessed to ascertain whether a correlation exists between activity and overall catalytic stability. Additionally, the comparison of stability between PPCs synthesised with GMA and OEGMA was explored. To this end, half-lives were extracted from the *p*NA assay conducted on aliquots of **CT-POEGMA** conjugate solutions incubated at 40 °C, pH 8.0 by assuming an exponential decay and subsequently normalised to the half-life of the corresponding batch of α -CT (Figure 4.15).

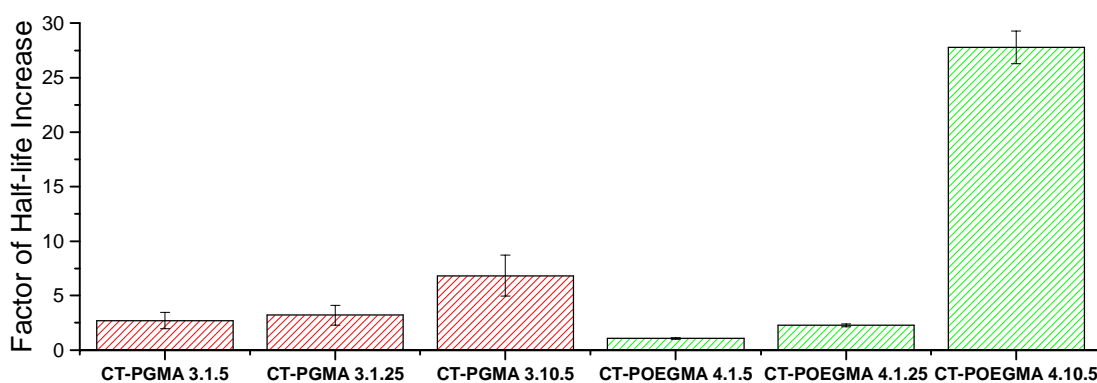


Figure 4.15 Factor of activity half-life increase for **CT-PGMA** and **CT-POEGMA** PPC species compared with native α -CT at 40 °C and pH 8.0 extracted from the linear regression of $\ln(\text{residual activity})$ against time.

It is evident that the same trends in stability are observed for both GMA and OEGMA conjugates; the increase in polymeric grafting density or molecular weight of a singly grafted polymer were observed to enhance the stability further. However, **CT-POEGMA** PPCs with a single grafted polymer, **4.1.5** and **4.1.25**, were found to have lower stability than the corresponding **CT-PGMA** analogue. As the variable that was kept constant between GMA and OEGMA analogues was molecular weight of the overall PPC, the OEGMA conjugates have a lower degree of polymerisation and therefore a shorter grafted polymer. It is hypothesised that the degree of

polymerisation has a greater impact upon the stability and the potential to prevent interactions between protein and solvent when a low grafting density is employed.

Although a decrease in stability was found with **CT-POEGMA** PPCs with a singly grafted polymer, there is the significant increase in stability observed by **CT-POEGMA 4.10.5**. In comparison to native α -CT, **CT-POEGMA 4.10.5** was found to have an increased stability by a factor of 27, which is 4-fold enhancement from the **CT-PGMA 3.10.5** species. Despite the degree of polymerisation being smaller than **CT-PGMA 3.10.5**, it is postulated that the high degree of grafting density along with the comb-like structure can cover the surface of the protein more effectively and form a network to prevent interactions with the solvent (Figure 4.16).

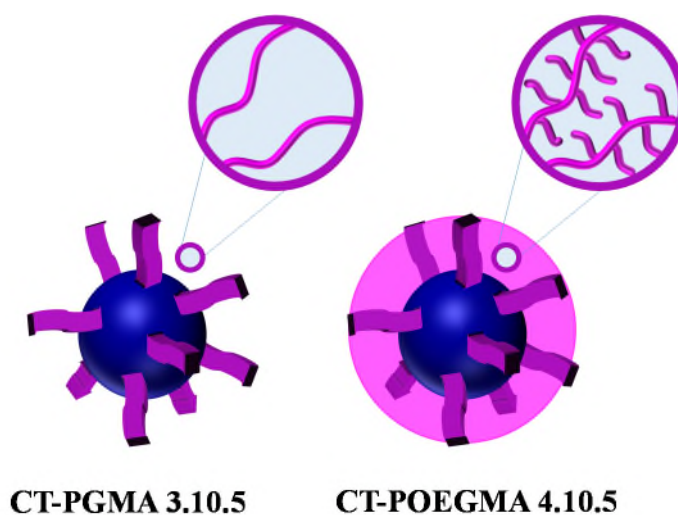


Figure 4.16 Schematic representation of possible morphologies of **CT-PGMA 3.10.5** and **CT-POEGMA 4.10.5**.

Despite the reduction in stability observed in singly grafted species, it is apparent that the comb-like structure of OEGMA enables more effective stabilisation of α -CT at higher grafting densities than linear hydrophilic monomers. As such, PPCs with grafted POEGMA were further investigated to examine the effect on stability of parameters including molecular weight and comb-length.

4.3.3 Comparison of Molecular Weight of Comb-Like Hydrophilic Polymers

As discussed in Section 4.3.2.3, the molecular weight of singly grafted polymers had a positive effect on the observed catalytic stability. Additionally, the large increase in stability observed from the POEGMA ten site grafted PPCs, **CT-POEGMA 4.10.5**, has aimed an investigation towards investigated the effect on molecular weight of the ten-site grafted species using the monomer OEGMA₃₆₀. Aiming towards PPCs of varying molecular weight polymers whilst maintaining grafting density, **CT-MI 2.1.10** was utilised to synthesise **CT-POEGMA 4.10.2-4.10.20** and the resulting conjugates were characterised using SDS-PAGE and UV-Vis spectroscopy (Table 4.7).

Table 4.7. Summary **CT-POEGMA 4.10.2-4.10.20** characterisation with UV-Vis spectroscopy and SDS-PAGE analysis.

PPC	Target Polymer M_w /kDa	Target PPC M_w /kDa	PPC M_w /kDa (UV-Vis)	PPC M_w /kDa (SDS-PAGE)
CT-POEGMA 4.10.2	2	45	44.5	68.8
CT-POEGMA 4.10.5	5	75	81.0	144.5
CT-POEGMA 4.10.10	10	125	140.4	163.8
CT-POEGMA 4.10.20	20	225	194.3	188.8

Successful polymerisations were observed in all cases and PPCs with a constant grafting density and a range of molecular weights were synthesised, which were carried forward to be examined for changes in activity and stability.

Prior to analysis of the stability of these species, the initial activities of **CT-POEGMA 4.10.2-4.10.20** were assessed by calculating the Michaelis-Menten parameters from the *p*NA hydrolysis assay at varying substrate concentrations by employing Lineweaver-Burk plots (Table 4.8). As PPCs were synthesised from two different batches of

α -CT, conjugates have been grouped for comparison purposes with their corresponding batch of native α -CT.

Table 4.8 Michaelis-Menten Parameters of α -CT and **CT-POEGMA 4.10.2-4.10.20** based on the *p*NA assay.

Sample	M_w /kDa (UV-Vis)	K_m / μ M	k_{cat} /sec ⁻¹	k_{cat}/K_m /sec ⁻¹ μ M ⁻¹
Native α -CT Batch 1	25.5	105 \pm 6	14.6 \pm 0.7	0.14 \pm 0.01
CT-POEGMA 4.10.5	81.0	108 \pm 4	8.3 \pm 0.2	0.08 \pm 0.01
Native α -CT Batch 2	25.5	64 \pm 4	12.8 \pm 2.0	0.20 \pm 0.03
CT-POEGMA 4.10.2	44.5	142 \pm 21	11.0 \pm 1.7	0.08 \pm 0.02
CT-POEGMA 4.10.10	140.4	71 \pm 17	5.3 \pm 1.1	0.08 \pm 0.02
CT-POEGMA 4.10.20	194.3	31 \pm 2	2.5 \pm 0.1	0.08 \pm 0.01

From Table 4.8, it is evident that as the molecular weight of the polymeric species increased, the catalytic constant was found to decrease. This correlates with the previous observation that the catalytic ability of the enzyme is not affected but the ability of the product of the assay to diffuse out of the active site through the polymer layer. Furthermore, the ability of the polymer to prevent the substrate from leaving the active site also has an impact upon the K_m of the system. The assay detects that the system has a greater affinity to exist in the enzyme-substrate conformation and lowers the K_m , which leads to the suggestion of uncompetitive inhibition.^{50, 51} Overall due to the changes in both K_m and k_{cat} , the catalytic efficiency of the systems remains independent of molecular weight of the polymeric species.

Despite the reduction in k_{cat} with increasing molecular weight of POEGMA₃₆₀, the stability of **CT-POEGMA 4.10.2-4.10.20** were examined at 40 °C, pH 8.0. Aiming towards analysing the dependency between molecular weight and stability, half-lives were extracted from the *p*NA assay conducted on aliquots of **CT-POEGMA 4.10.2-4.10.20** solutions by assuming an exponential decay and subsequently normalised to the half-life of the corresponding batch of α -CT (Figure 4.17).

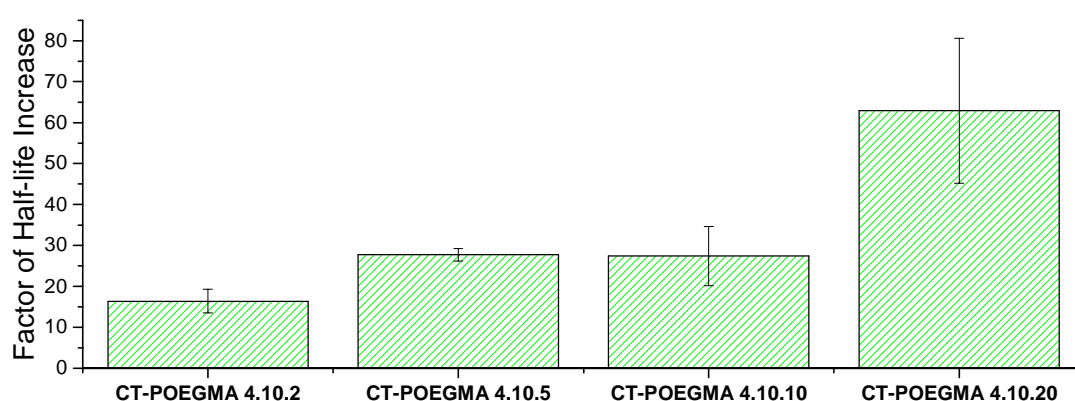


Figure 4.17 Factor of activity half-life increase for **CT-POEGMA 4.10.2-4.10.20** species compared to native α -CT at 40 °C and pH 8.0 extracted from the linear regression of $\ln(\text{residual activity})$ against time.

Although a decrease was observed in the catalytic constant when the molecular weight was increased, the stability was observed to have the opposite trend: as the molecular weight increases the stability also increases. This trend fits well with the theory proposed earlier in which the stability has a dependence upon the ability of the polymer to prevent solvent-protein interactions whereby as the polymer molecular weight increases the polymeric shell becomes thicker and therefore exhibits a higher degree of shielding for the protein.

Following the significantly enhanced stability under accelerated conditions at 40 °C, samples were carried forward to investigate if they exhibit a higher stability at both low and ambient temperature storage. Aiming towards identifying if the molecular weight has an impact on stability at varying temperatures, **CT-POEGMA 4.10.5** and **CT-POEGMA 4.10.20** were chosen

as the appropriate conjugates to study as they showed different stabilities with varying molecular weights under the accelerated testing. As described previously in Section 4.3.1.3.1, in order to be able to compare the samples with a high degree of accuracy, aliquots were taken at various time points and stored at $-20\text{ }^{\circ}\text{C}$ until the stability study was concluded at 28 days prior to analysis with the pNA assay. As a consequence of the previous reduction in activity during storage at $-20\text{ }^{\circ}\text{C}$, it was important to investigate if the same storage effects were observed for **CT-POEGMA** PPCs (Figure 4.18).

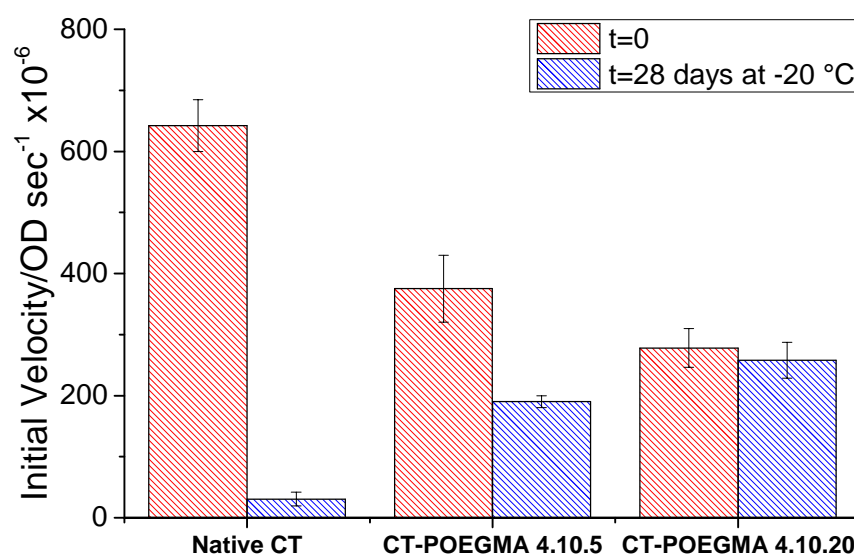


Figure 4.18 Initial velocity of α -CT, **CT-POEGMA 4.10.5**, and **CT-POEGMA 4.10.20** species at $t=0$ before and after storage at $-20\text{ }^{\circ}\text{C}$, pH 8.0. Each data point is based on the average of four repeats of pNA assay with standard deviation displayed as error.

The initial activity of native α -CT was found to decrease by 95% with prolonged storage at $-20\text{ }^{\circ}\text{C}$, whilst **CT-POEGMA 4.10.5** was shown to have a 50% stability retention, which is lower than the value observed for **CT-PGMA 3.10.5**. In contrast, **CT-POEGMA 4.10.20** was observed to have a significantly higher retention of activity, with only a 7% reduction in stability over 28 days storage at $-20\text{ }^{\circ}\text{C}$. To allow the stability of the two species to be more effectively compared at various storage temperatures, residual activity plots were extracted for **CT-POEGMA 4.10.5** and **4.10.20** at 4 and $20\text{ }^{\circ}\text{C}$ (Figure 4.19).

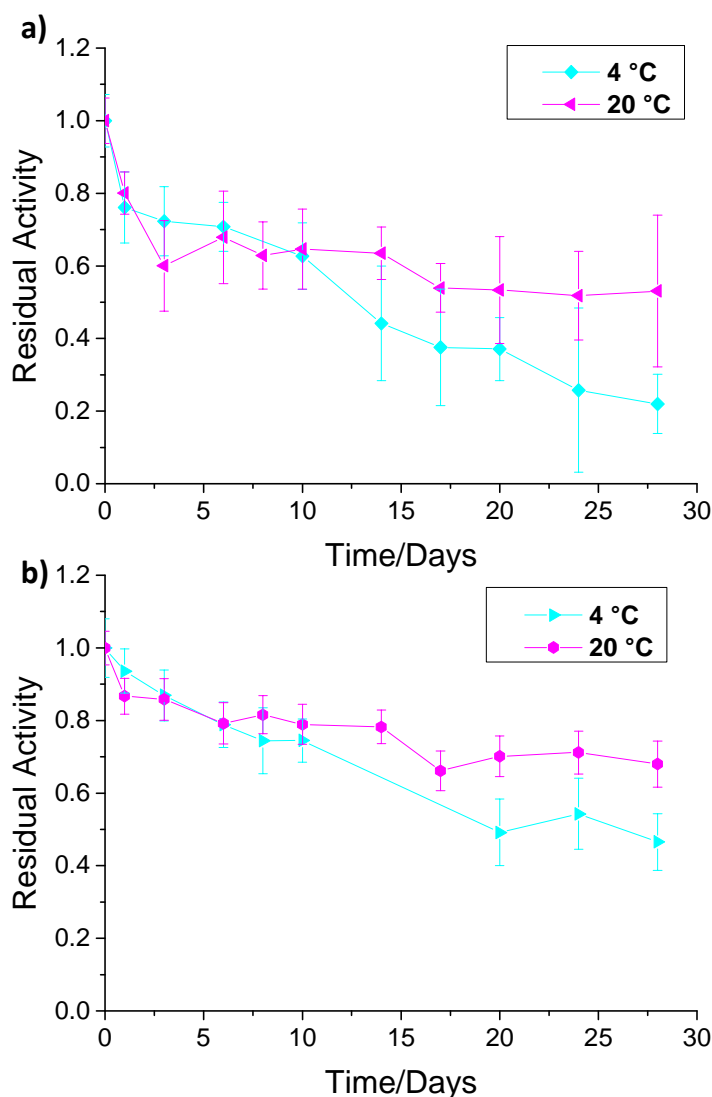


Figure 4.19 Residual activity stability profiles of a) **CT-POEGMA 4.10.5** and b) **CT-POEGMA 4.10.20**. All samples were incubated at pH 8.0 at both 4 and 20 °C. Each data point is based on the average of four repeats of *p*NA assay with standard deviation displayed as error.

As reported previously in the accelerated studies, **CT-POEGMA 4.10.20** was found to exhibit a higher degree of stability than **CT-POEGMA 4.10.5** at both temperatures suggesting that the molecular weight of the grafted polymers is a strong influencing factor independent of storage temperature. Although it was expected that as the storage temperature was decreased, the stability of the PPCs would increase as a lower thermal energy should induce less structural changes within α -CT, the opposite effect was nevertheless observed. At 4 °C, the stability profiles for both **CT-POEGMA 4.10.5** and **4.10.20** show a general decrease in activity over time, yet when stored

at ambient temperature, both samples appear to have a slower decrease but also a plateau of residual activity formed. Although POEGMA species has been observed to have an LCST transition in water,¹⁶ POEGMAs have been also been found in the literature to undergo UCST-type behaviours in solvents including ethanol and propanol,^{33, 52} therefore it was hypothesised that the grafted polymers could undergo a change of morphology at low temperatures. However, the literature has also reported the addition of water can affect the UCST-type behaviour with the incorporation of 1% of water to isopropanol causing a reduction in the observed transition by 12.5 °C.⁵² Therefore, it has been postulated that the grafted polymers would not undergo full aggregation but have the potential to retract or alter their morphology to reduce the solvent shielding ability at low temperatures.

Aiming towards identifying whether the grafted OEGMA polymers undergo a transition at low temperatures, dynamic light scattering (DLS) was employed to investigate the hydrodynamic diameter at varying temperatures. As it was expected to observe a larger difference in the hydrodynamic diameter with an increase in molecular weight, DLS analysis was performed on **CT-POEGMA 4.10.20** at pH 8.0 at both 5 and 25 °C (Figure 4.20).

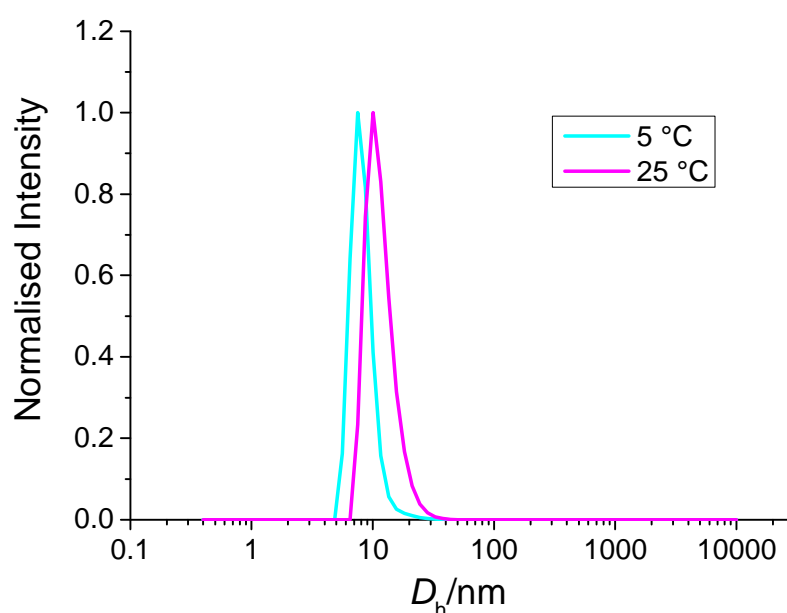


Figure 4.20 Number average size distributions of **CT-POEGMA 4.10.20** at 5 and 25 °C.

It was found from DLS analysis that the hydrodynamic diameter reduces from 11 nm to 8 nm when the temperature was decreased from 25 to 5 °C. This supports the theory of a potential UCST-type transitions occurring within **CT-POEGMA** PPCs. Despite the promising results observed, due to the dispersity of the samples and the error associated with the measurements, these samples would be deemed as within error. Further research would have to be conducted to identify whether UCST-type transitions exist within the grafted POEGMAs.

Furthermore, to allow the comparison of **CT-POEGMA** PPCs of different polymeric molecular weights at varying temperatures, half-lives exhibited by **CT-POEGMA 4.10.5** and **4.10.7** species have been extracted and compared to those observed for **CT-PGMA 3.10.5** (Table 4.9).

Table 4.9 Summary of catalytic half-lives for α -CT, **CT-PGMA 3.10.5**, **CT-POEGMA 4.10.5**, and **4.10.20** at 4 °C, 20 °C, and 40 °C. Half-lives at 40 °C have been normalised to a native α -CT half-life of 13.2 minutes.

	4 °C/days	20 °C/days	40 °C /mins
Native α -CT	-	-	13.2 \pm 3.4
CT-PGMA 3.10.5	19.3 \pm 1.1	18.1 \pm 4.5	89.9 \pm 9.1
CT-POEGMA 4.10.5	13.0 \pm 2.8	>28	367.0 \pm 19.8
CT-POEGMA 4.10.20	24.4 \pm 1.9	>28	830.3 \pm 233.6

In spite of the decrease in stability observed during low temperature storage, **CT-POEGMA** PPCs exhibit a higher stability in solution when exposed to ambient temperatures or 40 °C in contrast to the **CT-PGMA 3.10.5** species. Additionally, the stability is found to be dependent on the grafted polymer molecular weight at all temperatures examined, with a positive correlation observed between the length of the polymer and the catalytic stability.

4.3.4 Comparison of Comb-Length of Hydrophilic Monomers

As the molecular weight of the grafted polymer was found to have a significant impact upon the enzymatic stability, the comb-length of OEGMA was a factor that was deemed an imperative variable to be investigated. To this end, three monomer species were identified as appropriate for

this study, (triethylene glycol) methacrylate (TEGMA) and OEGMA with an average molecular weight of 450 and 900 Da (OEGMA₄₅₀ and OEGMA₉₀₀ respectively) (Figure 4.21). As a consequence of their commercial availability, ease of synthesis and the wide coverage of their properties in the literature, it is important to note that the end group utilised is a methyl ether as opposed to a free hydroxyl group that has been employed in the previous OEGMA studies.

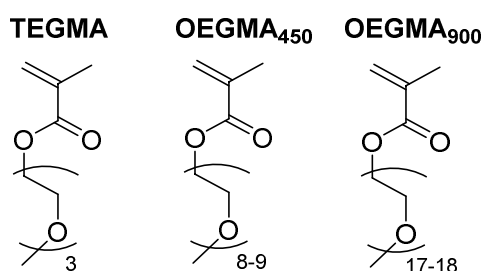


Figure 4.21 Chemical structures of TEGMA, OEGMA₄₅₀, and OEGMA₉₀₀.

Aiming towards PPCs of the same molecular weight and grafting density, **CT-MI 2.1.10** was utilised to synthesise **CT-PTEGMA 4.10.5**, **CT-POEGMA₄₅₀ 4.10.5**, and **CT-POEGMA₉₀₀ 4.10.5** from the corresponding monomers using the ATRP methodology previously described in Chapter 2. Subsequently, the resulting conjugates were characterised using SDS-PAGE and UV-Vis spectroscopy (Table 4.10)

Table 4.10. Summary of **CT-PTEGMA 4.10.5**, **CT-POEGMA₄₅₀ 4.10.5**, and **CT-POEGMA₉₀₀ 4.10.5** characterisation with UV-Vis spectroscopy and SDS-PAGE analysis.

PPC	Target PPC M_w /kDa	PPC M_w /kDa (UV-Vis)	PPC M_w /kDa (SDS-PAGE)
CT-PTEGMA 4.10.5	75	63.9	149.3
CT-POEGMA₄₅₀ 4.10.5	75	62.9	178.4
CT-POEGMA₉₀₀ 4.10.5	75	87.7	175.0

Indeed, successful polymerisations were observed in all cases and PPCs with similar molecular weights and a constant polymeric grafting density were obtained. However, it is apparent that

CT-POEGMA₉₀₀ 4.10.5 was found to have a slightly larger molecular weight than initially targeted, with grafted polymers of 6 kDa in comparison to 4 kDa found in **CT-PTEGMA 4.10.5** and **CT-POEGMA₄₅₀ 4.10.5**.

As it is well reported in the literature that polymers based on OEGMA tend to exhibit LCST-type behaviours,¹⁶ with a temperature dependence upon their comb-length, it was essential to examine the polymer morphology within the PPCs at varying temperatures. To this end, DLS analysis was performed upon **CT-PTEGMA 4.10.5**, **CT-POEGMA₄₅₀ 4.10.5**, and **CT-POEGMA₉₀₀ 4.10.5** at varying temperatures to ascertain any size changes within the temperature conditions utilised for stability testing.

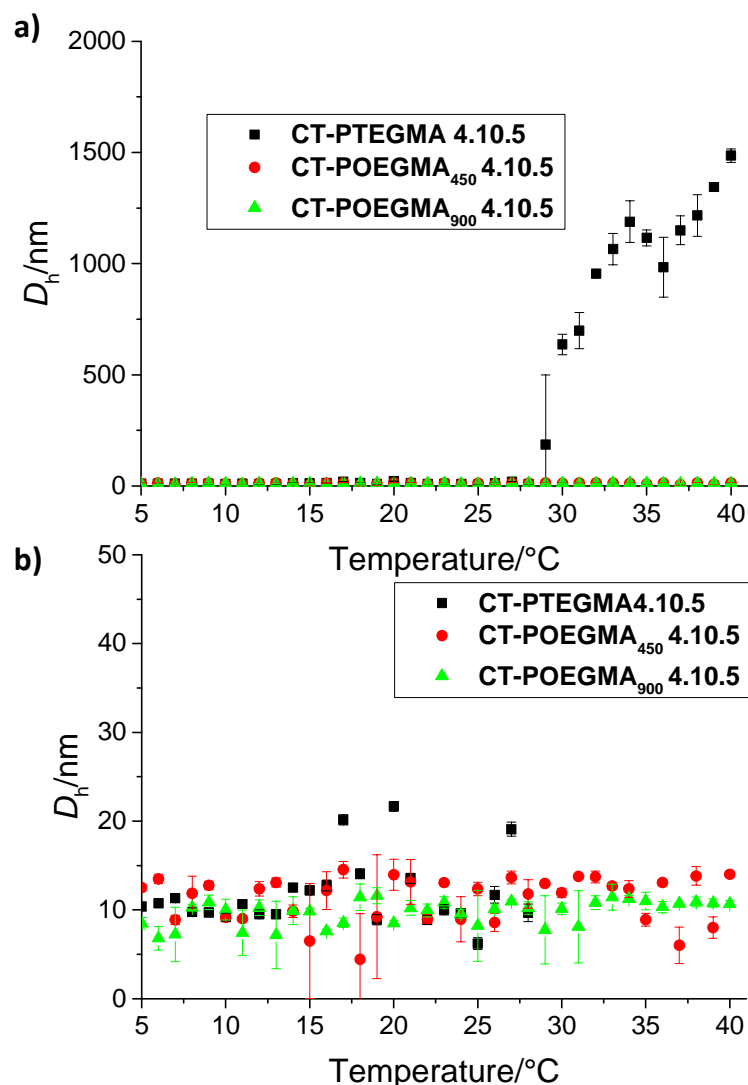


Figure 4.22 Dependence of hydrodynamic diameter of **CT-PTEGMA 4.10.5**, **CT-POEGMA₄₅₀ 4.10.5**, and **CT-POEGMA₉₀₀ 4.10.5** on temperature measured in pH 8.0 buffer. a) full range of observed D_h and b) displays an enlargement of the region from 0 to 50 nm.

As predicted from the literature,¹⁶ the PPC with the shortest comb-length, **CT-PTEGMA 4.10.5**, was observed to undergo a size transition with an onset of approximately 30 $^{\circ}\text{C}$ and form aggregates. In contrast, the two other conjugate species, **CT-POEGMA₄₅₀ 4.10.5** and **CT-POEGMA₉₀₀ 4.10.5**, were not found to undergo any significant size changes in the temperature range examined.

To investigate any variations in the initial activity of **CT-PTEGMA 4.10.5**, **CT-POEGMA₄₅₀ 4.10.5**, and **CT-POEGMA₉₀₀ 4.10.5**, the *p*NA hydrolysis assay was utilised

and subsequent extraction of Michaelis-Menten parameters by employing a Lineweaver-Burk plots (Table 4.11). As the *p*NA assay was performed at 25 °C, all polymers should therefore be in a non-aggregated hydrated state.

Table 4.11 Michaelis-Menten parameters of α -CT and **CT-PTEGMA 4.10.5**, **CT-POEGMA₄₅₀ 4.10.5**, and **CT-POEGMA₉₀₀ 4.10.5** based on the *p*NA assay.

Sample	$K_m/\mu\text{M}$	$k_{\text{cat}}/\text{sec}^{-1}$	$k_{\text{cat}}/K_m/\text{sec}^{-1} \mu\text{M}^{-1}$
Native α -CT Batch 2	64 ± 4	12.8 ± 2.0	0.200 ± 0.030
CT-PTEGMA 4.10.5	182 ± 15	2.8 ± 0.2	0.020 ± 0.010
CT-POEGMA₄₅₀ 4.10.5	305 ± 93	2.8 ± 0.9	0.010 ± 0.004
CT-POEGMA₉₀₀ 4.10.5	322 ± 22	2.5 ± 0.2	0.007 ± 0001

In all cases, the PPCs were found to have a significant decrease in catalytic constant, k_{cat} , and an increase in the Michaelis parameter, K_m . The reduction observed in k_{cat} for all conjugates is much larger than the decrease observed in **CT-POEGMA 4.10.5**, which is the OEGMA₃₆₀ analogue of these PPCs. It is hypothesised that this reduction could be as a result of the modification of the OEGMA end group from a free hydroxyl to a methyl ether by altering the hydrophilicity or interaction with the *p*NA assay substrate of the PPC. However, the increase in K_m is dependent upon the comb-length and moreover, as the comb-length increases the affinity for the substrate decreases. It is postulated that as the comb-length increases, the substrate has greater difficulty accessing the active site to form the enzyme-substrate complex due to the increase in density of the surrounding polymeric shell.

Aiming towards identifying variations in the catalytic stability, both above and below the size transition temperature exhibited by **CT-PTEGMA 4.10.5**, the stability of **CT-PTEGMA 4.10.5**, **CT-POEGMA₄₅₀ 4.10.5**, and **CT-POEGMA₉₀₀ 4.10.5** were investigated at 30 and 40 °C at pH 8.0. To this end, catalytic half-lives were extracted from the *p*NA assay by assuming an exponential decay (Figure 4.23).

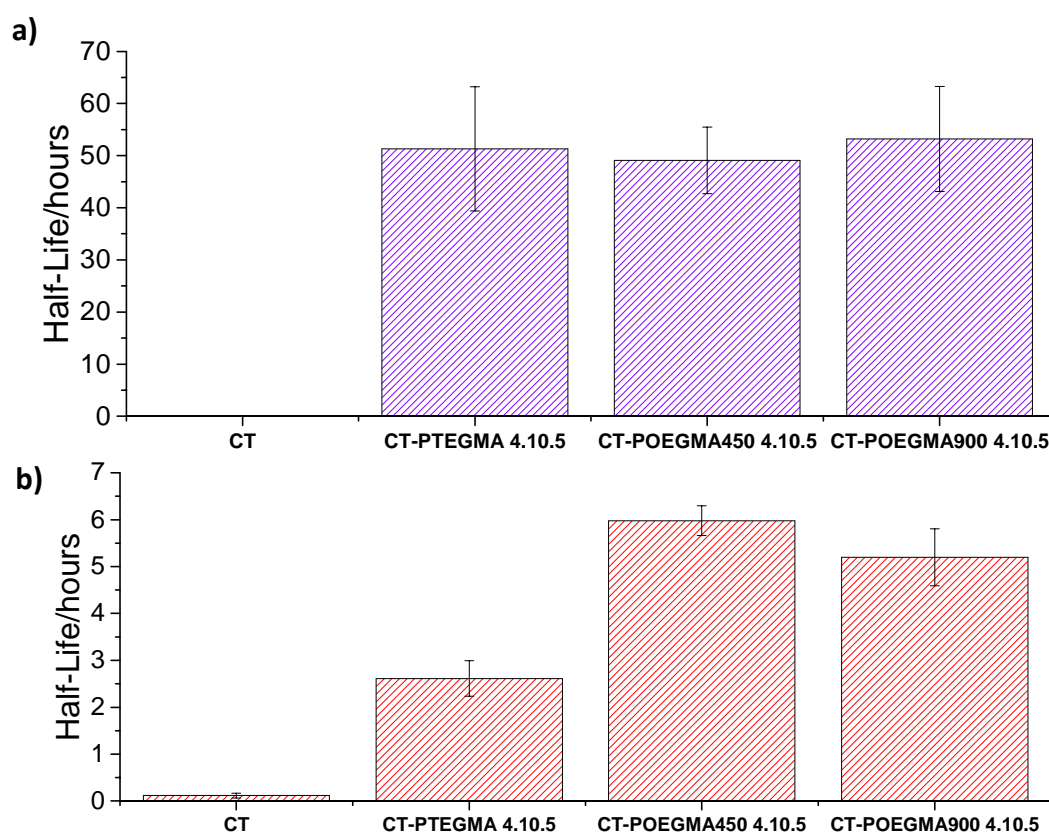


Figure 4.23 Catalytic half-lives for **CT-PTEGMA 4.10.5**, **CT-POEGMA₄₅₀ 4.10.5**, and **CT-POEGMA₉₀₀ 4.10.5** at pH 8.0 at a) 30 °C and b) 40 °C extracted from the linear regression of $\ln(\text{residual activity})$ against time. Accurate half-life values cannot be extracted for α -CT at 30 °C due to methodology described in Section 4.3.1.3.1.

It is evident that although at 30 °C, when all PPCs are in their extended hydrated state, the half-lives of all three PPCs examined are observed to have similar levels of enhancement yet upon increasing the temperature to 40 °C, **CT-PTEGMA 4.10.5** is noted to significantly decrease in stability in comparison to the other two conjugates. This is hypothesised to be a result of the change in hydrophilicity of the polymer causing the PPC to aggregate, which subsequently allowed an increase in protein-solvent interactions. Indeed, Murata *et al.* observed a similar behaviour with poly(*N,N*-dimethylamino ethyl methacrylate) (PDMAEMA); when PDMAEMA was conjugated with α -CT was at low pH and therefore in the extended conformation, an increase in stability was observed. However upon altering the pH to above the pK_a of the polymer causing the polymer to collapse on to the enzymes surface, no enhancement of α -CT stability was observed.⁵³

Although it was observed that the stability at 30 °C was within error for all conjugates, despite the molecular weights of **CT-PTEGMA 4.10.5**, **CT-POEGMA₄₅₀ 4.10.5**, and **CT-POEGMA₉₀₀ 4.10.5** being comparable, as a consequence of the differences in side-chain length, the degree of polymerisation varies greatly between the three samples. This results in a thicker and less dense polymeric shell for **CT-PTEGMA 4.10.5** while a smaller but denser shell for **CT-POEGMA₉₀₀ 4.10.5** (Figure 4.24).

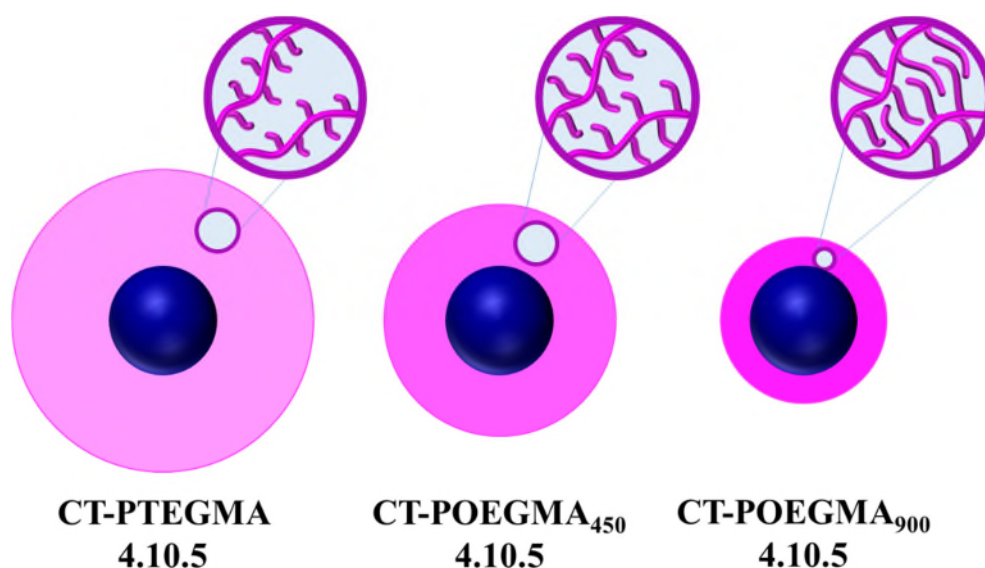


Figure 4.24 Schematic representation of the proposed effective structures of **CT-PTEGMA 4.10.5**, **CT-POEGMA₄₅₀ 4.10.5**, and **CT-POEGMA₉₀₀ 4.10.5**.

Although the conjugates vary in size and shell density, the stability of all samples was similar and therefore it was hypothesised that stability can be induced by either high density of the polymeric shell or high degrees of polymerisations forming thicker shells. These structures are postulated to be more difficult to penetrate and prevent interactions between solvent and protein.

4.4 Conclusions

To conclude, PPCs were successfully synthesised using both HPMA and OEGMA. Similarly to the **CT-PGMA** conjugates synthesised in the previous Chapter, a lack of control is observed due to the nature of ATRP conducted in aqueous systems. Despite the comparable stability of

CT-PHPMA PPC species to that of **CT-PGMA** at 40 °C, the observed stability at ambient and low temperature storage is considerably reduced. However, it is apparent that this may be due to the methodology of the testing, which required storage at -20 °C prior to analysis. Although the storage stabilities were either comparable or reduced in comparison to PGMA conjugates, **CT-PHPMA** PPCs provided better protection for a secondary enzyme in solution. This is hypothesised to be due to the amide functionality present providing competitive inhibition to the second enzyme in solution.

When analysing conjugates synthesised from OEGMA₃₆₀, single grafted polymers were found to provide a lower stability to 40 °C storage compared with the GMA conjugates. This property was potentially impacted by the length of the polymer, as although the molecular weights of the PPCs were comparable, the degree of polymerisation of the **CT-POEGMA** PPCs was smaller than that of **CT-PGMA** species. However upon synthesising **CT-POEGMA 4.10.5**, which had ten grafted OEGMA₃₆₀ polymers, the stability was found to be 4-fold higher than that seen by the GMA analogue, which was an increase by a factor of 27 compared with native α -CT.

Additionally, the stability can be enhanced further by increasing the molecular weight of the grafted polymers, as a positive correlation was observed between the two properties. However upon increasing the molecular weight, the catalytic constant was found to decrease and so the molecular weight of the grafted polymer must allow a compromise between the stability and activity dependent upon the desired application. Despite the enhanced stability observed in **CT-POEGMA** PPCs under accelerated and ambient testing conditions, storage at low temperatures, they were found to be reduced in comparison to **CT-PGMA** species but still an increase compared with native α -CT. This was hypothesised to be a result of UCST-type behaviour of the grafted POEGMA.

Furthermore, the alteration of the comb-length was shown to have no effect upon the stability when stored at ambient temperatures and additionally, it was hypothesised that this is a result of

the varying thicknesses and density of the polymeric shell formed. However, it is postulated that the stability has a dependence upon the length of the polymer as opposed to the molecular weight and so further investigation would have to be performed to explore the stability of PPCs with the same degree of polymerisation.

4.5 Experimental

4.5.1 Materials

All chemicals were obtained from Sigma-Aldrich and used without further purification unless stated otherwise. Ultrafiltration membranes with a 5 kDa MWCO were supplied by Amicon. SYPRO orange was supplied as a 5,000 \times concentrate in DMSO from Thermo Fisher. SDS-PAGE gradient gels were purchased from Biorad.

4.5.2 Instrumentation

4.5.2.1 *¹H Nuclear Magnetic Resonance (NMR) and ¹³C NMR Spectroscopy*

¹H NMR spectra were recorded on a Bruker DPX-300 or DPX-400 spectrometer at 300 MHz and 400 MHz, respectively with MeOD, D₂O, or CDCl₃ as the solvent. The chemical shifts of protons were quoted relative to tetramethylsilane (TMS) at $\delta = 0$ ppm when using CDCl₃, or relative to residual solvent protons when using MeOD (¹H: $\delta = 3.31$ ppm) and D₂O (¹H: $\delta = 4.79$ ppm). ¹³C NMR spectra were recorded on a Bruker DPX-300 or DPX-400 spectrometer at 75 MHz and 100 MHz, respectively with MeOD, D₂O, or CDCl₃ as the solvent. The chemical shifts of carbons were quoted relative to solvent carbons when using MeOD (¹³C: $\delta = 49.3$ ppm) and CDCl₃ (¹³C: $\delta = 77.0$ ppm).

4.5.2.2 *Ultraviolet-Visible (UV-Vis) Spectroscopy*

UV-Vis spectroscopy for the determination of protein concentrations were conducted on a Perkin Elmer Lambda 35 UV/Vis spectrometer recording absorbance at $\lambda = 280$ nm. Utilising the Beer-Lambert law and the molar extinction coefficient for α -CT of 50,585 L mol⁻¹ cm⁻¹, percentage protein and the theoretical molecular weights were extracted. UV-Vis spectroscopy for kinetic measurements was conducted on a FLUOstar OPTIMA multi-well microplate reader. 96-well polystyrene plates were used with an excitation filter of $\lambda = 405$ nm, unless otherwise stated. Data was analysed using MARS v3.01 software.

4.5.2.3 Sodium Dodecyl Sulfate Poly(acrylamide) Gel Electrophoresis (SDS-PAGE)

SDS-PAGE gel analysis was carried out using 4-12 % BioRad SDS-PAGE gels. Gels were run at a constant voltage, 150 V, for 60 minutes and subsequently stained with Coomassie Brilliant Blue. Samples were prepared by heating protein solutions combined with loading buffer in a 1:1 ratio for 5 minutes at 80 °C. Densitometric analysis was performed on the resulting gels using ImageJ software and determining the grayscale profile of the lane length.

4.5.2.4 Dynamic Light scattering (DLS)

DLS measurements were conducted on a Malvern Zetasizer Nano ZS instrument equipped with a 4 mW He-Ne 633 nm laser module and a detector at 173°. Samples were prepared at 1 mg/mL in water and filtered using a 0.22 μ m nylon filter prior to analysis. All experiments were run in triplicate with twelve acquisitions per repeat.

4.5.2.5 Thermal Shift Assay

Thermal shift assay measurements were conducted on an Agilent MX3005P rtPCR with an excitation filter of $\lambda = 492$ nm and an emission filter of $\lambda = 610$ nm used unless otherwise stated. 10 μ L of enzyme (50 mg/mL) was added to 90 μ L SYPRO orange solution (12.5x conc.). Heating ramps were performed at a rate of 1 °C min⁻¹.

4.5.3 Enzyme Kinetic Studies

4.5.3.1 pNA Protease Assay

To assess initial hydrolysis rate, 20 μ L of enzyme (2 μ g/mL protein concentration) was added to 160 μ L of 50 mM Tris-HCl buffer (pH 8). 20 μ L of *N*-succinyl-Ala-Ala-Pro-Phe-*p*-nitroanilide in methanol, at 1 mM, was added to the enzyme solution. The initial rate of hydrolysis of the peptide substrate was monitored by recording the increase in absorption at $\lambda = 405$ nm at 25 °C. Background hydrolysis was subtracted to give initial rates of hydrolysis.

4.5.3.2 *CT Stability Assays*

Enzyme species (2 $\mu\text{g}/\text{mL}$ protein concentration) were incubated in 50 mM of Tris-HCl buffer at pH 8.0. For samples incubated at 40 $^{\circ}\text{C}$, the assay was performed immediately after the aliquot had been taken to prevent samples degrading over time. For samples incubated at 4 $^{\circ}\text{C}$ or 20 $^{\circ}\text{C}$, the samples were stored at -20 $^{\circ}\text{C}$ until the 28th day study was completed. The residual activity was calculated as a ratio of initial rates of hydrolysis, calculated as described above, at given incubation time over the initial activity. Activity half-lives were extracted from a linear plot of the natural logarithm of residual activity against time; all stability profiles were assumed to be based on an exponential decay. Half-life values were subsequently normalised to factor of half-life increase by dividing by the half-life of the corresponding batch of α -CT to alleviate issues of batch-to-batch variations.

4.5.3.3 *Michaelis-Menten Kinetics and Parameters*

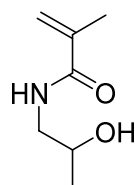
Michaelis-Menten parameters were established by performing the pNA protease assay (see Section 4.5.3.1) with varying *N*-succinyl-Ala-Ala-Pro-Phe *p*-nitroanilide substrate concentrations. A range of *N*-succinyl-Ala-Ala-Pro-Phe *p*-nitroanilide solutions were prepared by diluting with methanol to 10, 5, 2, 1, 0.5, 0.2 mM solutions; the initial hydrolysis rate was recorded as before. MARS data analysis software was used to extract values of K_m , k_{cat} and k_{cat}/K_m from a plot of the reciprocal of substrate concentration against the reciprocal of initial hydrolysis rate.

4.5.3.4 *Glucose Oxidase Stability Assays*

Native α -CT and α -CT-PPCs (5 mg/mL protein concentration) were incubated with glucose oxidase (GO_x) (0.5 units/mL) in 50 mM sodium acetate buffer at pH 5.0 at 30 $^{\circ}\text{C}$. Aliquots (50 μL) were collected and the activity assay was performed immediately. The residual activity of GO_x was calculated as a ratio of initial rates of activity at given incubation time over the initial activity. To assess initial activity rate a 10 μL of GO_x (0.5 units/mL) was added to 190 μL of a solution of glucose (1.72% w/v), *o*-dianisidine (0.17 mM) and horseradish peroxidase (PO_x)

(3 Purpogallin units/mL). The initial rate of oxidation of *o*-dianisidine was monitored by recording the increase in absorption at $\lambda = 492$ nm at 25 °C. Background hydrolysis was subtracted to give initial rates of hydrolysis. PO_x was used in a large excess and stored in aliquots at -20 °C to ensure that this is not the limiting factor in enzyme kinetics.

4.5.4 Synthesis of *N*-(2-Hydroxypropyl)methacrylamide (HPMA)



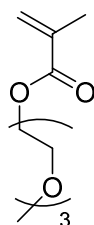
Synthesis previously reported by Vaisocherová-Lísalová *et al.*⁵⁴ A mixture of methacryloyl chloride (8.0 g, 76 mmol) and dichloromethane (10 mL) was slowly added to a solution of 2-hydroxypropyl amine (6.0 g, 80 mmol) and sodium hydrogen carbonate (7.2 g, 88 mmol) in dichloromethane (150 mL) at 0 °C, and then the mixture was stirred at room temperature for 3 h. After filtering out the precipitated salt, the solution was evaporated to remove the solvent. HPMA was isolated by recrystallisation from acetone. ¹H NMR: (300 MHz, D₂O): δ (ppm) 5.64 (s, 1H, CH₃C=CHH), 5.39 (s, 1H, CH₃C=CHH), 4.00-3.79 (m, 1H, O=CNHCH₂CHOHCH₃), 3.34-3.10 (m, 2H, O=CNHCH₂CHOHCH₃), 1.87 (s, 3H, CH₃C=CH₂) and 1.11 (d, 3H, ³J_{H-H} = 6.3 Hz, O=CNCH₂CHOHCH₃). ¹³C NMR (75 MHz, D₂O): δ (ppm) 172.1, 139.1, 121.0, 66.2, 46.2, 19.4, 17.7 ESI-MS (*m/z*): [2M+Na]⁺ calcd. for C₇H₁₃NO₂: 309.1584; found: 309.1407.

4.5.5 Typical Polymerisation of HPMA/OEGMA to Synthesise α -CT-PPCs

In a typical polymerisation reaction, a solution of HPMA (115 mg, 0.8 mmol), and **CT-MI 2.1.10** (20 mg, 0.0092 mmol of initiator groups) in deionised water (7 mL) was sealed and bubbled with nitrogen in an ice bath for 20 min. Deoxygenated catalyst solutions of HMTETA (10 μ L, 0.04 mmol) and Cu(I)Br (5 mg, 0.04 mmol) in deionised water (3 mL) was then added to the conjugation reactor under nitrogen bubbling. The mixture was sealed and stirred for 18 h at 4 °C. CT-PPMA conjugates were isolated by ultrafiltration using a Millipore stirred filtration cell and

a 5 kDa MWCO membrane against deionised water and then lyophilised. The successful production of the PPCs was confirmed by UV-Vis spectroscopy and SDS-PAGE analysis.

4.5.6 Synthesis of Triethylene Glycol Methyl Ether Methacrylate (TEGMA)



Synthesis previously reported by Jones *et al.*⁵⁵ A mixture of methacryloyl chloride (6.48 g, 70 mmol) and tetrahydrofuran (10 mL) was slowly added to a solution of triethylene glycol (10.0 g, 60 mmol) and triethylamine (9.34 mL, 70 mmol) in tetrahydrofuran (100 mL) at 0 °C, and then the mixture was stirred at room temperature for 16 h. After filtering out the precipitated salt, the solution was evaporated to remove the solvent. The resulting compound was redissolved in dichloromethane and washed with water (100 mL), sodium hydrogen carbonate solution (2 x 100 mL) and finally again with water (2 x 100 mL). The organic layer was dried with magnesium sulfate before isolating the crude product by evaporating solvent. Flash column chromatography (6:1 petroleum ether:ethyl acetate) was utilised to obtain purified TEGMA as a clear liquid. ¹H NMR: (300 MHz, CDCl₃): δ (ppm) 6.13 (s, 1H, CH₃C=CH \mathbf{H}), 5.58 (s, 1H, CH₃C=C \mathbf{H} H), 4.30 (t, 2H, ³J_{H-H} = 3.4 Hz, O=COCH $\mathbf{2}$ CH $\mathbf{2}$ O), 3.77 (t, 2H ³J_{H-H} = 3.4 Hz, O=COCH $\mathbf{2}$ CH $\mathbf{2}$ O), 3.71-3.59 (m, 8H, CH $\mathbf{2}$ O(CH $\mathbf{2}$ CH $\mathbf{2}$ O) $\mathbf{2}$ CH $\mathbf{3}$), 3.38 (s, 3H, O(CH $\mathbf{2}$ CH $\mathbf{2}$ O) $\mathbf{3}$ CH $\mathbf{3}$) and 1.95 (s, 3H, CH $\mathbf{3}$ C=CH $\mathbf{2}$). ¹³C NMR (75 MHz, D₂O): δ (ppm) 167.1, 136.0, 125.5, 71.8, 70.5, 70.4, 69.0, 63.7, 58.8, 25.3 18.4. ESI-MS (*m/z*): [M+Na]⁺ calcd. for C₁₁H₂₀O₅: 255.3692; found: 255.3688.

4.6 References

1. C. Barner-Kowollik, A. S. Goldmann and F. H. Schacher, *Macromolecules*, 2016, **49**, 5001-5016.
2. J. E. Elliott and C. N. Bowman, *Macromolecules*, 2001, **34**, 4642-4649.
3. V. V. Korshak, *Acta Polym.*, 1983, **34**, 603-611.
4. K. A. Günay, P. Theato and H.-A. Klok, in *Functional Polymers by Post-Polymerization Modification*, Wiley-VCH Verlag GmbH & Co. KGaA, 2012, pp. 1-44.
5. M. A. Gauthier, M. I. Gibson and H.-A. Klok, *Angew. Chem. Int. Ed.*, 2009, **48**, 48-58.
6. R. Kakuchi and P. Theato, *Polym. Chem.*, 2014, **5**, 2320-2325.
7. J. S. Oakdale, L. Kwisnek and V. V. Fokin, *Macromolecules*, 2016, **49**, 4473-4479.
8. J. Lee, E. W. Lin, U. Y. Lau, J. L. Hedrick, E. Bat and H. D. Maynard, *Biomacromolecules*, 2013, **14**, 2561-2569.
9. R. J. Mancini, J. Lee and H. D. Maynard, *J. Am. Chem. Soc.*, 2012, **134**, 8474-8479.
10. H. Murata, C. S. Cummings, R. R. Koepsel and A. J. Russell, *Biomacromolecules*, 2014, **15**, 2817-2823.
11. Z. Ding, C. J. Long, Y. Hayashi, E. V. Bulmus, A. S. Hoffman and P. S. Stayton, *Bioconjugate Chem.*, 1999, **10**, 395-400.
12. F. D. Jochum and P. Theato, *Chem. Soc. Rev.*, 2013, **42**, 7468-7483.
13. S. Dai, P. Ravi and K. C. Tam, *Soft Matter*, 2008, **4**, 435-449.
14. G. Kocak, C. Tuncer and V. Butun, *Polym. Chem.*, 2016.
15. D. J. Phillips and M. I. Gibson, *Polym. Chem.*, 2015, **6**, 1033-1043.
16. J.-F. Lutz, *J. Polym. Sci. Part A: Polym. Chem.*, 2008, **46**, 3459-3470.
17. H. Yamauchi and Y. Maeda, *J. Phys. Chem. B*, 2007, **111**, 12964-12968.
18. M. Heskins and J. E. Guillet, *J. Macromol. Sci., Part A: Pure Appl. Chem.*, 1968, **2**, 1441-1455.
19. H. Lai, G. Chen, P. Wu and Z. Li, *Soft Matter*, 2012, **8**, 2662-2670.
20. I. Idziak, D. Avoce, D. Lessard, D. Gravel and X. X. Zhu, *Macromolecules*, 1999, **32**, 1260-1263.

21. P. A. Woodfield, Y. Zhu, Y. Pei and P. J. Roth, *Macromolecules*, 2014, **47**, 750-762.
22. H. G. Schild and D. A. Tirrell, *J. Phys. Chem.*, 1990, **94**, 4352-4356.
23. G. Fundueanu, M. Constantin and P. Ascenzi, *Int. J. Pharm.*, 2009, **379**, 9-17.
24. A. Chilkoti, G. Chen, P. S. Stayton and A. S. Hoffman, *Bioconjugate Chem.*, 1994, **5**, 504-507.
25. Z. Ding, G. Chen and A. S. Hoffman, *Bioconjugate Chem.*, 1996, **7**, 121-125.
26. C. A. Lackey, N. Murthy, O. W. Press, D. A. Tirrell, A. S. Hoffman and P. S. Stayton, *Bioconjugate Chem.*, 1999, **10**, 401-405.
27. T. Shimoboji, Z. Ding, P. S. Stayton and A. S. Hoffman, *Bioconjugate Chem.*, 2001, **12**, 314-319.
28. P. S. Stayton, T. Shimoboji, C. Long, A. Chilkoti, G. Ghen, J. M. Harris and A. S. Hoffman, *Nature*, 1995, **378**, 472-474.
29. P. Tae Gwan and A. S. Hoffman, *J. Biomater. Sci., Polym. Ed.*, 1993, **4**, 493-504.
30. D. J. Keddie, *Chem. Soc. Rev.*, 2014, **43**, 496-505.
31. A. Mühlebach, S. G. Gaynor and K. Matyjaszewski, *Macromolecules*, 1998, **31**, 6046-6052.
32. F. Käfer, F. Liu, U. Stahlschmidt, V. Jérôme, R. Freitag, M. Karg and S. Agarwal, *Langmuir*, 2015, **31**, 8940-8946.
33. P. J. Roth, T. P. Davis and A. B. Lowe, *Macromolecules*, 2012, **45**, 3221-3230.
34. I. Cobo, M. Li, B. S. Sumerlin and S. Perrier, *Nat. Mater.*, 2015, **14**, 143-159.
35. C. Cummings, H. Murata, R. Koepsel and A. J. Russell, *Biomacromolecules*, 2014, **15**, 763-771.
36. O. Naksuriya, Y. Shi, C. F. van Nostrum, S. Anuchapreeda, W. E. Hennink and S. Okonogi, *Eur. J. Pharm. Biopharm.*, 2015, **94**, 501-512.
37. B. Obereigner, M. Burešová, A. Vrána and J. Kopeček, *J. Polym. Sci. Polym. Symp.*, 1979, **66**, 41-52.
38. M. V. Solovsky, K. Ulbrich and J. Kopeček, *Biomaterials*, 1983, **4**, 44-48.
39. L. Šprincl, J. Exner, O. Štěrba and J. Kopeček, *J. Biomed. Mater. Res., Part B*, 1976, **10**, 953-963.
40. K. Matyjaszewski and J. Xia, *Chem. Rev.*, 2001, **101**, 2921-2990.
41. M. Teodorescu and K. Matyjaszewski, *Macromolecules*, 1999, **32**, 4826-4831.

42. M. Teodorescu and K. Matyjaszewski, *Macromol. Rapid Commun.*, 2000, **21**, 190-194.
43. J. T. Rademacher, M. Baum, M. E. Pallack, W. J. Brittain and W. J. Simonsick, *Macromolecules*, 2000, **33**, 284-288.
44. J. J. Lavinder, S. B. Hari, B. J. Sullivan and T. J. Magliery, *J. Am. Chem. Soc.*, 2009, **131**, 3794-3795.
45. M.-C. Lo, A. Aulabaugh, G. Jin, R. Cowling, J. Bard, M. Malamas and G. Ellestad, *Anal. Biochem.*, 2004, **332**, 153-159.
46. M. W. Pantoliano, E. C. Petrella, J. D. Kwasnoski, V. S. Lobanov, J. Myslik, E. Graf, T. Carver, E. Asel, B. A. Springer, P. Lane and F. R. Salemme, *J. Biomol. Screen.*, 2001, **6**, 429-440.
47. S. Üzgün, Ö. Akdemir, G. Hasenpusch, C. Maucksch, M. M. Golas, B. Sander, H. Stark, R. Imker, J.-F. Lutz and C. Rudolph, *Biomacromolecules*, 2010, **11**, 39-50.
48. D. Rinaldi, T. Hamaide, C. Graillat, F. D'Agosto, R. Spitz, S. Georges, M. Mosquet and P. Maitresse, *J. Polym. Sci. Part A: Polym. Chem.*, 2009, **47**, 3045-3055.
49. M. Liu, P. Tirino, M. Radivojevic, D. J. Phillips, M. I. Gibson, J.-C. Leroux and M. A. Gauthier, *Adv. Funct. Mater.*, 2013, **23**, 2007-2015.
50. J. M. Berg, J. L. Tymoczko and L. Stryer, *Biochemistry, Fifth Edition*, W.H. Freeman, 2002.
51. W. W. Cleland, *Biochim. Biophys. Acta*, 1963, **67**, 173-187.
52. P. J. Roth, F. D. Jochum and P. Theato, *Soft Matter*, 2011, **7**, 2484-2492.
53. H. Murata, C. S. Cummings, R. R. Koepsel and A. J. Russell, *Biomacromolecules*, 2013, **14**, 1919-1926.
54. H. Vaisocherová-Lísalová, F. Surman, I. Víšová, M. Vala, T. Špringer, M. L. Ermini, H. Šípová, P. Šedivák, M. Houska, T. Riedel, O. Pop-Georgievski, E. Brynda and J. Homola, *Anal. Chem.*, 2016, **88**, 10533-10539.
55. M. W. Jones, M. I. Gibson, G. Mantovani and D. M. Haddleton, *Polym. Chem.*, 2011, **2**, 572-574.

5 Synthesis of Protein-Polymer Conjugates from Laundry-Specific Enzymes

5.1 Abstract

The work in this Chapter highlights the effectiveness of protein-polymer conjugates within liquid laundry detergent for a stain-removal application. α -chymotrypsin and α -chymotrypsin protein-polymer conjugates, introduced in previous chapters, were not observed to enhance stain removal when examined *via* application testing. Therefore, Unilever Protease 1 and Lipex, enzymes that have been optimised for stain removal applications within high surfactant environments, were investigated. The conjugation reagent required for the synthesis of protein-polymer conjugates was found to inhibit both Unilever Protease 1 and Lipex and therefore purification was needed to remove the excess reagent. Enhancement of catalytic half-life was observed upon the synthesis of macro-initiators from Unilever Protease 1, however upon the transformation to protein-polymer conjugates using poly(glycerol methacrylate), enzyme stability was found to revert back to that of native Unilever Protease 1. In contrast, the synthesis of macro-initiators from Lipex was observed to cause a decrease in stability. Further destabilisation was found upon the synthesis of poly(glycerol methacrylate) polymer-protein conjugates, with the conjugate species becoming insoluble in aqueous solution. It is hypothesised that the grafted polymer disrupts the hydrophobic interactions within the Lipex resulting in a reduction in solubility, activity, and stability.

5.2 Introduction

5.2.1 Laundry Formulations

Laundry formulations are made up of many different components including surfactants, bleaches, water softeners, fragrances, fabric softeners, and anti-redeposition agents.¹ Surfactants are a key component to all laundry formulations and have been utilised by civilisations as far back as 2800 BC for laundry and cleaning applications.² Surfactants are amphiphiles with a hydrophilic head group and a hydrophobic alkyl chain, thus allowing surfactants to interact with hydrophobic stains and increase the solubility of the material allowing for the removal of water immiscible

compounds (Figure 5.1). Anti-redeposition agents were incorporated into laundry detergents to prevent the reattachment of stains during the washing cycle.

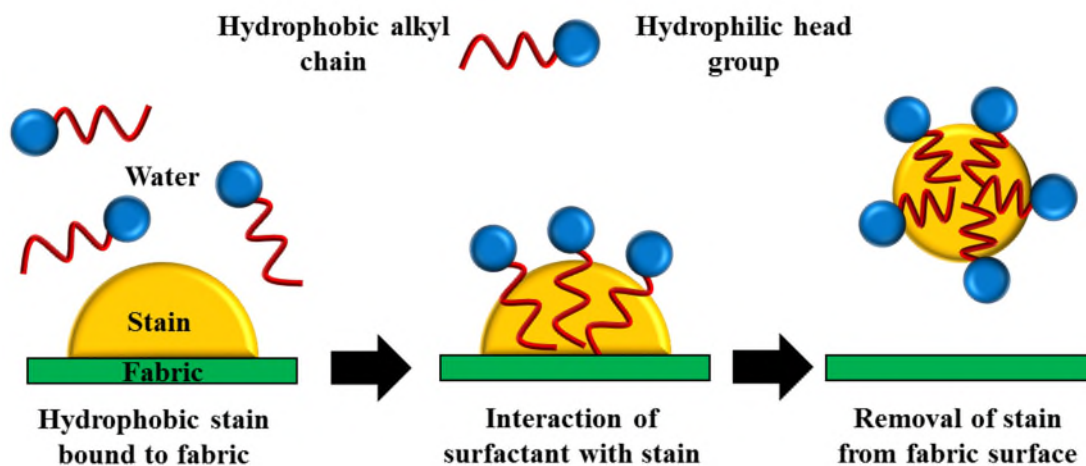


Figure 5.1 Schematic representation of the interaction of surfactants with hydrophobic stains

The effectiveness of surfactants can be hindered by the presence of calcium and magnesium ions as they react to form insoluble complexes that can precipitate out of aqueous solution.³ As such, locations with high water hardness can require increased surfactant concentrations to obtain the same level of cleaning. To alleviate this problem, many laundry detergents contain water softeners. Original water softeners removed calcium and magnesium ions by the precipitation of their respective salts. Although this method was effective, iron salts were also observed to precipitate causing clothing to become yellow in colour.¹ Water softeners were rapidly changed to compounds that complexed the ions such as sodium triphosphate,⁴ however, as a result of phosphate regulations that were introduced because of eutrophication issues,⁴ current laundry formulations tend to employ zeolites for this role.¹

Despite the ability of surfactants to provide high degrees of stain removal, the low biodegradability of synthetic surfactants has been found to be problematic. Legislation was implemented in Germany in 1961 stating that all detergents must be 80% biodegradable and in the following years many other countries followed suit and adopted this legislation.¹ In recent years, industry has been encouraged to produce more sustainable products and so the use of sugar

based surfactants has increased. This has also led to the development of more concentrated formulations pioneered by the Unilever scheme in 2006 of “Small and Mighty”.^{5, 6}

Due to the changes in washing practices including the progression from hand to machine washing and new environmental legislations, laundry formulations constantly have to adapt to suit their purpose. Enzymes were introduced into laundry formulation in 1959,¹ the first enzymes to be introduced were proteases. Amylases, cellulases and lipases were added over the next decade to formulations to improve stain removal capacity. Enzymes are biological catalysts that have very high specificity and activity rates and so allow laundry to be washed at lower temperatures than non-enzymatic washing powder. The addition of enzymes to laundry formulations has been shown to increase stain removal by over 25%.⁷

The major limitation with the application of enzymes into liquid laundry formulations is the narrow range of conditions at which the enzyme remains active. Native enzymes are intolerant to small changes in their external environment; alterations in the environment can cause changes in the tertiary structure of the protein causing their activity to rapidly decrease. Factors that affect the stability of enzymes include pH, temperature and concentration of salts. Proteases, which are common enzymes used in laundry formulations, also pose a problem as autolytic digestion can occur. Due to these problems, the development of more stable enzymes is required to withstand the storage conditions within laundry detergents.

5.2.2 Laundry-Specific Protease Enzymes

Since enzymes were introduced into laundry formulations in 1959,¹ many protease enzymes have been utilised to enhance industrial stain removal.⁷⁻⁹ Much research has been conducted to modify the protein’s primary structure to induce higher stability within surfactant containing environments.¹⁰⁻¹³ Proteases that are ideal for a laundry-based application have a low specificity and can digest peptide bonds at numerous locations within protein or peptide compounds. The work in this Chapter focuses on subtilisins, a range of serine proteases that are non-specific

endoproteases. Subtilisins have been found to possess the same catalytic triad as present within the active site of α -chymotrypsin (α -CT).

The current subtilisin enzyme of interest is Unilever Protease 1 (UL1). Whilst the structure of UL1 is relatively unknown, the enzyme is derived from modifying the expression of savinase. As such, savinase will be utilised as a model for UL1 to help determine the number of possible modification sites and other characteristics including absorption coefficients and microenvironments of residues. savinase has been found to have optimum activity at pH 10.0 and a wide range of thermal activity between 20 and 60 °C.^{14, 15} However, it has been found that savinase can be inhibited by compounds that are naturally present in some food sources including eggs and potatoes.¹⁶

5.2.3 Laundry-Specific Lipase Enzymes

As many different stains exist, different types of enzyme are required to target stains made up of both proteins and fats. Lipases are a subclass of esterases that can catalyse the hydrolysis of ester bonds. Lipases are specific to the hydrolysis of triglycerides into glycerol and their substituent fatty acids (Figure 5.2). Lipase enzymes have many industrial applications including food manufacture, the production of biodiesel and enhancement of stain removal in laundry formulations.¹⁷⁻²⁰

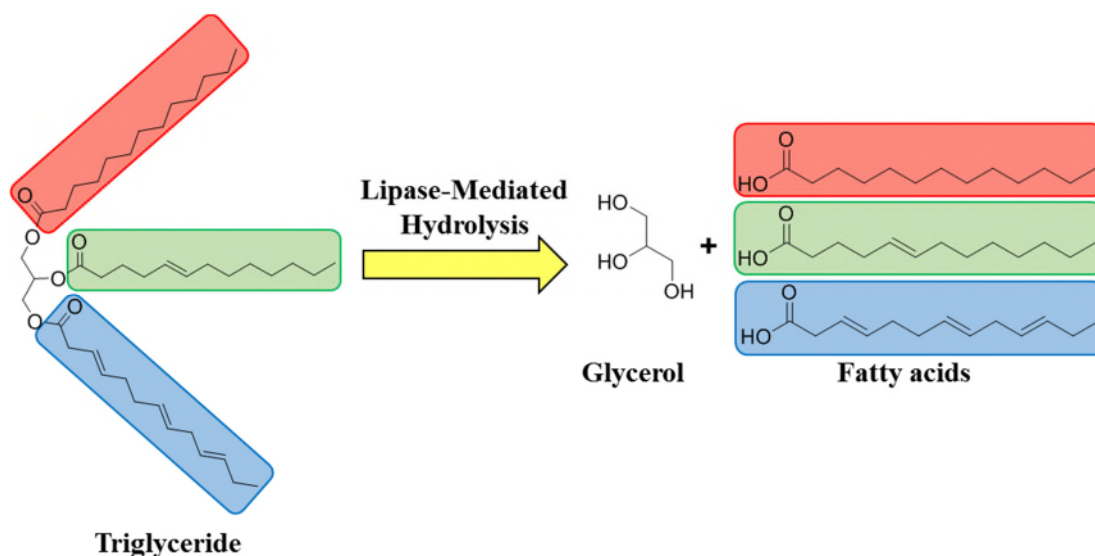


Figure 5.2 Schematic representation of the hydrolysis of triglycerides to form glycerol and fatty acid chains.

Enzymes, including lipases, which originate from thermophilic organisms tend to have an increased optimum temperature in comparison to other species. As such the Lipase from *Thermomyces Lanuginosa* (TLL) was identified as an enzyme of high industrial interest due to its activity at high operating temperatures. It was also noted that TLL contains the same catalytic triad present in both α -CT and UL1 with hydrolysis of substrates being controlled by the nucleophilicity of the L-serine residue and by employing the use of an oxyanion hole.²⁰⁻²²

Although the catalytic site has many similarities to α -CT and UL1, the access to lipase is hindered by the presence of a helical loop referred to as the “lid”.²³ In a solely aqueous environment, the “lid” remains closed and access to the active site is low. The introduction of a hydrophobic substrate induces a morphology change to the open conformation. Figure 5.3 highlights the exposure of the active site upon the protein adopting the open “lid” conformation.

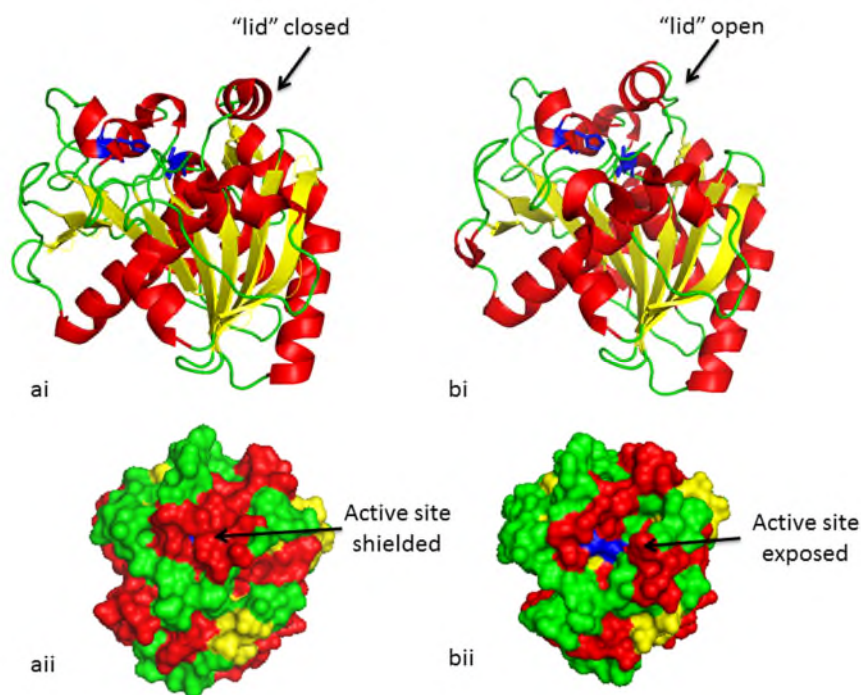


Figure 5.3 Crystal structure of TLL in the a) closed (**1DU4**), and b) open (**1EIN**) positions with the active site shown in blue.²¹ The structure is represented as i) the secondary structure ii) the surface structure. PDB crystal structure references are identified in bold. With thanks to Dr. Katherine Farrance.

The mobility of the “lid” has been studied through the analysis of the structure at varying surfactant concentrations.^{10, 21, 24} Brzozowski *et al.* identified Arg84, Cys22, and Cys268 as the key residues involved in the “lid” mechanics.²¹ The two L-cysteine residues are present in the closed morphology as a left handed disulfide bond and upon exposure to surfactants can isomerise to form a right handed bond. This in turn allows Arg84, which is located within the hinge of the “lid”, to form hydrogen bonds with the Cys268 residue. The newly formed hydrogen bonds induce a morphological change and cause the “lid” to move into the open conformation. When employing TLL in laundry applications, the presence of high levels of surfactant in the detergent ensure the “lid” remains in the open morphology.

With an aim to develop enzymatic species that are stable to the conditions within laundry detergent and retain their high stain removal capabilities, α -CT macro-initiators and protein-polymer conjugates (PPCs) synthesised in the preceding chapters were compared to

corresponding analogues synthesised from laundry-specific protease and lipase enzymes, UL1 and Lipex. With the additional aim of creating a one-pot formulation with multiple enzymes present, the stability of Lipex and UL1 polymer conjugate species were investigated in the presence of each other to further examine the protection provided by the addition of grafted polymeric species.

5.3 Results and Discussion

5.3.1 Effectiveness of α -Chymotrypsin and α -Chymotrypsin PPCs in Laundry Applications

Although α -CT has been utilised as a model enzyme throughout the previous chapters, α -CT has not been selectively modified for exposure to environments that contain high levels of surfactants typically found in laundry formulations. To explore the tolerance of α -CT when exposed to these environments, the activity of α -CT was investigated in solutions containing varying concentrations of Ecoboost™ formulation in both pH 8.0 buffer and distilled water (Figure 5.4). Ecoboost™ formulation is a trademarked liquid formulation from Unilever containing 15 wt.% surfactant, which is a combination of anionic and non-ionic surfactants, with calcium binders. The retention of the catalytic activity of α -CT was examined by the *p*-nitroaniline (*p*NA) assay (introduced in Section 2.3.5) and subsequently normalised to residual activity with respect to α -CT in pH 8.0 Britton-Robinson buffer.

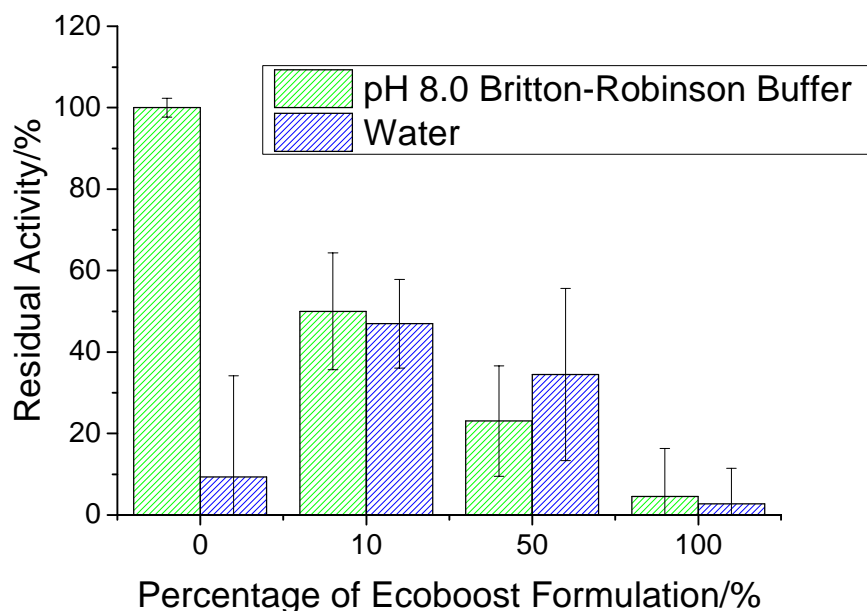


Figure 5.4 The effect of Ecoboost™ formulation upon activity of α -CT. Each data point is based on the average of four repeats of *p*NA assay with standard deviation displayed as error.

The activity of α -CT was found to decrease as the percentage of Ecoboost™ formulation was increased in buffered solution. The addition of 10% formulation led to a 50% decrease in activity

compared with α -CT in 100% pH 8.0 buffer (0% Ecoboost™). It is noteworthy that α -CT prepared in deionised water, without any additives, only has 10% of the activity of α -CT in pH 8.0 buffer. However, upon addition of Ecoboost™ formulation, which has a pH of 7.8, the activities appear to be independent of the solvent used to prepare samples, either water or buffer. It is hypothesised that as deionised water has a pH of approximately 6.8 compared with the pH 8.0 buffer, the active site of α -CT exists in a different conformation at these different pH values owing to the presence of charged residues within the protein's structure. Upon the addition of Ecoboost™ formulation, it is proposed that the increase in pH allows an increase in activity compared to samples prepared in 100% water, yet the presence of surfactants leads to an overall decrease in activity.

Despite the observed decrease in activity upon addition of formulation, it was still important to analyse the stain removal capabilities of α -CT and α -CT PPCs synthesised in previous chapters to determine if these species are suitable for the intended application. The most common industrial method for determining stain removal efficiency of enzymes is to perform stain tests. These tests incubate stained fabric with laundry formulation, buffer and enzymes at elevated temperatures to represent the conditions present in a washing machine (Figure 5.5). The treated fabric is then rinsed and allowed to dry prior to analysis. As enzymes can exhibit substrate specificity a range of stains are employed to investigate variations in degree of cleaning observed. Common stains that are utilised to analyse the efficiency of protease enzymes are based on blood, milk and ink.

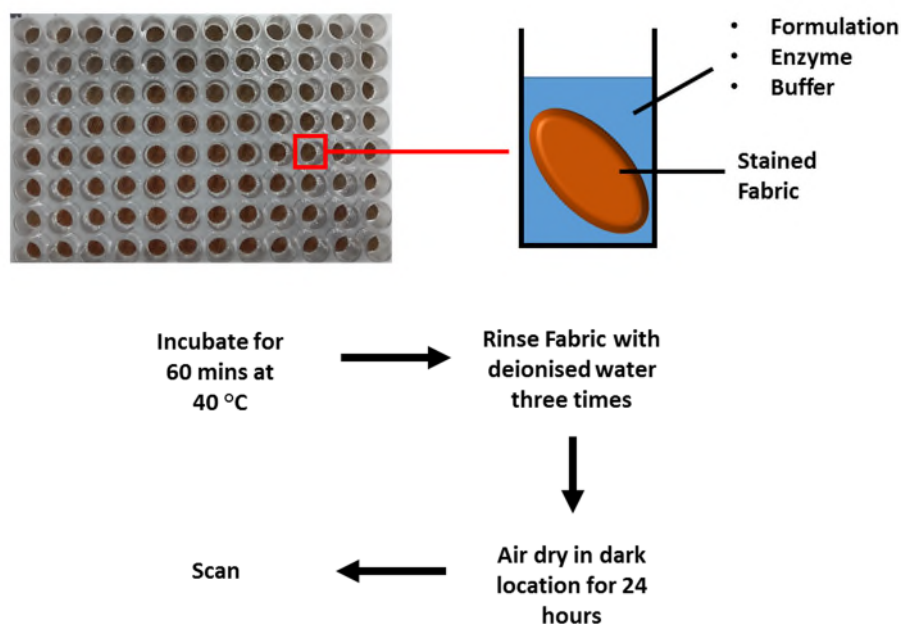


Figure 5.5 Experimental procedure for industrial stain testing.

The stained fabric was then analysed to determine the degree of stain removal by comparing the colour profile in relation to an unstained cotton fabric calibrant. The colour profiles of the fabric was analysed by employing Hunter's LAB analysis, which is most commonly used to analyse variations in colour within the food industry.²⁵ Change in colour, ΔE , is calculated based upon the relationship described in Equation 5.1 (a) where L , a , and b represent the brightness, redness to greenness, and yellowness to blueness respectively.²⁶ The stain removal index (SRI) based upon colourimetry was introduced by Neiditch *et al.* as a superior method for reporting stain removal compared to previous methods, which were largely based upon reflectance, as the colourimetry method allowed greater accuracy in the analysis of coloured stains.²⁷ The change in SRI (ΔSRI) can be used to analyse increases or decreases in stain removal ability based upon additives, such as enzymes, to the formulation.

Equation 5.1 (a-c) Hunter's LAB analysis, SRI and ΔSRI equations.

$$(a) \Delta E = \sqrt{(L_0 - L)^2 + (a_0 - a)^2 + (b_0 - b)^2}$$

$$(b) SRI = 100 - \Delta E$$

$$(c) \Delta SRI = \text{Experimental SRI} - \text{Control SRI}$$

To investigate their suitability for a stain removal application, α -CT PPCs synthesised in previous Chapters were explored. The conjugates were chosen to cover a range of polymer functionalities and based upon their high retention of initial activity and significant enhancements in thermal stability, reported in previous Chapters, **CT-PGMA 3.10.5**, **CT-PHPMA 4.10.5**, **CT-POEGMA 4.10.5** and **CT-POEGMA 4.10.20** were selected. As the activity of α -CT was significantly reduced in the presence of the laundry formulation, the stain tests were conducted in buffer to ascertain stain removal capabilities at high α -CT enzymatic activity. The stain removal efficiency of native α -CT and **CT-PGMA 3.10.5**, **CT-PHPMA 4.10.5**, **CT-POEGMA 4.10.5** and **CT-POEGMA 4.10.20**, were examined with stain tests using fabric stained with blood and blood, milk, and ink (Figure 5.6). Control experiments were performed without the presence of enzymatic species to allow the observation of enhanced stain removal.

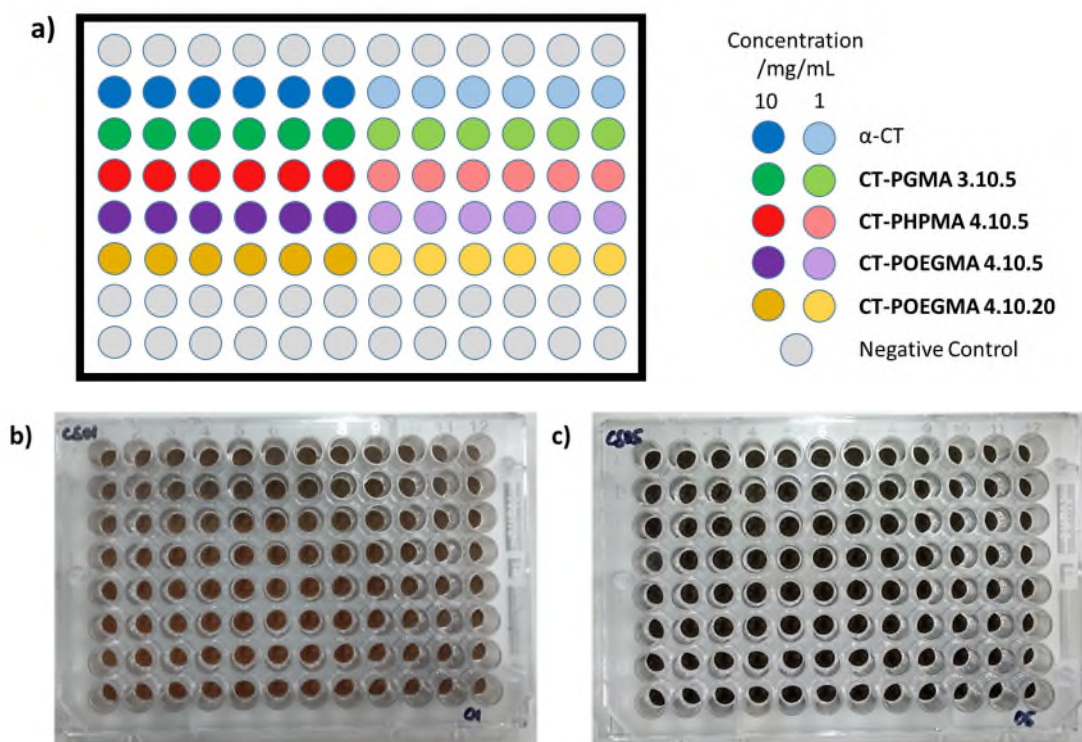


Figure 5.6 a) Layout of samples in stain plates and resulting stain test plates after exposure to α -CT, **CT-PGMA 3.10.5**, **CT-PHPMA 4.10.5**, **CT-POEGMA 4.10.5** and **CT-POEGMA 4.10.20** with b) blood and c) blood, milk and ink.

Although the observation of enhanced stain removal was expected in samples containing α -CT and α -CT PPCs, Δ SRI was found to be zero in all cases suggesting that the enzymes could not hydrolyse the stain from the surface of the fabric. It is hypothesised that the selectivity of α -CT prevents stain removal in these tests, as α -CT can only cleave peptide bonds next to aromatic residues. It is also postulated that the active site of α -CT cannot access a substrate that is bound to a surface preventing stain removal.

Therefore, as a result of the low activity exhibited by α -CT in laundry formulation and the lack of stain removal observed with both α -CT and α -CT PPCs, it was concluded that α -CT is not an appropriate enzyme for a stain removal application. As such, the chemistries that have been applied to α -CT to synthesise PPC species with enhanced stability will also be employed to synthesise PPCs from enzymes that are currently utilised for stain removal and laundry applications. The overall aim is to generate enzymes that are both stable to storage with themselves and other enzymes yet also exhibit high stain removal efficiency.

5.3.2 Laundry-Specific Protease Enzymes

5.3.2.1 Structure and Properties of Laundry-Specific Protease Enzymes

As mentioned in Section 5.2.2, the current proteolytic enzyme of interest is UL1, which is derived from savinase. As the structure of UL1 is unknown, the structure of savinase will be employed to aid in the analysis of UL1. In contrast to α -CT, which contains 17 potential amine modification sites, savinase only contains 5 L-lysine residues and 1 N-terminus and therefore 6 possible conjugation sites. Figure 5.7 identifies the locations of these residues, in pink and yellow, and highlights that the residues are not evenly spread across the enzyme but concentrated into a specific area. It is possible that this could lead to areas of the enzyme remaining unprotected by the grafted polymeric species.

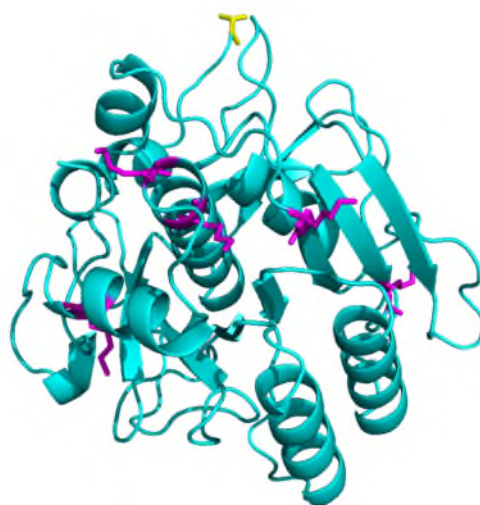


Figure 5.7 Crystal structure of savinase (1SVN).¹⁴ L-Lysine residues have been highlighted in pink and the *N*-terminus highlighted in yellow.

Previous theories from Section 2.3.4 indicate that the conjugation of initiator species using an active ester is dependent upon the pK_a of the amine group. To this end, the DEPTH server was utilised to predict the pK_a values of the ionisable groups within savinase, based on the microenvironment in which the residue is found.²⁸ savinase was submitted to the DEPTH server in the monomeric form of the crystal structure of 1SVN (Figure 5.8).¹⁴

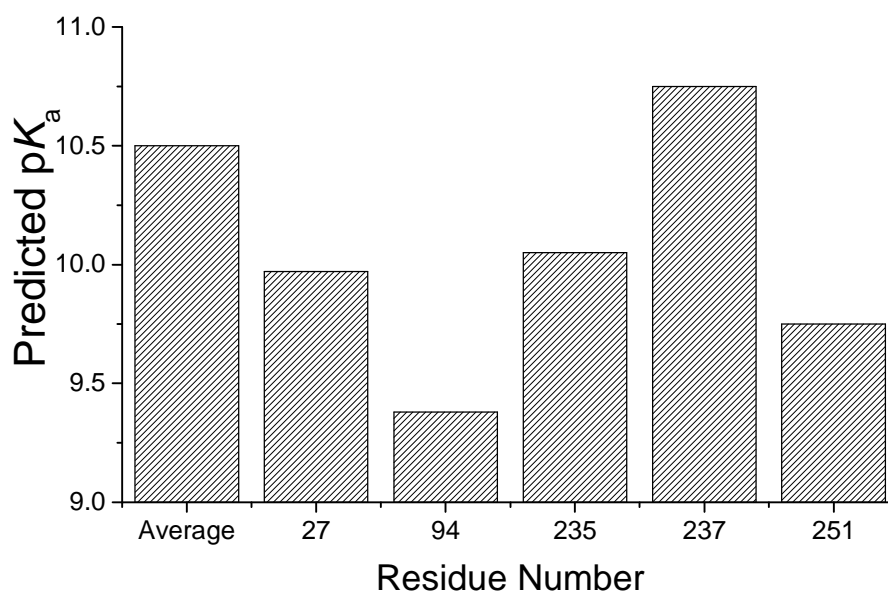
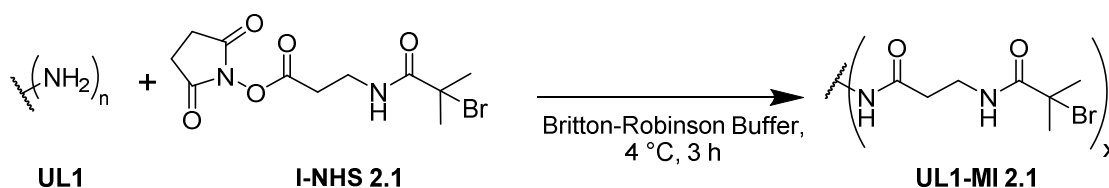


Figure 5.8 Predicted pK_a values of amine groups in L-lysine residues within savinase compared with the average pK_a of L-lysine at 10.5. All values have been calculated by the DEPTH server.²⁸

Although not computed by the DEPTH server, the *N*-terminus is predicted to have the lowest pK_a from previous literature reports.²⁹ In addition to the *N*-terminus, the predicted pK_a values of savinase indicate that residue 94 is the next most probable residue to undergo conjugation. It is noteworthy that the pK_a values are in a similar range to that observed by α -CT and therefore it is predicted that a similar conjugation profile will be observed for UL1.

5.3.2.2 *Synthesis of Macro-Initiators from Laundry Specific Protease Enzymes*

To ascertain whether the conjugation to UL1 is comparable to that observed previously with α -CT in Section 2.3.2, UL1 macro-initiators (**UL1-MI 2.1s**) were synthesised with varying concentrations of the active ester species **I-NHS 2.1**, as used in Chapter 2, per amine at different pH values (pH 8.0, 10.0 and 12.0) (Scheme 5.1). The efficiency of the conjugation reaction was assessed after 3 hours using matrix-assisted laser desorption/ionisation time-of-flight (MALDI-ToF) mass spectrometry without any further purification (Figure 5.9 and Table 5.1).



Scheme 5.1 Reaction of primary amines on UL1 with **I-NHS 2.1** to form **UL1-MI 2.1**.

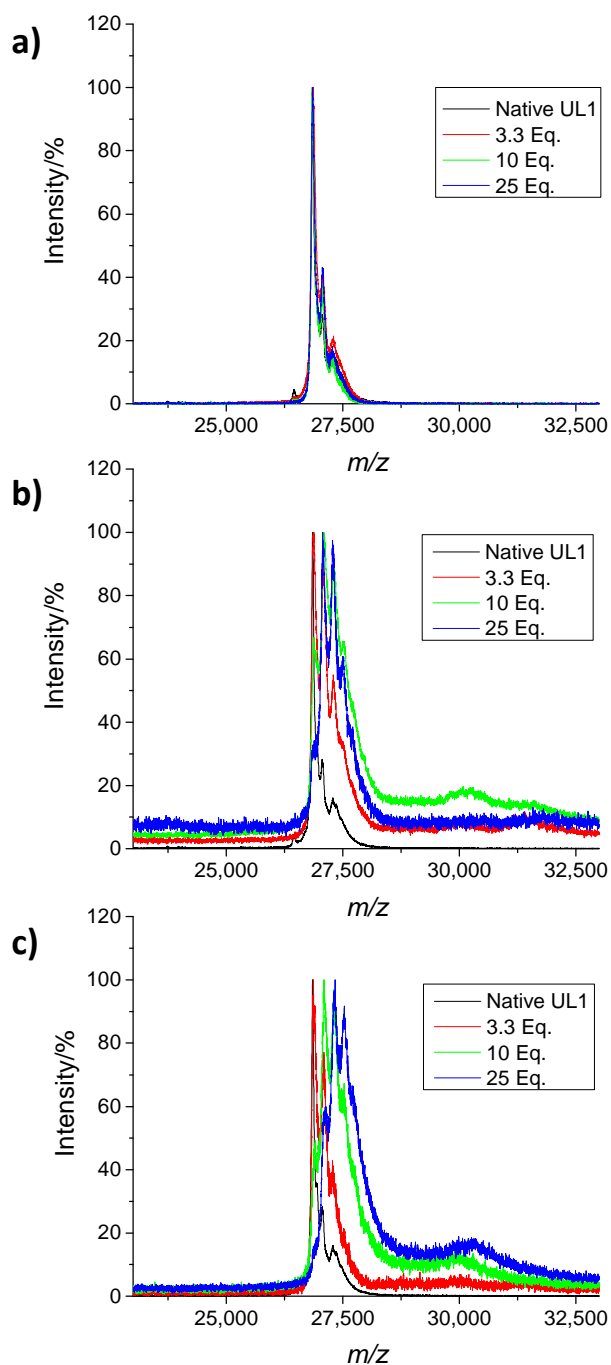


Figure 5.9 MALDI-ToF mass spectra of **UL1-MI 2.1** species formed at varying concentrations of **I-NHS 2.1** when the conjugation reaction was carried out at a) pH 8.0, b) pH 10.0, and c) pH 12.0.

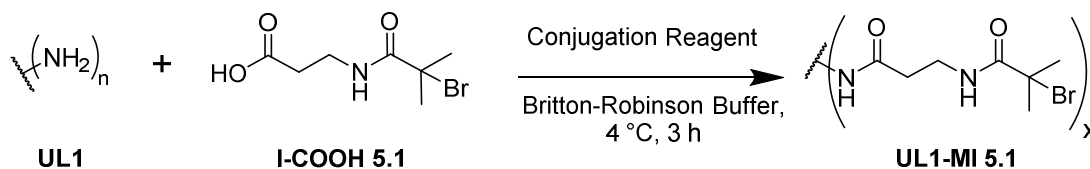
Table 5.1. Average degree of attachment of **I-NHS 2.1** initiator for **UL1-MI 2.1** species synthesised at varying pH values and concentrations of initiator as determined by MALDI-ToF analysis. Errors are reported as the standard deviation of the distribution based on the assumption of a Gaussian fit of the MALDI-ToF mass spectra.

	Equivalents of Initiator Added per Amine		
	3.3	10	25
pH 8.0	0	0	0
pH 10.0	0	1 ± 1	1 ± 1
pH 12.0	0	1 ± 1	2 ± 1

When conjugation was conducted at pH 8.0, the resulting **UL1-MI 2.1** species were all observed to have an unaltered molar mass of 26.8 kDa, the mass of UL1. In contrast to α -CT, which was able to undergo high levels of modification at pH 8.0, this indicates that no modification of UL1 was achieved at pH 8.0. Upon increasing the pH to 10.0, single-site conjugation was observed when employing over 10 equivalents of initiator per amine. A further increase in pH to 12.0 resulted in modification of an additional site, generating a **UL1-MI** with 2 initiator sites. It is evident from MALDI-ToF analysis that the conjugation profile at varying pH and concentration does not mimic that observed with α -CT. It is hypothesised that the reduction in modified sites may be due to the location of the amine groups that are inaccessible and unfavourable for reaction.

As discussed in Chapter 3, a high polymeric grafting density appears to be the most effective method of producing stable protein species, as such further synthetic methods were investigated to prepare **UL1-MI** with an increased number of initiators conjugated to the surface. To this end, a range of typical amide coupling reagents were explored in an attempt to promote higher degrees of initiator incorporation on the surface of UL1. **I-COOH 5.1**, the carboxylic acid analogue of initiator **I-NHS 2.1**, was employed so that the resulting macro-initiator species would have the same chemical structure independent of the synthetic route. Benzotriazol-1-yl-oxytripyrrolidinophosphonium hexafluorophosphate (PyBOP),³⁰ 2-(1H-benzotriazol-1-yl) 1,1,3,3-tetramethyluronium hexafluorophosphate (HBTU),³⁰ 1-[bis(dimethylamino)methylene]

1H-1,2,3-triazolo[4,5]pyridinium 3-oxid hexafluorophosphate (HATU),³¹ 2-(1H benzotriazole-1-yl)-1,1,3,3-tetramethyluronium tetrafluoroborate (TBTU),³² 4-dimethylaminopyridine (DMAP),³³ and *N*-(3-dimethylaminopropyl)-*N'*-ethylcarbodiimide hydrochloride (EDC.HCl) were selected as appropriate reagents to trial to assess a broad range of potential amide coupling catalysts.³⁴ A large excess of the amide coupling reagents (1000 equivalents per amine) and initiator species, **I-COOH 5.1**, (10 equivalents per amine) were utilised to synthesise macro-initiators from UL1 (Scheme 5.2). Although the conjugations were all performed at pH 8.0, the addition of triethylamine (TEA) was also explored with select reagents to investigate if this could further promote attachment of initiators. It was thought that the introduction of a basic species, such as TEA, could promote the deprotonation of the basic L-lysine residues and therefore enhance the amide coupling reaction. It should also be noted that the addition of 10 equivalents of *N*-hydroxysuccinimide (NHS) is required for the conjugation with EDC.HCl. The resulting **UL1-MI 5.1s** were analysed using MALDI-ToF mass spectrometry without any further purification to quantify the number of initiators successfully conjugated to UL1 (Figure 5.10).



Scheme 5.2 Reaction of primary amines on UL1 with **I-COOH 5.1** to form **UL1-MI 5.1**.

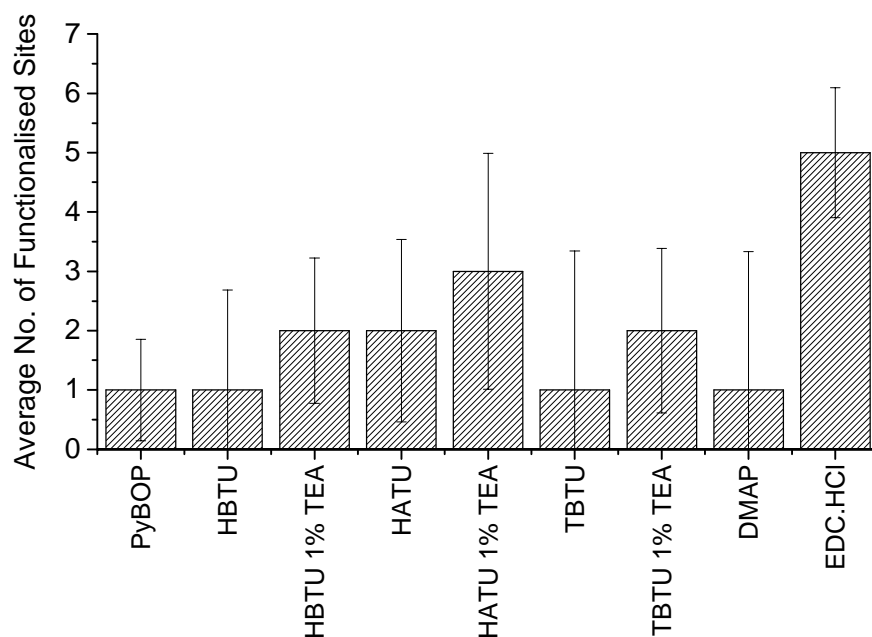


Figure 5.10 Average number of initiator functionalised sites of UL1 as determined by MALDI-ToF with **I-COOH 5.1** and various conjugation reagents. Error bars are displayed as the standard deviation of the distribution of sites functionalised based on the assumption of a Gaussian fit of the MALDI-ToF mass spectra.

All reagents were observed to form **UL-MI 5.1** species with a minimum of one initiator unit conjugated to the enzyme. The addition of TEA enabled modification of a further site in all cases. It is hypothesised that due to most of these reagents having been designed for use in solid-phase amide synthesis, which is conducted in *N,N*-dimethylformamide (DMF), the reagents are not optimised for use within an aqueous system. It is evident that EDC.HCl was the most successful coupling reagent, enabling the conjugation of initiator groups in 5 out of the 6 possible modification sites.

Following effective conjugation employing EDC.HCl, the ability to tune the system to synthesise macro-initiators with a range of initiator grafting densities, through variation of the concentration of EDC.HCl, was assessed. The resulting macro-initiators were analysed using MALDI-ToF mass spectrometry (Figure 5.11 and Table 5.2).

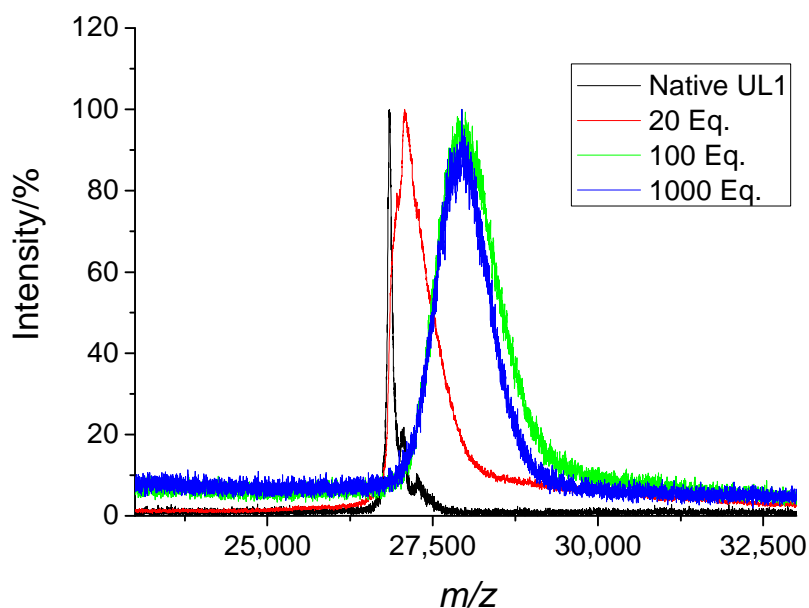


Figure 5.11 MALDI-ToF mass spectra of **UL1-MI 5.1** species formed at pH 8.0 using 10 equivalents of **I-COOH 5.1** and varying concentrations of EDC.HCl.

Table 5.2. Average degree of attachment of **I-COOH 5.1** initiator for **UL1-MI 5.1** species synthesised at varying pH values and concentrations of EDC.HCl as determined by MALDI-ToF analysis. Errors are reported as the standard deviation of the distribution based on the assumption of a Gaussian fit of the MALDI-ToF mass spectra.

	Equivalents of EDC.HCl Added per Amine		
	20	100	1000
pH 8.0	1 ± 1	5 ± 2	5 ± 2

Upon varying the concentration of EDC.HCl, the synthesised macro-initiators were observed to have varying initiator grafting densities. Using 20 equivalents of EDC.HCl generated a **UL1-MI 5.1** species with a molar mass of 27.0 kDa, which corresponds to a single initiator attachment. It is evident that the addition of 100 and 1000 equivalents of EDC.HCl result in the same initiator species with an average of 5 initiator sites attached. Whilst both reactions led to the same product, upon increasing the scale of the reaction from 5 mL to 500 mL, aggregation was observed when using 1000 equivalents of EDC.HCl. It is hypothesised that as a consequence of the exothermic reaction between EDC.HCl and amine moieties, the resultant heat generated was

not adequately dissipated upon increase of reaction scale, causing aggregation. However, it was found that using 100 equivalents of EDC.HCl at the larger 500 mL scale did not result in aggregation.

5.3.2.3 *Activity of Macro-Initiators from Laundry Specific Protease Enzymes*

Following the successful synthesis of **UL1-MI 5.1s**, it was important to establish if the synthesis caused any alterations to the enzyme's activity and stability profiles. As previously discussed in Section 2.3.5, NHS was found to inhibit the catalytic ability of α -CT and therefore it was essential to examine whether the **UL1-MI 5.1** species were subject to inhibition from the conjugation conditions. The retention of the catalytic activity of UL1 and **UL1-MI** species with 1 and 5 conjugated initiators, **UL1-MI 5.1.1** and **UL1-MI 5.1.5** respectively, were examined using the *p*NA assay. The residual activity was calculated as a percentage of the initial activity of native UL1 (Figure 5.12).

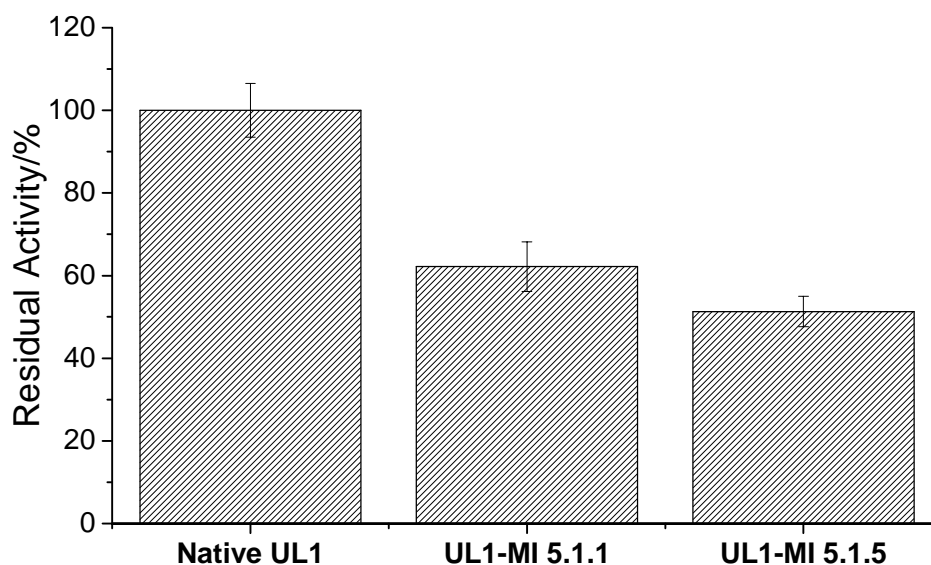
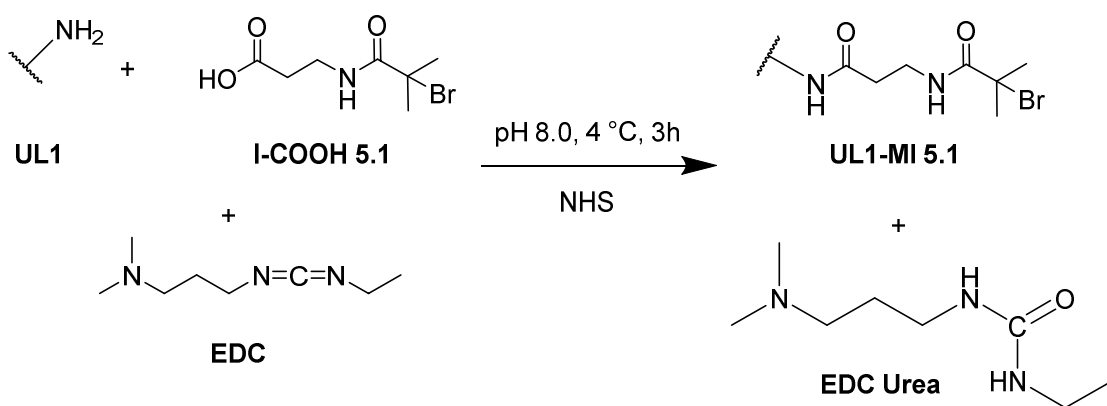


Figure 5.12 Residual activity of **UL1-MI 5.1** species after purification by dialysis for 48 hours against deionised water. Each data point is based on the average of four repeats of the *p*NA assay with standard deviation displayed as error bars.

The activity of **UL1-MI 5.1.1** and **5.1.5** was observed to decrease to 62% and 51% of the initial value respectively after exposure to the reaction conditions followed by dialysis against deionised water. It is evident from these observations that inhibition occurs upon exposure of UL1 to the conjugation conditions, which is not unexpected based on previous results of α -CT and NHS in Section 2.3.5.

Following the decrease in activity observed for **UL1-MI 5.1** species, it was deemed important to investigate whether the observed decrease was due to the presence of an inhibitor or alterations to the proteins tertiary structure. To this end, all components of the conjugation reaction were examined for inhibitory response with UL1. In addition to EDC.HCl and NHS that are actively introduced to the system, 1-(dimethylamino)-3-(3-ethylureido)propane (EDC urea) is formed over the course of the reaction as a side product that may also impact the protein's activity (Scheme 5.3).



Scheme 5.3 Reaction of primary amines on UL1 with **I-COOH 5.1** to form **UL1-MI 5.1** with the production of EDC urea from EDC.

To establish which reaction components can act as an inhibitor to UL1, the activity of UL1 was investigated at varying concentrations of additives. To this end, the *p*NA assay was conducted on native UL1 in the presence of increasing concentrations of NHS, EDC.HCl and EDC urea (Figure 5.13).

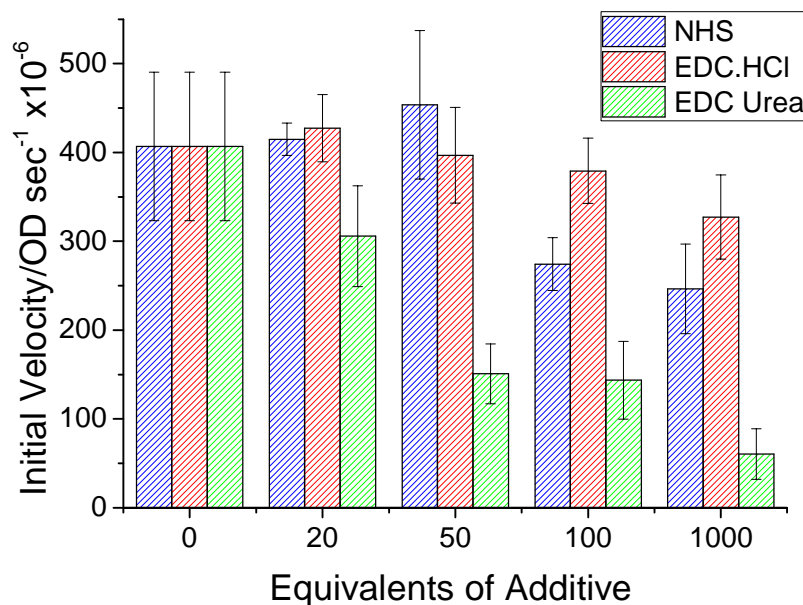


Figure 5.13 Initial velocity of native UL1 upon exposure to varying concentrations of NHS, EDC.HCl, and EDC urea. Equivalents of the additive were calculated as equivalents per amine. Each data point is based on the average of four repeats of the *pNA* assay with standard deviation displayed as error bars.

Figure 5.13 reveals that the addition of NHS has a similar effect upon UL1's activity compared to α -CT. Although up to 50 equivalents of NHS had no significant impact on the activity of UL1, the addition of 100 and 1000 equivalents caused a reduction in activity of 33% and 40% respectively. In comparison, the addition of EDC.HCl was observed to not have a significant effect upon the activity of UL1 when exposed to concentrations up to 100 equivalents of EDC.HCl. When the concentration was increased further to 1000 equivalents of EDC.HCl, the activity of UL1 was observed to decrease from 407 to 327 $\text{OD sec}^{-1} \times 10^{-6}$, which is a 20% reduction in activity.

Despite the small reduction observed with the incorporation of EDC.HCl, EDC urea was observed to cause a significant reduction in activity of 63% upon the addition of only 50 equivalents of EDC urea. However, this is not unexpected as the presence of urea has been found to cause protein denaturation.^{35, 36} Indeed, Zou *et al.* discovered that urea binds to amide units within peptides and subsequently displaces water in the protein's solvation shell.³⁶ This leads to the disruption of

hydrophobic interactions within the protein and eventual denaturation. It is hypothesised that as EDC urea contains a urea functionality, it can undergo similar interactions with proteins, which lead to unfolding of the protein.

To establish whether the observed reductions in UL1 activity were reversible, various purification methods were investigated. To this end, **UL1-MI 5.1** was subjected to dialysis, precipitation in methanol, spin filtering, desalting columns and ultrafiltration. All samples were subsequently lyophilised and activity analysed using the *pNA* assay. The residual activity was calculated as a percentage of activity in comparison to native UL1 (Figure 5.14).

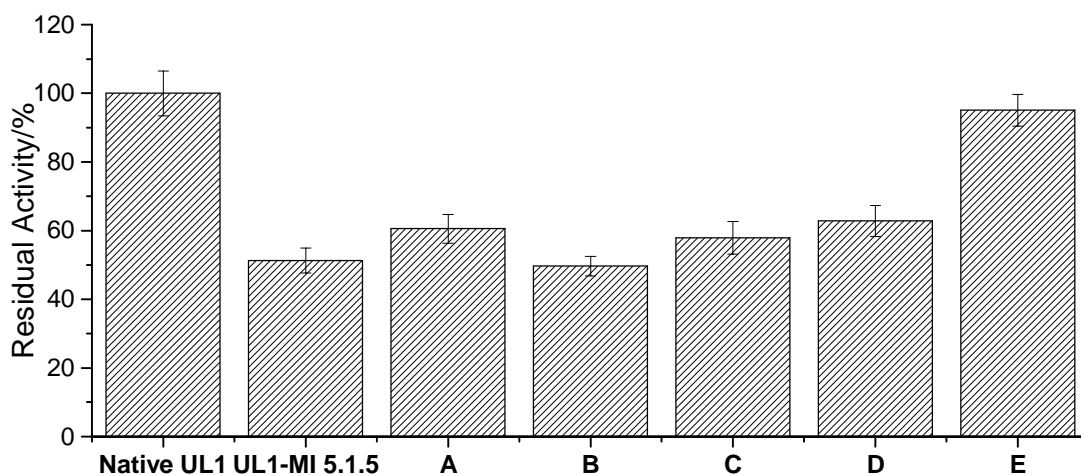


Figure 5.14 Residual activity of **UL1-MI 5.1.5** upon exposure to varying purification conditions relative to native UL1. A - purified by 96 hours of dialysis against deionised water, B – purified by precipitation into methanol, C – purified by spin filtering with a MWCO of 10 kDa, D – purified with a desalting column, E – purified by ultrafiltration with a MWCO of 5 kDa. Each data point is based on the average of four repeats of the *pNA* assay with standard deviation displayed as error bars.

Although most of the attempted methods were unsuccessful in the restoration of UL1 activity, similarly to the purification of **CT-MI 2.1** in Section 2.3.5, the most effective method to regain activity was ultrafiltration. This purification technique was able to restore the activity from 51% to 95% in comparison to native UL1. This suggests that the reduction in activity was caused by a reversible process, hypothesised to be linked to the removal of residual EDC urea and NHS from **UL1-MI 5.1.5**.

To allow comparison of the activity profiles between native UL1 and the purified **UL-MI 5.1** species with 1 and 5 conjugated initiators, **UL-MI 5.1.1** and **UL-MI 5.1.5** respectively, the Michaelis-Menten model of kinetics was employed. As discussed in Chapter 2, a Michaelis-Menten model of kinetics is one of the most commonly used models to assess the activity of enzymes.^{37, 38} A series of *p*NA assays was conducted with varying substrate concentrations and Michaelis-Menten parameters were extracted from the subsequent hydrolysis data by employing Lineweaver-Burk plots (Table 5.3).

Table 5.3 Michaelis-Menten Parameters of UL1 and **UL1-MI 5.1** species based on the *p*NA assay.

Sample	$K_m/\mu\text{M}$	$k_{\text{cat}}/\text{sec}^{-1}$	$k_{\text{cat}}/K_m/\text{sec}^{-1} \mu\text{M}^{-1}$
Native UL1	261 ± 40	1.9 ± 0.6	0.0078 ± 0.0008
UL1 5.1.1	335 ± 108	1.4 ± 0.5	0.0040 ± 0.0011
UL1 5.1.5	986 ± 177	1.5 ± 0.3	0.0015 ± 0.0004

The Michaelis constant, K_m , is an inverse measure of the affinity between enzyme and substrate. The K_m of the UL1 species was observed to increase relative to the number of initiators attached to the enzyme's surface. **UL-MI 5.1.5** has a K_m that is a 3-fold increase in comparison to native UL1. This suggests that a competitive inhibition process occurs and prevents the formation of an enzyme-substrate complex. Furthermore, this observation is hypothesised to result from changes to the surface charge distribution of the enzyme owing to the reduction in potentially ionisable groups on UL1 as observed for α -CT macro-initiators in Section 2.3.6.1.

In addition to the increase in K_m , a decrease in k_{cat} was also observed for both macro-initiator species. It is postulated that the decrease in k_{cat} may be an indication of a small percentage of denaturation as a result of exposure to the urea species generated during synthesis. As a consequence of the variations in K_m and k_{cat} , the overall efficiency, k_{cat}/K_m , was found to decrease by a factor of 5 compared with the native UL1 enzyme.

5.3.2.4 *Stability of Macro-Initiators from Laundry Specific Protease Enzymes*

Despite the decrease in activity observed in Section 5.3.2.3 for **UL1-MI 5.1s**, it was proposed that, if a significant increase was observed in the stability of **UL1-MI 5.1** species, the enzymes would still have a beneficial effect within an application that requires prolonged storage periods such as laundry detergents. As such, the stability of UL1 and **UL1-MI** with 1 and 5 initiator units covalently bonded to the surface of UL1 (**UL1-MI 5.1.1** and **5.1.5** respectively) was assessed under accelerated conditions in Ecoboost™ formulation at 40 °C. To this end, the catalytic activity of UL1, **UL1-MI 5.1.1**, and **UL1-MI 5.1.5** was monitored over time using the *p*NA assay (Figure 5.15). The residual activity was calculated as a ratio of initial rates of hydrolysis for a given incubation time over the initial activity. Half-life values were subsequently extracted by assuming an exponential decay.

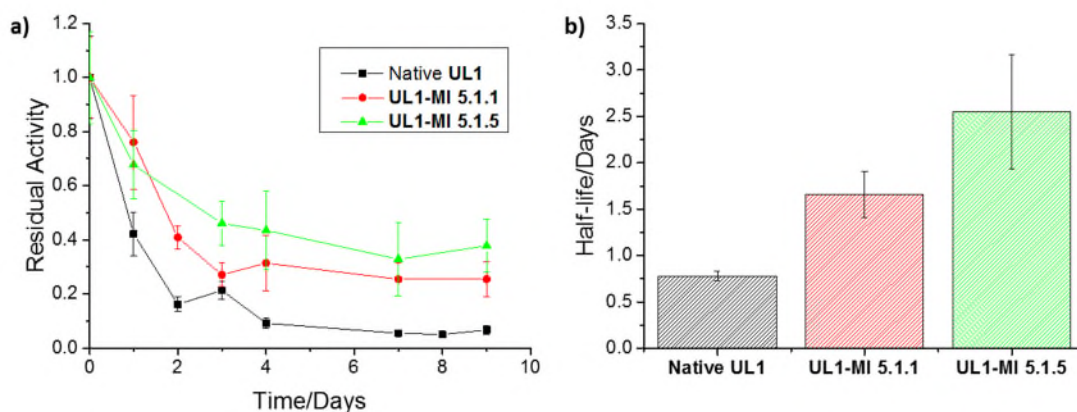


Figure 5.15 a) Thermal stability profiles of UL1 and **UL1-MI 5.1** species in Ecoboost™ formulation at 40 °C. Each data point is based on the average of four repeats of *p*NA assay with standard deviation displayed as error bars. b) Activity half-life at 40 °C for UL1 and **UL1-MI 5.1** species extracted from the linear regression of $\ln(\text{residual activity})$ against time.

Figure 5.15 reveals the stability enhancement of UL1 upon the addition of initiator species. The addition of 1 initiator unit shows an increase in stability by a factor of 2. The further addition of initiator units, to 5 initiators conjugated to the surface of UL1, led to a 3-fold increase of half-life increase from 0.75 to 2.5 days. This trend is the same as was observed for macro-initiators synthesised from α -CT-MI in Section 2.3.6. The resulting UL1-MI species have a reduced number

of potential ionisable groups and therefore it is hypothesised that the increase in stability also occurs as a consequence of altering the surface charge of UL1.

In an attempt to further analyse the thermal stability of **UL1-MIs**, the melting temperature, T_m , was investigated. Despite attempting to conduct thermal shift assays in Ecoboost™ formulation, due to the presence of surfactant, SYPRO orange was observed to fluoresce at all temperatures due to the formation of the detergent micelles within the formulation.^{39, 40} The high level of initial fluorescence dominated the spectra and masked the protein melt transition and so T_m could not be extracted. To alleviate the issue of surfactant, thermal shift assays were performed in aqueous solution using SYPRO orange, with methodology previously described in Section 2.3.6.1. T_m measurements were conducted for all UL1 and **UL1-MI 5.1** species (Figure 5.16).

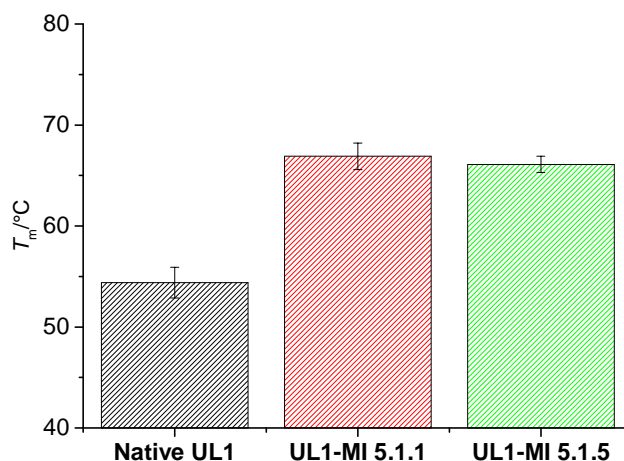


Figure 5.16 Graph displaying T_m of UL1 and **UL1-MI 5.1** species. T_m values were extracted from thermal shift assays at 5 mg/mL in water with SYPRO orange, excitation $\lambda = 492$ nm, emission $\lambda = 610$ nm. Values are obtained from triplicate repeats and error is displayed as standard deviation.

The T_m was shown to increase with the addition of initiator units whereby an increase of 13 °C and 12 °C was seen with the addition of 1 and 5 initiator units, respectively. Previously in Section 2.3.6.1, the T_m of α -CT macro-initiators was shown to increase with respect to the number of initiators bound to the surface. However, **UL1-MI 5.1** species exhibit similar T_m values independent of the number of initiators attached. This suggests that the location of the single-site modification has a significant role in the degree of stability achieved. It is also hypothesised that

the decrease of surface charge in microenvironments can form stronger intra-protein interactions and therefore increase T_m .

From the observed changes in both catalytic stability and T_m , it is concluded that altering the surface chemistry of UL1 exhibits similar behaviours to that observed by **CT-MI** species described previously in Chapter 2. However, it is noted that the stability of the **UL1-MI** appears to have a dependency upon the location of the modifications.

5.3.2.5 Synthesis and characterisation of Protein-Polymer Conjugates from Laundry-Specific Protease Enzymes

With an aim towards identifying whether different protease enzymes have comparable stability enhancements upon PPC synthesis, similar conjugates to those synthesised from α -CT and poly(glycerolmethacrylate) (PGMA) in Chapter 3 were targeted. To evaluate the effect of polymer conjugation upon the stability and activity of UL1, three different protein-polymer conjugates (PPCs) were designed and synthesised by employing the copper catalysed atom-transfer radical polymerisation (ATRP) methodology used in Section 3.3.1. **UL1-PGMA** PPCs were targeted to allow comparison between molecular weight and grafting density of the polymeric species. As the targeted **UL1-PGMA** PPCs are similar in morphology and molecular weights to that of the α -CT PPCs (Chapter 3), this will allow comparisons to be drawn between the α -CT and UL1 species. Analysis of the resulting **UL1-PGMA** PPCs was conducted by UV-Vis spectroscopy and summarised in Table 5.4. Sodium dodecyl sulfate poly(acrylamide) gel electrophoresis (SDS-PAGE) analysis was not utilised to analyse these conjugates as a result of difficulties encountered when visualising the protein using various staining techniques.

Table 5.4. Summary **UL1-PGMA** PPC characterisation from UV-Vis spectroscopy and SDS-PAGE analysis.

PPC	Target Polymer M_w /kDa	Average number of polymers attached	Target PPC M_w /kDa	PPC M_w /kDa (UV-Vis)
UL1-PGMA 5.1.10	10	1	37.5	32.7
UL1-PGMA 5.1.50	50	1	87.5	63.2
UL1-PGMA 5.5.10	10	5	87.5	99.5

In all cases the percentage protein extracted from UV-Vis spectroscopy at $\lambda = 280$ nm confirms the successful synthesis of **UL1-PGMA** conjugates. Although both conjugates with one conjugated polymer, **UL1-PGMA 5.1.10** and **5.1.50**, were observed to be slightly smaller by UV-Vis spectroscopy than initially targeted, this was not viewed to be problematic as a range of conjugate molecular weights was still achieved. Therefore all conjugates were utilised in the assessment of variations in activity and stability between UL1 and α -CT.

Following the successful synthesis of **UL1-PGMA** PPCs, the conjugates species were analysed to explore differences in their initial activity. To this end, *p*NA assays were conducted with varying substrate concentrations and Michealis-Menten parameters extracted from the subsequent hydrolysis data by employing Lineweaver-Burk plots (Table 5.5).

Table 5.5 Michaelis-Menten Parameters of UL1 and **UL1-PGMA** PPCs based on the *p*NA assay.

Sample	$K_m/\mu\text{M}$	$k_{\text{cat}}/\text{sec}^{-1}$	$k_{\text{cat}}/K_m/\text{sec}^{-1} \mu\text{M}^{-1}$
Native UL1	261 ± 40	1.9 ± 0.6	0.0078 ± 0.0008
UL1-PGMA 5.1.10	989 ± 176	1.3 ± 0.2	0.0013 ± 0.0003
UL1-PGMA 5.1.50	1782 ± 315	0.7 ± 0.2	0.0004 ± 0.0001
UL1-PGMA 5.5.10	2265 ± 408	0.6 ± 0.1	0.0002 ± 0.0001

All **UL1-PGMA** species show an increase in K_m in comparison to native UL1. This suggests the polymer is preventing the formation of the enzyme-substrate complex by hindering access to the active site. For PPCs with a singly grafted polymeric species, the increase in K_m was dependent upon the molecular weight of the polymer. For example, the increase in polymeric molecular weight from **UL1-PGMA 5.1.10** to **5.1.50** is 30 kDa, which leads to a 2-fold increase in K_m . A decrease in k_{cat} was also observed for all species, which also led to a decrease in overall catalytic efficiency with increasing molecular weight of the PPC.

It is worth noting the presence of calcium binding sites within the precursor to UL1, savinase. It is hypothesised that the calcium binding sites may interact with the copper ions employed in ATRP as both copper and calcium are divalent. This could potentially lead to inhibition by altering the tertiary structure of UL1, leading to a decrease in hydrolytic activity for the conjugate species.

Following the observed reduction in activity, it was important to establish whether the stability of the **UL1-PGMA** PPCs correlated to the observed decrease in catalytic efficiency. To assess alterations in the stability of the conjugates in comparison to the native UL1, the catalytic activity of UL1 and **UL1-PGMA** PPCs in Ecoboost™ formulation at 40 °C was monitored over time using the *p*NA assay (Figure 5.17). The residual activity was calculated as a ratio of initial rates of hydrolysis for a given incubation time over the initial activity. The half-life data was subsequently extracted by assuming an exponential decay.

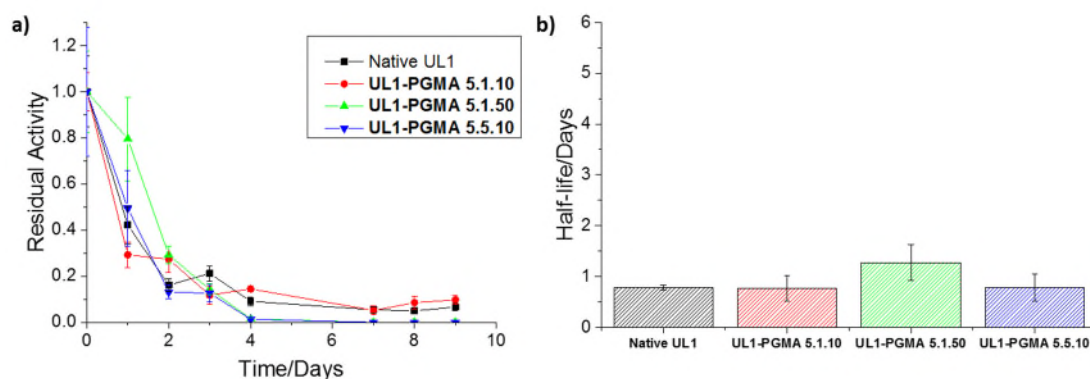


Figure 5.17 a) Thermal stability profiles of UL1 and **UL1-PGMA** PPC species in Ecoboost™ formulation at 40 °C. Each data point is based on the average of four repeats of pNA assay with standard deviation displayed as error bars. b) Activity half-life at 40 °C for UL1 and **UL1-PGMA** PPC species extracted from the linear regression of $\ln(\text{residual activity})$ against time.

A similar stability was observed for native UL1 and UL1 PPCs, **UL1-PGMA 5.1.10** and **5.5.10**. However, a small increase in half-life was observed for **UL1-PGMA 5.1.50** with an increase of a factor of 1.6. Despite the observed increase in stability, this increase is not very substantial when compared to the half-life of the corresponding α -CT analogue, **CT-PGMA 3.1.50**, which enhanced the stability of α -CT by a factor of 3.

To investigate whether the addition of grafted polymeric species had an impact upon the intra-protein interactions within the protein-polymer conjugates, variations in the melting temperatures, T_m , were explored. To extract T_m values, thermal shift assays were performed with SYPRO orange in aqueous solution with methodology previously described in Section 2.3.6.1, for all **UL1-PGMA** species (Figure 5.18).

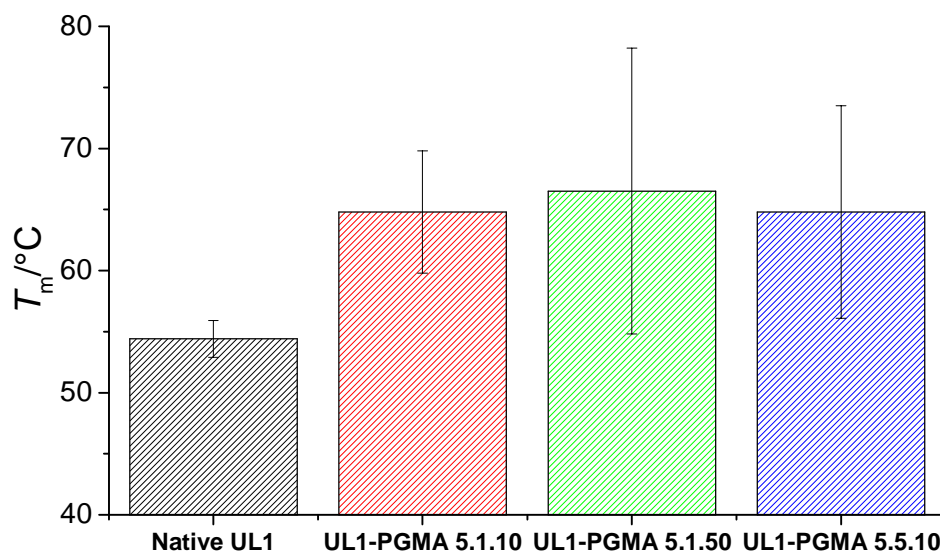


Figure 5.18 Graph displaying T_m of UL1 and **UL1-PGMA** PPC species. T_m values were extracted from thermal shift assays at 5 mg/mL in water with SYPRO orange, excitation $\lambda = 492$ nm, emission $\lambda = 610$ nm. Values are obtained from triplicate repeats and error is displayed as standard deviation.

An increase in T_m was observed for all conjugate species compared with native UL1. Despite this increase, no difference in T_m was observed between corresponding macro-initiator and PPC species. This suggests that the addition of grafted polymeric species does not affect the enhancement of T_m provided by macro-initiator formation but also does not provide any additional improvement.

Although an increase in T_m was observed for all **UL1-PGMA** species, as a result of the lack of increase in stability within Ecoboost™ formulation and a significant reduction in initial activity, **UL1-PGMA** PPCs were deemed not to be a viable option for use in an industrial laundry application.

5.3.3 Laundry-Specific Lipase Enzymes

5.3.3.1 Structure of Laundry Specific Lipase Enzymes

As a consequence of the observed reduction in activity without an improvement of the stability of UL1 in Section 5.3.2, other enzymes were investigated to establish if enhancements to stability

could be imparted onto other laundry-specific enzymes. As such, lipase enzymes were investigated as they are of high interest for incorporation into laundry formulations but have the major limitation of a low degree of stability.

As lipases can originate from numerous sources, lipase enzymes were selected from both bacterial and fungal origins to investigate if this factor influences the enzyme's ability to form successful PPC species. Lipases were selected based on stain removal capabilities within laundry detergent. As such, Lipase from *Pseudomonas fluorescens* (PFL) and Lipex were chosen as the key enzymes to be investigated.

Although Lipex is a key industrial enzyme, the primary and secondary structure of the enzyme is relatively unknown and therefore, Lipase from *Thermomyces Lanuginosa* (TLL), which is the precursor to the modified Lipex, will be analysed in tandem to Lipex to aid in analysis. Upon initial modification of TLL, an intermediate species, Lipolase, is formed with eight modified residues compared to the native TLL. Subsequently, the introduction of two L-arginine residues with the modifications T231R and N233R to Lipolase results in the formation of the Lipex species.

As some of the modifications from TLL to Lipex are unknown, it was important to establish variations between the two lipase species. Kyte-Doolittle plots are used to compare the hydrophobicity of proteins based upon the amino acid sequence.⁴¹ The hydrophobicity of the amino acids within a protein's sequence is dependent on surrounding residues. Therefore, the hydropathic value of each amino acid is averaged with the immediate neighbouring residues to produce a map of the hydrophobicity along the protein's sequence.⁴¹ Positive hydropathic scores indicate a hydrophobic segment within the protein, with the magnitude denoting the degree of hydrophobicity. Kyte-Doolittle plots for TLL and the modified lipases, Lipolase and Lipex, are shown in Figure 5.19.

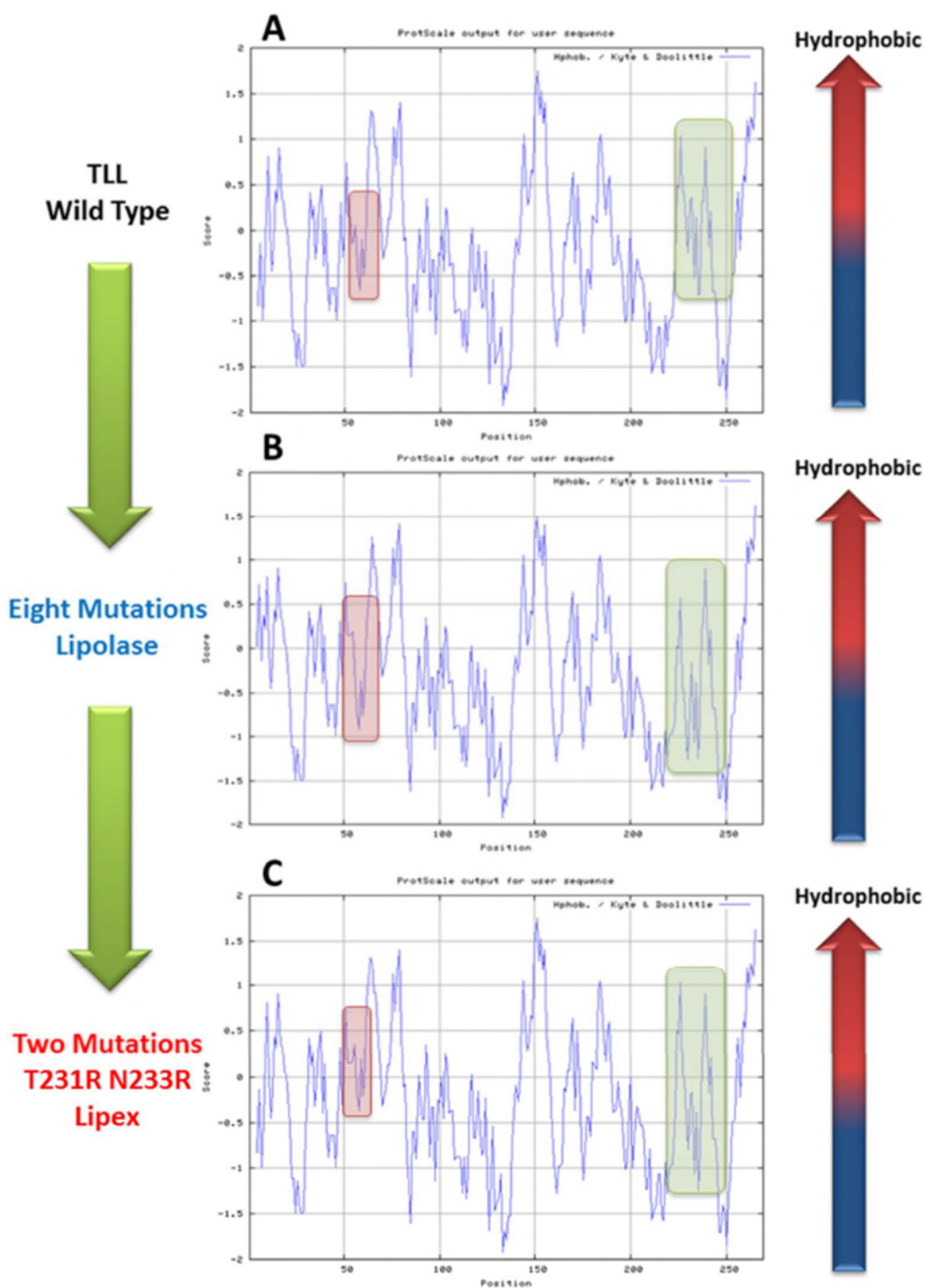


Figure 5.19 Kyte-Doolittle plot of (A) TLL, (B) Lipolase, and (C) Lipex. The highlighted boxes emphasise locations in which a change in the hydrophobicity is observed, with thanks to Dr Katherine Farrance and Dr Dietmar Lang.

Figure 5.19 reveals the locations of modification within the enzymes that cause a change to their hydrophobicity. There are two areas, which have been highlighted, that indicate an alteration to hydrophobicity from TLL to Lipex. The plots suggest an introduction of hydrophilic residues at position *ca.* 55 upon the formation of Lipolase. However, the transformation to Lipex reverts this segment back to a more hydrophobic region. The second highlighted region at approximately residue 230 indicates the addition of more hydrophilic residues for both Lipolase and Lipex. This observed change corresponds to the addition of two L-arginine residues within this region upon the transformations T231R and N233R from Lipolase to Lipex.

5.3.3.2 *Synthesis of Macro-Initiators from Laundry Specific Lipase Enzymes*

To assess the formation of macro-initiators from PFL, TLL and Lipex, the primary structures were examined to identify possible modification sites within the lipase species. It was found that PFL contains 15 L-lysine residues and 1 N-terminus compared with TLL, which contains only 7 L-lysine residues and 1 N-terminus. This results in 16 potential modification sites for PFL in comparison to only 8 for TLL. Although the full sequence for Lipex is unknown, it has been assumed that any modifications have not affected the number of primary amine groups present within Lipex compared to TLL.

The tertiary structures were subsequently analysed to locate the residues within the crystal structure of the lipases. Figure 5.20 highlights the locations of these residues within both PFL and TLL. Based on these structures it is therefore concluded that the potential sites for modification are spread evenly across the surface of both enzymes.

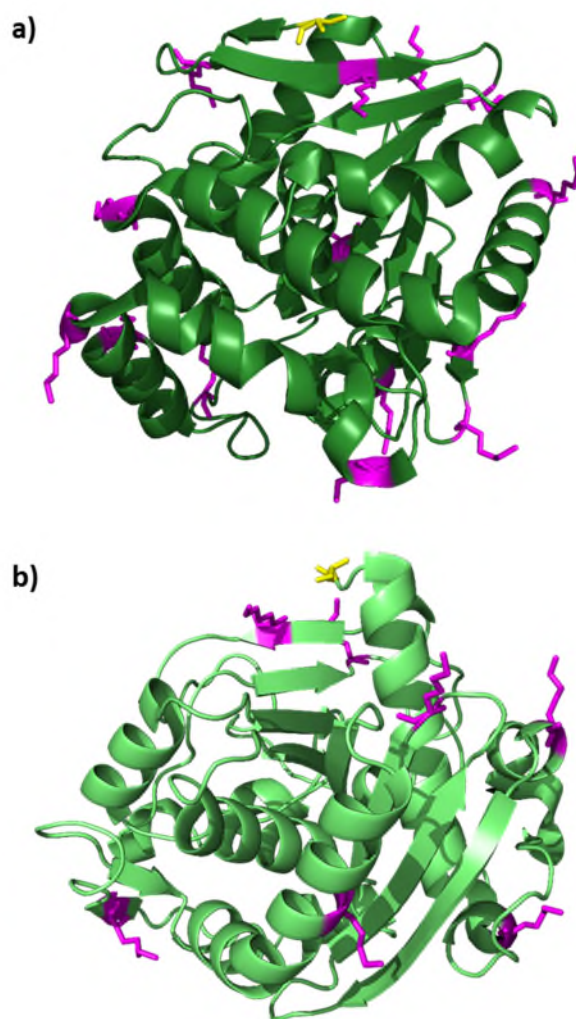


Figure 5.20 Crystal structure of a) PFL (**1VA4**),⁴² and b) TLL (**1DU4**).²¹ L-Lysine residues have been highlighted in pink and the *N*-termini highlighted in yellow. PDB crystal structure references are identified in bold.

PFL contains a similar distribution and number of potential modification sites to α -CT and so was selected as the initial enzyme to analyse. To ascertain whether the conjugation to PFL would proceed with an active ester initiator or require the addition of a conjugation reagent, such as EDC.HCl employed in Section 5.3.2.2, the conjugation of PFL was attempted with 3.3 equivalents of **I-NHS 2.1** at varying pH. The efficiency of the conjugation reaction was assessed after 3 hours using MALDI-ToF mass spectrometry (Figure 5.21 and Table 5.6).

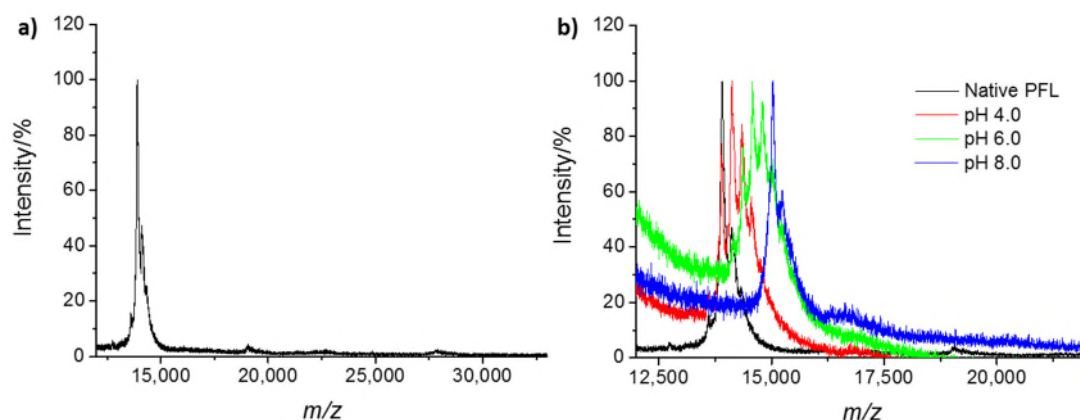


Figure 5.21 MALDI-ToF mass spectra of a) native PFL and b) PFL species formed using 3.3 equivalents of **I-NHS 2.1** per amine when the conjugation reaction was carried out at a range of pH values.

Table 5.6. Average degree of attachment of **I-NHS 2.1** initiator for **PFL-MI 5.1** species synthesised at varying pH values as determined by MALDI-ToF analysis. Errors are reported as the standard deviation of the distribution based on the assumption of a Gaussian fit of the MALDI-ToF mass spectra.

Equivalents of Initiator Added per Amine	pH		
	4.0	6.0	8.0
3.3 Eq.	1 ± 1	3 ± 1	5 ± 0

As discussed previously in Section 2.3.1, MALDI-ToF mass spectrometry has been employed to quantitatively assess the number of initiator sites bound to the protein.⁴³⁻⁴⁵ The mass spectra were fitted to a Gaussian distribution to facilitate the extraction of the average number of conjugate initiators species and the respective error. The mass spectrum of the previously analysed native enzymes of α -CT and UL1 displayed sharp peaks with minimal errors. In contrast, native PFL was observed as a broader peak and therefore the error within native PFL has been incorporated into the calculations for number of initiators conjugated.

Successful conjugation was observed at all pH values attempted. The same trend based upon pH dependency was observed for PFL as with α -CT, described in Section 2.3.2, with single-site modification occurring at pH 4.0 and conjugation of 5 sites at pH 8.0. An increase in dispersity

of the MALDI-ToF mass spectra was observed for samples modified at pH 4.0 and pH 6.0. The dispersity was observed to decrease for conjugations at pH 8.0, similar to the dispersity found for native PFL. This suggests that all potential sites have been modified and there is a single species present with 5 sites modified.

Despite the promising conjugation results observed for PFL, the native PFL species was observed to have a molar mass of 13.9 kDa. The expected molecular weight of PFL was 30.1 kDa, and therefore it was hypothesised that the observed peak is the doubly charged species. However, the peak distance between the species of PFL with n and $n+1$ conjugated initiators is 0.2 kDa, which is an accurate mass for the addition of a single initiator species. Although other analytical techniques including aqueous SEC, electrospray mass spectrometry, and SDS-PAGE analysis were employed, none were successful in correctly identifying the expected molecular weight of PFL. All techniques used to analyse the molecular weight of PFL were in agreement and identified a molecular weight of 13.9 kDa. Therefore, PFL was deemed unsuitable for further analysis and investigations were concentrated upon the fungal lipases, TLL and Lipex.

Investigations were focused upon the analysis of the native TLL as an analogue for Lipex. To establish the conjugation profile of TLL with an active ester initiator, TLL was reacted with 3.3 equivalents of **I-NHS 2.1** at varying pH values. The effectiveness of the conjugation reaction was quantified after 3 hours using MALDI-ToF mass spectrometry (Figure 5.22).

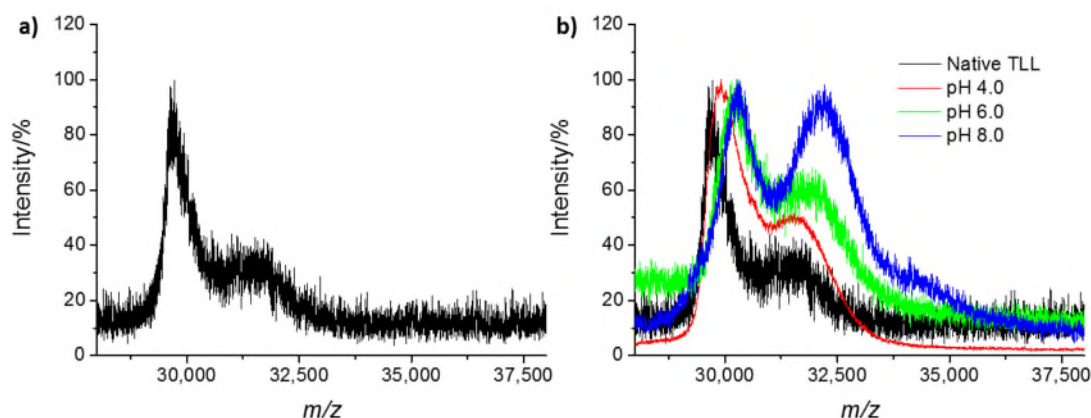


Figure 5.22 MALDI-ToF mass spectra of a) native TLL and b) TLL species formed using 3.3 equivalents of **I-NHS 2.1** per amine when the conjugation reaction was carried out at a range of pH values.

It was noted that the spectrum of the native TLL species contained a primary peak at the expected molar mass of 29.8 kDa, however a high molecular weight shoulder was also observed at 32 kDa. To investigate the possibility that the secondary peak occurs as a result of *N*-glycosylation of the protein, deglycosylation was performed. Deglycosylation was attempted using endoglycosidases, however, no differences were observed in the spectra prior and after deglycosylation. Therefore, it was assumed that the secondary peak was a result of the expression process of a fungal protein from a bacterial source. This could potentially lead to peptides utilised during synthesis remaining attached to the TLL species in the final product.

Upon conjugation, the molar mass of the primary peak was observed to increase dependent upon the pH at which the reaction was conducted. However, it was apparent that the intensity of the secondary peak with respect to the primary peak was dependent upon the pH of the reaction. As a result of the bimodal distribution and the variation in relative intensities, the number of initiators bound to the surface could not be extracted without implementing further assumptions. As such, TLL was determined to be unviable for continued analysis in the study.

In spite of the problems faced with the previous two lipase enzymes, Lipex, a modified version of TLL for use in high surfactant environments was examined. The conjugation profile of Lipex

with an active ester initiator was investigated at varying concentrations of **I-NHS 2.1** and at varying pH. The conjugation reaction was quantified after 3 hours using MALDI-ToF mass spectrometry (Figure 5.23 and Table 5.7).

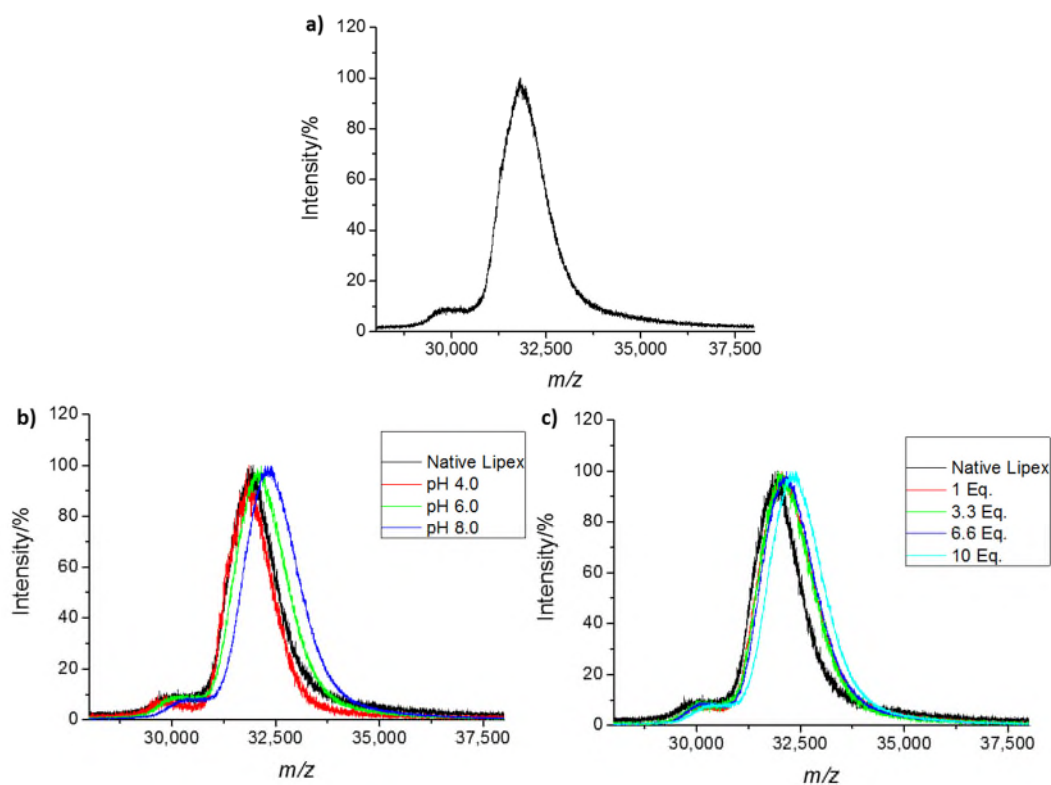


Figure 5.23 MALDI-ToF mass spectra of Lipex species formed a) native Lipex b) using 10 equivalents of **I-NHS 2.1** per amine at varying pH and c) at pH 8.0 using varying concentrations of **I-NHS 2.1**.

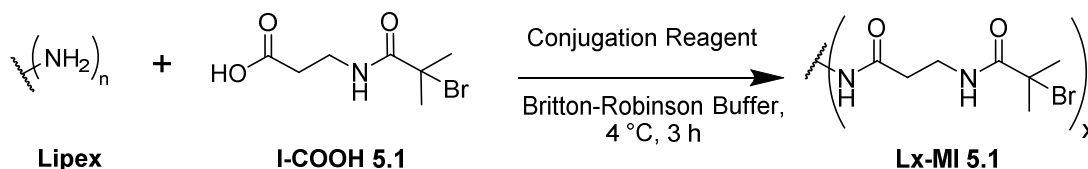
Table 5.7. Average degree of attachment of **I-NHS 2.1** initiator for **Lx-MI 2.1** species synthesised at pH 8.0 and varying concentrations of initiator as determined by MALDI-ToF analysis. Errors are reported as the standard deviation of the distribution based on the assumption of a Gaussian fit of the MALDI-ToF mass spectra.

	Equivalents of Initiator Added per Amine			
	1	3.3	6.6	10
pH 4.0				0 ± 0
pH 6.0				1 ± 0
pH 8.0	1 ± 0	1 ± 0	1 ± 0	2 ± 0

Native Lipex was observed to have a mono-modal peak at the expected molar mass of 31.9 kDa. However, the Gaussian fit of the mass distribution of the native Lipex was reasonably large with a peak width at half height of 1.4 kDa. Therefore, as with native PFL, the error within native Lipex has been incorporated into the calculations for number of initiators conjugated. Despite the dispersity within the native species, the dispersity is consistent throughout all macro-initiators.

The initiator conjugation to Lipex appears to be dependent upon both initiator concentration and pH as observed previously with the α -CT system in Section 2.3.2. The greatest degree of modification was observed at pH 8.0 with 10 equivalents of **I-NHS 2.1** per amine resulting in an increase of 0.4 kDa, which corresponds to 2 conjugated initiator units. Despite observing the successful attachment, the efficiency of the conjugation is relatively low with only 2 sites out of the possible 8 sites modified.

To investigate if higher initiator grafting densities could be achieved, EDC.HCl was employed to promote the conjugation reaction (Scheme 5.4). EDC.HCl was chosen as a suitable reagent as it was observed to be the most successful additive in the conjugation of initiator to UL1 (Section 5.3.2.2). To design an optimum system for the synthesis of Lipex macro-initiators, **Lx-MI**, the concentrations of the carboxylic acid initiator, **I-COOH 5.1**, and EDC.HCl were varied. MALDI-ToF mass spectrometry was employed to analyse the resulting **Lx-MI 5.1** species (Figure 5.24 and Table 5.8).



Scheme 5.4 Reaction of primary amines on Lipex with **I-COOH 5.1** to form **Lx-MI 5.1**.

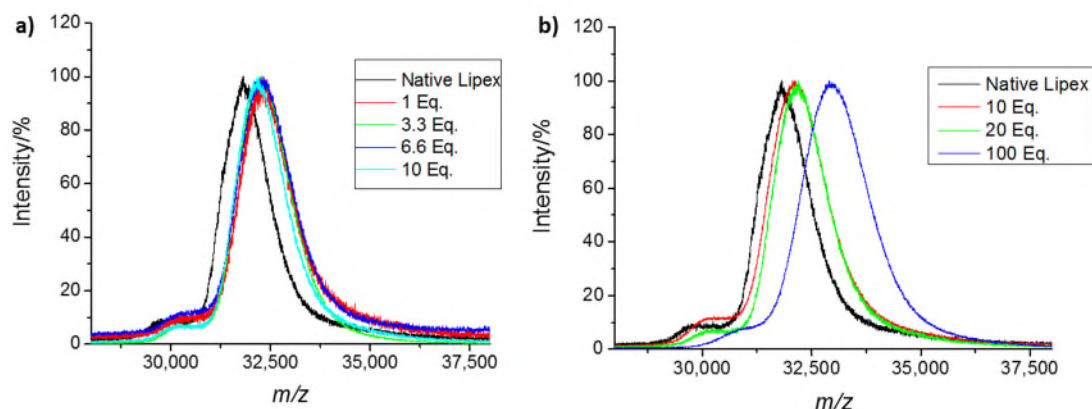


Figure 5.24 MALDI-ToF mass spectra of **Lx-MI 5.1** species formed at pH 8.0 using a) 20 equivalents of EDC.HCl and varying concentrations of **I-COOH 5.1** and b) 10 equivalents of **I-COOH 5.1** and varying concentrations of EDC.HCl.

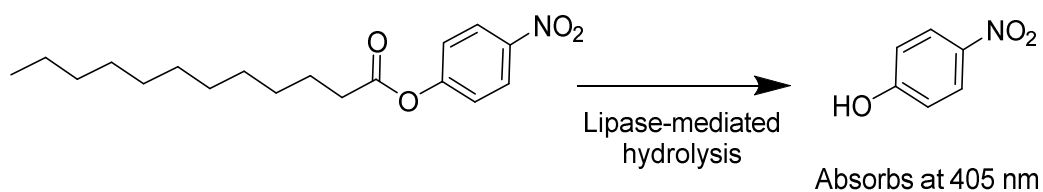
Table 5.8. Average degree of attachment of **I-COOH 5.1** initiator for **Lx-MI 5.1** species synthesised at pH 8.0 and varying concentrations of initiator and EDC.HCl as determined by MALDI-ToF analysis. Errors are reported as the standard deviation of the distribution based on the assumption of a Gaussian fit of the MALDI-ToF mass spectra.

Equivalents of EDC.HCl per Amine	Equivalents of Initiator Added per Amine			
	1	3.3	6.6	10
10				1 ± 0
20	2 ± 0	2 ± 0	2 ± 0	2 ± 0
100				5 ± 1

Upon changing the concentration of **I-COOH 5.1**, there was no change in the number of modification sites observed. The reaction was determined to be independent of the concentration of **I-COOH 5.1**. In contrast, altering the concentration of EDC.HCl resulted in the synthesis of macro-initiators with a range of initiator grafting densities from 1 to 5 site modifications. This was an enhancement in conjugation efficiencies compared with conjugation to **I-NHS 2.1**, from 25% to 63% for conjugation of initiators to 5 sites.

Following successful synthesis of **Lx-MI 5.1** species, it was important to investigate alterations to the enzyme's ability to catalyse reactions as any modifications to enzymes have the potential

to affect their catalytic activity.⁴⁶⁻⁴⁸ A common method to examine the activity of lipase enzymes is an assay in which the enzyme cleaves a hydrocarbon chain from *p*-nitrophenol (*p*NP) and the resulting hydrolysed *p*NP can be detected spectroscopically *via* an increase of absorption at $\lambda = 405$ nm (Scheme 5.5).⁴⁹ The length of the hydrocarbon chain can be varied to match the application, short chain substrates tend to be employed for investigating the activity of esterases instead of lipases due to the increased water solubility of esterases.^{50, 51} Longer chain substrates are employed for lipases as they have a preference to work at a water-oil interface.¹⁸ To this end, the substrate employed throughout the *p*NP assays in this study is 4-nitrophenyl dodecanoate.



Scheme 5.5 Hydrolysis of 4-nitrophenyl dodecanoate employed in the *p*NP assay for the detection of lipase activity.

Following the observed previous inhibition of both α -CT and UL1 caused by reagents employed in the conjugation reactions (Section 2.3.5 and 5.3.2.3), an inhibition test was performed to establish if the activity of Lipex is affected by the incorporation of additives and by-products present within the conjugation reaction. To this end, the activity of native Lipex was analysed by employing the *p*NP assay in the presence of varying concentrations of NHS, EDC.HCl, and EDC urea (Figure 5.25).

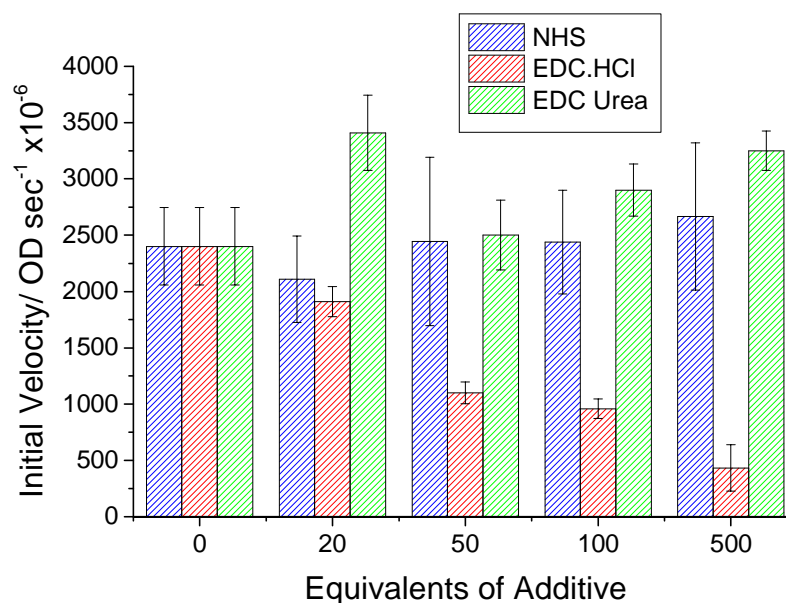


Figure 5.25 Initial velocity of native Lipex upon exposure to varying concentrations of NHS, EDC.HCl, and EDC urea. Equivalents of the additive (NHS, EDC.HCl or EDC Urea) were calculated as equivalents per amine. Each data point is based on the average of four repeats of *p*NP assay with standard deviation displayed as error bars.

Figure 5.25 reveals that the addition of NHS has no effect upon Lipex's activity and is able to maintain activity at all concentrations of NHS examined. In contrast to UL1, where EDC.HCl was observed to cause minimal changes to the activity, EDC.HCl is observed to decrease the activity of Lipex from 2400 to 1100 OD sec⁻¹ x 10⁻⁶ upon the addition of 50 equivalents of EDC.HCl, which is an 55% reduction. A further increase to 500 equivalents of EDC.HCl resulted in a decrease to 18% of the initial activity.

Despite the significant decrease in activity upon the addition of EDC.HCl, the addition of EDC urea was observed to have a positive impact on activity within Lipex. It is hypothesised that due to the alterations in hydrophobic interactions caused by the urea functionality,³⁶ the lid of the Lipex, which protects the active site, transitions to a permanently "open" position in the presence of EDC urea. Therefore, accessibility to the active site has been increased and results in an increase in observed activity.

As a result of the observed effects of additives on Lipex activity, it was deemed imperative to purify the resulting **Lx-MI 5.1** species before analysing for variation in activity resulting from initiator conjugation. Lipex macro-initiators with 1 and 5 initiators conjugated to the surface of the enzyme, **Lx-MI 5.1.1** and **Lx-MI 5.1.5** respectively, were subjected to purification by ultrafiltration prior to analysis. Subsequently, a series of *p*NP assays was conducted with varying substrate concentrations and Michaelis-Menten parameters were extracted from the subsequent hydrolysis data by employing Lineweaver-Burk plots (Table 5.9).

Table 5.9 Michaelis-Menten Parameters of Lipex and **Lx-MI 5.1** species based on the *p*NP assay.

Sample	$K_m/\mu\text{M}$	$k_{\text{cat}}/\text{sec}^{-1}$	$k_{\text{cat}}/K_m/\text{sec}^{-1} \mu\text{M}^{-1}$
Native Lipex	77 ± 6	1122 ± 81	14.5 ± 1.6
Lx-MI 5.1.1	83 ± 7	1017 ± 173	12.3 ± 2.2
Lx-MI 5.1.5	69 ± 13	1175 ± 190	17.0 ± 4.2

By comparing the three enzymes tested, parameters K_m and k_{cat} are within error of each other suggesting that the catalytic ability of Lipex was not compromised when attaching initiator molecules or as a result of the reaction conditions that the enzymes were exposed to. Although variations are observed within the efficiency parameter, k_{cat}/K_m , the magnitude of the errors is relatively large and so could be a contributing factor to the observed differences.

Following the successful synthesis of Lipex macro-initiators with unaltered activity profiles, the stability of these enzymatic species was also investigated. The catalytic activity of Lipex and **Lx-MI** with 1 and 5 initiator units covalently bonded to the surface of Lipex (**Lx-MI 5.1.1** and **5.1.5** respectively) was monitored over time in Ecoboost™ formulation at 40 °C using the *p*NP assay. The residual activity was calculated as a ratio of initial rates of hydrolysis for a given incubation time over the initial activity. To allow a quantitative comparison of these stability profiles, their half-lives were extracted from a linear plot of the natural logarithm of residual

activity against time (Figure 5.26); all stability profiles were assumed to follow an exponential decay.

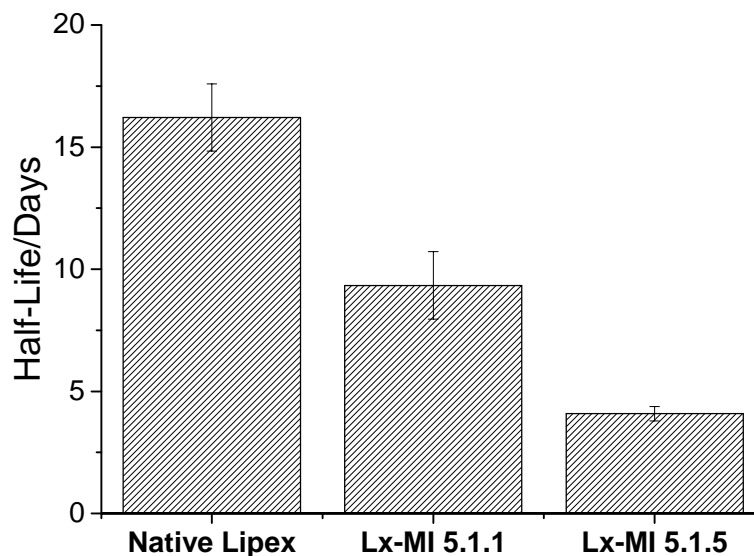


Figure 5.26 Activity half-life at 40 °C in Ecoboost™ formulation for Lipex and **Lx-MI 5.1** species extracted from the linear regression of $\ln(\text{residual activity})$ against time from aliquots analysed with the *p*NP assay. Each data point is based on the average of four repeats of *p*NP assay with standard deviation displayed as error bars.

In contrast to the previous results observed for both α -CT and UL1 (Section 2.3.6.1 and 5.3.2.4), a decrease in stability was observed for Lipex macro-initiator species in comparison to the native enzyme. Furthermore, the stability decrease was observed to have a dependency upon the number of initiators attached. For example, the conjugation of 1 initiator unit was observed to cause a 43% decrease in half-life in comparison to native Lipex, whereas the addition of 5 initiator units led to a half-life decrease of 74%. This suggests that the initiator species destabilise the Lipex enzyme and therefore reduce the catalytic half-life.

To establish the impact of the conjugation of initiator species to Lipex on the stability of the intra-protein interactions, T_m values of the **Lx-MI 5.1** species were explored. To extract the T_m values for the **Lx-MI 5.1** species, thermal shift assays were performed employing the dye SYPRO orange. T_m measurements were conducted for all **Lx-MI 5.1** species (Figure 5.27).

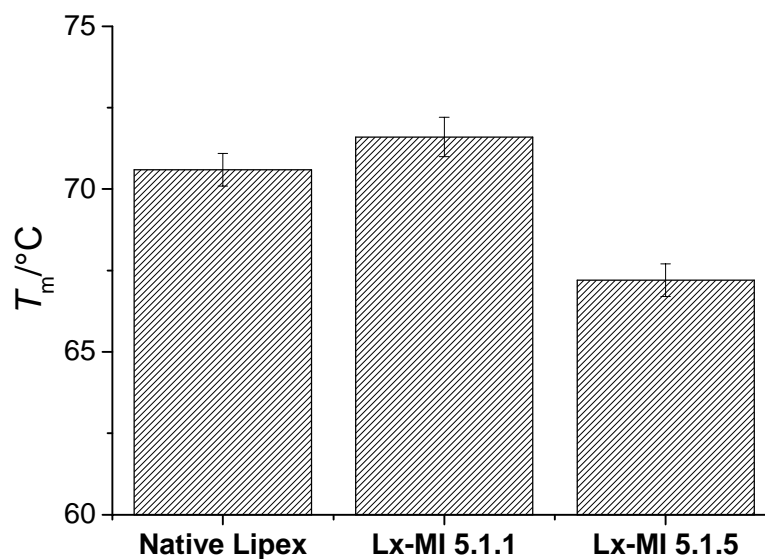


Figure 5.27 Graph displaying T_m of Lipex and **Lx-MI 5.1** species. T_m values were extracted from thermal shift assays at 5 mg/mL in water with SYPRO orange, excitation $\lambda = 492$ nm, emission $\lambda = 610$ nm. Values are obtained from triplicate repeats and error is displayed as standard deviation.

The T_m was shown to increase slightly with the addition of 1 initiator, but the addition of 5 initiators causes a decrease in T_m from the native Lipex from 71 °C to 67.5 °C. It is hypothesised that the addition of these initiator species could change the hydrophobic/hydrophilic interactions within the protein and result in a reduction in T_m .

Despite maintaining the initial catalytic activity, **Lx-MI 5.1** species were observed to have a decreased stability. It is hypothesised that the changes in stability are potentially caused by a change in intra-protein interactions. To confirm this theory, the tertiary structure of **Lx-MI 5.1** could be analysed by circular dichroism or small-angle X-ray scattering.

5.3.3.3 Synthesis and Characterisation of Protein-Polymer Conjugates from Laundry-Specific Lipase Enzymes

Aiming towards restoring and further enhancing the stability of Lipex in laundry detergent storage conditions, the synthesis of protein-polymer conjugates from Lipex was investigated. To evaluate the effect of conjugated polymeric species upon the stability and activity of Lipex, three different

PPC species were designed (Table 5.10). Analysis of the resulting **Lx-PGMA** PPCs was conducted by UV-Vis spectroscopy and densitometric analysis of SDS-PAGE gels (Table 5.10).

Table 5.10. Summary of **Lx-PGMA** PPC characterisation from UV-Vis spectroscopy and SDS-PAGE analysis.

PPC	Target Polymer M_w /kDa	Average number of polymers attached	Target PPC M_w /kDa	PPC M_w /kDa (UV-Vis)	PPC M_w /kDa (SDS-PAGE)
Lx-PGMA 5.1.10	10	1	37.5	37.5	52.1
Lx-PGMA 5.1.50	50	1	87.5	-	112.7
Lx-PGMA 5.5.10	10	5	87.5	-	123.2

Both analytical techniques confirm the successful synthesis of the **Lx-PGMA 5.1.10** conjugate, however slightly larger polymers than targeted were observed by SDS-PAGE. **Lx-PGMA 5.1.50** and **Lx-PGMA 5.5.10** could not be analysed using UV-Vis spectroscopy as they were both found to be insoluble in aqueous systems. It is hypothesised that the conjugated hydrophilic polymers caused alteration to the enzyme tertiary structure and exposed a higher percentage of hydrophobic segments of the protein, resulting in aggregation and subsequently precipitation. In spite of their lack of solubility in aqueous environments, SDS-PAGE analysis was able to confirm the successful synthesis of the two PPCs.

Following the synthesis **Lx-PGMA** PPCs, the conjugate species were analysed to explore differences in their initial activity in relation to their observed solubility. To this end, *p*NA assays were conducted with varying substrate concentrations and Michealis-Menten parameters extracted from the subsequent hydrolysis data by employing Lineweaver-Burk plots for **Lx-PGMA** PPCs (Table 5.11).

Table 5.11 Michaelis-Menten Parameters of Lipex and **Lx-PGMA** PPCs based on the *p*NP assay.

Sample	$K_m/\mu\text{M}$	$k_{\text{cat}}/\text{sec}^{-1}$	$k_{\text{cat}}/K_m/\text{sec}^{-1} \mu\text{M}^{-1}$
Native Lipex	77 ± 6	1122 ± 81	14.5 ± 1.6
Lx-PGMA 5.1.10	168 ± 57	767 ± 157	4.6 ± 1.7
Lx-PGMA 5.1.50	162 ± 43	134 ± 35	0.8 ± 0.3
Lx-PGMA 5.5.10	271 ± 43	137 ± 21	0.5 ± 0.1

An increase in K_m was observed for all Lipex conjugates and furthermore appears to be related to the polymeric grafting density. For example, the two PPCs that contain a singly conjugated polymer, **Lx-PGMA 5.1.10** and **5.1.50**, have similar K_m values in comparison to the **Lx-PGMA 5.5** species, which has a K_m value approximately 2-fold larger. Significant differences are also observed in k_{cat} , with a decrease being observed for all PPC species compared to native Lipex. Noteworthy is the large decrease observed for the Lipex conjugates that are insoluble in aqueous systems, with a decrease of 88% observed for both **Lx-PGMA 5.1.50** and **5.5.10**.

It was hypothesised that the addition of an organic solvent, to aid in solubility, could restore the activity of **Lx-PGMA 5.1.50** and **5.5.10**. To test this theory, the activity of both species was explored in relation to the concentration of added dimethyl sulfoxide (DMSO) by employing the *p*NP assay (Figure 5.28).

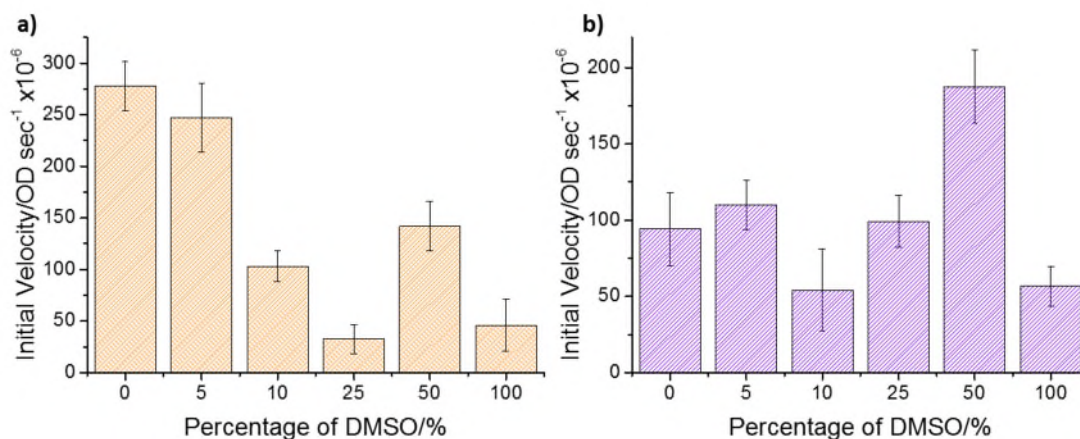


Figure 5.28 Initial velocity of a) **Lx-PGMA 5.1.50** and b) **Lx-PGMA 5.5.10** upon exposure to varying concentrations of DMSO. Each data point is based on the average of four repeats of *p*NP assay with standard deviation displayed as error bars.

Lx-PGMA 5.1.50 was observed to decrease in activity from 100% to 12% upon the increase of DMSO from 0% to 25%. It is hypothesised that this result is caused by DMSO interrupting the hydrogen bonding within Lipex leading to a reduction in activity. The further increase of DMSO from 25% to 50% led to an increase in activity from 12% to 51% in relation to the PPC's activity at 0% DMSO incorporation. It is postulated that between 25% and 50% DMSO is the threshold to solubilise **Lx-PGMA 5.1.50** and this increase in solubility leads to an increase in observed activity. Upon increasing the concentration of DMSO to 100%, the activity of the conjugate decreases again, which suggests that the increase in solubility is negated by the interactions between DMSO and the network of hydrogen bonding within Lipex.

The results observed for **Lx-PGMA 5.5.10** exhibit similar trends to that of **Lx-PGMA 5.1.50**. The introduction of 10% DMSO leads to a decrease in activity, however a further increase of up to 50% incorporation of DMSO was observed to have an increase in activity. At a concentration of 50% DMSO, **Lx-PGMA 5.5.10** activity was 2-fold larger than **Lx-PGMA 5.5.10** in 100% buffer. However, although an increase in activity was observed, in comparison to the native Lipex, the improved activity was still a reduction of approximately 80%.

Despite the increase in activity observed within **Lx-PGMA 5.1.50** and **5.5.10** upon solubilisation with DMSO, the reduction in activity was too significant for the PPCs to be viable options for use in industrial applications. As such, the only conjugate that was examined for changes in stability was **Lx-PGMA 5.1.10**. To this end, the catalytic activity of Lipex and **Lx-PGMA 5.1.10** in Ecoboost™ formulation at 40 °C was monitored over time using the *p*NP assay (Figure 5.29). The residual activity was calculated as a ratio of initial rates of hydrolysis for a given incubation time over the initial activity.

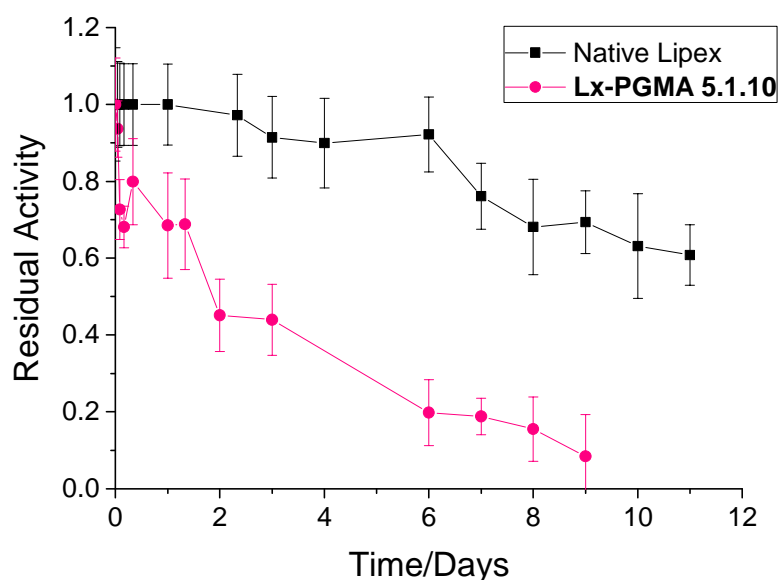


Figure 5.29 Thermal stability profiles of Lipex and **Lx-PGMA 5.1.10** species in Ecoboost™ formulation at 40 °C. Each data point is based on the average of four repeats of *p*NP assay with standard deviation displayed as error bars.

Figure 5.29 reveals that **Lx-PGMA 5.1.10** is less stable than native Lipex. **Lx-PGMA 5.1.10** was found to have a half-life of 1.8 days compared to that of Lipex of 14.3 days, which is an 87% reduction. It is evident that the conjugation of a polymeric species destabilises the Lipex enzyme, resulting in a reduction in catalytic half-life.

Following the unsuccessful enhancement of Lipex stability, the melting temperatures of the Lipex PPCs were explored to investigate the effects of polymer conjugation upon protein interactions. To this end, thermal shift assays were performed on Lipex and **Lx-PGMA** PPCs by employing

SYPRO orange dye and the previously described methodology (Section 2.3.6.1). T_m values were subsequently extracted from the thermal assay profiles (Figure 5.30).

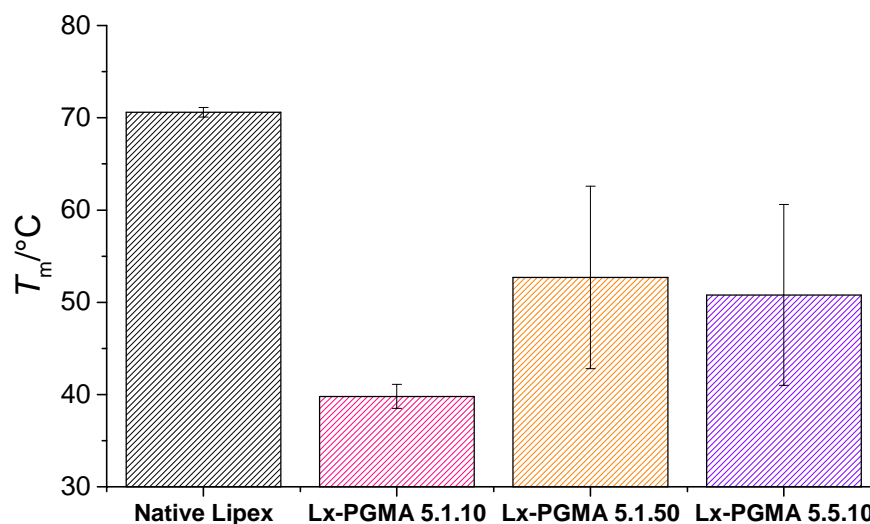


Figure 5.30 Graph displaying T_m of Lipex and **Lx-PGMA** PPC species. T_m values were extracted from thermal shift assays at 5 mg/mL in water with SYPRO orange, excitation $\lambda = 492$ nm, emission $\lambda = 610$ nm. Values are obtained from triplicate repeats and error is displayed as standard deviation.

In all cases, **Lx-PGMA** PPCs were observed to exhibit a decrease in T_m in comparison to native Lipex. For example, the T_m of **Lx-PGMA 5.1.10** was observed to decrease by 30 °C. This suggests that the addition of the polymeric species has weakened the intra-protein bonds causing T_m to dramatically decrease. Although **Lx-PGMA 5.1.50** and **5.5.10** were observed to have an increased T_m in comparison to that of **Lx-PGMA 5.1.10**, large associated errors were also observed. It is hypothesised that these errors result from the insolubility of the PPCs in aqueous solution and that the observed melt to corresponds to the solubilisation temperature. It is upon solubilisation that the hydrophobic regions of the protein were exposed and therefore the protein was then able to bind to the dye indicating a protein melt.

In contrast to α -CT, the addition of polymeric species to Lipex appears to reduce the stability and produce conjugates with lower catalytic half-lives and T_m values. It is concluded that the synthesis

of Lipex conjugates using poly(glycerol methacrylate) is not a viable route for the stabilisation of this enzyme.

5.3.4 Towards One-Pot Storage of Protease and Lipase Enzymes

Following the unsuccessful stabilisation of lipase enzymes through the formation of protein-polymer conjugates, the aim was to create a system in which lipase is able to maintain its stability in the presence of other enzymes. Aiming towards the generation of a laundry formulation that contains multiple enzymes that are stable to storage in the presence of each other, the stability of Lipex was analysed in the presence of UL1 and **UL1-PGMA** PPCs synthesised in Section 5.3.2.5. To this end, UL1 and **UL1-PGMA** PPC species were incubated with Lipex at 40 °C for 8 days with aliquots tested for Lipex activity with the *p*NP assay (Figure 5.31).

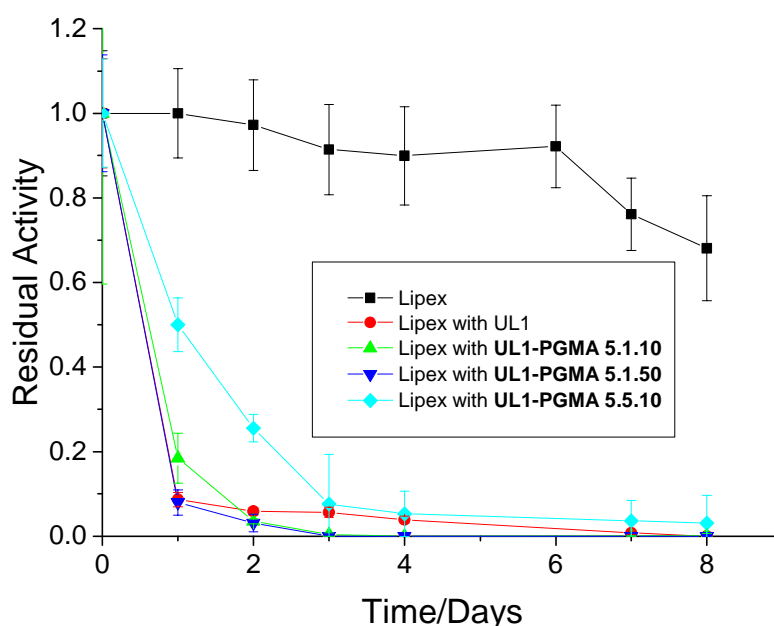


Figure 5.31 Stability profiles of Lipex incubated with UL1 and **UL1-PGMA** PPC species at various time intervals in Ecoboost™ formulation at 40 °C. Each data point is based on the average of four repeats of *p*NP assay with standard deviation displayed as error bars.

Although some serine protease enzymes such as α -CT can catalyse the *p*NP assay, UL1 alone was shown to have no catalytic effect on the assay used to assess Lipex activity. Lipex without the presence of protease was relatively stable in formulation at 40 °C and only reduced in activity to 80% after 7 days. However, Lipex incubated in the presence of native UL1 was observed to reduce in activity by 90% after only 24 hours. Exposing Lipex to PPC species containing one grafted

polymer, **UL1-PGMA 5.1.10** and **5.1.50**, provided no protection for Lipex with a 90% reduction also observed after 24 hours. In contrast, the addition of **UL1-PGMA 5.5.10**, which has 5 polymers grafted to the surface, shows a small increase in the half-life of Lipex by about 1.7-fold compared to incubation with native UL1.

Although an improvement is observed when employing **UL1-PGMA 5.5.10**, when compared to the Lipex without protease the reduction in activity is still significant and therefore would not be suitable for use within an application that requires long-term storage such as laundry detergents.

5.4 Conclusions

To conclude, although α -CT exhibited improved stability upon conjugate synthesis, lack of stabilisation in high surfactant systems such as Ecoboost™ formulation lead to a low activity. It was also observed that α -CT and subsequent conjugates were not optimised for laundry applications and no additional stain removal was found compared with negative controls.

By employing the same chemistries utilised in the formation of α -CT PPCs, protein-polymer conjugates were synthesised from several enzymes designed for using in laundry detergents. UL1, which is a protease enzyme based upon savinase, was found to require the addition of a conjugation reagent to allow the successful reaction to form macro-initiators. The resulting macro-initiators have reduced catalytic efficiencies but an increase in observed stability. Upon formation of **UL1-PGMA** PPCs, the stability reverted back to that of the native enzyme. As a consequence of the lack of stability enhancement it was hypothesised that the location of the polymeric graft was an important factor in controlling the stability of the enzymatic species.

The application of the chemistries to Lipex was also unsuccessful in achieving the desired increase in enzymatic stability. The formation of the initiator species was observed to maintain the enzyme's catalytic efficiency but resulted in a reduction of catalytic half-life. The formation of PPCs further reduced the activity and stability and also induced the precipitation of the PPCs. The decrease in solubility was postulated to be as a result of undesired interactions between

hydrophobic segments of the protein and the grafted hydrophilic polymer altering the tertiary structure of the protein and causing aggregation. The addition of organic solvent aided in solubility but was also detrimental to the enzymatic activity. As such it was concluded that the stabilisation of Lipex utilising grafted PGMA polymers was not a viable approach.

Whilst aiming towards a one-pot system with multiple enzymes, Lipex was incubated with protease PPCs. Protease conjugates with a single grafted polymer were ineffective at protecting the Lipex species from digestion by the protease species. In contrast, a slight increase in protective stability was observed from the incubation of protease with 5 grafted polymers in comparison to exposure of Lipex to the native protease. However, introduction of any protease species caused a detrimental effect on the stability of the Lipex enzyme. It is concluded that the synthesis of protein-polymer conjugates from UL1 and PGMA was not an effective method for protecting secondary enzyme species in solution. As a consequence of the lack of increase in stability within laundry detergent, the PPCs synthesised throughout this Chapter were deemed unsuitable for use in laundry applications.

5.5 Experimental

5.5.1 Materials

All chemicals were obtained from Sigma-Aldrich and used without further purification unless stated otherwise. Ultrafiltration membranes with a 5 kDa MWCO were supplied by Amicon. SYPRO orange was supplied as a 5,000× concentrate in DMSO from Thermo Fisher. SDS-PAGE gradient gels were purchased from Biorad. Unilever Protease 1 (UL1), Lipase from *Pseudomonas fluorescens* (PFL), Lipase from *Thermomyces lanuginosus* (TLL), and Lipex were all supplied by Unilever from their supplier Novozyme. Ecoboost™ formulation was provided by Unilever. Desalting columns (PD MidiTrap G-10) were supplied from GE Healthcare Life Sciences.

5.5.2 Instrumentation

5.5.2.1 *¹H Nuclear Magnetic Resonance (NMR) and ¹³C NMR Spectroscopy*

¹H NMR spectra were recorded on a Bruker DPX-300 or DPX-400 spectrometer at 300 MHz and 400 MHz, respectively with MeOD, D₂O, or CDCl₃ as the solvent. The chemical shifts of protons were quoted relative to tetramethylsilane (TMS) at $\delta = 0$ ppm when using CDCl₃, or relative to residual solvent protons when using MeOD (¹H: $\delta = 3.31$ ppm) and D₂O (¹H: $\delta = 4.79$ ppm). ¹³C NMR spectra were recorded on a Bruker DPX-300 or DPX-400 spectrometer at 75 MHz and 100 MHz, respectively with MeOD, D₂O, or CDCl₃ as the solvent. The chemical shifts of carbons were quoted relative to solvent carbons when using MeOD (¹³C: $\delta = 49.3$ ppm) and CDCl₃ (¹³C: $\delta = 77.0$ ppm).

5.5.2.2 *Industrial Stain testing*

The following procedure is a general protocol for stain testing. To a plate preloaded with the stained fabric, 20 μ L of 10 mg/mL α -CT solution (PPCs quantities were calculated based on their molecular weight) and 75 μ L of 50 mM Tris-HCl buffer solution was added. The total volume was made up with 12 French Hard (FH) (2:1 Ca:Mg) water to 150 μ L. A control test was carried out omitting α -CT. The plates were shaken at 250 rpm for 30 minutes at 30 °C. The wells were

then rinsed three times with deionised water with a 30 second shake between each wash. The stained fabric was left to dry overnight in a dark environment and scanned using a flatbed scanner.

5.5.2.3 Matrix-Assisted Laser Desorption/Ionization Time-of-Flight (MALDI-ToF) Mass Spectrometry

MALDI-ToF mass spectrometry was conducted on a Bruker Autoflex MALDI ToF/ToF spectrometer. The acceleration voltage was 20 kV in a positive linear mode. Protein solution (1.0-2.0 mg/mL) was mixed with an equal volume of matrix (0.5 mL of water, 0.5 mL of acetonitrile, 2 μ L of trifluoroacetic acid, and 8 mg of 4-hydroxy-3,5-dimethoxycinnamic acid), and 2 μ L of the resulting mixture was spotted on the target plate. Samples were calibrated against native α -CT. Number of sites conjugated and associated errors were extracted from a Gaussian fit of the MALDI-ToF mass spectra.

5.5.2.4 Ultraviolet-Visible (UV-Vis) Spectroscopy

UV-Vis spectroscopy for the determination of protein concentrations was conducted on a Perkin Elmer Lambda 35 UV/Vis spectrometer with absorbances recorded at $\lambda = 280$ nm. Utilising the Beer-Lambert law and the molar extinction coefficient for savinase (used as an approximation for UL1) and TLL (used as an approximation for Lipex) of 26,930 and 37,275 L mol⁻¹ cm⁻¹ respectively, percentage protein and the theoretical molecular weights were extracted. UV-Vis spectroscopy for kinetic measurements was conducted on a FLUOstar OPTIMA multi-well microplate reader. 96-well polystyrene plates were used with an excitation filter of $\lambda = 405$ nm, unless otherwise stated. Data was analysed using MARS v3.01 software.

5.5.2.5 Sodium Dodecyl Sulfate Poly(acrylamide) Gel Electrophoresis (SDS-PAGE)

SDS-PAGE gel analysis was carried out using 4-12 % BioRad SDS-PAGE gels. Gels were run at a constant voltage, 150 V, for 60 minutes and subsequently stained with Coomassie Brilliant Blue. Samples were prepared by heating 1mg/mL protein solutions combined with loading buffer in a

1:1 ratio for 5 minutes at 80 °C. Densitometric analysis was performed on the resulting gels using ImageJ software and determining the grayscale profile of the lane length.

5.5.2.6 Thermal Shift Assay

Thermal shift assay measurements were conducted on an Agilent MX3005P rtPCR with an excitation filter of $\lambda = 492$ nm and an emission filter of $\lambda = 610$ nm used unless otherwise stated. 10 μ L of enzyme (50 mg/mL) was added to 90 μ L of SYPRO orange solution (12.5x conc.). Heating ramps were performed at a rate of 1 °C min⁻¹.

5.5.3 Software

All protein crystal structure images were produced using The PyMOL Graphics System, Version 1.3, Schrodinger LLC.

5.5.4 Enzyme Kinetic Studies

5.5.4.1 pNA Protease Assay

To assess initial hydrolysis rate, 20 μ L of enzyme (2 μ g/mL protein concentration) was added to 160 μ L of 50 mM Tris-HCl buffer (pH 8). 20 μ L of *N*-succinyl-Ala-Ala-Pro-Phe-*p*-nitroanilide in methanol at 1 mM was added to the enzyme solution. The initial rate of hydrolysis of the peptide substrate was monitored by recording the increase in absorption at $\lambda = 405$ nm at 25 °C. Background hydrolysis was subtracted to give initial rates of hydrolysis.

5.5.4.2 pNP Lipase Assay

To assess initial hydrolysis rate, 20 μ L of enzyme (100 ng/mL protein concentration) was added to 160 μ L of 50 mM Tris-HCl buffer (pH 8). 20 μ L of *p*-nitrophenol laurate in methanol at 1 mM was added to the enzyme solution. The initial rate of hydrolysis of the ester substrate was monitored by recording the increase in absorption at $\lambda = 405$ nm at 25 °C. Background hydrolysis was subtracted to give initial rates of hydrolysis.

5.5.4.3 Stability Assays

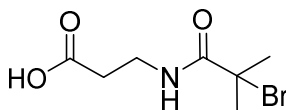
Enzyme species (2 µg/mL for proteases and 100ng/mL for lipases) were incubated in Ecoboost™ formulation. Samples were incubated at 40 °C with aliquots taken at frequent time intervals and stored at -20 °C until the study was concluded. These samples were subsequently defrosted and analysed with either the *p*NA or *p*NP assay. The residual activity was calculated as a ratio of initial rates of hydrolysis, calculated as described above, for a given incubation time over the initial activity. Activity half-lives were extracted from a linear plot of the natural logarithm of residual activity against time; all stability profiles were assumed to be based on an exponential decay.

5.5.4.4 Michaelis-Menten Kinetics and Parameters

Michaelis-Menten parameters were established by performing the *p*NA protease assay (see Section 5.5.4.1) or *p*NP (see Section 5.5.4.2) at varying substrate concentrations. A range of substrate solutions were prepared by diluting with methanol to 10, 5, 2, 1, 0.5, 0.2 mM solutions; the initial hydrolysis rate was recorded as before. MARS data analysis software was used to extract values of K_m , k_{cat} and k_{cat}/K_m from a plot of the reciprocal of substrate concentration against the reciprocal of initial hydrolysis rate.^{37, 52}

5.5.5 Synthesis of ATRP Initiators

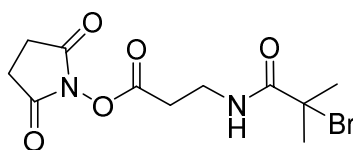
5.5.5.1 Synthesis of Carboxylic Acid Initiator 3-(2-Bromo-2-methylpropionylamino)propionic acid (I-COOH 5.1)



Synthesis previously reported by Murata *et al.*⁵³ A mixture of 2-bromo-2-methylpropionyl bromide (3.1 mL, 25 mmol) and dichloromethane (12 mL) was slowly added to a solution of β-alanine (2.23 g, 25 mmol) and sodium hydrogen carbonate (5.25 g, 62 mmol) in deionised water (50 mL) at 0 °C, and then the mixture was stirred at room temperature for 2 h. The aqueous phase

was washed with dichloromethane (25 mL \times 3) and adjusted to pH 2 with 1.0 M HCl. The product was extracted with ethyl acetate (20 mL \times 6) and the organic phase was dried with MgSO₄, filtered, and evaporated under vacuum. 3-(2-Bromo-2-methylpropionylamino)propionic acid was isolated by recrystallisation from a mixture of diethyl ether and *n*-hexane (1/9 volume ratio). The product was isolated in a 65% yield. ¹H NMR (300 MHz, CDCl₃): δ (ppm) 7.23 (broad s, 1H, CH₂NHC=O), 3.56 (td, 2H, ³J_{H-H} = 6.0 Hz, CH₂CH₂NHC=O), 2.65 (t, 2H, ³J_{H-H} = 6.0 Hz, HOOCCH₂CH₂NH), 1.95 (s, 6H, NHC=OC(CH₃)₂Br). ¹³C NMR (100 MHz, CDCl₃): δ (ppm) 177.6, 172.5, 62.3, 35.6, 32.4, 30.5. ESI-MS (*m/z*): [M+Na]⁺ calcd. for C₇H₁₂BrNO₃: 259.9892; found: 259.9894.

5.5.5.2 Synthesis of *N*-Hydroxysuccinimide Initiator 2,5-Dioxo-1-pyrrolidinyl 3-(2-bromo-2-methylpropionylamino) propionate (**I-NHS 2.1**)



Synthesis previously reported by Murata *et al.*⁵³ *N,N'*-Diisopropylcarbodiimide (0.86 mL, 6 mmol) was slowly added to a solution of **I-COOH 5.1** (1.2 g, 5 mmol), and *N*-hydroxysuccinimide (0.625 g, 6 mmol) in dichloromethane (50 mL) at 0 °C. The mixture was stirred at room temperature for 4 h. After filtering out the precipitated urea, the solution was evaporated to remove the solvent. The product was purified by recrystallisation from 2-propanol. Product isolation was achieved with an 83% yield. ¹H NMR (300 MHz, CDCl₃): δ (ppm) 7.18 (broad s, 1H, CH₂NHC=O), 3.68 (td, 2H, ³J_{H-H} = 5.8 Hz, CH₂CH₂NHC=O), 2.91-2.84 (m, 6H, O=CCH₂CH₂NH and ONC=OCH₂CH₂C=O), 1.95 (s, 6H, NHC=OC(CH₃)₂Br). ¹³C NMR (100 MHz, CDCl₃): δ (ppm) 179.3, 177.6, 172.5, 62.3, 35.9, 32.2, 31.3, 25.6. ESI-MS (*m/z*): [M+Na]⁺ calcd. for C₁₁H₁₅BrN₂O₅: 357.0092; found: 357.0055.

5.5.6 Typical Synthesis of Protein Macro-Initiators

The protocols listed are general procedures for the synthesis of protein macro-initiators and have been used to synthesise macro-initiators from UL1, PFL, TLL, and Lipex.

5.5.6.1 Utilising I-NHS 2.1

Lipex (1.0 g, 0.21 mmol of amine groups) was dissolved in Britton-Robinson buffer (100 mL) at 0 °C. After the addition of **I-NHS 2.1** (231 mg, 0.69 mmol), the solution was stirred at 3 °C for 3 h. The Lipex macro-initiator was purified by ultrafiltration using a Millipore stirred filtration cell and a 5 kDa MWCO membrane against deionised water, and isolated by lyophilisation and characterised by MALDI-ToF mass spectrometry.

5.5.6.2 Utilising I-COOH 5.1

Lipex (240 mg, 0.05 mmol of amine groups) was dissolved in Britton-Robinson buffer (30 mL) at 0 °C. *N*-(3-Dimethylaminopropyl)-*N*'-ethylcarbodiimide hydrochloride (EDC.HCl) (950 mg, 5.0 mmol), *N*-hydroxysuccinimide (NHS) (480 mg, 4.2 mmol), and **I-COOH 5.1** (118 mg, 0.3 mmol) were added to the Lipex solution. The resulting solution was stirred at 3 °C for 3 h. The Lipex macro-initiator was purified by ultrafiltration using a Millipore stirred filtration cell and a 5 kDa MWCO membrane against deionised water, and isolated by lyophilisation.

5.5.7 Synthesis of Glycerol Methacrylate (GMA)

Glycidyl methacrylate was passed over basic alumina before use. A solution of glycidyl methacrylate (3 mL) in deionised water (27 mL) was refluxed at 80 °C for 9 hrs. The monomer was synthesised with a 99% yield; the product was not isolated from the reaction solution but used for polymerisations with no further processing or purification. ¹H NMR: (300 MHz, MeOD): δ (ppm) 6.01 (s, 1H, CH₃C=CHH), 5.59 (s, 1H, CH₃C=CHH), 4.00-4.15 (m, 2H, O₂CCH₂), 3.87 (quin, ³J_{H-H} = 5.3 Hz, 1H, O₂CCH₂CHOH), 3.46-3.58 (m, 2H, CH₂OH) and 1.78 (s, 3H, CH₃C=CH₂). ¹³C NMR (75 MHz, MeOD): δ (ppm) 169.5, 135.7, 127.0, 75.7, 69.5, 62.3, 17.4. ESI-MS (*m/z*): [M+Na]⁺ calcd. for C₇H₁₂O₄: 183.0592; found: 183.0964.

5.5.8 Typical Polymerisation of GMA to Synthesise Protein-Polymer Conjugates (UL1-PGMA and Lx-PGMA)

This protocol is general procedures for the synthesis of protein-polymer conjugates and has been used to synthesise conjugates from UL1 and Lipex. A solution of GMA (10% v/v) (1200 μ L, 0.75 mmol), and **Lx-MI 5.1.5** (100 mg, 0.015 mmol of initiator groups) in deionised water (10 mL) was sealed and bubbled with nitrogen in an ice bath for 20 min. A deoxygenated catalyst solution of HMTETA (16 μ L, 0.06 mmol) and Cu(I)Br (9 mg, 0.06 mmol) in deionised water (5 mL) was then added to the conjugation reactor under nitrogen bubbling. The mixture was sealed and stirred for 18 h at 4 °C. **Lx-PGMA** conjugate was isolated by ultrafiltration using a Millipore stirred filtration cell and a 5 kDa MWCO membrane against deionised water and then lyophilised. The production of the PPC, **Lx-PGMA 5.5**, was confirmed by UV-Vis spectroscopy and SDS-PAGE analysis.

5.6 References

1. E. Smulders, W. Rähse, W. von Rybinski, J. Steber, E. Sung and F. Wiebel, in *Laundry Detergents*, Wiley-VCH Verlag GmbH & Co. KGaA, 2003, pp. 1-6.
2. W. A. Poucher, *Perfumes, Cosmetics and Soaps: With Special Reference to Synthetics*, D. Van Nostrand Company, Incorporated, 1941.
3. W. Crookes, *Chemical News and Journal of Industrial Science*, Chemical news office, 1773.
4. A. R. Baldwin, *Second World Conference on Detergents: Looking Towards the 90's : Proceedings*, American Oil Chemists' Society, 1987.
5. C. Edser, *Focus on Surfactants*, 2012, **2012**, 1-2.
6. C. Edser, *Focus on Surfactants*, 2007, **2007**, 1-2.
7. C. Hemachander and R. Puvanakrishnan, *Process Biochem.*, 2000, **35**, 809-814.
8. D. Kumar, T. N. Savitri, R. Verma and T. Bhalla, *Res. J. Microbiol.*, 2008, **3**, 661-672.
9. H. Lund, S. G. Kaasgaard, P. Skagerlind, L. Jorgensen, C. I. Jørgensen and M. van de Weert, *J. Surfactants Deterg.*, 2012, **15**, 265-276.
10. J. Skjold-Jørgensen, J. Vind, A. Svendsen and M. J. Bjerrum, *Biochemistry*, 2014, **53**, 4152-4160.
11. D. A. Cowan and R. Fernandez-Lafuente, *Enzyme Microb. Technol.*, 2011, **49**, 326-346.
12. D. Otzen, *Biochim. Biophys. Acta*, 2011, **1814**, 562-591.
13. A. D. Nielsen, L. Arleth and P. Westh, *Biochim. Biophys. Acta*, 2005, **1752**, 124-132.
14. C. Betzel, S. Klupsch, G. Papendorf, S. Hastrup, S. Branner and K. S. Wilson, *J. Mol. Biol.*, 1992, **223**, 427-445.
15. G. Lange, C. Betzel, S. Branner and K. S. Wilson, *Eur. J. Biochem.*, 1994, **224**, 507-518.
16. R. J. Siezen and J. A. M. Leunissen, *Protein Sci.*, 1997, **6**, 501-523.
17. R. D. Schmid and R. Verger, *Angew. Chem. Int. Ed.*, 1998, **37**, 1608-1633.
18. M. Schmidt and U. T. Bornscheuer, *Biomol. Eng.*, 2005, **22**, 51-56.
19. K.-E. Jaeger and T. Eggert, *Curr. Opin. Biotechnol.*, 2002, **13**, 390-397.
20. R. Fernandez-Lafuente, *J. Mol. Catal. B: Enzym.*, 2010, **62**, 197-212.

21. A. M. Brzozowski, H. Savage, C. S. Verma, J. P. Turkenburg, D. M. Lawson, A. Svendsen and S. Patkar, *Biochemistry*, 2000, **39**, 15071-15082.
22. G. H. Cohen, E. W. Silverton and D. R. Davies, *J. Mol. Biol.*, 1981, **148**, 449-479.
23. Y. Cajal, A. Svendsen, V. Girona, S. A. Patkar and M. A. Alsina, *Biochemistry*, 2000, **39**, 413-423.
24. J. Skjold-Jørgensen, J. Vind, A. Svendsen and M. J. Bjerrum, *Biochemistry*, 2016, **55**, 146-156.
25. J. Ahmed, U. S. Shivhare and P. Singh, *Food Chem.*, 2004, **84**, 605-611.
26. M. Maskan, *J. Food Eng.*, 2001, **48**, 169-175.
27. O. W. Neiditch, K. L. Mills and G. Gladstone, *J. Am. Oil Chem. Soc.*, 1980, **57**, 426-429.
28. K. P. Tan, T. B. Nguyen, S. Patel, R. Varadarajan and M. S. Madhusudhan, *Nucleic Acids Res.*, 2013, **41**, W314-W321.
29. G. R. Grimsley, J. M. Scholtz and C. N. Pace, *Protein Sci.*, 2009, **18**, 247-251.
30. J. D. Carter and T. H. LaBean, *J. Nucleic Acids*, 2011, **2011**, 8.
31. W. Tai, R. S. Shukla, B. Qin, B. Li and K. Cheng, *Mol. Pharm.*, 2011, **8**, 901-912.
32. R. Chinchilla, D. J. Dodsworth, C. Nájera and J. M. Soriano, *Tetrahedron Lett.*, 2000, **41**, 2463-2466.
33. S. S. Wang, J. P. Tam, B. S. H. Wang and R. B. Merripield, *Int. J. Pept. Protein Res.*, 1981, **18**, 459-467.
34. N. Nakajima and Y. Ikada, *Bioconjugate Chem.*, 1995, **6**, 123-130.
35. M. Abu-Hamdiyyah, *J. Phys. Chem.*, 1965, **69**, 2720-2725.
36. Q. Zou, S. M. Habermann-Rottinghaus and K. P. Murphy, *Proteins: Struct., Funct., Bioinf.*, 1998, **31**, 107-115.
37. L. Michaelis and M. M. L. Menten, *FEBS Lett.*, 2013, **587**, 2712-2720.
38. K. A. Johnson and R. S. Goody, *Biochemistry*, 2011, **50**, 8264-8269.
39. T. Menzen and W. Friess, *J. Pharm. Sci.*, **102**, 415-428.
40. M. Kohlstaedt, I. von der Hocht, F. Hilbers, Y. Thielmann and H. Michel, *Acta Crystallogr., Sect. D: Biol. Crystallogr.*, 2015, **71**, 1112-1122.
41. J. Kyte and R. F. Doolittle, *J. Mol. Biol.*, 1982, **157**, 105-132.
42. J. D. Cheeseman, A. Tocilj, S. Park, J. D. Schrag and R. J. Kazlauskas, *Acta Crystallogr., Sect. D: Biol. Crystallogr.*, 2004, **60**, 1237-1243.

43. E. Szájli, T. Fehér and K. F. Medzihradsky, *Mol. Cell. Proteomics*, 2008, **7**, 2410-2418.
44. M. W. Duncan, H. Roder and S. W. Hunsucker, *Briefings in Functional Genomics*, 2008, **7**, 355-370.
45. M. Bucknall, K. Y. C. Fung and M. W. Duncan, *J. Am. Soc. Mass Spectrom.*, 2002, **13**, 1015-1027.
46. P. Tae Gwan and A. S. Hoffman, *J. Biomater. Sci., Polym. Ed.*, 1993, **4**, 493-504.
47. K. Velonia, A. E. Rowan and R. J. M. Nolte, *J. Am. Chem. Soc.*, 2002, **124**, 4224-4225.
48. C. T. Walsh, S. Garneau-Tsodikova and G. J. Gatto, *Angew. Chem. Int. Ed.*, 2005, **44**, 7342-7372.
49. R. Gupta, P. Rathi, N. Gupta and S. Bradoo, *Biotechnol. Appl. Biochem.*, 2003, **37**, 63-71.
50. P. Desnuelle and P. Savary, *J. Lipid Res.*, 1963, **4**, 369-384.
51. H. Chahinian, L. Nini, E. Boitard, J.-P. Dubès, L.-C. Comeau and L. Sarda, *Lipids*, 2002, **37**, 653-662.
52. H. Lineweaver and D. Burk, *J. Am. Chem. Soc.*, 1934, **56**, 658-666.
53. H. Murata, C. S. Cummings, R. R. Koepsel and A. J. Russell, *Biomacromolecules*, 2013, **14**, 1919-1926.

6 Conclusions and Future Work

6.1 Conclusions

To conclude, the synthesis of protein-polymer conjugates of α -chymotrypsin (α -CT) with varying monomer functionality and grafting densities was successful. The resulting activity and stability profiles were also studied for each protein-polymer conjugate. To facilitate high polymeric grafting densities, a “grafting from” approach was employed *via* the synthesis of protein macro-initiators. The conjugation of an active ester species to the *L*-lysine residues on the surface of α -CT was able to be tuned by varying the pH of the reaction and the concentration of active ester species. The methodology allowed for simple production of protein macro-initiators with varying densities of surface-grafted initiator. Although various methods were attempted, the location of the modification sites were not able to be elucidated and therefore it was not possible to conclude whether the initiators that were synthesised were site-specific at varying pH or underwent random conjugation caused by autolytic behaviour. α -CT macro-initiator species were found to retain the catalytic activity profile of the native enzyme and also enhance the thermal stability. Indeed, the thermal stability was found to correlate to the surface charge of the protein with an increase in melting temperature, which indicated stronger intra-protein interaction with a reduction in surface charge.

Three monomers, glycerol methacrylate (GMA), *N*-(2-hydroxypropyl) methacrylamide (HPMA), and oligo(ethylene glycol) methacrylate (OEGMA), were successfully polymerised by atom-radical transfer polymerisation (ATRP) from the surface of α -CT. The subsequent analysis of the protein-polymer conjugates revealed that the grafting density was more influential on the catalytic stability than the overall molecular weight of the conjugates produced from all three monomers. Conjugates possessing high polymeric grafting densities were the most effective conjugate at providing enhanced stability. It was postulated that the observed increase in stability was related to the polymers’ ability to shield the protein residues interacting with the surrounding environment.

Investigation of the monomeric functionality revealed that protein-polymer conjugates synthesised from GMA and HPMA impart similar stability to the protein. In contrast, conjugates with grafted poly(OEGMA) were found to have a 4-fold increase in catalytic stability in comparison to the more linear species of GMA and HPMA. Additionally, increasing the molecular weight of the grafted polymeric species can further enhance stability, however this introduces limitations upon the catalytic ability of the conjugate species. In turn, this creates the need to establish a compromise between the desired stability and activity based upon the application of the resulting protein-polymer conjugate.

Whilst synthesising conjugates at the same overall molecular weight, the length of the pendent chain of the OEGMA monomer was found to have no effect upon the stability when stored below the lower critical solution temperature. As it was hypothesised that this is a result of the varying thicknesses and density of the polymeric shell formed, the stability was determined to have a dependence upon the length of the polymer as opposed to the molecular weight. This introduces the possibility of future investigations into the dependency of stability on the polymer length and the potential synthesis of species with tuneable stability suited to the final usage.

The grafted polymers of PGMA and PHPMA on the surface of α -CT provide protection to a secondary enzyme in solution from proteolytic digestion. It is hypothesised that the polymers perform molecular sieving to prevent larger substrates such as proteins reaching the active site but allows smaller molecules such as peptides through. The additional stability imparted from the grafted polymers allows advances towards the production of a one-pot formulation containing multiple stable enzymes.

Finally, the same chemistries employed to produce protein-polymer conjugates from α -CT were utilised in the synthesis of conjugated species from enzymes designed for a stain removal application. Although protein-polymer conjugates were successfully synthesised from both Unilever Protease 1 (UL1) and Lipex, the resulting conjugates did not exhibit the enhanced

stability previously observed with α -CT analogues. The lack of enhancement was hypothesised to be connected to the location of the polymeric graft and possible interactions with the existing intra-protein bonding. Therefore, it was concluded that the stabilisation of UL1 and Lipex by introducing grafted PGMA polymers was not a viable route and further research would have to be conducted to examine the other possible methods of stabilisation.

6.2 Future Work

Having established procedures for the successful synthesis of protein-polymer conjugates from the surface of several enzymes, there are many opportunities for further investigation. It would be desirable to locate the modification sites within α -CT when forming macro-initiators as to investigate the effect of the modification site upon degree of stability. This could be achieved by modifying proteins that do not undergo autolytic processes and performing tryptic digestions followed by high performance liquid chromatography mass spectrometry analysis.

The surface charge was found to be a key variable in the stability of α -CT and the introduction of charged polymeric species could be explored to determine the relationship between the protein's stability and the density of anionic or cationic substituents. The existing polymers could also be developed to include hydrophobic segments, which could be used to investigate the effect on enzymes that are optimised to a more hydrophobic environment such as lipase enzymes. This could be achieved by the synthesis of a scaffold protein-polymer conjugate with varying degrees of a modifiable monomer and performing subsequent post-polymerisation modification to incorporate a variety of functionalities

Despite the significant increase in stability observed for α -CT protein-polymer conjugates, activity was found to decrease as a result of restricted access to the active site. The development of a cleavable group connecting the polymer to the protein upon an external stimuli could create enzymatic species that are stable to storage and can be activated upon exposure to light, pH, temperature or light.

The successful protection of a second enzyme in the presence on α -CT protein-polymer conjugates, showed the selectivity to digest exclusively small peptides over macromolecular proteins. Many enzymes have been found to irritate skin and cause allergic reactions and therefore the protected enzymatic species have the potential to provide protection for the skin from the enzymatic activity. Further investigations should be performed into the skin sensitivity of the protein-polymer conjugates for possible use in other cleaning products that could benefit from the addition of enzymatic cleaning such as multi-purpose surface cleaners.

Although successful results were observed with the synthesis of protein-polymer conjugates from α -CT, applying these chemistries to various industrially relevant enzymes was not successful. As such, further research should be conducted into the effects on the tertiary structure of Lipex and UL1 upon synthesis of the conjugate species and to this end, circular dichroism and small-angle X-ray scattering analysis may provide some insight. This could uncover and highlight the differences between α -CT, UL1, and Lipex, and aid in selection of proteins that are suitable to be used as the catalytic core of protein-polymer conjugate species.